Digital measurement of power system frequency

Padilla, Rene David Carranza L.

Award date:
1994

Awarding institution:
University of Bath

DIGITAL MEASUREMENT

OF

POWER SYSTEM FREQUENCY

Submitted by René David Carranza López Padilla

For the degree of Ph.D.

School of Electronic and Electrical Engineering

University of Bath, U.K.

1994

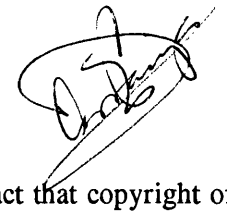

ProQuest LLC
789 East Eisenhower Parkway
P.O. Box 1346
Ann Arbor, MI 48106-1346

ABSTRACT

This thesis describes the investigation conducted on the development of a new technique for the measurement of power system frequency by digital means.

Information on power system frequency is carried by a signal composed of a fundamental component plus nonstationary additive noise. It is shown that a correct estimation of power system frequency will be accomplished if an adaptive extraction of the fundamental from noise is provided, and also, if amplitude variations in the fundamental component are discriminated with respect of variations of the fundamental frequency. The new frequency measurement technique incorporates a novel bandpass and orthogonal filtering process which extracts the signal from additive noise and correctly discriminates the effects of amplitude variations of the signal. A phase differentiation estimator uses the orthogonal components of the signal to calculate the frequency of the signal. Unit gain bandpass and orthogonal decomposition of the input signal are achieved irrespective of the frequency.

Results are presented for accuracy and evaluation time of the frequency measurement algorithm. Initially, the algorithm was tested against signals with known amplitude and frequency characteristics. Effects of nonstationary additive noise were also investigated. A set of computer based simulations of power system conditions was further developed. Particular attention was placed on the algorithm's response to dynamic power system frequency conditions. It is shown that the new technique is able of tracking rapid variations of frequency while providing accurate frequency estimates with evaluation times less than two power system cycles.

This thesis also describes the microprocessor implementation and laboratory testing of the new measurement technique using a power system simulator. The power system model basically consists of a micromachine and a transmission line model which can be synchronized to the mains supply. Power swing conditions between the micromachine and the mains supply can be generated by the simulator. Results are presented for correct operation and reliability of the measurement technique for on-line applications. The results confirm the reliability and accuracy of the new technique as predicted by the computer based experimental investigation.

ACKNOWLEDGEMENTS

I would like to thank Dr. Philip J Moore, who was my supervisor during this project, without whose excellent guidance I would have never achieved what is described herein. Under his supervision, I had the advantage of his profound expertise on power systems and digital signal processing which form the basis of this research work. I also wish to thank Dr. Moore for his many valuable comments and suggestions on this thesis.

Especial appreciation is expressed to Professor Allan T Johns, for precious discussions and his continuous interest on the progress of this project.

I would like to express my gratitude to those many people whose work in the fields of power system and signal processing has enabled me to endeavour this project.

During my staying as student in the Power and Energy Systems Group at the University of Bath, I had the benefit of friendship and expert discussions from my colleagues. I would like to thank Bruce Stedall, Haiyu Li, Y H Song, David Fitton for their comradeship. I wish to thank Vick Gott and Brian Ross for their helpful assistance on the conduction of the experimental investigation stages of this project.

I would like to express my gratitude to Sandra, my wife, for her admirable understanding and invaluable discussions on this work which rendered a continuous source of inspiration, for her patience and loving support during those many difficult stages throughout this work. I would like to thank David, my son, for his patience during those many days working late at the university.

I would like to thank my parents and my sisters for their endless support and encouragement advices throughout this work.

I wish to thank the Departament of Electrical Engineering of CINVESTAV-IPN for its support throughout my studies in Bath. I am also grateful to CONACYT-Mexico for financial support.

This thesis is dedicated to Sandra and David,
a blessing from God.

CONTENTS

LIST OF ILLUSTRATIONS

LIST OF ABBREVIATIONS AND SYMBOLS

Abbreviations

A/D = Analogue to Digital converter

ALE = Adaptive Line Enhancer

ALU = Arithmetic Logic Unit

AM = Amplitude Modulation

AR = Auto Regressive

AVR = Automatic Voltage Regulator

cpu = central program unit

C.P.V. = Cauchy's Principal Value of an integral operation

D/A = Digital to Analogue converter

DFT = Discrete Fourier Transform

DTFT = Discrete Time Fourier Transform

DP-RAM = Dual Port-Random Access Memory

DSP = Digital Signal Processing

e.m.f. = electromotive force

FFT = Fast Fourier Transform

FIR = Finite Impulse Response

FM = Frequency Modulation

FT = Fourier Transform

HT = Hilbert Transform

IF = Instantaneous Frequency

IIR = Infinite Impulse Response

I/O = Input/Output

ISR = Interrupt Service Routine

LMS = Least Mean Squares

m.m.f. = magnetomotive force

PC = Personal Computer

PC/C31 = DSP board containing the TMS320C31 cpu and the I/O module

PPS = Positive Phase Sequence

RLS = Recursive Least Squares

ROCOF = Rate of Change of Frequency

SCL = Short Circuit Level

Z[x] = Z transform of the variable x

Symbols

0,1 = relating to zero and positive phase sequence (subscripts)

ac = alternating current

'a', 'b', 'a' = relating to phases a, b, c

D = dependence of the load on frequency

dc = direct current

f = linear frequency, variable in the frequency domain

f_0 = linear power system frequency

f_s = sampling frequency

H_0 = equivalent single mass inertia time constant

L = order of an adaptive filter

n = time, variable in the discrete time domain

N = number of coefficients of a FIR filter

pf = power factor

p.u. = per unit

s = second

S/H = sample and hold circuit

t = time

T = sampling period

w = angular frequency, continuous time domain = $2\pi f$

w_0 = angular power system frequency

δ = load angle

θ = phase argument

π = angle in radians

σ = speed governor gain : droop

ϕ = angular phase offset

Ω = angular normalized frequency, discrete time domain = $2\pi f/f_s$

CHAPTER 1

INTRODUCTION

This Chapter describes, in an introductory manner, some aspects in the field of power system frequency measurement motivating the work which is the subject of this thesis.

The first section of the Chapter will address the necessity of an accurate measurement of power system frequency in relation to the correct operation of a power system. A brief description of the main problems associated with the measurement of power system frequency is given. The aims and objectives of the present research work are presented in the last part of the Chapter together with the structure of the thesis.

1.1 Power System Frequency

The value of the frequency in a power system is a reliable parameter which can be used to assess the magnitude and direction of any imbalance between generated and consumed power. The possibility of deviations of the frequency in modern power systems is kept to a minimum since most of the mechanical energy in the system consists of rotating machinery, both on the generation and on the load sides of the system, which represents a large amount of inertia which is always available in the form of a flywheel effect. However, in the case of a severe disruption of energy supply, the correct operation of the system can be threatened by the risk of a partial or total collapse due to the time needed to release prime mover power to assist the system during the generation-demand imbalance condition.

The dynamics of a large system are determined by the aggregate of the components that comprise the system. In systems with a large scale of integration, fluctuations of the operating points are assisted by the flow of power along the system. During contingency conditions, variations of the frequency due to plant outages are

restricted by releasing reserve generating capacity provided by generating plants operating at less than full output, or by gas turbine generators which can be started automatically by underfrequency relays.

Severe disturbances in a power system can convey the system to a generating deficiency period. A faulted generating unit, or the loss of a major tie are generally associated with this type of disturbances. In such cases the generating capacity of the system may become inadequate to meet the demand. Provisions are normally taken to ensure that, given the case of a forced plant shortage, there will be sufficient running generating capacity to allow a contained drop in the frequency. During the stage of power commitment planning, a determined amount of energy is set apart from the rest of the running generating plant capacity to accomplish these provisions. This energy is allocated throughout the whole system according to the rating of the generating units to ensure that the time spent to release the energy into the consumption areas will not result in overloading other generating plants. In modern industrial areas, a significant amount of the demand consists of frequency sensitive load, such as synchronous motors that perform like synchronous compensators when the frequency decreases, thus helping to reduce the overload of the system in the case of a generation deficiency. Generally, utility boards guarantee excursions of the system's frequency within 1% in periods of 24 hours.

If the severity of a disturbance in a system results in a section of the system becoming separated from the main system, the frequency of the islanded system will increase if the available running reserve exceeds the demand, while an excessive demand will result in a frequency decline. In the case of a frequency decline period, the initial rate of change of the frequency will be proportional to the generation-demand imbalance. If the generating capacity is not adequate to satisfy the demand, some of the load will have to be disconnected to prevent a possible collapse of the islanded system. Under these circumstances, load shedding schemes will be put into operation in power stations and substations in order to gradually arrest the decline of frequency. Many heavy rotating machines in use in power systems depend on under-frequency relaying procedures to avoid the risk of operating under extremely

low rotor speeds. Load shedding schemes are based on the accurate measurement of frequency deviations and on the rate of change of frequency (ROCOF) which allows to estimate the optimum amount of load to be disconnected. The necessity of an accurate and rapid measurement of the power system frequency during any of the above circumstances is critical for the correct operation of a load shedding scheme. Either an incorrect estimation of the frequency or a delayed measurement of frequency, will result in inadequate amounts of load being disconnected. Generally, a sub-optimal amount of disconnected load will lead to a reinforcement of the over-loading.

The above circumstances will be addressed in Chapter 2 in relation to the nature of frequency in power systems.

1.2 The Problem of Measuring Power System Frequency

Even during steady state conditions in a power system, the presence of electromagnetic noise present throughout the system can corrupt the measurement of power system frequency. Typical frequency spectra of signals taken at a power system busbar have shown that information on the system's frequency is carried by a signal centred at the system's frequency and immersed in additive broad band noise. For the correct measurement of power system frequency, the nonstationary nature of the noise has to be considered. An adaptive extraction of the fundamental component signal from the noise will ensure that time varying events will not affect the estimation of frequency. On the other hand, under dynamic power system conditions, variations of the transfer of power in the system will result in variations of amplitude and frequency of the signal under observation. It will be shown that under dynamic power system frequency conditions, the measurement of frequency is affected by variations of the amplitude of the signal, and also, that the measurement of the frequency taken at different points along the power system will produce different estimates of the system's frequency.

There are many well established power system frequency measurement techniques.

The commonest approach is to consider that the power system frequency remains stationary for a period of time long enough to neglect variations in the statistics of the signal under observation. For a stationary signal, its frequency is given as the inverse of its period. However, under this approach, it is not possible to remove the biasing effects of very low frequency components produced during power system disturbances on the frequency estimates.

A different approach is based on the spectral analysis of a signal taken at a power system busbar. Fourier Transform based techniques produce estimates of the frequency by locating the frequency components in the spectrum of the incoming signal. The correct application of these techniques requires that the sampling frequency must be an integer multiple of the product of the fundamental frequency times the number of samples to be included in the Fourier Transform calculation, and that every frequency component of the spectrum must be an integer multiple of the fundamental frequency. Incorrect use of these techniques results in spectral smearing or spectral leakage, respectively.

Chapter 3 is devoted to describe the characteristics of some of the most relevant power system frequency measurement techniques. Particular attention is placed on the recently developed adaptive power system frequency measurement techniques. These adaptive methods permit to account for the nonstationary nature of a power system and allow the rapid tracking of variations of the frequency during dynamic power system conditions.

The new power system frequency measurement technique, the subject of this thesis, is based on the definition of the instantaneous frequency (IF) of a signal, where the frequency of a signal is expressed as the derivative in time of the angular phase of the signal. The measurement of power system frequency is performed from a voltage or a current signal taken from a busbar. The signal is composed of a fundamental component centred at the power system's frequency and additive noise components. This technique provides an adaptive extraction of the fundamental component with respect of the nonstationary noise, and an optimum discrimination of the effects of

amplitude variations of the fundamental component.

The theoretical background supporting the development of the new power system frequency technique is addressed in Chapter 4. It will be shown that the correct estimation of a signal's frequency should account for the random variations of amplitude and frequency of the fundamental component. The concept of the IF of a signal provides an optimum discrimination of amplitude variations in the signal which is achieved by performing an orthogonal decomposition of the fundamental component. Then, a new frequency estimate is calculated from the derivative in time of the phase of the orthogonal components. In the new frequency measurement technique, the orthogonal decomposition is provided by two finite impulse response (FIR) filters which also allow extraction of the fundamental component from noise in addition.

The main features of the new power system frequency measurement technique are:

- This technique exhibits the shortest evaluation time among the current power system frequency measurement techniques, particularly during amplitude modulation processes and dynamic power system conditions.

- It provides the lowest variance estimate when dealing with amplitude modulation processes even in the presence of nonstationary noise.

- The numerical nature of the measuring algorithm in this technique has lead to the implementation of the technique on a digital signal processor based board.

1.3 Aims and Objectives of the Present Research Work

The work in this research project is aimed to produce an accurate and high speed technique for the measurement of power system frequency by digital means. The technique should correctly discriminate amplitude modulation from frequency modulation events in the fundamental component carrying information on the power

system frequency. The time varying nature of the signal and its environment will be considered, and the measuring algorithm should be able to adapt itself to such changes in the signal.

The following objectives were proposed for the development of the current research work:

1. A literature survey will be performed to ascertain the state of the art in this field. This will produce a set of technical references for purposes of comparison of performances among the different techniques.

2. Development of the new frequency measurement algorithm. The initial work on the new frequency measurement algorithm was introduced by Moore and Johns in 1991 [1]. This thesis will present the work performed to establish the theoretical background of a new power system frequency technique based on the work of Moore and Johns.

3. Experimental investigation to ascertain the performance of the new technique. Initially, a series of experiments developed by computer modelling are used to assess the accuracy and evaluation time of the new technique. This investigation will be accomplished in several stages. Firstly, it is intended to show the abilities of the technique for dealing with known signals whose main parameters can be determined in advance. The sensitivity of the technique to additive broad band noise is evaluated at this stage. Secondly, a collection of realistic power system conditions, developed by using computer modelling, will be used to evaluate the reliability and correct operation of the technique under dynamic power system frequency conditions.

4. Experimental investigation conducted on a power system simulator. Initially, the requirements for the digital implementation of the frequency measurement technique on a digital signal processing board (DSP) will be ascertained. Secondly, an experimental investigation using the DSP based frequency measurement technique will be conducted on a power system simulator. This simulator was originally

developed in the University of Bath for power system transient and dynamic studies. The rig basically consists of a micromachine and a transmission line model which can be synchronized onto the mains laboratory. The system model enables the simulation of a power swing of the micromachine against the mains supply. A series of tests will be conducted on this laboratory rig in order to assess the performance of the frequency measurement equipment when dealing with realistic frequency transient conditions.

1.4 The Structure of the Thesis

This section provides a description of the contents of the Chapters in this thesis:

The concept of the instantaneous frequency of a signal and the characteristics of the frequency in power systems will be discussed in the second Chapter. The necessity of accuracy and fast evaluation times during the measurement of frequency in power system will be discussed in relation to the dynamics of a power system and the development of frequency based protective schemes. It is shown in this Chapter, that the time varying nature of a power system imposes a set of restrictions which should be observed for the correct measurement of power system frequency.

Different approaches to the measurement of power system frequency have been developed over the years. A discussion on the most relevant frequency measurement techniques will be addressed in Chapter 3.

The development of the new frequency measurement technique is presented in Chapter 4. A theoretical background has been developed to support the validity of the new technique for its use in power system applications.

An assessment of the measuring algorithm's performance is included in Chapter 5. Results are presented for accuracy and evaluation time using computer based simulation of signals with known parameters and modelling of dynamic power system conditions

The measurement of frequency from a positive phase sequence (PPS) vector by using the new technique is addressed in Chapter 6. The development of the PPS frequency measurement algorithm is described in this Chapter. Results from the evaluation of performance of the PPS frequency measurement algorithm are included.

The digital implementation of the frequency measurement technique on a DSP board is discussed in Chapter 7. Results from the investigation conducted on the power system simulator using the DSP based technique are presented in this Chapter.

Chapter 8 presents a summary of this work. Conclusions on the work accomplished and some recommendations on further research work are included in this Chapter.

CHAPTER 2

FREQUENCY IN POWER SYSTEM APPLICATIONS

This Chapter will discuss the attributes of frequency in a power system. For a signal taken at a power system busbar, either a voltage or a current, it will be shown that unique information about the power system frequency is provided if such a signal is considered as an amplitude and frequency modulated process. This signal is in fact a single frequency component immersed in broad band noise. Analysis in both the time and the frequency domain of typical power system signals will confirm this approach. The last part of the Chapter will address how information about the dynamics of a power system can be obtained by observing the variation of the system's frequency as a function of time. Finally, this chapter will consider the effects of accuracy and time of evaluation during the measurement of frequency on the performance of frequency based protective schemes.

2.1 The Concept of Power System Frequency

The instantaneous value of the frequency (IF) is a well defined concept for a sinusoidal signal centred at a particular carrier frequency. This concept is frequently used in communication applications. If a signal exhibits more than a single frequency component it would be meaningless to define its instantaneous frequency because it would not render any physical significance. Instead, a frequency analysis of the signal will identify the different components in the signal's frequency spectrum.

Many physical phenomena changing in time may be correctly represented by single component signals even in cases where other interference sources may contaminate the signal with the addition of more components. In such circumstances it is correct to speak about the IF of the phenomenon under observation. This is true in the case of additive noisy components which are mainly due to the nonlinear nature of some elements within the same system. It is very likely that these components will exhibit a higher spectral energy content as compared to other noisy components generated

outside the system. In the system's frequency spectrum these components will lie in a frequency bandwidth close to the system's fundamental frequency, i.e.: harmonics of the fundamental. Even when these components are dependent on the occurrence of the fundamental, their amplitude and phase exhibit nonstationary characteristics, that is, their statistics will be different from one time of observation to another. The same random and time varying nature is displayed by the other noisy components contaminating the system's spectrum.

Let a real function ***x(t)*** to represent a signal taken from a power system bus, either a voltage or a current signal. From the nature of the represented system, this function may be regarded as the sum of a term centred at the system's fundamental frequency w_0 plus additive broad band noise. Hence, ***x(t)*** can be depicted as:

$$x(t) = s(t) + v(t) \qquad (2.1)$$

where the last term ***v(t)*** represents any other component apart from the fundamental, such as: dc, harmonics, travelling waves, arcing voltages, induced radio frequencies, etc. Equation (2.1) may provide a physical interpretation of the frequency of the represented power system if, and only if the fundamental component ***s(t)*** can be extracted from the additive noise. An adaptive bandpass filter will have to be used for this purpose.

It should be noticed that the term ***s(t)*** is centred at the fundamental frequency of an electrical signal since ***x(t)*** represents a signal taken from either a voltage or a current in the power system. It is only during steady state conditions in the power system when the frequency driving this term (electrical frequency) will exactly correspond to the rotor speed (mechanical frequency) of any generating unit in the system. Under these particular conditions, the electrical frequency can be measured at different nodes along the system and the same value will be displayed. It will be graphically shown from simulation results in Chapter 5 that this statement does not hold true during disturbances affecting the power system. See also [2], [3] and [4].

The fundamental component ***s(t)*** in the spectrum of ***x(t)*** can be expressed as:

$$s(t) = a(t)\cos[\theta(t)] \tag{2.2}$$

where the argument of the cosine function is:

$$\theta(t) = w_0 t + \Delta w(t) + \alpha(t) \tag{2.3}$$

The instantaneous frequency of ***s(t)*** is defined as [5]:

$$w_i(t) = \frac{d\theta(t)}{dt} \tag{2.4}$$

hence,

$$w_i(t) = w_0 + \frac{d\Delta w(t)}{dt} + \frac{d\alpha(t)}{dt} \tag{2.5}$$

Equation (2.2) represents a monocomponent signal with amplitude ***a(t)*** and centred at a frequency $w_i(t)$. Note that during steady state conditions the deviation of frequency $\Delta w(t)$ equals zero and the phase angle $\alpha(t)$ is constant, therefore, the centre frequency is $w_i(t) = w_0$. However, during the influence of a disturbance in the system, both $\Delta w(t)$ and $\alpha(t)$ may change according to:

- the initial conditions of the system preceding a disturbance,
- the type and magnitude of the disturbance,
- the electrical distance between the measuring point and the fault location,
- if the disturbance affects the generation/demand balance of the system, then the changes of the frequency in the system will result in changes in the reactance of the network elements located between the generating units and the point of measurement, thus the angle $\alpha(t)$ will vary with time.

In equation (2.2), both the amplitude **a(t)** and the phase $\theta(t)$ may be considered as random modulation processes. During steady state conditions in a power system and for an ideal zero noise, i.e: $v(t) = 0$, the conditional expected values of these processes should approach: $\mathbf{E\{a(t) \mid v(t) = 0\}} = V$ or I, *i.e*: the nominal voltage or current values, and $\mathbf{E\{w_i(t) \mid \alpha(t) = constant\ and\ \Delta w(t) = 0\}} = w_i$, *i.e*: the nominal power system frequency.

2.1.1 Amplitude/Frequency Modulated Signals in Power Systems

The term **a(t)** in equation (2.2) is intended to represent dynamic variations of the amplitude of ***s(t)***. In the case of a voltage signal taken at a power system busbar, **a(t)** will account for events such as: terminal voltage fluctuations in a generating unit following the dynamical response of an AVR, swings of power across the system, a generator transformer tap change, a sudden over-loading at the receiving end, etc. The effects of these events will be reflected on the amplitude of the voltage and/or the current. Note that ***s(t)*** in equation (2.2) is not accounting for the effects of additive noise in the signal ***x(t)***. It should also be noticed that fluctuations on the amplitude **a(t)** will be restrained by controlling schemes in the generating side of a power system, i.e.: AVR, power system stabilizers. In practice, the effects of restricting any possible excursion of the amplitude **a(t)** to a minimum will render a frequency spectrum **A(w)** of **a(t)** which will be bounded within a narrow frequency bandwidth about dc.

In order to show the effects of typical power system conditions on the amplitude and on the frequency of the fundamental component, the simulation of a single generator connected to a remote load has been carried out by using the Electro Magnetic Transients Program (EMTP) [6]. This simulation displays the performance of the generator following the application of an additional load at the remote end. An outline of the configuration of the system is shown in Figure 2.1. Before the fault inception, the generator is set at 75% of its rating. At time t = 30 s, an additional load rated at 10% of the generator rating is connected at the remote end. In this simulation the generator is assisted by a speed governor and by an AVR.

The generator terminal voltage is shown in Figure 2.2. This figure shows the impact of the additional load on the amplitude of the terminal voltage which is modulated by the dynamics of the fault. The new frequency measurement algorithm, as referred in Chapter 4, has been used to show the trajectory of both the frequency and the envelope of the voltage at the generator's terminal. Figure 2.6 shows the frequency and the terminal voltage in per unit. It can be seen that the rate of decay of the

voltage amplitude is steeper than that of the frequency since the frequency is assisted by the mechanical inertia of the generator which has a longer time constant as compared to that of the generator's exciter.

Figures 2.3 and 2.4 show the behaviour of the frequency measured by the new technique at the terminal voltage and at the receiving end, respectively. In both cases, the generator's rotor speed has been included for purposes of comparing the dynamics of the measured frequency at an electric point against the mechanical frequency. A proper discussion on the different trajectories of the frequency when measured at different points as shown in Figure 2.5, will be given until Chapter 5 during the assessment of the performance of the measuring algorithm.

2.1.2 Instantaneous Frequency of an AM/FM Signal

The concept of instantaneous frequency (IF) is used to provide a practical interpretation of the time varying nature of some oscillatory phenomena. In this way, the IF of a signal represents the location in the spectrum of the signal of its fundamental component as it varies with time. In other research areas such as acoustics, seismic, radar and sonar, the IF conveys information about the progress in time of the signal and it also provides a description of the media where the signal is present.

It has been shown that the IF of a signal can be obtained by forming a complex representation of the signal. In 1946, Gabor [7] proposed a method to represent a real signal by a complex one: from a signal like ***s(t)*** in equation (2.2), a complex representation ***z(t)*** is given as:

$$z(t) = s(t) + j\,HT[s(t)] \qquad (2.6)$$

where **HT[*s(t)*]** is the Hilbert Transform of ***s(t)***. From its definition, the Hilbert Transform of a signal ***s(t)*** yields:

$$HT[s(t)] = C.P.V.\int_{-\infty}^{\infty} \frac{s(t)}{\pi(t-\tau)}\,d\tau \qquad (2.7)$$

$$FT\{HT[s(t)]\} = -j\,S(w)\,sgn(w) \qquad (2.8)$$

where equation (2.7) is the time domain expression of the Hilbert Transform **HT[*s(t)*]** of **s(t)**, and equation (2.8) describes the Fourier Transform of the Hilbert Transform. The Cauchy's principal value (C.P.V.) in equation (2.7) avoids the singularity in the denominator of the integral at $t = \tau$. Since **HT[*s(t)*]** produces a 90° phase shift in ***s(t)*** for all frequencies within $\mathbf{0 \le w \le \infty}$, then, equation (2.6) can be expressed as:

$$z(t) = s(t) + j\,\hat{s}(t) \qquad (2.9)$$

z(t) is called the analytic signal associated with ***s(t)***. By definition, ***z(t)*** has a spectrum limited to positive frequencies only:

$$Z(w) = \begin{cases} 2S(w) & for\ w \ge 0 \\ 0 & for\ w < 0 \end{cases} \qquad (2.10)$$

that is, $s(t) = -HT[\hat{s}(t)]$ and $s(t) = -H^2[s(t)]$, i.e: ***s(t)*** and **ŝ*(t)*** are orthogonal to each other and contain the same spectral components.

Using the analytic signal representation of a real process, as shown by Gabor, Ville [8] has shown that the IF of a signal like ***s(t)*** can be given by:

$$f_i(t) = \frac{1}{2\pi}\frac{d\,arg[z(t)]}{dt} \qquad (2.11)$$

Equation (2.11) leads to the canonical definition of the IF of a single component signal ***s(t)*** which is given as the derivative in time of its phase. From Appendix 1, the IF of ***s(t)*** can be expressed as:

$$f_i(t) = \frac{1}{2\pi}\frac{\frac{d\,\hat{s}(t)}{dt}s(t) - \hat{s}(t)\frac{d\,s(t)}{dt}}{s^2(t) + \hat{s}^2(t)} \qquad (2.12)$$

Mandel [9] and later Papoulis [10], have shown that ***z(t)*** can uniquely represent the real signal ***s(t)*** as a process modulated both in amplitude by an envelope **a(t)** and in frequency by a phase $\theta(t)$, if the quadrature component ***ŝ(t)*** in the analytic signal

representation $z(t)$ is the Hilbert Transform of $s(t)$. This assumption is correct under the following conditions:

1. There must not exist spectral overlap between the envelope **a(t)** and the frequency carrier term $cos[\theta(t)]$. That is, the spectrum of **a(t)** should not interfere with the spectrum of $cos[\theta(t)]$. This requirement can be achieved by forming an orthogonal decomposition procedure leading to the complex signal $z(t)$ as in equation (2.9). For a discrete time implementation of $z(t)$, let two finite impulse response (FIR) filters $h_i(t)$ and $h_q(t)$, be used to provide in phase $i(t)$ and quadrature $q(t)$ components of the signal $s(t)$ as in Figure 2.7, where the symbol * represents a convolution in the time domain. The orthogonal decomposition of the signal $s(t)$ must be such that the orthogonal components can be expressed as:

$$i(t) = |s(t)|\angle[w_o t + \Delta w(t) + \alpha(t) + \phi] \qquad (2.13.a)$$

$$q(t) = |s(t)|\angle[w_o t + \Delta w(t) + \alpha(t) + \phi - \frac{\pi}{2}] \qquad (2.13.b)$$

Note that: a) there is -90° phase difference between $i(t)$ and $q(t)$, b) both FIR filters contribute with an equal phase delay ϕ without modifying the amplitude of $s(t)$, and, c) the angle ϕ is not a function of time, thus $\mathbf{d\phi/dt = 0}$.

It should also be noted that neither $i(t)$ nor $q(t)$ are the Hilbert transform of the input signal $s(t)$, but they are the Hilbert Transform of each other. From equation (2.9) and Figure 2.7, the analytic signal $z(t)$ can be expressed as:

$$z(t) = |z(t)|\exp[j\,\gamma(t)] \qquad (2.14)$$

where:

$$|z(t)| = (i^2 + q^2)^{1/2}$$

$$\gamma(t) = \tan^{-1}[\frac{q(t)}{i(t)}] \qquad (2.15)$$

If the frequency response of the orthogonal FIR filters $H_i(w)$ and $H_q(w)$ exhibit unit gain and equal group delay such that the quadrature component $q(t)$ equals the Hilbert Transform of the in-phase component $i(t)$, then, from equations (2.2) and

(2.14), the analytic signal $z(t)$ can be expressed as:

$$z(t) = a(t)\cos[\gamma(t)] + j\,HT\{a(t)\cos[\gamma(t)]\}$$
$$z(t) = a(t)\cos[\gamma(t)] + j\,a(t)HT\{\cos[\gamma(t)]\}$$
$$z(t) = a(t)\exp[j\gamma(t)] \qquad (2.16)$$

According to Bedrosian [11], equation (2.16) holds true if the spectrum $A(w)$ of the amplitude envelope **a(t)** does not overlap with the spectrum $C(w)$ of the carrier component $cos[\theta(t)]$. That is, the envelope **a(t)** in the second equation of (2.16) can be factorized outside of the Hilbert Transform term only if no overlap exists, otherwise, phase distortion will occur. For power system applications this condition is satisfied in practice by automatic voltage regulators in the generating side of the system which restrain the oscillations of the terminal voltage amplitude within few hertz close to dc in the system's spectrum. Typical power system conditions show that the commonest amplitude modulation is usually displayed in the form of a slow exponentially decaying function.

2. An implementation of the Hilbert Transform by digital means implies an approximated discrete time impulse response $ht[k]$ [12] with a discrete time Fourier Transform $dHT(\Omega)$ as follows:
where $\Omega = 2\pi f/f_s$, **f** is the independent variable in the frequency domain and f_s is the sampling frequency. Note that equation (2.17) is only an approximation to the continuous time Hilbert Transform as given in equation (2.7). This approximation is valid provided that a unit gain and a linear phase are achieved by the discrete time Hilbert Transform filter about the fundamental component of $s(t)$. See Berthomier [13] for an implementation of an IF estimation technique. Hence, for a digital implementation of the complex representation $z(t)$, its corresponding discrete time Fourier Transform $Z(\Omega)$ becomes:

$$Z(\Omega) = \begin{cases} 2S(\Omega) & for\ \ 0 \le \Omega < \pi \\ 0 & for\ \ -\pi < \Omega \le 0 \end{cases} \qquad (2.18)$$

3. A wrong estimation of the IF of $s(t)$ will result if the implementation of the analytic signal $z(t)$ allows any noise component of $v(t)$ in $x(t)$ to trespass into the

$$HT[k] = \begin{cases} \frac{2}{\pi}\frac{\sin^2[\frac{\pi k}{2}]}{k} & for\ k \neq 0 \\ 0 & for\ k = 0 \end{cases}$$

$$dHT(\Omega] = -j\ sgn(\Omega) \qquad (2.17)$$

spectrum of *z(t)*. The reasons are: a) from equation (2.16), the Hilbert Transform inherently selects the cosine component with the highest frequency and replaces it with a complex exponential, thus, spectral overlapping may occur; b) the differential operation in equation (2.11) will perform as a high pass filter amplifying any noise.

From this theoretical background, it can be seen that the frequency of a power system can be correctly estimated by digital means if the component *s(t)* centred at the fundamental power system frequency is properly extracted from the additive noise. The complex representation of the monocomponent signal will render a correct estimate of the IF provided that the in-phase and quadrature components of *s(t)* exhibit a unit gain and equal group delay about the fundamental.

2.2 Frequency Related to Power System Dynamics

Large scale integrated power systems have large amounts of mechanical inertia which will allow them to run synchronously at power frequency. These systems are virtually immune to changes in the loading or excitation of the individual generating units integrated to these systems. The high degree of integration of the system means that local demand is assisted from a virtual single supply which is fed by all the generating plants. For practical purposes, an infinite busbar is created and consists of a network of transmission and distribution lines connecting generating centres with demand areas not necessarily in physical proximity. Small fluctuations of loading or voltage are compensated by the flow of power along the system such that it remains in a steady-state stability condition. It can be said that the dynamics of the main system is determined by the aggregate of the components that comprise the system.

It may happen that a severe disturbance, for instance, the loss of a generating plant or the tripping of a transmission circuit, causes the separation of a section from the main system. These particular circumstances may also arise, for instance, when an industrial generating unit becomes disconnected from the utility. The islanded section is then run under its own dynamical conditions, facing the problem of a frequency decline if the generating capacity is inadequate to meet the local demand. The rate of fall of frequency is proportional to the overloading of the generating plant. Therefore, power system frequency becomes an important parameter in power and energy studies.

The case of an islanded power system will easily show how frequency is related to the power system dynamics. In this case, the electromechanical dynamics of the islanded system can be represented approximately by the dynamics of a single generating unit model [14], [15], [16], [17]. The complexity of the representation increases as the size of the system becomes larger. Some power system dynamics analysis have approached the problem through a coherency based dynamic equivalent where the model is composed of physical elements integrated in coherent groups [18]. A more practical approach is based in a transient energy function which reduces the system to a single generator located at the centre of inertia of the large system. In the second approach: 1) the system frequency corresponds to the average of the individual frequencies of the generating units within the system [14], [15], thus, synchronizing oscillations among machines are eliminated; 2) the impedance seen by the generating units at the time of separation is included as a single impedance representing the generator transformer, the transmission and distribution impedances plus a loading at the receiving end which is dependent on both voltage and frequency [19]; 3) if the model has to include a spare generating capacity, the dispatch of this energy is included in the model as driven by the dynamics of the machine's speed governing system; 4) the equivalent inertia time constant of the model represents similar inertias of the generators within the islanded system; 5) it is also assumed that the represented generators are operating at similar load levels. This model represents a linear equivalent of the whole system and it is suitable to estimate the performance of the system under the effects of several disturbances. A

better understanding of the behaviour of an islanded system should include the non linear nature of the elements in the system. The equivalent electromechanical model can be described by the following differential equation:

$$M\frac{d}{dt}\Delta f^*(t) = \Delta P^*(t) - D_{fv}(t)\Delta f^*(t) \qquad (2.19)$$

where $M = 2H_o$, H_o [kWs/kVA] is the inertia time constant of the equivalent generator running at synchronous speed w_0 ; $\Delta f^*(t) = f_o - f(t)$ is the change in frequency; $\Delta P^*(t) = P_{mech} - P_{elec}$ is the electromechanical power equation, positive values denote an excess of mechanical input power to the generator's shaft, negative values denote an excess of loading taken as a decelerating torque by the machine. The star * indicates per unit values. The availability of spare generating capacity may be included in this model by adding the dynamics of a speed governor driven by a first order differential equation where only the largest time constants dominating the response of the equivalent generator are included. In Figure (2.8) is shown the transfer function of a typical speed governor [14]. The following equation represents the time domain expression of the diagram:

$$\sigma T_R\frac{dP^*_{mech}}{dt} + \sigma P^*_{mech} = K_M F_H T_R\frac{d\Delta f^*}{dt} + K_M\Delta f^* \qquad (2.20)$$

where $K_M = pf(1 - SR)$ is the total mechanical power gain and it is affected by the power factor and by the spinning reserve SR; σ, is equal to the governor regulation gain, *i.e*: $\sigma = 2\pi$*droop; F_h is the fraction of the power generated by the high pressure turbine and T_R is the long time constant of typical reheaters. By substituting P^*_{mech} in $\Delta P^*(t)$ in equation (2.19), the frequency of the system as a function of time is given by:

$$\Delta f^*(t) = \frac{\sigma P^*_{step}}{D_{fv}\,\sigma + K_M}\left[1 + A\,e^{-\alpha t}\sin(w_R t + \phi)\right] \qquad (2.21)$$

A description of the terms in equation (2.21) is given in Appendix 2.

The factor D_{fv} denotes the dependence of the loading on both voltage and frequency. In [16], [17] this double dependence is expressed as:

$$D_{fv}(t) = \Delta f(t) + K\Delta V(t) \qquad (2.22)$$

where $\Delta f(t) = f_o\ \delta P_{elec}/P_o \delta f$ denotes the dependence on frequency; $\Delta V(t) = V_o \Delta P_{elec}/P_o \Delta V$ denotes the dependence on voltage and $K = f_o \Delta V/V_o \Delta f$ is a voltage to frequency ratio to compensate for changes in voltage with respect of changes in frequency. This factor must be estimated from on-line measurements.

From equation (2.21) it can be shown that the initial rate of frequency decline in the separated system becomes proportional to the value of the equivalent inertia time constant H_o and to the magnitude of the overload. That is:

$$\left.\frac{d\Delta f^*(t)}{dt}\right|_{t = separation} \simeq \frac{P^*_{step}}{2H_o} \qquad (2.23)$$

It should be noted that the use of this equivalent system model is for providing an insight into the performance of a very tight system where the distances among generating and consuming areas in the system are small and all rotating machines display similar parameter values. In genuine power system applications some other considerations have to be made. Baldwin's comments to the dynamic energy approach [20], point out the case of generators within the islanded system operating in an under-excitation condition before the time of separation when the generators would be drawing all their magnetizing current from the main system (consuming lagging VARs). The response of the AVR of an under-excited generator facing a sudden generation-demand imbalance would be to increase the exciter input, and thus the output voltage, to correct the reactive output. This situation will increase momentarily the overload [18] but it will not have a direct impact on the initial rate of frequency decay since some time delay may be expected due to the inertia of the exciter.

It may be seen that if the D factor in equation (2.21) were correctly accounting for the dependency of the load on voltage variations, then, the typical voltage drop that accompanies a frequency decline when a system becomes islanded, would help to reduce the magnitude of the overload. The response of voltage regulators is to raise the terminal voltage following the power imbalance for a given overload where the

power factor remains the same, but this voltage recovering action will be observed after one or two seconds after the separation time. See Figure 2.6. On the other hand, most of the load in power systems have a large content of frequency dependent load, such as synchronous motors and capacitor banks, some of them for purposes of power factor correction in industrial areas. The impedance of this load will increase as the frequency declines, thus helping to attenuate the magnitude of the overload [19]. In the model proposed by Anderson *et al* [14], as in equation (2.21), the factor D is cascaded with the governor regulating gain σ, or droop, which has typical values between 2% to 5%, thus, the product $D\sigma$ as in equation (2.21) does not represent a severe impact on the initial rate of frequency decay. It should also include the inertia of the load which will slow the frequency dependency response of the load. However, the factor D does determine the maximum excursion of the frequency decline and the final steady state value of $\Delta f^*(t)$.

It should be noted that a loss of generation also implies a loss of reactive power since power factor in everyday power systems are far from unity. The problem with reactive power is that it is not evenly distributed throughout the system since reactive power sources and power factor compensators are close to each other but far from generating centres. Therefore, the occurrence of a power system encountering a generation inadequacy may result not only in a frequency collapse but also in a voltage collapse if the reactive power at the generating side of the system does not match the loading reactive power. This situation can be better appreciated in terms of the rotor angle δ of an equivalent single generator feeding a load at a remote end. A change in δ will result in a change in the generator rotor speed and terminal voltage. Due to its dependence on voltage and frequency, the load will also experience the effects of the changes in δ. If the rotor angle reaches its maximum at 90°, then, the terminal voltage $\mathbf{V_t}$ will no longer be proportional to the excitation voltage $\mathbf{E}$, and changes in the latter voltage will result in large excursions of the generating reactive power. That is, at $\delta = \pi/2$:

$$\frac{dE}{dV_t} = 0 \quad ; \qquad \frac{dQ_g}{dE} = -\infty \quad ; \qquad \frac{dQ_g}{dV_t} = -\infty \tag{2.24}$$

2.3 Frequency Based Protective Schemes

Within a particular utility, the available amount of generation is balanced by a corresponding amount of demand on the consumer side. During healthy conditions both the voltage and the frequency of the system are determined and preserved by well accounted generating reserves. The stability of such a system, however, can be at risk of collapse whenever a severe loss of generation occurs. A common cause is the loss of an infeed tie connecting the utility with a main system. The remaining generating units within the islanded utility may be facing a demand exceeding the committed rating of the generating capacity and thus, the angular velocity of the generating units will start a rapid decelerating trend. The worst situation can be depicted when the decoupling is accompanied by a demand which has a low percentage of frequency/voltage depending load and when the available spinning reserve is not adequate to prevent the overload.

An easy and reliable way to arrest the frequency decline and to restore the power balance in an islanded system is to disconnect some of the load until a new balance status is reached. Within the islanded system, the fall of the frequency will also affect rotating machinery which will be running at dangerous low speeds. High costs are involved in maintaining an appropriate provision of generating capacity to encounter situations of generation deficiency, thus, this provision is kept to a minimum. During the system planning stage a spare generating capacity is allocated and distributed geographically throughout the system; the allocated amount being just enough to assist the system if a breakdown occurs. However, given the case of a system becoming islanded from a main system, the time spent to use this spare capacity for restoring the generation-demand power imbalance implies that some generators must be operated at a maximum capacity which would require a fast response of input prime movers and governor systems. This procedure may be longer than the time required for the frequency decline excursion to reach a point where an irreversible damage to the system has been made. The use of under-frequency load shedding schemes is justified by these economical and practical constraints.

At the time of the overload, the initial trend of the frequency decay is the only indication of the magnitude of the disturbance. From the previous section, it was seen that the initial rate of change of frequency is proportional to the ratio between the magnitude of the overload and the equivalent inertia time constant of the system. The accurate and fast measurement of this initial rate, better known as ROCOF, is used by load shedding procedures to assess the magnitude of the generation-demand imbalance as it progresses in time.

There are some practical requirements and constraints concerning the application of the ROCOF in load-shedding schemes:

- As shown in section 2.2, for an interconnected system undergoing a generation deficiency, the frequency at a given node is different from the frequency at other nodes [2], [3], [15], [21]. If a load-shedding scheme is to be started at a given substation, the local frequency will be equal to the average of the frequencies arriving at that node, but it may not be equal to the system frequency. That is, the local frequency will exhibit a random walk describing a nonlinear trajectory which is driven by the different dynamics of the individual machines within the system. An attempt to shed some part of the load at one substation may alleviate the load of some generating units but may worsen the response of others. Adaptive estimation of the dynamics of the system behind the load shedding location may be possible from the estimation of the ROCOF.

- In small systems undergoing a generation shortage, it is feasible to account with an adequate knowledge of the dynamic response of the generating units and of the dimensions and distribution of load which will enable a load-shedding scheme to be successfully started since during the planning of the system this provision can be made [23]. In medium and large size power systems there is no way to foreseen the correct amount of load to be shed and the restoration of the frequency decline may result in a weaker generation-demand balance. This is the main drawback of conventional under-frequency load-shedding schemes. Nevertheless, ROCOF based techniques also require of an adequate knowledge of the system. A correct evaluation

of the system status can be obtained by using recent information about power and frequency in the system as it is produced during the disturbance. Adaptive techniques as proposed by Elkateb *et al* [24] have been envisaged to extract this information in order to provide an optimum shedding of load.

- Frequency and voltage sensitive load will reduce the magnitude of the overloading as the frequency falls, affecting the initial rate of change of frequency. The load shedding procedure may disconnect some of this load worsening the disruption. A continuous and accurate estimation of the ROCOF, assuming that a short time is involved in the estimation, will display the trajectory of the overloading reflecting the dependence of the load with respect of variations of voltage and frequency.

- In order to account for fluctuations of power in the system which are due only to small disturbances from which it is possible to recover by controlling the export and import of power among areas in the system, a ROCOF based load shedding scheme must be programmed to start the measurement of the rate of change of frequency only if the frequency falls below a predetermined level. Typical levels range from 49.5 Hz depending on the physical location of the load shedding equipment and provided that the local rotating machines will not be damaged by this extent on the frequency decline. Local utilities usually guarantee frequency variations within 1% of its nominal value.

- In the case of available spinning reserve, the use of the ROCOF enhances the sensitivity of the assessment of the overloading with respect of the parameters of an equivalent speed governor driving the spare energy as this energy is being used for recovering the power system frequency deceleration.

The operating strategies of a power system will determine the design of a proper load shedding scheme. The design will take account of the distribution of the load in the system and provide an adaptive estimator of the dynamics of the load since it is likely to vary with time. Additional back-up, under-frequency relaying procedures are included in practice should the frequency remain below a safe level.

This condition may arise as a result of a sub-optimal estimation of the load to be shed.

From these circumstances it can be appreciated that ROCOF based load shedding schemes provide a more reliable means to encounter the frequency decline during a generation-demand imbalance. Power system frequency measurement plays an important role on the successful application of these schemes. There are, however, two significant issues concerning the measurement of frequency during these incidents:

- Firstly, at a given node on the system, the local frequency is only an average of the frequencies of the signals arriving at that node, and it does not necessarily equal the frequency of the overall system. Some authors [4], [21] point out that the oscillations in the measured local frequency should be extracted to estimate the real frequency trend of the system. As seen in Figure (2.5), the different frequencies observed at node SEND and at LOAD result from the changes of the electrical phase between the points. With respect to the rotor speed, the frequency at SEND is the frequency of the electromagnetic field in the generator which becomes different from the rotor speed which is assisted by a large mechanical inertia. Other authors [21], [22] consider that the positive phase sequence (PPS) voltage vector should be used for estimation of the power system frequency because this vector carries information of the real rotating electromagnetic field vector in the generator and thus it is insensitive to a given asymmetry of the phases occurring during the imbalance. The advantages of using the PPS voltage vector for frequency measuring will be shown in Chapter 6.

- And secondly, high energy content noisy components such as harmonics created during a generation deficiency which are driven in magnitude and phase by the power swinging across the system, makes the noise to be coloured rather than white. As it will be seen in the next Chapter some adaptive frequency measuring algorithms are based on the assumption that the noise contaminating the fundamental component is white, for instance Kalman estimation techniques. Even when provisions are taken

to calculate the statistics of the noise by adaptive algorithms, the estimates of frequency are sub-optimal in the sense that the initial values of the adaptive algorithm parameters have to be defined from *a priori* values which are based on intuitive approximations to the expected values of the modelled noise. The best performance of a frequency measuring algorithm will be achieved if it is able to extract the fundamental component in the power system signal from the additive noise as it was explained at the beginning of the present Chapter.

2.4 Conclusions

1° Information on the frequency of power system is conveyed by a single component process centred at the system's fundamental frequency immersed in additive broad band noise. Typical power system conditions confirm that this process is modulated both in amplitude and frequency.

2° A complex representation of the monocomponent real signal can be used for the estimation of the power system frequency. It has been shown that the analytic function associated with a monocomponent signal naturally leads to the canonical definition of the instantaneous frequency of the signal. An unbiased frequency estimator can be implemented by digital means if the complex representation is performed by an orthogonal decomposition of the signal with FIR filters which must feature unit gain and equal group delay about the fundamental frequency.

3° The dynamics of a power system can be better estimated by observing the changes of the frequency since this parameter is directly related to the magnitude and direction of flow of power in the system The steady conversion of rotating mechanical energy on the generating side of a power system into electrical energy during healthy conditions is reflected on the system's frequency. Should the system be facing a period of generation deficiency, the frequency will decline following a trajectory which is driven by the variation of the dynamics of the elements within the system. For a practical assessment of the performance of these elements, the whole system can be represented by a single equivalent generator located at the

inertia centre of the system. From this model it has been shown that the initial rate of frequency decay is proportional to the magnitude of the overload and to the system's inertia time constant. The response of other elements within the system during such disturbances will also affect the trend of the frequency, i.e. speed governing systems dispensing spare generating capacity, voltage/frequency dependent load reducing the magnitude of the overload as the frequency declines, automatic voltage regulators restoring the voltage amplitude and sometimes reinforcing the overload. It has also been seen that during a period of generating capacity shortage, the power system may be at risk of both voltage and/or frequency collapse, where the cause of the breakdown is very likely a difference between the generating reactive power and the load reactive power.

4° In order to assist a system during a sudden generation/demand imbalance for recovering its frequency, load shedding schemes are started when the frequency falls below a predetermined level, since no other corrective action can be taken before the frequency decline had made serious damages to the system. Optimum load shedding schemes are based on the measurement of both the frequency and the rate of change of frequency since the latter is proportional to the magnitude of the overload. ROCOF based load shedding schemes are more sensitive to the main parameters driving the electrical and mechanical dynamics of a power system. Adaptive estimation of frequency and power during the application of a ROCOF based load shedding scheme will result in a stronger restoration of the system since optimum amounts of load will be shed.

5° Adaptive estimation of frequency and power at a load shedding location will assist the protective scheme to estimate the correct amount of load to be shed.

6° It has been shown that an optimum control of the dynamics of a power system can be achieved if a proper measurement of the system's frequency is carried out. It is imperative, therefore, that accuracy and fast evaluation times must prevail on the measurement of power system frequency.

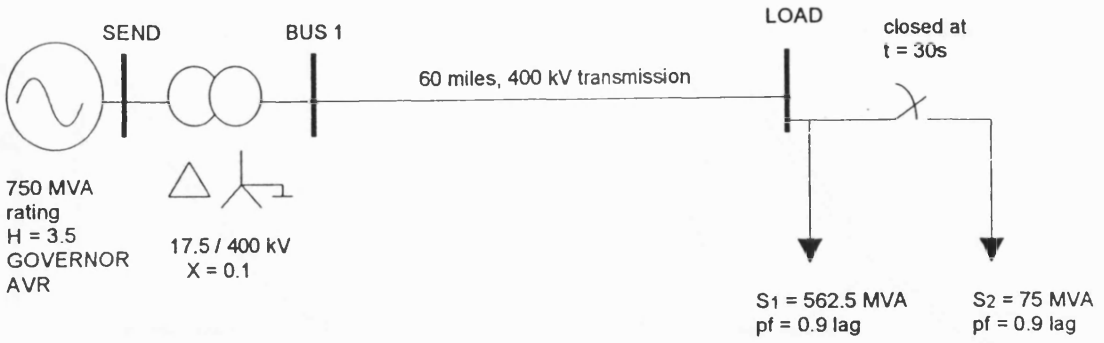

Figure 2.1. EMTP simulation of the application of an additional load at the remote end.

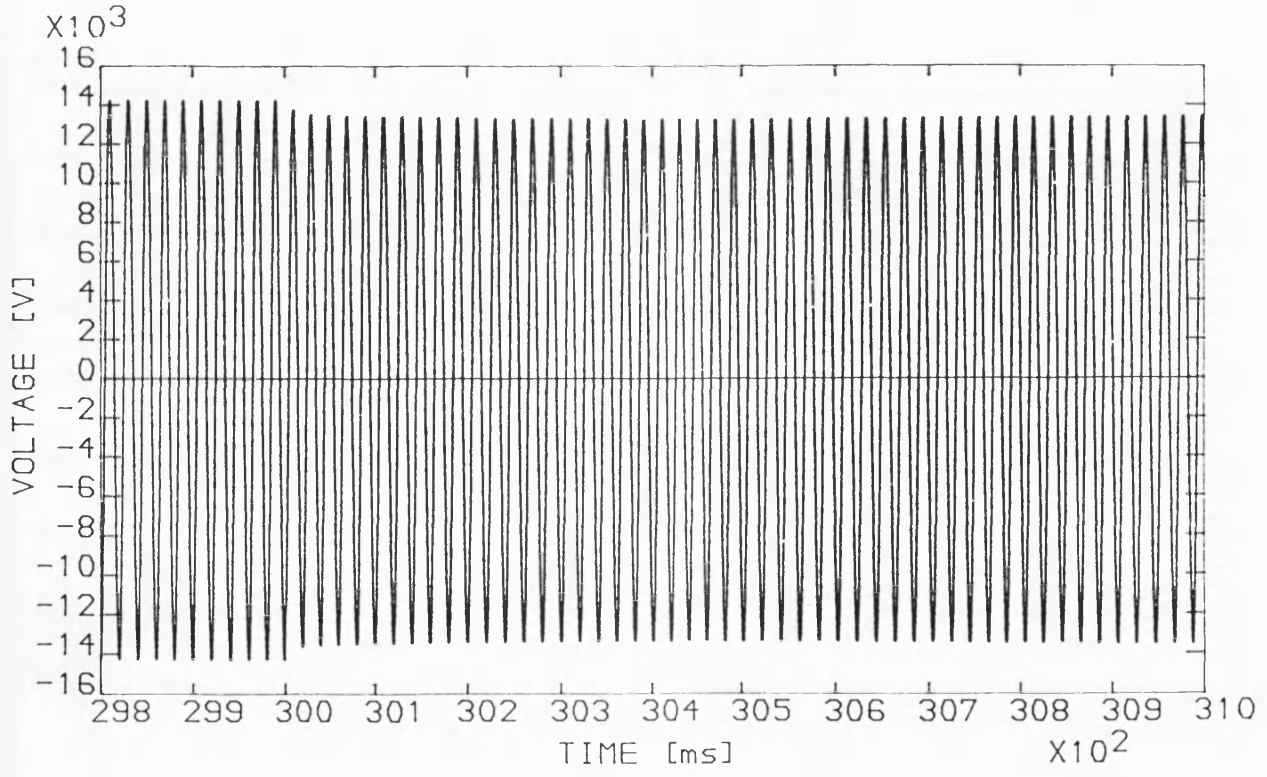

Figure 2.2. Modulation of voltage at busbar SEND.

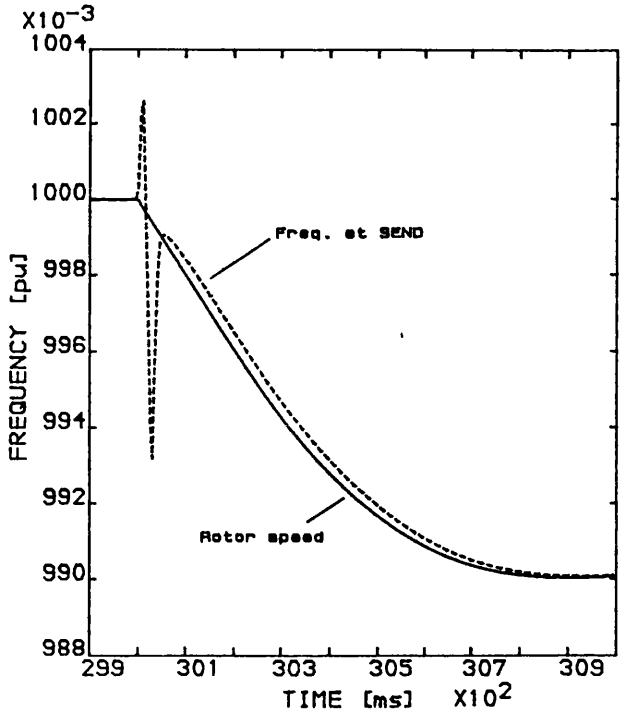

Figure 2.3. Generator rotor speed and frequency measured at busbar SEND.

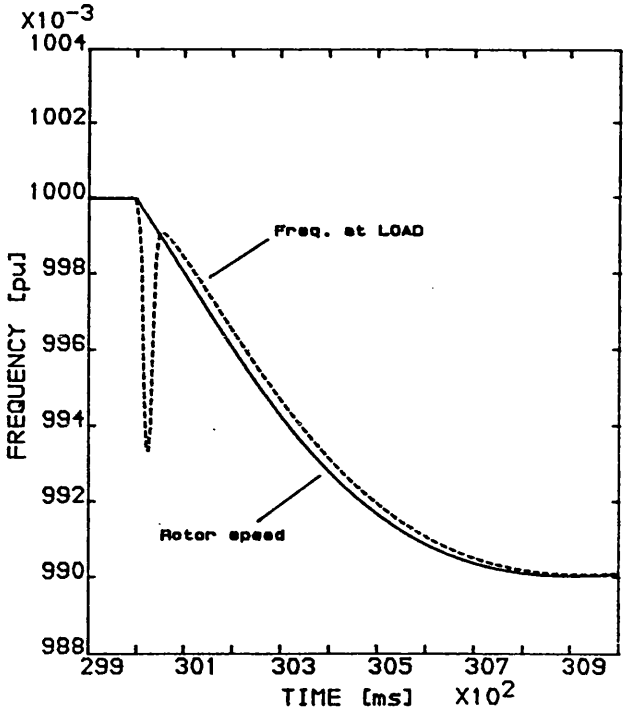

Figure 2.4. Generator rotor speed and frequency measured at busbar BUS1.

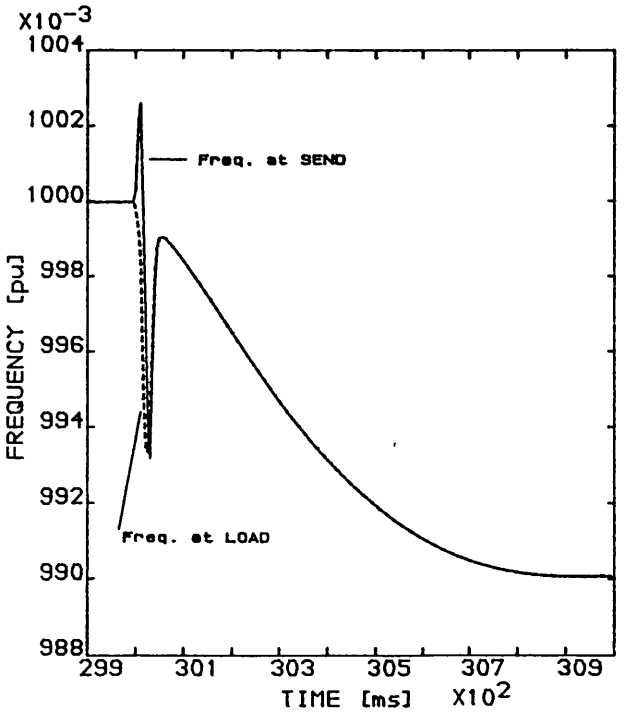

Figure 2.5 Measured frequency at SEND (solid line) and at BUS1 (broken line).

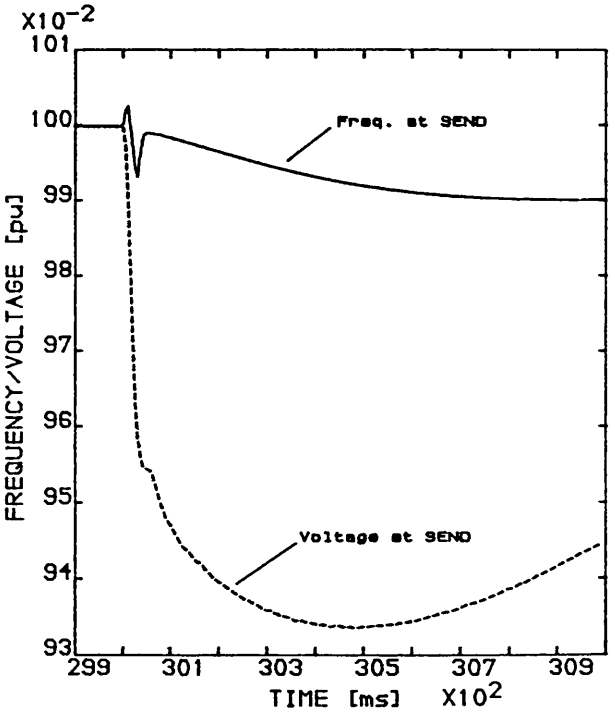

Figure.2.6. Voltage amplitude and frequency at busbar SEND.

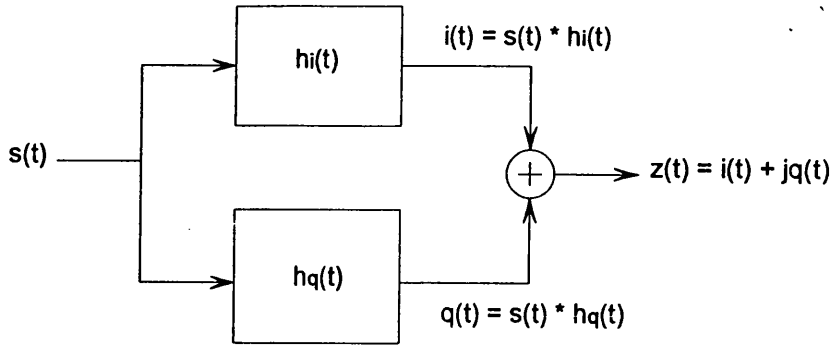

Figure 2.7. Schematic diagram of the complex representation **z(t)** of the single component signal **s(t)**.

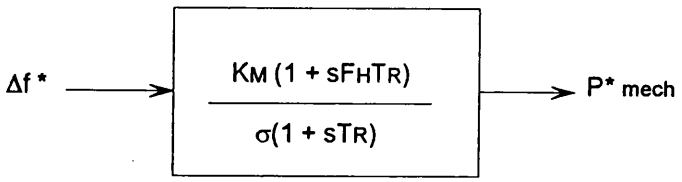

Figure 2.8. Transfer function of a typical speed governing system.

CHAPTER 3

FREQUENCY MEASUREMENT TECHNIQUES

Any attempt for obtaining information on the frequency of a power system will face the presence of additive nonstationary noise contaminating the source of information. Until recently, research in the area of measurement of power system frequency has considered that frequency is also a nonstationary event, therefore, the time varying nature of this parameter should not be neglected during its estimation. Recursive tracking of the frequency as it varies with time has been achieved by the introduction of adaptive filters. The effects of the additive noise contaminating the information about the power system frequency have been significantly reduced by the use of these filters.

It will be seen in this Chapter, that it is the concept of power system frequency supporting the development of a particular technique that renders a correct measurement of this parameter. This Chapter will address some of the main techniques for power system frequency measurement. These techniques have been grouped according to the approach undertaken. The last part of this Chapter will discuss the principle of operation of the new frequency measurement technique as proposed by this thesis.

3.1 Frequency of a Stationary Process

If frequency of a power system is associated with the rotational speed of a generator, then, huge amounts of mechanical inertia will restrain fast excursions of the frequency such that its statistics should be viewed as remaining stationary in the time. In this sense, the first order expectations of the frequency would be the same just to provide enough time for a frequency measurement to be accomplished. This approach results from the assumption that in a large integrated power system, voltage and frequency throughout the system are insensitive to local variations on generators or loads.

3.1.1 Zero Crossing Techniques

For a stationary signal, its frequency is given as the inverse of its period, that is, the times at which the signal goes through a given level, in this case, the time axis when the signal vanishes to zero. Alternatively, the frequency can be considered as half the time interval between consecutive zero crossings. This concept of frequency can be expressed as **f = 1/P** and **f = Z/2**, where **P** is the period of the signal and **Z** is the zero crossing rate taken as a function of time.

A digital implementation of this approach is straightforward. If the zero crossings are assumed to fall exactly on sample points, then a linear average of this rate will approximate the frequency of the signal within the observation interval:

$$f_i(t) \approx \frac{1}{M} \sum_{t-\tau}^{t} Z(t) \qquad (3.1)$$

where τ is the length of the observation interval and **M** is an averaging constant. If the interval between zero crossings contains a non integer number of samples, then, quantization noise will be introduced increasing the variance of the estimate. In order to reduce the variance of the estimate, the observation window should be increased. In that case, the estimate will exponentially reach the real value.

The implementation of many of these techniques are microprocessor based [25], [26], [27], [28], [29]. More sophisticated algorithms include the information from samples occurring at non zero crossing levels [30]. Compensating algorithms have been incorporated to reduce the effects of errors on the measured frequency: analogue input low pass filters to reduce the influence of additive noise [28], detection of the direction of the slope of the observed signal to reduce detection of false zero crossings [26]; weighting functions to reduce the influence of samples taken at times far from zero crossing levels [30].

The main problem to be solved by zero crossing techniques is the presence of non 50 Hz frequency components in the observed signal. Extensive use of lowpass filters has been made to overcome the problem of high frequency noise, starting from the

harmonics of the fundamental, which will produce false zero crossing detections. However, the major source of inaccuracy will be a dc component appearing in the signal's spectrum since the signal under observation will be mounted on this component and the crossing level will not be zero.

3.1.2 Fourier Transform Based Techniques

The frequency of a signal is usually associated with the Fourier Transform of the signal. The Fourier Transform is a representation in the frequency domain of the frequency contents of a signal and results from integrating the time convolution between the signal and a time "sweeping" factor. The integration should be performed over the entire history of the signal. This transformation removes the time variable from the frequency domain and thus it is not a function of time. The magnitude component of the Fourier Transform is related to the phase component in the sense that the latter may indicate the time of occurrence of the former. This information is difficult to extract unless the signal is a deterministic one. On the other hand, the instantaneous location of a frequency component at a particular instant of time, which conveys to the concept of instantaneous frequency, is given as a function of time and is extracted from local information as taken from the most recent evolution of the signal.

By using a fast Fourier Transform (FFT) based algorithm, Girgis *et al* [31], calculated deviations of frequency from its nominal value. Any deviation from the fundamental will "leak out" on the signal's spectrum. That is: for a finite observation window sequence of N samples, where $N = f_s/f_0$, f_s and f_0 are the sampling and fundamental frequencies, respectively, the FFT will not produce a leakage provided that N is an integer multiple of the fundamental frequency. This algorithm is almost linear within 5 Hz about the fundamental, but only for pure sinusoidal waveforms. A zero crossing detector is used to ascertain a positive slope on the waveform in order to start the FFT algorithm. To correct for the presence of additive noise on the measured waveform, a Kalman filter is added to the resulting estimated frequency. This filter was designed from *a priori* estimates of the

frequency statistics and, thus, it must be adjusted for the application of the measuring algorithm on a different power system.

3.2. Frequency in Time Varying Processes

Recursive algorithms have been developed to track variations in time of the frequency of a power system. Some techniques were designed to adjust only a single parameter in the measuring algorithm to compensate the algorithm's performance for time varying deviations of the frequency regardless of the nonstationary nature of the amplitude of the fundamental component or of the surrounding noise. On the other hand, adaptive filter theory has been used by more sophisticated techniques in order to account for the nonstationary statistics of the observed signal. The design of many adaptive frequency measuring algorithms includes some sort of adaptive narrow bandpass filter centred at the fundamental which recursively extracts this component from the power system additive noise providing correct information about the amplitude and frequency of the fundamental. Different techniques are utilised after this signal enhancement for calculating the frequency from the bandpass filtered signal.

3.2.1 Frequency Estimation From a Phasor Measurement

Under this approach, the speed of rotation of a voltage vector is taken as the frequency of the voltage signal. To account for deviations of frequency, the angle of the vector is related to a certain reference angle which is rotating at synchronous speed. Frequency measurement results from a phasor estimation, that is, the real and imaginary parts of the fundamental component are recursively tracked, and the derivative in time of the angle described by the complex parts yields the frequency estimate.

Phadke *et al* [32], proposed a recursive positive sequence phasor estimator based on the real and imaginary parts as they are generated by a discrete Fourier Transform (DFT) centred at the fundamental. A FIR filter was based on the phasor description

of the DFT to recursively produce the complex components of an input signal, *i.e:* a new phasor estimate is based on the estimation of previous phasors. The rate of change of the most recent estimated complex phasor yields the input signal frequency. According to the authors, small deviations of frequency result in large evaluation times. If larger frequency estimation errors were allowed, the evaluation times would be reduced. The DFT-FIR filters do not provide a complete rejection of noise outside their main frequency sidelobes, and this paper does not give any indication of the use of an additional noise reduction stage. The same phasor estimation principle is used by Benmouyal [33] to recursively adjust the sampling frequency of a similar DFT-FIR filter. Longer evaluation times are expected for small frequency deviations. Thorp *et al* [34] used a least squares polynomial fitting algorithm to smooth the influence of noise on the estimated voltage phasor following the technique developed by Phadke.

3.2.2 Adaptive Estimation of Power System Frequency

Initial work on the measurement of the frequency of a signal by using adaptive filter theory is attributed to Griffiths in 1975 [35]. A FIR transverse all pass filter, provides a connection between the coefficients of the filter and the power spectrum of the signal. The filter is made adaptive by using the least mean squares (LMS) algorithm of Widrow and Hoff. A similar approach was undertaken by Reddy [36]: a recursive least squares (RLS) lattice filter provides the location of frequency components in the signal's spectrum. These techniques have been considered as adaptive spectral estimators. They are better known as adaptive auto-regressive (AR) models which provide a practical means for estimating the IF of a FM process by locating the frequency at which the AR power spectrum attains its peak value at a given instant of time. The transfer function of an adaptive AR model of order L is given as:

$$H(e^{j\Omega}) = \frac{1}{1 + a_1 e^{-j\Omega} + a_2 e^{-j2\Omega} \ldots + a_n e^{-jM\Omega}} \qquad (3.2)$$

The power spectrum of a time varying process $x(t)$ and its time convolution with this

AR filter can be expressed as:

$$S(\Omega) = S_x^2(\Omega)\,|H(e^{j\Omega})| = \frac{S_x^2(\Omega)}{\left|1 + \sum_{k=1}^{M} a_k\, e^{-jk\Omega}\right|^2} \qquad (3.3)$$

The coefficients a_k of the adaptive filter are related to the location of the frequency components of $x(t)$. Frequency is estimated as a function of time for a given observation data window.

Most of these implementations have undesirable practical characteristics: long evaluation times since a FFT algorithm has to be used to locate the frequency components from the estimated power spectrum, frequency resolution being dependent on the length of the observation data window, and finally, the length of the decorrelation factor in the line enhancement stage must be adjusted in order to decorrelate the input signal with the fundamental's harmonics in the case that the former could drift from its nominal value. Recently, Chambers [38] and Chicharo [39] have incorporated a LMS filter from Widrow and Stearns [40] to implement infinite impulse response (IIR) notch filters to track the fundamental component. LMS algorithms suffer from longer convergence times as compared to other adaptive techniques due to the occurrence of noisy components which result in the spread of eigenvalues in the correlation matrix.

A significant improvement over the previous techniques has been afforded by the Kalman filter theory. For a nonstationary signal immersed in white noise, a precise rejection of the noise can be achieved in terms of the Kalman equations. For power system applications, the design of the Kalman approach will yield: a process equation to describe the dynamics of the fundamental component of the observed signal in terms of a state vector which includes the presence of white noise contaminating the signal, and a measurement equation which relates the dynamics of the signal to the measurement errors. The error between an estimate and a real value provides a measure to make recursive the algorithm. For a nonstationary signal to be observed, the process equation is modified to account for some form of

variation of the signal, for instance, a random constant, a random walk or a combination of both. In order to extract the real features of the observed signal from additive noise, a precise model of the signal must be used to evaluate the variables of the process equation. Kalman filtering exhibits faster convergence rates that LMS. However, they are computational complex and may lead to numerical instability if low precision arithmetic is used.

Sachdev and Shen [41] used a Kalman filter for smoothing of frequency measurement results. Kamwa and Grondin [42] used the Kalman theory to form a recursive identification of a voltage phasor as described by a Taylor series expansion for application on power system frequency measurement. Sachdev, Wood and Johnson [43] designed a Kalman filtering method for estimation of rotating phasors for power system relaying applications.

The most relevant research work on Kalman filter theory for power system applications is attributed to Girgis *et al.* It should be helpful to have a quick review to his work. Girgis and Hwang [44] used a linear two-state Kalman filter to estimate the quadrature components of a voltage phasor; frequency is calculated from the rotation of the phasor angle. A three-state extended Kalman filter was later used instead of the two-state filter in order to estimate the frequency as one of the state variables. The simulations presented on this paper included the presence of white noise with different standard deviations. Girgis concluded that noise affects the estimation of the phasor angle in the two-state filter and the estimates of frequency in the three-state filter. It was also noticed that the sampling frequency affects the settling time of the filters: higher sampling rates yield a faster filter response. The effects of the noise on the three-state filter are reflected by an initial overshoot of the filter output during the convergence period of the filter, however, the noise does not have effect on the final steady state of the estimates. The results presented on this paper does not include variations of the amplitude of the underlying signal which would reveal the robustness of the Kalman approach. Tracking of time varying harmonics in power systems was addressed by Girgis, Chang and Makran [45]. The problem of time varying amplitude of the fundamental is met on this paper. The

number of state variables depends on the possible number of harmonics to be estimated.

A later study on power system frequency deviation and its rate of change based on an adaptive Kalman filter was presented by Girgis and Peterson [46] in 1990. A two stage filter is proposed as in [43] for estimation of quadrature components leading to frequency and rate of change of frequency measurement. The first stage calculates the frequency from the adaptive estimation of the rotating voltage phasor, while the second filter models the frequency deviation calculated by the first stage as a linear walk plus a random ramp process; the rate of frequency change is found from the slope of the random ramp. A significant improvement over previous Kalman work is presented on this paper. That is, the noise statistics contaminating the power system information are recursively estimated by a noise variance estimator for on-line applications. Girgis accepts that this estimator is sub-optimal in the sense that the true value of the statistics of the time varying noise can not be accurately determined. However, the estimates will show a lower variance as compared to previous Kalman filter implementations. Under the presence of noise, this paper shows that the combined response of the two stages filter converges within 0.2 seconds.

It is seen from these Kalman filter applications that the state model of the process to be observed should clearly express the statistics of additive noise. The Kalman filter is sensitive to the relationship between the estimated process and the measurement equation on the assumption that the noise must be white [47]. In order to account for this inconvenience the state variable vector may be augmented and added to the original state vector [48].

3.2.3 Phase Differentiating Estimators

From the orthogonal decomposition of a bandpass signal into its in-phase and quadrature components, an estimation of frequency of the signal can be given as the speed of rotation of the angle between the orthogonal components. There are two

similar approaches to this concept. On the first one, a demodulation procedure renders the orthogonal components of the bandpass signal; frequency is calculated from the differentiation of the angle between the components. On the second approach, a complex representation of the bandpass signal is given in terms of an analytic signal as described in Chapter 2; the complex representation is achieved by the digital implementation of an approximated Hilbert Transform.

3.2.3.1 Signal Demodulation

The positive phase sequence voltage vector was used by Eckhardt *et al* [21] to calculate power system frequency. The three phases at a given node are used to form a complex PPS vector. Frequency is calculated from the derivative with respect to time of the angle between the imaginary and the real parts of the vector. Three moving average filters with different group delays are used to low pass the frequency estimates. Denys *et al* [22] used the conventional quadrature demodulation procedure applied to a PPS voltage vector:

$$V(t) = \frac{A(t)}{2}[e^{j\phi(t)} + e^{-j[\phi(t) + 2w_o t]}] \tag{3.4}$$

where $A(t)$ is the amplitude of the fundamental signal $v(t)$:

$$v(t) = A(t)\cos[w_o t + \phi(t)] \tag{3.5}$$

The demodulation consists on the time multiplication of the input signal $v(t)$ by a complex signal centred at $w = w_0$. The resulting convolution in the frequency domain separates the spectrum of $v(t)$ into two frequency components, one located at dc and the other at the second harmonic of the fundamental $w = 2w_0$. This process is similar to the well known AM demodulation process. An IIR low pass filter close to dc is added after the demodulated PPS signal $V(t)$ to remove noise from the split component. Denys used the Prony's method for analysing the spectra of the orthogonal components in order to estimate the fundamental frequency. A third order notch filter follows the frequency estimates to remove the influence of amplitude variations on the input signal. He does not use the differentiation of the phase to avoid noise amplification due to the implementation of the phase derivative.

Begović *et al* [49] proposed a frequency measurement based on the conventional demodulation procedure, as previously described, followed by an IIR Bessel lowpass filter to remove noise starting at the second harmonic. An approximation to the finite central difference algorithm of the phasor angle yields the frequency deviation estimate.

A severe problem to be dealt with by using a difference algorithm during the calculation of the frequency from the rotation of the angle spanned by the orthogonal components is the "wrapping" of the angle. A complicated numeral algorithm must be implemented to remove this discontinuity which otherwise will affect the frequency results.

3.2.3.2 Hilbert Transform Approximation

In order to implement the complex representation of a real signal, as described in Chapter 2, some frequency measuring techniques have developed different approximations to the Hilbert Transform by the use of FIR filters. From equation (2.17), it is seen that the Hilbert Transform impulse response **HT[k]** is infinite in duration and noncausal. From the work of Rabiner and Schafer [50], a suitable implementation of the Hilbert Transform by digital means has been afforded. The design will produce a bandpass filter with symmetry about half the bandpass, with an equi-ripple magnitude and a linear group delay equal to half the number of coefficients of the filter. The bandwidth of the approximated Hilbert Transform needs only to cover a narrow bandwidth about the frequency components of interest just enough to preserve the Nyquist bandwidth criterion for digital applications. This FIR filter approach renders a good 90° phase shifter to provide the quadrature component for frequencies within a required bandwidth. The linear group delay caused by this filter has to be matched by another bandpass FIR with equal group delay which should yield the in-phase component. Berthomier [13] used the Hilbert Transform as proposed by Rabiner and Gold [12] for analysing the time-frequency variation of a real multi-component signal. The objective of this particular technique was to associate the energy contents of the frequency components of a signal to their

occurrence at a given instant of time.

There are two main problems related to the use of the discrete Hilbert Transform: the first one is the equi-ripple magnitude about the bandpass resulting from the discrete time approximation to the continuous time. This non-unit magnitude must be compensated for to avoid frequency estimate errors when the observed frequency drifts from its nominal value; the second problem, is that to produce a suitable bandpass filter requires the use of a high order FIR filter to achieve a narrow bandwidth about the fundamental, otherwise non 50 Hz components will trespass into the frequency calculation.

Sun and Sclabassi [51] developed a numerical algorithm to implement an alternative form to the discrete Hilbert Transform by using the DFT complex representation of a real signal. Calculation of frequency is performed by a central difference algorithm over the angle of the complex signal. Phase unwrapping is needed to unfold the angle at $\pm \pi$. A smoothing procedure is applied to the frequency results by using a linear regression estimator followed by a lowpass filter.

3.3 Approach Proposed by the New Frequency Measurement Technique

It was envisaged by Moore and Johns [1] that a bandpassing plus orthogonal decomposition filter will be achieved from the design of two symmetric FIR filters with a 90° phase shift in between. It can be shown that the resulting filters provide an equal group delay, and that their frequency responses are centred at the power system nominal frequency and exhibit zeros at dc and at each one of the subsequent harmonics of the fundamental. Since the frequency response of the filters is not equal at other frequencies apart from the fundamental, a magnitude compensation algorithm is included to compensate the output of the filter before the calculation of the frequency. These filters provide an optimum approximation to the discrete complex representation of a real single component signal. Rejection of non 50 Hz components is achieved without distortion of the phase of the orthogonal estimates. A new frequency estimate is calculated from the ratio between the slopes of the

orthogonal components and their magnitude as given in Chapter 2 by equation (2.12). As it will be shown in Chapter 4, this technique produces the best approximation to the concept of the instantaneous frequency of a single component AM/FM signal immersed in broad band noise. It is also shown in Chapter 4, that variations in the amplitude of the fundamental component result in inaccurate estimates of frequency. It will be shown that the complex representation approach undertaken by this technique allows an optimum discrimination of the effects of amplitude variations.

According to the categorization of the different frequency measurement techniques as discussed in the previous paragraphs, the new technique can be classified as related to the last group for its approximation to the analytic signal representation leading to the instantaneous frequency of a real signal. The design of the algorithm has allowed an easy implementation of the measuring technique on a digital signal processing board for power system applications. Frequency estimates are afforded in less than one and half 50 Hz cycles. Chapter 4 will describe the design and development of this technique.

3.4 Related Work on Instantaneous Frequency Measurement

Extensive research in the area of Signal Processing on the problem of the measurement of the IF of a signal has sustained the development of different frequency measuring techniques for application fields other than power systems. The main concept addressed by these techniques is the development of time-frequency representations of real signals for on-line applications. The starting point of this approach is given by the discrete short time Fourier Transform [52]. The time-frequency information resulting from this technique is corrupted by the spread of frequency sidelobes resulting from the observation of short time data windows. Different smoothing techniques, such as Hamming, Hanning and other FIR filters, help to reduce the Gibbs phenomenon which results from truncation of the observed signal. Other techniques have resulted from the short time Fourier transform: wavelet transform and Gabor expansion.

A significant improvement has been given by the Wigner-Ville time-frequency transformation. The resulting information on the location of frequency components is given as a function of time. A complex representation provided by a previous orthogonal decomposition of the observed signal is necessary before the application of this transform. The distribution of energy located at the different frequency components of a signal at a given instant of time, operates like a time-spectral representation of the signal.

Correct use of these techniques requires initialisation of the filter parameters according to a particular application. It seems that the problem of tracking a single component signal located close to dc and to its first harmonics, such is the case of information taken from a power system busbar, implies an expensive computational task for these techniques for on-line power system applications. There exists a compromise between the length of the observed data window and the resolution of the time-frequency representation. This dilemma has been depicted as the problem associated with the bandwidth-time product in the Fourier Transform. Essentially, there is no way to measure the energy of a particular frequency component at a particular instant of time. Instead, energy is associated to a finite bandwidth and to information from a finite data window. The resulting problem is a lack of resolution in the time-frequency representations. Excellent tutorial information on these techniques has been gathered by Boashash [53] and Hlawatsch *et al* [54].

3.5 Summary

1° The assumption of stationary statistics of power system frequency resulted in the development of fast zero crossing and FFT frequency measurement techniques. Due to the time varying nature of power system parameters, adaptive filter theory has superseded stationary based techniques. An optimum tracking of the power system fundamental has been afforded by these filters.

2° Adaptive frequency measurements started with the estimation of voltage phasor and the calculation of the speed of rotation of the angle described the estimated

phasor complex components. Long evaluations resulted from the phasor estimation and the frequency calculation which produces accurate estimates from pure sinusoidal signals only.

3° Adaptive estimation based on LMS and RLS algorithms rendered the development of adaptive AR filters. These techniques are particular well suited for tracking multicomponent signals. Resolution of frequency components in the signal spectrum is related to the length of the observed data window.

4° The application of Kalman filtering theory to the problem of frequency measurement created a new generation of fast estimators. Kalman filtering is sensitive to round off noise unless high precision arithmetic is used. Insufficient precision of the state variable modelling of the signal or process to be estimated, results in a weak estimator which may steer the filter into instability. This condition assumes that the model of the noise is intuitively well known to initiate the filter. Sub-optimal noise estimators may be added to the Kalman algorithm when dealing with nonstationary environments. Kalman filtering can not assume that the observed process is always constant. Therefore, some sort of noise should be added to the model, for instance a random walk or a random ramp. The use of Kalman filtering is better accommodated for tracking a process whose noise statistics can be accurately known.

5° Measurement of frequency can be obtained from the derivative in time of the angle of the orthogonal components of a complex signal. Phase unwrapping is required to unfold the phase angle between the orthogonal components. The differences between measuring techniques lie in the orthogonal decomposition techniques which are used to yield a complex representation of a real signal, and also, on the use of the orthogonal components for the calculation of frequency.

6° Signal demodulation, as used in communication applications allows observation of the deviation of the frequency of the input signal from its nominal value which will result in a deviation of the split frequency components. Lowpass filtering is

required to extract the complex components near dc from the remainder of the demodulated spectrum. These complex low frequency components exhibit a 90° phase shift between each other. A bandpass filter usually precedes the frequency convolution to remove non-50 Hz components.

7° Digital implementation of the Hilbert Transform has been proposed by many authors. The algorithm of Rabiner and Gold produces an equi-ripple bandpass filter which requires compensation for its group delay and for its magnitude at frequencies other than the fundamental.

8° The new frequency measurement, as proposed on this thesis, is based on the orthogonal decomposition of a signal performed by two bandpass FIR filters. Equal group delays and a constant 90° phase shift between the complex components is provided. A magnitude compensation algorithm produces unit gain orthogonal components. Frequency is not calculated from the derivative of the angle of the complex components. Instead, the ratio between a combination of the trend of variation of the slope of the orthogonal components and their magnitude results in high accuracy frequency estimates avoiding problems such as phase unwrapping. The FIR orthogonal and bandpass filters permit a fast tracking of frequency variations and produces frequency estimates insensitive to the effect of harmonics.

CHAPTER 4

A NEW FREQUENCY MEASUREMENT TECHNIQUE

A very simple and elegant frequency measurement algorithm based on the ratio of the trend of the slopes of the orthogonal components of a phasor vector and their magnitude, was envisaged by Moore and Johns in 1991 [1]. It was visualized that this algorithm would be well appointed for its application on power system frequency measurements.

The initial algorithm of Moore and Johns has established the basis for developing a new frequency measuring technique. Following the objectives of the present research project the main features of the initial algorithm have been investigated. This investigation work rendered the theoretical performance of the algorithm allowing a direct comparison with other power system frequency measuring algorithms. It was seen that the initial algorithm needed to be made adaptive for dealing with the time varying nature of a power system.

Extensive work has been performed to define and evaluate the theoretical background of the new measuring technique in order to show the validity of its use on power system applications. It will be shown, on the second part of this Chapter, that the main features of the frequency measuring algorithm are well supported by this background and permit the proper implementation of the algorithm for power system frequency measurement.

4.1 Initial Work

The use of microprocessor based frequency measuring techniques, such as zero crossing and FFT algorithms, has lost popularity in recent years. Dealing with nonstationary parameters for practical power system conditions led to the use of adaptive filter theory for power system applications. One of the main factors motivating the work of Moore and Johns, and also determining the objectives of the

present research project, has been the development of a digital frequency measurement technique which could employ the approach given by the adaptive filter theory in order to overcome the major weaknesses of other measuring techniques as shown on the previous chapter.

4.1.1 The Starting Point of the Initial Algorithm

The initial work of Moore and Johns, is based on the orthogonal decomposition of a signal for calculating its frequency. For a voltage or a current phasor ***s(t)***, its in-phase and quadrature components are:

$$s_i(t) = A\cos(w_0 t + \phi) \tag{4.1}$$

$$s_q(t) = A\sin(w_0 t + \phi) \tag{4.2}$$

then,

$$s_i(t)\frac{ds_q(t)}{dt} = A^2 w_0 \cos^2(w_0 t + \phi) \tag{4.3}$$

$$s_q(t)\frac{ds_q(t)}{dt} = -A^2 w_0 \sin^2(w_0 t + \phi) \tag{4.4}$$

It is seen that w_0 can be obtained by subtracting equation (4.4) from (4.3):

$$s_i(t)\frac{ds_q(t)}{dt} - s_q(t)\frac{ds_i(t)}{dt} = A^2 w_0 \tag{4.5}$$

Since the magnitude of the phasor ***s(t)*** equals ***A***, then:

$$|s(t)| = \sqrt{s^2{}_i(t) + s^2{}_q(t)} = A \tag{4.6}$$

Hence,

$$s^2(t) = A^2 \tag{4.7}$$

From equations (4.5) and (4.7):

$$w_0 = \frac{s_i(t)\frac{ds_q(t)}{dt} - s_q(t)\frac{ds_i(t)}{dt}}{s^2{}_i(t) + s^2{}_q(t)} \tag{4.8}$$

Equation (4.8) shows the frequency or rotation speed of the phasor ***s(t)*** expressed as

a ratio of the trend of the slopes of the orthogonal components and their magnitude. This ratio, in fact, extracts the information of the speed of rotation of the angle spanned by the orthogonal components $s_i(t)$ and $s_q(t)$, and, at the same time, removes the dependency of the vector on the amplitude A. The validity of this statement for a discrete time implementation of the frequency measurement algorithm will be shown later in this Chapter .

For the digital implementation of equation (4.8), the input signal $s(t)$ is sampled at a fixed rate T_s. The discrete time sequence $s[nT_s]$ results from this sampling process where $nT_s = t$; henceforth, $s[nT_s]$ will be simply expressed as $s[n]$.

Two symmetric FIR filters with 90° phase shift between each other are used to produce the orthogonal decomposition of $s[n]$. The impulse responses of the orthogonal filters have been taken from the expression of the Discrete Fourier Transform as used to evaluate the frequency contents of a sequence signal at a given discrete frequency; in this case, at the power system fundamental frequency. Thus:

$$S(\Omega_0) = \sum_{k=0}^{N-1} s[k]\, e^{-j\left(\frac{2\pi k f_o}{f_s} + \phi\right)} \qquad (4.9)$$

where $N = f_s/f_0, f_s = 1/T_s$ and f_0 is the power system fundamental frequency. Thus, $\Omega_0 = 2\pi f_o/f_s$. The angle ϕ has been selected to be equal to π/N. From this finite and causal time convolution, the impulse response of the orthogonal FIR filters are expressed as:

$$h_i[k] = \sin\left[\frac{\pi(2k+1)}{N}\right] \qquad (4.10.a)$$

$$h_q[k] = \cos\left[\frac{\pi(2k+1)}{N}\right] \qquad (4.10.b)$$

for $k = 0, 1, .. N - 1$. The frequency responses $H_i(\Omega)$ and $H_q(\Omega)$ of the FIR filters, show that only at $f = 50$ Hz, $H_i(\Omega)$ equals $H_q(\Omega)$, see Figure 4.1. Moore and Johns used a closed expression of the real frequency response of the FIR filters to compensate their different gain at frequencies apart from f_0. The frequency response expressions are given as:

$$G_i(f) = \frac{T_0}{T}[g(f - f_0) + g(f + f_0)] \qquad (4.11.a)$$

$$G_q(f) = \frac{T_0}{T}[g(f - f_0) - g(f + f_0)] \qquad (4.11.b)$$

where

$$g(f) = \frac{\sin(2\pi f T_0)}{2\pi f T_0} \qquad (4.12)$$

$T_0 = 0.5/f_0$, $T = 1/f$, where f is the frequency domain independent variable.

The output of the FIR filters is normalized by using the reciprocal value of $G_i(f)$ and $G_q(f)$. At time n, the value of the frequency $f[n]$ which will be used to normalize the output $s_i[n]$ and $s_q[n]$ from the FIR filters, has to be predicted from previous frequency estimates; *i.e.*: this is a one-step predictor process. Moore and Johns used the value of the frequency calculated p samples before. Thus, the gain equations (4.11.a) and (4.11.b) become:

$$G_i[f] = \frac{f[n-p]}{f_0}[g(f[n-p] - f_0) + g(f[n-p] + f_0)] \qquad (4.12.a)$$

$$G_q[f] = \frac{f[n-p]}{f_0}[g(f[n-p] - f_0) - g(f[n-p] + f_0)] \qquad (4.12.b)$$

The derivative of the orthogonal components was implemented as a one-sample backwards difference equation:

$$\frac{ds_i(t)}{dt} \approx s'_i[n] = \frac{s_i[n] - s_i[n-1]}{T_s} \qquad (4.13.a)$$

$$\frac{ds_q(t)}{dt} \approx s'_q[n] = \frac{s_q[n] - s_q[n-1]}{T_s} \qquad (4.13.b)$$

This approximation to the derivative is performed at some time between the current and the previous sample, then:

$$s_i[n] = \frac{s_i[n] + s_i[n-1]}{2} \qquad (4.14.a)$$

$$s_q[n] = \frac{s_q[n] + s_q[n-1]}{2} \qquad (4.14.b)$$

From equations (4.13) and (4.14), the frequency calculation as given by equation (4.8) becomes:

$$f_0 = \frac{1}{2\pi T_s} \frac{s_q[n]\, s_i[n-1] - s_q[n-1]\, s_i[n]}{s^2{}_i[n] + s^2{}_q[n]} \qquad (4.15)$$

The use of equation (4.15) to approximate the continuous time derivative produces a constant error in the frequency calculation. By using the first two terms of the McLaurin series expansion of the input signal ***s[n]***, this error can be expressed as:

$$f_\epsilon = \frac{2}{3} \frac{\pi^2 f^3}{f_s^2} \qquad (4.16)$$

This value must be added to the frequency result. Appendix 3 describes the procedure leading to equation (4.16).

4.1.2 Limitations of the Initial Technique

1° The procedure leading to the frequency calculation equation (4.8) was developed by using the orthogonal components $s_i(t)$ and $s_q(t)$, given as functions in the continuous time domain. Therefore, it is possible to assume that the amplitude factor *A* of the input signal ***s(t)*** is automatically cancelled out by the frequency calculation equation (4.8). In fact, for power system applications, the amplitude *A* in ***s(t)*** should be regarded as a time varying function ***A(t)***. For a digital implementation of the frequency calculation equation, the orthogonal decomposition of the input signal must be achieved by causal, linear and finite impulse response filters such that they exhibit a linear phase response and stable numerical properties. After the digital orthogonal decomposition, the amplitude sequence ***A[n]*** of the input signal will be present on both $s_i[n]$ and $s_q[n]$. Since every output sample from the orthogonal filters results from the convolution of the input signal sequence ***s[n]*** with a FIR function within a finite observation window, then, any variation of the amplitude ***A(t)***

exhibited by $s(t)$ within the observation window will be reflected on the orthogonal outputs. It will be shown in the second part of this chapter that the variations of the amplitude must be smaller than the variations of frequency such that an optimum complex representation of the real input signal can be properly achieved by digital means. Otherwise, the estimated frequency will reflect any possible variation of the amplitude $A(t)$.

2° The frequency response of the orthogonal filters as given in equation (4.11) is formulated in a closed expression. An analysis of the impulse response of the orthogonal filters by using the Z Transform, will produce a more explicit connection with the Hilbert Transform approximation.

3° In order to normalize the output of the orthogonal filters at a time n, a one-step prediction of the frequency value $f[n]$ should be performed. It will be shown that by estimating the normalizing frequency from a weighted ratio of the amplitude and frequency, the normalization of the gain of the filters will produce an optimum orthogonal decomposition, in the sense that the influence of a time varying amplitude on the finite convolution window will be minimized.

4° It will be shown later in this chapter that the frequency response of the orthogonal filters may allow noisy components to corrupt the frequency calculations, therefore, an additional signal enhancement has to be provided.

4.2 Theory Development to Support a New Algorithm

As shown in Chapter 2, the calculation of the frequency as given by equation (4.8), is well supported by the concept of the IF of a real single component signal. Therefore, this equation will be essentially followed to support a new frequency measuring algorithm. Proper account of the limitations shown by the initial measuring algorithm will be undertaken by the development of the new technique.

It was seen in the previous section, that one of the main limitations of the initial

measuring algorithm, particularly at the stage of the formation of the orthogonal components, is concerned with the influence of a time varying amplitude of the fundamental component. Since the orthogonal decomposition is to be carried out by FIR filters for its digital implementation, then, variations of the amplitude of the fundamental component will be present within the finite observation windows used by the filters. In order to assess the causes and effects of this problem, it is required to analyze the time and frequency response of the orthogonal decomposition stage.

4.2.1 Time and Frequency Response of the Orthogonal Filters

The truncated duration of the impulse response of the filters $h_i[k]$ and $h_q[k]$ as given in equation (4.10), can be viewed as the product of two symmetric real sequences $c_i[n]$ and $c_q[n]$ which display a 90° phase shift each other, with a unit gain rectangular window $p[k] = u[k] - u[k - N]$:

$$h_i[k] = p[k] \times c_i[n] \qquad (4.17.a)$$

$$h_q[k] = p[k] \times c_q[n] \qquad (4.17.b)$$

where $u[k] = 1$ for $k \geq 0$, and $u[k] = 0$ for $k < 0$. Figure 4.2 shows the rectangular window $p[k]$ for a specific length of 80 coefficients, and the orthogonal components $c_i[n]$ and $c_q[n]$ where:

$$c_i[n] = \cos\left[\frac{\pi(2n + 1)}{N}\right] \qquad (4.18.a)$$

$$c_q[n] = \sin\left[\frac{\pi(2n + 1)}{N}\right] \qquad (4.18.b)$$

$$p[k] = 1 \quad for\ k = 0,1,\ldots N-1 \qquad (4.18.c)$$

Figure 4.3 shows a picture of the $c_i[n]$ and $c_q[n]$ after being truncated by $p[k]$. The value of N has been chosen to afford particular features from the orthogonal filters as it will be shown from the analysis of their frequency response as follows.

In the frequency domain, the Fourier Transform of a discrete-time sequence is given by the Z Transform. For the rectangular window $p[k]$, its Z Transform is:

$$P(z) = \frac{z - z^{N-1}}{z + 1} \qquad (4.19)$$

Equation (4.18) has been taken from the impulse response of the orthogonal filters. Thus, an expansion of equation (4.17) yields:

$$h_i[k] = p[k]\cos\left(\frac{2\pi k}{N}\right)\cos\left(\frac{\pi}{N}\right) - p[k]\sin\left(\frac{2\pi k}{N}\right)\sin\left(\frac{\pi}{N}\right) \qquad (4.20.a)$$

$$h_q[k] = p[k]\sin\left(\frac{2\pi k}{N}\right)\cos\left(\frac{\pi}{N}\right) + p[k]\cos\left(\frac{2\pi k}{N}\right)\sin\left(\frac{\pi}{N}\right) \qquad (4.20.b)$$

The Z Transform of the first term on the right side of equation (4.20.b) yields:

$$Z\left\{p(k)\sin\left(\frac{2\pi k}{N}\right)\cos\left(\frac{\pi}{N}\right)\right\} = \frac{j}{2}\cos\left(\frac{\pi}{N}\right)\left[P(ze^{j\Omega_0}) - P(ze^{-j\Omega_0})\right] \qquad (4.21)$$

Similarly for the second term:

$$Z\left\{p(k)\cos\left(\frac{2\pi k}{N}\right)\sin\left(\frac{\pi}{N}\right)\right\} = \frac{1}{2}\cos\left(\frac{\pi}{N}\right)\left[P(ze^{j\Omega_0}) + P(ze^{-j\Omega_0})\right] \qquad (4.22)$$

where $\Omega_0 = 2\pi/N$. From equations (4.19), (4.20) and combining them with (4.21) and (4.22), the Z Transform of the in-phase and quadrature sequences $h_i[k]$ and $h_q[k]$ is given as [55]:

$$H_i(z) = \frac{z\cos\left(\frac{\Omega_0}{2}\right)(1 - z^{-N})(z - 1)}{z^2 - 2z\cos(\Omega_0) + 1} \qquad (4.23.a)$$

$$H_q(z) = \frac{z\sin\left(\frac{\Omega_0}{2}\right)(1 - z^{-N})(z + 1)}{z^2 - 2z\cos(\Omega_0) + 1} \qquad (4.23.b)$$

The following points about the frequency response of the orthogonal filters as given in equation (4.23) should be noticed:

1° At $\Omega = \Omega_0$, the terms $\cos(\Omega_0/2)[z + 1]$ and $\sin(\Omega_0/2)[z - 1]$ will allow that the magnitude of the frequency responses of equations (4.23.a) and (4.23.b) to be equal: $|H_i(\Omega)|$ and $|H_q(\Omega)| = N/2$. This feature is possible because of the phase factor π/N present in the impulse response of both filters.

2° The factors $[z - 1]$ and $[z + 1]$ produce a natural 90° phase shift between $H_i(\Omega)$

and $H_q(\Omega)$ for all frequencies within $-\pi \leq \Omega \leq \pi$. This particular point will be better appreciated later from equations (4.25.b) and (4.26.b).

3° For a value of N equal to $N = f_s/f_0$, *i.e.*: the number of coefficients N of the orthogonal filters equals one 50 Hz cycle, then, the factors z and $[1 - z^{-N}]$ in both (4.23.a) and (4.23.b) will produce zeros for both $H_i(\Omega)$ and $H_q(\Omega)$ at $\Omega = 0$, $2\Omega_0$, $3\Omega_0$, and subsequent harmonics of the fundamental.

4° Since the orthogonal filters are linear, time-invariant and causal, we can use the *one-sided* Z Transform [56] of equation (4.23), where $z = re^{j\Omega}$, for $r = 1$ in the unit circle plane and Ω is the normalized frequency $\Omega = 2\pi f/f_s$. Thus, equation (4.23) becomes:

$$H_i(e^{j\Omega}) = -e^{-j\Omega(\frac{N-1}{2})} \frac{2\cos(\frac{\Omega_0}{2})\sin(\frac{N\Omega}{2})\sin(\frac{\Omega}{2})}{\cos(\Omega) - \cos(\Omega_0)} \qquad (4.24.a)$$

$$H_q(e^{j\Omega}) = j\,e^{-j\Omega(\frac{N-1}{2})} \frac{2\sin(\frac{\Omega_0}{2})\sin(\frac{N\Omega}{2})\cos(\frac{\Omega}{2})}{\cos(\Omega) - \cos(\Omega_0)} \qquad (4.24.b)$$

Equation (4.24) can be depicted in terms of its magnitude and phase as functions of the frequency Ω:

$$|H_i(\Omega)| = \frac{2\cos(\frac{\Omega_0}{2})\sin(\frac{N\Omega}{2})\sin(\frac{\Omega}{2})}{\cos(\Omega) - \cos(\Omega_0)} \qquad (4.25.a)$$

$$\phi_i(\Omega) = -e^{-j\frac{\Omega}{2}(N-1)} \qquad (4.25.b)$$

and:

$$|H_q(\Omega)| = \frac{2\sin(\frac{\Omega_0}{2})\sin(\frac{N\Omega}{2})\cos(\frac{\Omega}{2})}{\cos(\Omega) - \cos(\Omega_0)} \qquad (4.26.a)$$

$$\phi_q(\Omega) = j\,e^{-j\frac{\Omega}{2}(N-1)} \qquad (4.26.b)$$

5° At $\Omega = \Omega_0$, both equations (4.24.a) and (4.24.b) show a singularity in both the numerator and denominator. By using the rule of L'Hôpital, Appendix 4 shows that the magnitude of the filters becomes: $| H_i(\Omega_o) | = | H_q(\Omega_o) | = N/2$. Note that the phase response of the filters does not show any singularity at this frequency. If the frequency response of the filters had been obtained by using the Discrete-time Fourier Transform, the use of sums by this transformation would had overcome this double singularity but at the expense of a very lengthy evaluation.

6° From equations (4.25) and (4.26), it is seen that the magnitude response of the in-phase filter is almost equal to that of the quadrature filter. Figure 4.4 shows the transfer function magnitude of the orthogonal filters for $N = 80$. As pointed out in the first note: a) at $\Omega = \Omega_o$, the gain of the filters equal $N/2$, and b) there are zeros at dc and at the subsequent harmonics of the fundamental

7° From equations (4.25.b) and (4.26.b), the phase response of the filters can be expressed in a linear form as:

$$\phi_i(\Omega) = \angle -e^{-j\frac{\Omega}{2}(N-1)} \rightarrow 180^o - \frac{\Omega}{2}(N-1) \qquad (4.27.a)$$

$$\phi_q(\Omega) = \angle je^{-j\frac{\Omega}{2}(N-1)} \rightarrow 90^o - \frac{\Omega}{2}(N-1) \qquad (4.27.b)$$

It is noticed that the transfer function of the quadrature filter lags by 90° the response of the in-phase filter at all frequencies as pointed out previously. Figure 4.5 shows the phase of the frequency response of the filters. The group delay of the filters can be calculated from the last equation:

$$g_i(\Omega) = -\frac{d\phi_i(\Omega)}{d\Omega} = \frac{N-1}{2} \qquad (4.28.a)$$

$$g_q(\Omega) = -\frac{d\phi_q(\Omega)}{d\Omega} = \frac{N-1}{2} \qquad (4.28.b)$$

The two filters show the same group delay irrespective of the frequency.

4.2.2 Approximation to the Hilbert Transform

Figures 4.6.a and 4.6.b show the magnitude and phase functions, respectively, in the frequency domain, of a Hilbert Transform filter as described in Chapter 2 and included here for practical purposes:

$$HT(t) = C.P.V. \int_{-\infty}^{\infty} \frac{s(t)}{\pi(t-\tau)} dt \qquad (4.29.a)$$

$$HT(\Omega) = -j\ sgn(\Omega) \qquad (4.29.b)$$

If the magnitude of the transfer function of the orthogonal filters $H_i(\Omega)$ and $H_q(\Omega)$ as given by equations (4.24.a) and (4.24.b), respectively, can be normalized to unit gain with respect of the frequency Ω, then:

$$mag_i(\Omega) = mag_q(\Omega) = 1.0 \qquad (4.30)$$

Thus, equations (4.25) and (4.26) become:

$$H_i(\Omega) = -1.0\ e^{-j\frac{\Omega}{2}(N-1)} \qquad (4.31.a)$$

$$H_q(\Omega) = j\ 1.0\ e^{-j\frac{\Omega}{2}(N-1)} \qquad (4.31.b)$$

Equating (4.31.a) to (4.31.b), then:

$$1.0 = \frac{-H_i(\Omega)}{e^{-j\frac{\Omega}{2}(N-1)}} \qquad (4.32.a)$$

$$1.0 = \frac{H_q(\Omega)}{j\ e^{-j\frac{\Omega}{2}(N-1)}} \qquad (4.32.b)$$

Hence,

$$H_q(\Omega) = -jH_i(\Omega) \quad for\ -\pi \le \Omega \le \pi \qquad (4.33)$$

Equation (4.33) shows that the frequency response of the quadrature filter approaches the frequency response of the Hilbert Transform -equation (4.29.b), of the in-phase filter at all frequencies in the unit plane for $-\pi \le \Omega \le \pi$, if the magnitude of both filters is normalized to unit gain. It will be shown in the next Chapter that this statement can be achieved for a narrow bandwidth centred at f_0 = 50 Hz.

As stated in Chapter 2, an optimum complex representation of a real single component signal can be achieved if the orthogonal decomposition approaches correctly the Hilbert Transform: 90° phase shift between the orthogonal components, unit gain and equal and constant group delay within a bandwidth centred at the fundamental frequency. In this sense, the frequency analysis of the proposed orthogonal filters confirms the validity of their use for measuring power system frequency by digital means.

4.2.3 One-Step Predictor for Frequency Response Normalization

It was seen in section 4.1, that, at a given time n, the value of the frequency $f[n]$ is used to normalize the gains of the orthogonal filters. However, at time n, the value of $f[n]$ is yet unknown. This value has to be predicted one-step in advance; that is: $f[n]$ has to be estimated in terms of the most recent results of the frequency:

$$\hat{f}[n] = E\{ f[n] \mid f[n-1], \ldots f[n-1-M] \} \qquad (4.34)$$

where $E\{\cdot\}$ denotes the best estimate of $f[n]$ based on its last samples. The use of a one-step frequency predictor is needed for two reasons:

1° To normalize the gain of the orthogonal filters as already discussed.

2° The following discussion will show that the influence of a time-varying amplitude of the fundamental component on the formation of an optimum complex representation of the input signal $s[n]$, by a correct orthogonal process yielding $s_i[n]$ and $s_q[n]$, can be minimized if the one-step frequency predictor is formed from the history of both the magnitude of the orthogonal components of the input signal and its frequency.

4.2.3.1 Optimum Frequency One-Step Predictor

In his studies on optical coherence, Mandel [9] pointed out the problem of producing an optimum envelope or magnitude representation of a real function like $s(t)$. As

discussed in Chapter 2, this representation can be afforded from the complex representation of $s(t)$ by using the analytic signal $z(t)$, such that the envelope becomes the magnitude of the orthogonal components $s_i(t)$ and $s_q(t)$ of $s(t)$. The envelope $|\, z(t) \,|$, as a function of time, is already familiar:

$$|z(t)| = \sqrt{s_i^2(t) + s_q^2(t)} \qquad (4.35)$$

Hence, $z(t)$ is expressed as:

$$z(t) = |z(t)| e^{j[w_0 t + \phi(t)]} \qquad (4.36)$$

It should be noticed that under this approach, the following discussion about the problem of an optimum envelope representation is to be related to the continuous time domain. Nevertheless, in the discrete time domain, our problem concerning the variations of the amplitude of $s[n]$ within the FIR filters observation window is the same in the sense that it is necessary that the influence of the variations of the amplitude over the estimation of the frequency can be minimized.

For a real signal like $s(t)$, its complex representation $z(t)$ can be expressed as:

$$z(t) = i(t) + j\hat{i}(t) \qquad (4.37)$$

where $\hat{i}(t)$ is the Hilbert Transform of the in-phase component of $s(t)$ as given already in Figure 2.7. In order to understand the behaviour of the envelope which results from the use of $z(t)$, another complex envelope $e(t)$ will be used, such that variations in the envelope of $z(t)$ will be directly reflected by $e(t)$. By using $z(t)$ and a complex modulation factor, $e(t)$ will be given as:

$$e(t) = z(t)\, e^{jw_0 t} \qquad (4.38)$$

accordingly, the in-phase component of $s(t)$ is:

$$i(t) = Re[\, e(t)\, e^{-jw_0 t}] \qquad (4.39)$$

It is seen that $e(t)$ will reflect any variation of the amplitude $A(t)$ in $s(t)$. Now, it is necessary to observe when $e(t)$ will display the slowest variations. That is,: we need to find the point where the energy M of $e(t)$ will reach a minimum value in a least-

square sense. From Parseval's theorem:

$$M = 2\pi\ E\left\{\left|\frac{de(t)}{dt}\right|^2\right\} \qquad (4.40)$$

where $\mathbf{E}\{\cdot\}$ is the expected value. From Appendix 5, M can be expressed as:

$$M = \int_{-\infty}^{\infty} (w-w_0)^2 S_{zz}(w)\, dw \qquad (4.41)$$

Equation (4.41) shows the counterpart of the Parseval's theorem in the frequency domain where $S_{zz}(w)$ is the power spectrum of $z(t)$. $S_{zz}(w)$ is the Fourier Transform of the autocorrelation function of $z(t)$: $\mathbf{FT}\{R_{zz}(\tau)\} = \mathbf{FT}[\mathbf{E}\{z(t)z(t+\tau)]$. Minimizing M with respect of w_0 gives:

$$\frac{dM}{dw_0} = 2w_0\int_{-\infty}^{\infty} S_{zz}(w)\, dw - \int_{-\infty}^{\infty} wS_{zz}(w)\, dw = 0 \qquad (4.42)$$

thus:

$$w_0 = \frac{\int_{-\infty}^{\infty} w\ S_{zz}(w)\, dw}{\int_{-\infty}^{\infty} S_{zz}(w)\, dw} \qquad (4.43)$$

Hence, minimizing the complex representation $e(t)$ of the envelope of $z(t)$, in a least square sense, implies that w_0 is the centre of mass of $S_{zz}(w)$, *i.e*: w_0 is the mean frequency of the power spectrum of complex function $z(t)$ representing the real signal $s(t)$. Equation (4.43) shows that a variation of the amplitude $\mathbf{a(t)}$ in $s(t)$ will be displayed in the power spectrum of $z(t)$ both in the numerator and in the denominator, thus, if $\mathbf{a(t)}$ were a constant in the time axis, then $w_0 = w$. Appendix 6, shows that w_0 can be given in terms of the spectrum of the real signal $s(t)$:

$$w_0 = \frac{\int_0^{\infty} w\, S_{ss}(w)\, dw}{\int_0^{\infty} S_{ss}(w)\, dw} \qquad (4.44)$$

It is seen that due to the use of the Hilbert Transform in $z(t)$, the integral functions in equation (4.44) are evaluated for positive frequencies only. For a digital implementation of this equation, the integral functions are approximated by finite sums within the interval $0 \leq \Omega \leq \pi$. Appendix 6 also shows that w_0 can be given in terms of the ratio of the expected values of the product magnitude times frequency divided by the expected value of the magnitude:

$$w_0(t) = \frac{E\{a^2(t)\, w_0(t)\}}{E\{a^2(t)\}} \qquad (4.45)$$

Equation (4.45) displays, in a clearer form, the minimization of the influence of a time varying amplitude **a(t)** in the estimation of the frequency $w_o(t)$. According to Papoulis [10], this frequency corresponds to a weighted average of the instantaneous frequency $w_0(t)$ of $s(t)$.

Equation (4.45) renders the best estimate of the instantaneous frequency $w_0(t)$ of $s(t)$ in the sense that the influence of any variation of the amplitude **a**(t) will be diminished. Equation (4.45) is the basis of the one-step frequency predictor to normalize the gain of the FIR orthogonal filters. A digital implementation of this equation has been accomplished by using two moving average (MA) filters which provide the best estimate to the expectation functions of equation (4.45). This approximation is valid on the assumption that the variations of the amplitude are wide sense stationary ergodic, *i.e*: the average of amplitude variations observed within a time interval will approach the average of observations performed at other times. Hence, the one-step frequency predictor can be given as:

$$w_0[n] = \frac{\frac{1}{P}\sum_{k=0}^{P-1} a^2[n-k]\, w_0[n-k]}{\frac{1}{P}\sum_{k=0}^{P-1} a^2[n-k]} \qquad (4.46)$$

where P is the length of the MA filters.

4.2.3.2 Amplitude-Weighted Instantaneous Frequency

According to Ström [58], the instantaneous frequency is well defined for real signals with constant amplitude. However, the use of the analytic signal to produce a complex representation of a time-varying amplitude/frequency real signal, for purposes of estimating the IF of the signal, may lead to IF estimates with infinite variance. If the amplitude of the signal to be represented is constant in time, then the representing envelope will also be constant. Ström proposes an amplitude-weighted instantaneous frequency which should reduce the variance of the estimates of the IF of a narrow band pass signal like $s(t)$, thus:

$$w^k(t) = \frac{a^k(t)\, w(t)}{E\{a^k(t)\}} \qquad for = 1, 2, 3, \ldots \qquad (4.47)$$

where $\mathbf{a(t) = s^2_i(t) + s^2_q(t)}$. For $k = 1$, the frequency given by equation (4.47) is very close to the weighted average frequency given by equation (4.44). In the case of a single component FM deterministic signal, Sun and Sclabassi [51] have similarly shown that the variance of the IF of a signal given by a complex representation, approaches the variance of the frequency given by its Fourier Transform since the Fourier Transform does not treat the amplitude modulation as a separated process due to the complex representation leading to the IF of a signal. Even when we are more concerned with AM/FM signals, this statement also points out the influence of the amplitude on the complex representation of a real signal.

Using different approaches, the association of the amplitude with the IF is shown to arise from the use of a complex representation of a real signal. In this sense, the frequency $w_0(t)$ provides a physical meaning only for a single component AM/FM

real signal and it makes possible an optimum envelope representation of the signal by using a complex function.

4.2.4 Amplitude Compensation in the Difference Algorithm

Digital implementation of equation (4.8) for the calculation of the frequency w_0 implies an approximation to the continuous time derivative of the orthogonal components $ds_i(t)/dt$ and $ds_q(t)/dt$ as already expressed by equations (4.13) and (4.14). A discrete time equivalent to w_0 has already been given in equation (4.15). It will be shown that assuming piecewise linearity between consecutive samples when using the one-sample backwards differentiation, exhibits a factor which is related to the amplitude of the input signal and, therefore, it must be considered during the calculation of w_0. It will be seen that this factor specially accounts for a time varying amplitude.

For a given sampling rate T_s, the continuous time expression of a one-sample backwards difference equation may be given as:

$$\frac{ds_i(t)}{dt} \approx s'_i(t) = \frac{s_i(t) - s_i(t-\Delta T)}{\Delta T} \qquad (4.48.a)$$

$$\frac{ds_q(t)}{dt} \approx s'_q(t) = \frac{s_q(t) - s_q(t-\Delta T)}{\Delta T} \qquad (4.48.b)$$

where $\Delta T = T_s$. To avoid numerical instability for a digital implementation, the samples at time t are given as:

$$s_i(t) = \frac{s_i(t) + s_i(t-\Delta T)}{2} \qquad (4.49.a)$$

$$s_q(t) = \frac{s_q(t) + s_q(t-\Delta T)}{2} \qquad (4.49.b)$$

Hence, from equation (4.15), the calculated frequency $f_0 = w_0/2\pi$ will be:

$$f_0 = \frac{s_q(t)\,s_i(t-\Delta T) - s_q(t-\Delta T)\,s_i(t)}{2\pi\Delta T[s^2{}_i(t) + s^2{}_q(t)]} \qquad (4.50)$$

From the definition of the real signal ***s(t)***, the orthogonal components should be:

$$s_i(t) = a(t)\cos(w_0 t) \qquad (4.51.a)$$

$$s_q(t) = a(t)\sin(w_0 t) \qquad (4.51.b)$$

and

$$s_i(t-\Delta T) = a(t-\Delta T)\cos[w_0(t-\Delta T)] \qquad (4.52.a)$$

$$s_q(t-\Delta T) = a(t-\Delta T)\sin[w_0(t-\Delta T)] \qquad (4.52.b)$$

Thus, f_0 becomes:

$$f_0 = \frac{\sin(w_0\Delta T)}{2\pi\Delta T}\left[\frac{a(t)\,a(t-\Delta T)}{s_i^2(t) + s_q^2(t)}\right] \qquad (4.53)$$

From equation (4.51), **a*(t)*** and **a*(t - ΔT)*** can be expressed as:

$$a(t) = \sqrt{s_i^2(t) + s_q^2(t)} \qquad (4.54.a)$$

$$a(t-\Delta T) = \sqrt{s_i^2(t-\Delta T) + s_q^2(t-\Delta T)} \qquad (4.54.b)$$

The term $\sin(w_0\Delta T)$ in equation (4.53) can be expressed in terms of the first two terms of its McLaurin expansion:

$$\sin(w_0\Delta T) = 2\pi f_0\Delta T - \frac{4\pi^3 f_0{}^3\Delta T^3}{3}$$

Hence, equation (4.53) becomes:

$$f_0 = [f_0 - \frac{2\pi^2 f^3{}_0\Delta T^2}{3}]\sqrt{\frac{s_i^2(t-\Delta T) + s_q^2(t-\Delta T)}{s_i^2(t) + s_q^2(t)}} \qquad (4.55)$$

The discrete time expression of equation (4.55) is:

$$f_0 = [f_0 - \frac{2\pi^2 f_0^3}{3f_s^2}]\sqrt{\frac{s_i^2[n-1] + s_q^2[n-1]}{s_i^2[n] + s_q^2[n]}} \qquad (4.56)$$

It can be noticed that if the amplitude of the input signal ***s(t)*** is constant, then:

$$f_0 = f_0 - \frac{2\pi^2 f_0^3}{3f_s^2} \qquad (4.57)$$

Equation (4.56) is equal to equation (4.15) including the error given by equation (4.16). If the amplitude **a*(t)*** is varying in time, use of the one-sample backwards difference equation must include the amplitude compensation of equation (4.56).

4.2.5 Bandpass Selectivity Enhancement

It can be seen from Figure 4.4 that the frequency response of the orthogonal filters is far from an ideal bandpass filter even when it does provides zeros at dc and at the 50 Hz harmonics. As stated in Chapter 2, any noise component entering the bandpass interval will affect the complex representation leading to the frequency estimation. The principal matter of concern in the present section is the extent of the main and the second sidelobes of the frequency response of the filters, since for a fundamental frequency drifting away from 50 Hz, the harmonics will certainly intrude within the nearby sidelobes. In fact, even if the fundamental component remains constant at 50 Hz, some other sort of high frequency noise may randomly appear within any of the frequency sidelobes at any time.

A further enhancement of the bandpass selectivity of the FIR orthogonal filters has been accomplished by two means: a) a FIR time invariant lowpass filter, and, b) a FIR adaptive bandpass line enhancer. The line enhancer filter should precede the orthogonal filtering stage.

4.2.5.1 Time Invariant Filtering

Two different lowpass filters have been tested: a Kaiser filter designed by the Remez

exchange procedure and a Hamming filter. These two filters display a finite impulse response, and, thus, a linear phase response with a constant group delay. A Kaiser lowpass filter, was designed to cut very close to dc as required for this application. It has been observed that the implementation of the Kaiser filter requires a higher number of coefficients of its impulse response to achieve the same performance in the stop band as a Hamming filter. On the other hand, the design of the Hamming filter allows location of a zero at a given frequency by changing the number of coefficients. The impulse response of a Hamming filter is given as:

$$hamming[k] = \alpha - (1-\alpha)\cos[\frac{2\pi k}{N}] \quad for\ k=0,1\ldots N-1 \qquad (4.58)$$

where $\alpha = 0.54$. For $N = f_s/f_0$, the first zero will occur at $f = 2f_0$; while, for $N = f_s/2f_0$, the first zero will lie at $f = 4f_0$. The frequency response of equation (4.58), as shown in Appendix 7, is expressed as:

$$H(\Omega) = \alpha \frac{\sin(\frac{\Omega N}{2})}{\frac{\Omega}{2}} e^{-j\frac{\Omega}{2}(N-1)} - j\frac{(1-\alpha)\sin(\frac{\Omega N}{2})\,[e^{j\Omega}-\cos(\Omega_0)]\,e^{-j\frac{\Omega N}{2}}}{\cos(\Omega)-\cos(\Omega_0)} \qquad (4.59)$$

At $\Omega = 0$, the magnitude equals αN. At $\Omega = \Omega_0$, the magnitude equals $(1 - \alpha)N/2$. The group delay is approximately $(N - 1)/2$. The frequency response of a Hamming lowpass filter as shown in Figure 4.7 for $f_s = 4$ kHz and $f_0 = 50$ Hz, results in a 80-coefficients filter. The same figure also shows a Kaiser lowpass filter with an equal cut off frequency but with a length of 103 coefficients for an attenuation of -40 dB and a ripple of 0.1 dB in pass and stop bands.

4.2.5.2 Adaptive Bandpass Filtering

Additionally, an adaptive line enhancer (ALE) was developed to extract the fundamental component from noise. The ALE is based on a recursive least squares algorithm implemented with a lattice structure in order to provide a faster convergence as compared to LMS algorithms. Figure 4.8 shows the diagram of the RLS-ALE filter. The components of the input signal $y[n]$ are the fundamental

component $s[n]$ and the additive noise $v[n]$.The delta Δ box is a decorrelation factor; it basically performs a delay of **d** samples which renders a decorrelation between the fundamental component $s[n]$ and the additive noise $v[n]$ in order to extract $s[n]$ from the noise. Then, the output $y[n]$ of the filter will yield the best estimate of the fundamental component $s[n]$ in a least-square sense.

In figure 4.8, the error $\mathbf{e}^{\Delta}_{L-1}[n]$ corresponds to the difference between the input signal $y[n]$ and the expected value of the decorrelated signal $y[n-\Delta]$. If $\mathbf{e}^{\Delta}_{L-1}[n]$ is uncorrelated with $y[n]$, then $y[n] = s[n]$. For a white noise sequence corrupting $y[n]$, a value of $\Delta = 1$ will produce an effective decorrelation. However, for the second and third harmonics of 50 Hz, which typically exhibit a higher energy content as compared to any other noisy component within a bandwidth close to the fundamental, this value of decorrelation is not enough. It was found that for a sampling rate of 4 kHz, the optimum value of Δ was 40 samples; that is, the second harmonic located at $f = 200$ Hz $\pm \Delta f$, would be found by the orthogonal FIR filters with a length of 40 coefficients. It will be seen in Chapter 5 that during exponentially decaying patterns of the fundamental frequency, the second harmonic also decays from $2f_o$ at twice the speed of decay of f_o, while the third harmonic falls three times faster, thus the decorrelation factor must be adjusted correspondingly.

In Chapter 5 will be shown the use of a RLS-ALE filter with a decorrelation factor of 40 samples and an order of 10 lattice adaptive stages. It has been seen that this order of the filter is good enough to track $s[n]$ without requiring a very hard-handling filter. However, as already stated, an adaptive adjustment to the value of Δ has to be included to track deviations of the fundamental in order to remove the first harmonics appearing in the input signal.

Figure 4.9 shows a block diagram of the new frequency measuring algorithm. The normalizing stage is indicated as the Frequency Response of the filters: for a given weighted frequency value, the magnitude of the frequency response of both filters is computed by equations (4.25) and (4.26). For the implementation of this algorithm on a digital signal processing board, the normalizing stage has been achieved by

using a *look-up table* containing the frequency response of both filters.

4.3 Conclusions

1° The initial frequency measuring algorithm of Moore and Johns is based on the digital implementation of equation (4.8). The development of this equation has been given in the continuous time domain, and thus, it eliminates the influence of the amplitude A of the input signal $s(t)$ at a given time t. As it was shown later, this assumption may not be correct for a digital implementation of the frequency measuring algorithm.

2° In the initial algorithm, the digital implementation of the frequency calculation equation (4.8) has been accomplished by using two FIR orthogonal filters. A closed frequency response of the filters was presented by Moore and Johns. It was seen that the gain of the filters should be normalized at frequencies other than the fundamental. A normalizing value can be given from a one-step predictor estimation. The initial algorithm proposed to use the value of frequency estimated **p** samples before.

3° Approximation to the continuous time derivative of the orthogonal components has shown that an error, given as a function of the frequency, has to be added to the final estimates to smooth the effects of the discrete time approximation.

4° The main limitations of the initial measuring algorithm are: a) frequency estimates are sensitive to variations of the amplitude of the input signal; this sensitivity is due to the nature of the discrete-time implementation which requires the use of FIR filters, b) harmonics of the fundamental and other noisy components will be removed by the natural zeros of the frequency response of the filters, provided that these components fall close to the zeros of the frequency response, otherwise, the frequency calculation will be corrupted.

5° It has been shown from the frequency analysis of the orthogonal filters as

proposed by the initial algorithm, that their frequency response expressions effectively provide an optimum complex representation of an AM/FM real signal, in the sense that the quadrature filter becomes the Hilbert Transform of the in-phase filter. This holds true provided that the gain of both filters is normalized about the fundamental, since it has been confirmed that the orthogonal outputs of the filters exhibit a 90° phase shift each other and equal group delays irrespective of the frequency. The orthogonal filters also provide natural zeros at dc and at every other harmonic of the fundamental. The bandpass filtering interval about 50 Hz is afforded with a short and constant group delay. It was shown in Chapter 3 that other orthogonal transformation techniques like the discrete Hilbert Transform and the AM demodulation process, do not afford the unique features exhibited by the FIR orthogonal filters concerning the orthogonal decomposition and the bandpass filtering characteristics which are required for power system applications. Therefore, the current frequency analysis validates the use of this complex representation for the measurement of power system frequency by digital means.

6° Analysis of the approximation to the derivative of the orthogonal components when using a one-sample backwards difference equation, has shown that a compensation factor should be added to the frequency estimates in order to cope with variations of the amplitude of the input signal.

7° It has been shown that an optimum reduction of the effects of a time varying amplitude on the complex representation procedure, can be achieved if a normalizing frequency value is predicted one-step in advance. The predicted frequency is produced by an estimation strategy based on the weighted average of the frequency. The average is formed from the ratio of the expected value of the product of the magnitude times the frequency, divided by the expected value of the magnitude. This ratio also shows that variations in time of the amplitude in the observed input signal can be minimized. Different authors have pointed out the need of weighting the frequency when a complex representation is used in order to reduce the influence of a time varying amplitude in the observed signal, and thus, to reduce the variance of the frequency estimates. An approximation to the expectations forming the weighted

amplitude-frequency ratio has been achieved by using moving average filters.

8° From the frequency response analysis of the filters, it was seen that a further signal enhancement should precede the orthogonal decomposition stage in order to remove the influence of noisy components falling within the neighbour frequency sidelobes of the filters. The principal matter of concern is the intrusion of the second and third harmonics into the bandpass interval of the filters if the fundamental frequency drifts away from its nominal value. Three different techniques were analyzed: two FIR fixed lowpass filters and an adaptive line enhancer. It was observed that the use of a Hamming lowpass filter offered a better performance concerning a shorter impulse response and a smoothed bandpass magnitude as compared to a Kaiser filter design. The adaptive line enhancer was developed as a recursive least-squares filter with a lattice structure. A decorrelation factor provides good rejecting features of harmonics provided that the fundamental frequency does not drift away from 50 Hz; otherwise, a very expensive computational algorithm would have to be used in order to feed back the frequency estimates into this adaptive filter for recursively adjusting the decorrelation parameter. Therefore, the Hamming lowpass pre-filter has been used throughout this work.

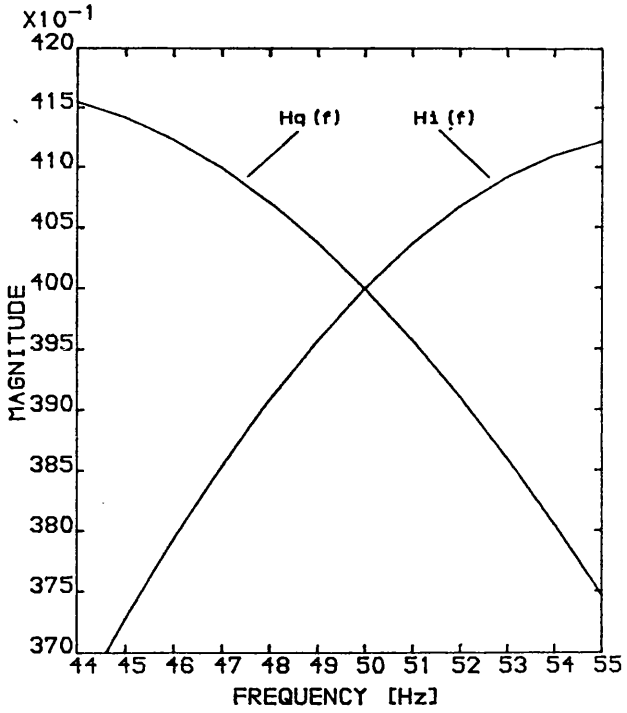

Figure 4.1 Gain of the orthogonal filters about 50 Hz.

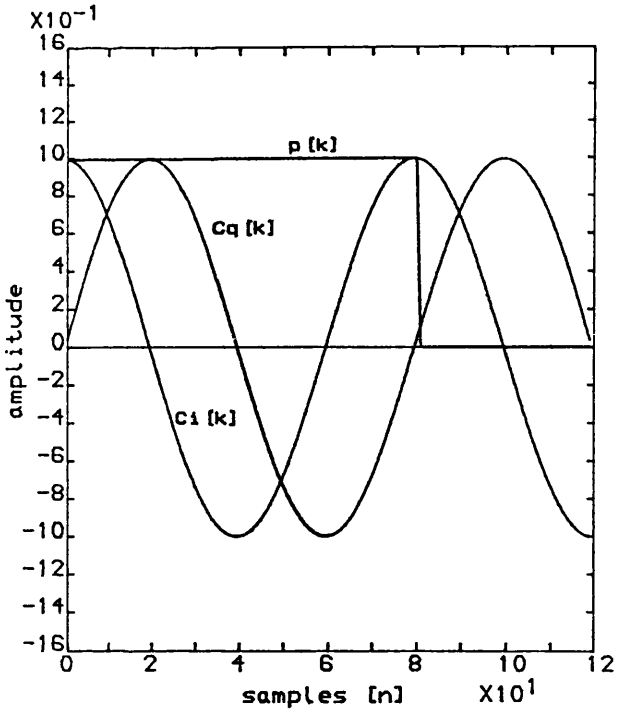

Figure 4.2 Two symmetric and orthogonal functions $c_i[n]$ and $c_q[n]$ and a 80-points unit rectangular window **p[k]**.

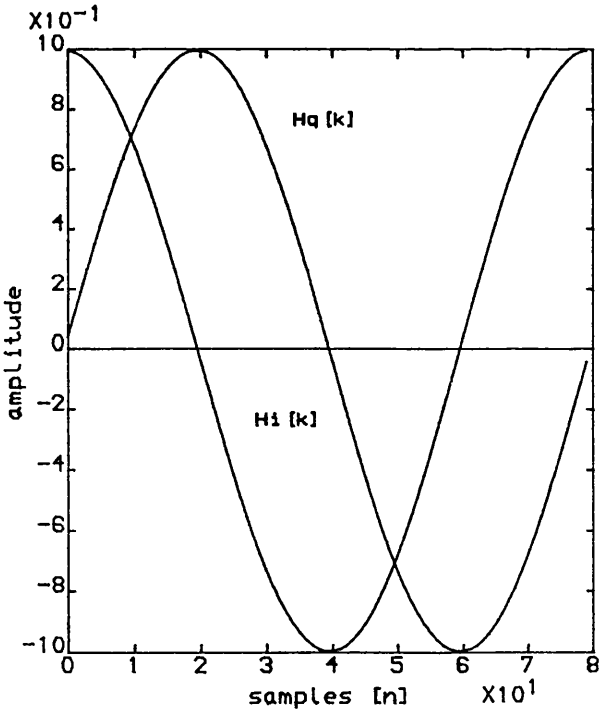

Figure 4.3. Finite duration of the impulse responses $h_i[k]$ and $h_q[k]$ for N = 80.

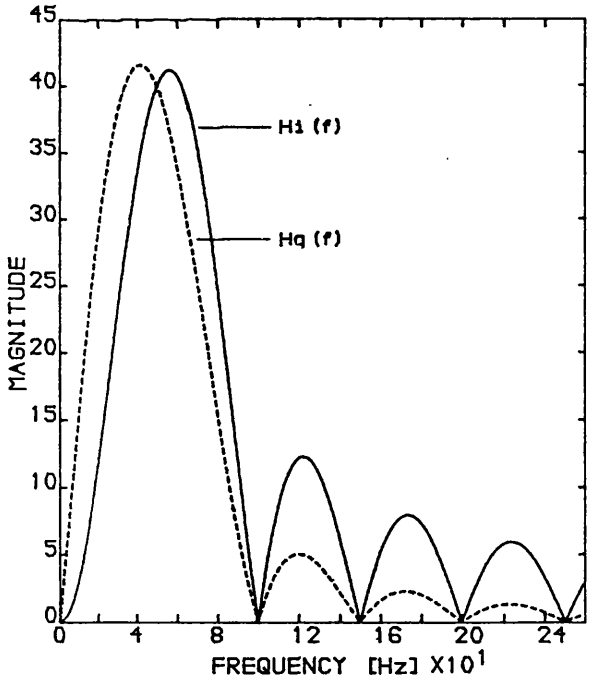

Figure 4.4 Magnitude of the frequency response of the orthogonal filters.

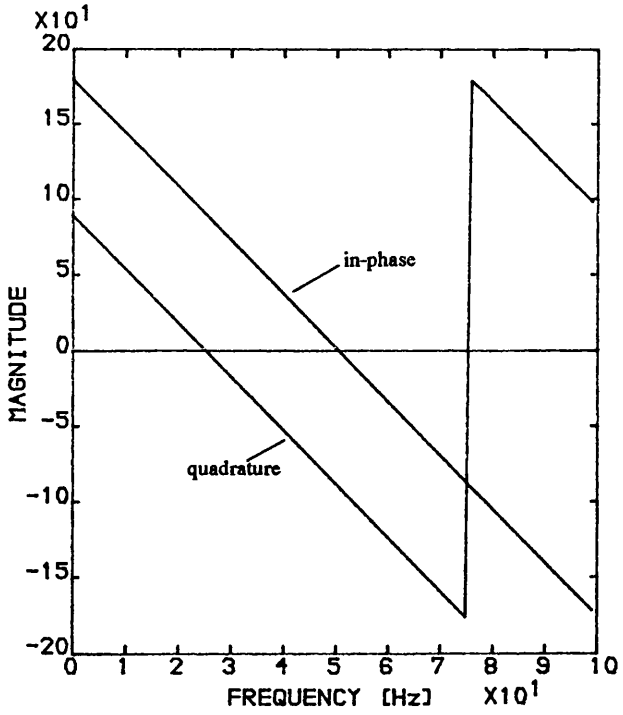

Figure 4.5 Phase of the frequency response of the orthogonal filters.

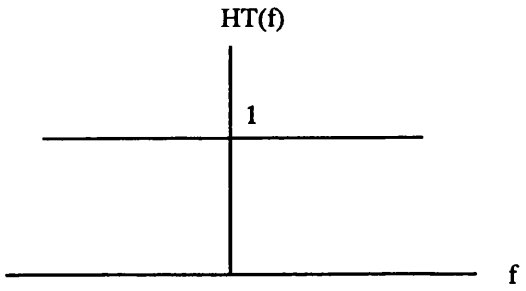

Figure 4.6.a. Magnitude of the frequency response of a Hilbert Transform filter.

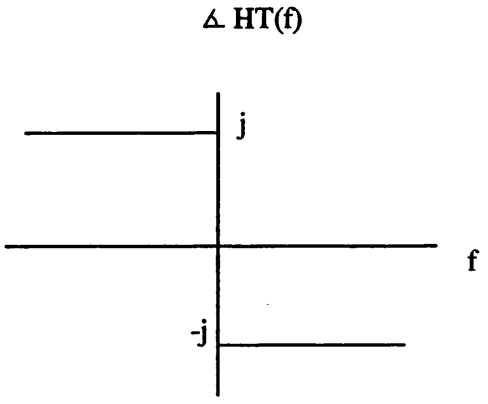

Figure 4.6.b Phase of the frequency response of a Hilbert Transform filter.

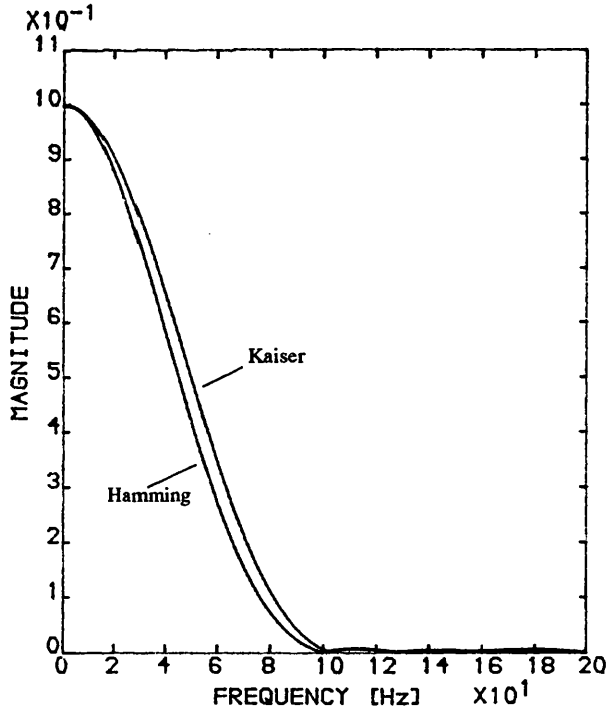

Figure 4.7 Frequency response of a Hamming and a Kaiser lowpass filters, for 80 and 103 points, respectively.

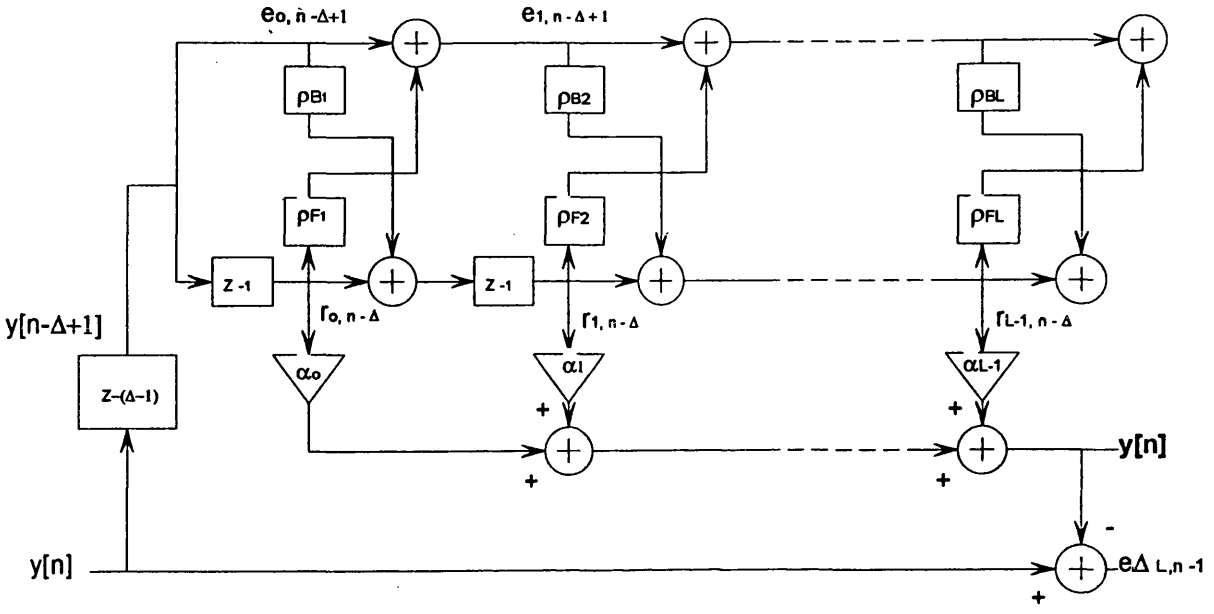

Figure 4.8 Block diagram of the RLS-ALE lattice filter.

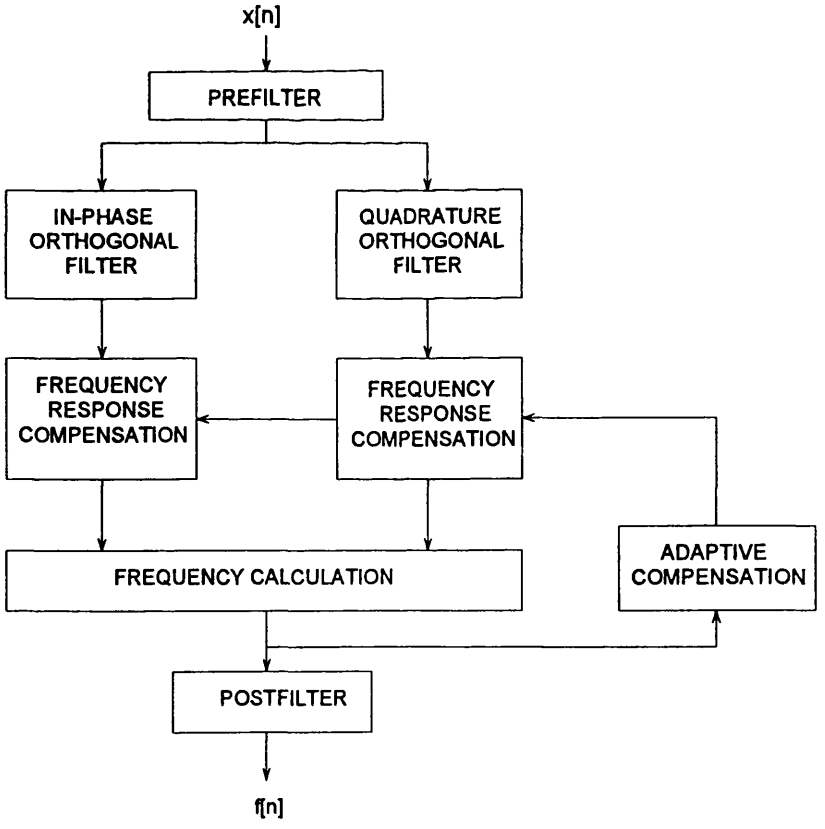

Figure 4.9 Block diagram of the new frequency measurement technique.

CHAPTER 5

PERFORMANCE ASSESSMENT OF THE ALGORITHM

The theory supporting the new frequency measuring algorithm was presented in the last Chapter. It was shown that this algorithm provides the best approximation to the complex representation of a real signal for the estimation of its frequency, thus, it can provide accurate estimates of the instantaneous frequency of a signal which can be taken from a power system busbar. Frequency estimates result from the weighted ratio of the gradient of the orthogonal components of a real signal. The orthogonal decomposition of the real signal is accomplished by two symmetric and orthogonal FIR filters which, additionally, provide a bandpass filtering of the signal about its fundamental component.

The assessment of the performance of the frequency measuring algorithm is addressed in this Chapter. It is aimed to certify that the method of the complex representation of a single component real signal may convey to the correct estimation of the IF of the signal. Two main stages have been proposed to ascertain the validity of the algorithm. Firstly, a set of deterministic testing signals has been implemented in order to evaluate the main features of the algorithm. In this group, the parameters of the signals, such as amplitude, frequency and noise interference, can be defined during the implementation of the testing signals. In this way, the performance of the algorithm can be compared against known patterns which determine the variation of these parameters. Secondly, a collection of simulations of typical power system conditions has been developed by using computer-based power system models. It is expected to establish the extent of the effectiveness of the measuring algorithm for power system applications.

5.1 Assessment of the Main Features

At this stage, it is required to determine the response of the measuring algorithm with respect of variations of the main parameters of the signal under observation,

that is: its amplitude and frequency. It is also needed to estimate the influence of additive noise on the algorithm's performance.

During the present series of deterministic simulations, the term *fault* will be used to denote the type of disturbance simulated during a particular study case.

5.1.1 Algorithm's Sensitivity to Amplitude and Frequency Variations

A signal modulated both in amplitude and in frequency is shown in Figure 5.1. Both modulation parameters follow an exponential decay pattern. The following equation describes this signal as a function of time:

$$x_i(t) = K[1 + \mu A(t)]\sin(2\pi f_o t - \Delta f[t + T_{FM}\, e^{-t/T_{FM}}]) \qquad (5.1)$$

where K is a constant determining the maximum excursion of the amplitude of $x_i(t)$; μ is the amplitude modulation index. The amplitude modulation function $A(t)$ is given as:

$$A(t) = e^{-t/T_{AM}} \qquad (5.2)$$

The following values have been assigned to the main parameters of equation (5.1): $f_0 = 50$ Hz; $K = 0.5$; $\mu = 0.5$; $T_{AM} = 0.2$ s; $\Delta f = 2.0$ Hz; $T_{FM} = 1.0$ s. The sampling frequency is $f_s = 4$ kHz. The effect of the exponential decay modulation is started at $t = 110$ ms, this is intended to be indicative of some power system fault. Figure 5.2 shows the trajectory of the estimated frequency (broken line) by using the delay predictor as proposed by Moore and Johns [1]. The length of the delay is 4 samples. The next equation defines the frequency $f(t)$ of the test signal which corresponds to the derivative in time of the phase argument of $x_i(t)$:

$$f(t) = f_o - \Delta_f[1 - e^{t/T_{FM}}] \qquad (5.3)$$

The same figure displays $f(t)$ which provides a means of reference for the evaluation of the measuring algorithm. The trajectory of the reference frequency about $t = 100$ ms is displayed in Figure 5.3. In the same figure, the broken line corresponds to the frequency estimated by the delay predictor technique, whereas the solid line shows

the frequency obtained from the weighted one-step predictor as described in Chapter 4. The influence of the exponential decay of the amplitude on the trajectory of both frequency predictors, is shown in the same figure. It is seen that the delay predictor exhibits higher oscillations as compared to the weighted predictor.

The input signal and its in-phase component, as produced by the measuring algorithm based on the weighted predictor, are shown in Figure 5.4. For clarity, the quadrature component of the input signal has been omitted in this figure. Two cycles before the fault are included in this figure in order to show how the in-phase component (broken line) is accurately tracking the input signal. At the time when the fault is up, and during the first negative half cycle of the input signal, it is seen that the in-phase component is attempting to track the sudden reduction of the amplitude of the input signal, from 100% to 80% which occurs in less than 5 ms. During this time, the trace of the input signal lies behind the trace of the in-phase component. With respect of the delay time between the traces of the signals, it can be said, that if the rotation of angular phase of the input signal were retarded, a similar delay effect would be observed irrespective of any change in the amplitude of the input signal. This is to explain the response of the frequency measurement algorithm to the sudden reduction of the amplitude of the signal. Correspondingly, a negative excursion of the measured frequency is produced as shown in Figure 5.3.

It can be seen during the following second half of the first negative cycle, that the trace of the input signal now leads the trace of the in-phase component. Then, the measured frequency exhibits a positive overshoot at $t = 115$ ms as shown in Figure 5.3. This leading effect stops at time $t = 120$ ms at the zero crossing. At this time, the trace of the input signal lies behind the in-phase component once again and a negative excursion of the measured frequency is produced.

Following the transient in the frequency due to the abrupt reduction of the amplitude, a small ripple appears on the trace of the frequency as shown in Figure 5.3. This ripple corresponds to the effects of the amplitude modulation process which is not completely over. As seen in figure 5.2, the mean value of the measured

frequency exactly follows the trace of the reference frequency (solid line).

The influence of an AM process on the estimation of frequency was pointed out in Chapter 4. It was shown by Ström [58], a infinite variance in the estimation of the frequency of signals modulated in amplitude. It was also shown in that Chapter, that the formulation of the frequency algorithm in the continuous time domain did differ from the discrete time domain due to the group delay of the digital filters. In Figure 5.4 is clearly shown the time taken by the adaptive frequency one-step predictor to track the input signal at the time of the fault occurrence. Therefore, the ripple imposed on the measured frequency does not correspond to variations of the underlying frequency and, thus, they must be removed. This problem will be accounted for in the next study.

In Figure 5.5 is displayed a test signal whose amplitude follows an exponential decay but its frequency remains constant. The analytic expression of the testing input signal follows the same description as given by equation (5.1) for the first study, except that the frequency is constant. The parameters describing the amplitude modulation pattern are equal to those given in the first simulation. This study is intended to show the effects of an AM process of a constant frequency signal upon the response of the frequency measurement algorithm.

In Figure 5.6 is shown the response of the weighted predictor compared to the delay predictor. It is noticed that the decaying pattern of the amplitude modulation process results in a reduced ripple in the weighted predictor as compared to the delay predictor. In this study, the amplitude of the input signal also undergoes a sudden reduction at t = 110 ms. Therefore, the frequency estimates exhibit the same pattern as in the first study due to the amplitude decay. Figure 5.7 shows the weighted predictor frequency for the complete simulation. It is seen that the mean value of the deviations of the measured frequency exactly corresponds to the trajectory of the reference frequency. Hence, a one-cycle Hamming lowpass post-filter has been added to smooth the frequency results. Figure 5.8 displays the lowpass filtered frequency calculated with the weighted predictor. It is seen that, except for the

swing of the measured frequency due to the sudden amplitude change, the measured frequency follows exactly the same trajectory as the reference frequency.

As a result of the performance of the weighted predictor and the use of the one-cycle Hamming lowpass post-filter, the following experimental studies were carried out by using this arrangement.

A test signal with constant amplitude and sinusoidal modulated frequency is shown in Figure 5.9. This experiment is intended to show the ability of the frequency measurement algorithm to track rapid variations of the underlying frequency.

The analytic expression of the test signal is given in the following equation:

$$x_i(t) = \sin(2\pi f_0 t + \Delta f \sin(2\pi f_M t)) \qquad (5.4)$$

The frequency modulation process $f(t)$ driving the argument of $x_i(t)$ is given as:

$$f(t) = f_0 + (\Delta f)(f_M)\cos(2\pi f_M t) \qquad (5.5)$$

The values of the parameters of the test signal are: $f_0 = 50$ Hz, $f_M = 2$ Hz and the amplitude of the frequency oscillations is $\Delta f = 0.5$, thus, the maximum excursion of the fundamental frequency of $x_i(t)$ is $\Delta f * f_M = 1$ Hz. The value of the parameters are aimed to be indicative of some power system disturbance.

In Figure 5.10 is shown the weighted-predictor frequency following the trajectory of the reference frequency as given by equation (5.5). It may be observed that at the occurrence of the fault, the measured frequency undergoes a sudden overshoot. Figure 5.11 displays the input test signal and its in-phase component near the time of the fault. An abrupt variation in the phase of the input signal can be observed at time $t = 100$ ms when the sinusoidal FM process is started. Now, the in-phase component lies behind the input signal. It is also noticed at time $t = 110$ ms, that the in-phase component crosses the time axis 1 ms after the input signal attempting to gain track of this sudden change in the phase of the input signal. This change in the phase can be seen as a rapid acceleration of the angular phase of the input signal.

Hence, the response of the frequency measurement algorithm is a positive excursion of the frequency as shown in Figure 5.10.

It can be seen in Figure 5.10 that the measured frequency accurately follows the reference frequency throughout the complete simulation. The rapid rate of change of the frequency is due to the value of the modulating frequency. Although this rapid acceleration of the frequency is unlikely to be observed in practical power systems, this simulation shows the accuracy and fast evaluation times of the frequency measurement algorithm.

A one-cycle lowpass Hamming post-filter is used in the current FM simulation to smooth the measured frequency. Figure 5.12 displays the weighted frequency, and the Hamming filtered frequency against the reference frequency. The trace of the frequencies are shown in dotted, broken and solid lines, respectively. It is seen that the Hamming lowpass frequency follows exactly the reference frequency with an additional group delay of 10 ms as compared to the weighted frequency.

5.1.2 Sensitivity of the Algorithm to Additive Noise

It was shown in Chapter 4 that the frequency response of the orthogonal filters exhibit zeros at dc and at the harmonics of 50 Hz. However, any other additive noisy component may randomly fall within the sidelobes of the frequency response of the filters. In this case, the calculated frequency will be corrupted by the intruding components. The most severe case will result if the harmonics of the fundamental frequency are present and the fundamental is decaying from its nominal value. This condition may occur in some particular power system circumstances.

A test signal corrupted by harmonics of the fundamental is used to verify the performance of the measuring algorithm under the presence of harmonics when the fundamental component is falling from 50 Hz. The test signal is amplitude and frequency modulated by an exponential decaying pattern similar to the signal described by equation (5.1); the same parameters have been used in this study.

Figure 5.13 displays the waveform of the test signal. The effects of the harmonics on the signal waveform have been included from the beginning of the simulation at time $t = 0$ in order to show how the response of the orthogonal filters to the harmonics when the fundamental frequency is 50 Hz.

Nine harmonics have been included in this study; the following are their corresponding values with respect of the amplitude of the fundamental component: the second harmonic at 25%; the third harmonic at 20%; the fourth harmonic at 15%; the fifth harmonic at 10%; the sixth harmonic at 5%; the seventh harmonic at 1%; the eighth harmonic at 1% and the ninth harmonic at 15%. The amplitude and frequency decline start at time $t = 120$ ms. For the purposes of the present study, the value of the maximum frequency excursion of the fundamental is $\Delta f =$ 10 Hz in order to show the influence of the harmonics moving into the frequency response of the orthogonal filters.

The discrete time Fourier Transform (DTFT) of the test signal is shown in Figure 5.14. The individual drift of the harmonics in the signal's spectrum can be appreciated, *i.e*: while the fundamental has fallen 1 Hz, the ninth will have fallen 9 Hz. However, there is no way to know the time of occurrence of the frequency drifts from this figure.

The frequency measured by the algorithm is shown in Figure 5.15 together with the reference frequency which is driven by equation (5.3). Before the AM/FM process is started, it is seen that the presence of harmonics do not affect the frequency calculations since the frequency response of the orthogonal filters removes these components. Following the starting of the fault, the reference frequency is seen to fall down to 48 Hz, in 80 ms approximately. At this time, the harmonics clearly exhibit their influence on the frequency estimates; as the frequency decay progresses, the calculated frequency undergoes a nonsense path. This frequency trajectory is a combination of the influence of the harmonics and of the evolution of the amplitude modulation pattern. Both modulation processes are seen to disappear about $t = 550$ ms.

In order to reduce the sensitivity of the orthogonal filters to the presence of additive noise, a recursive least squares (RLS) adaptive line enhancer (ALE) was implemented as proposed in the last Chapter. Figure 5.18 shows the results of the frequency measurement by using this filter. The implementation of the filter is based on a lattice structure as shown in Figure 4.8 in Chapter 4. The order **L** of the filter is 10 and the decorrelation factor Δ is 40 which corresponds to the number of samples of one-cycle of the second harmonic which is the closest noise component to the fundamental frequency. From Figure 18, it is seen that the trajectory of the measured frequency follows closer the reference frequency during the first 100 ms after the fault. It is also seen that by time t = 300 ms, when the fundamental has fallen to 47 Hz, the tracking capability of the ALE filter is diminished. At this frequency, the value of the decorrelation factor as used in this application is not longer effective. Figure 5.17 shows the discrete time Fourier Transform of the input signal before and after the ALE pre-filter. The reduction of noise afforded by the ALE pre-filter is about 60%. From this figure it is noticed that the ALE filter is not able to reduce the harmonics' presence beyond the fifth harmonic component. Nevertheless, the second harmonic still represents the main problem to the frequency response of the orthogonal filters. These filters will greatly attenuate any noisy components beyond 300 Hz but they are defenceless with respect of the second and third harmonics.

In order to improve the frequency response of the orthogonal filters, a one-cycle lowpass Hamming filter with a stop-band starting at 100 Hz, has been included in the measuring algorithm. This filter precedes the orthogonal filtering stage in order to attenuate the influence of noise. Figure 5.18 shows the reference and the measured frequencies of the Hamming pre-filtered input signal. It is seen that below 47 Hz, the presence of the second harmonic is still present, but now, it results in a small ripple in the measured frequency. A larger impulse response Hamming pre-filter could remove this effect at the expense of a larger group delay.

As a result from this study, it was decided to use the one-cycle Hamming pre-filter preceding the orthogonal filters. Therefore, the complete frequency measurement

algorithm has a total group delay of 37.5 ms, the first 17.5 ms corresponding to the orthogonal filters and to the adaptive predictor, and the remaining 20 ms corresponding to the pre-filter and post-filter Hamming lowpass filters.

5.2 Modelling of Typical Power System Conditions

A collection of different simulations of realistic power system conditions has been developed to evaluate the performance of the frequency measuring algorithm. These simulations are aimed to reproduce the conditions to determine the reliability of the frequency measurement algorithm for its application in power systems.

5.2.1.1 Performance of the Algorithm During a Power Swing

The conditions which can result in a power swing are shown in Figure 5.19 [59]. A limited generating unit is connected via a transmission line to a busbar R which is part of a large source network. A second transmission line connects busbar R to busbar S. At time t = 10 ms, a three-phase fault occurs in the line R-S, close to busbar R. The fault is cleared 200 ms later. Details of this study are given in Appendix 8.

Due to this fault, the power, which had been transmitted from P to R during steady state conditions, now has the effect of increasing the angle of the voltage V_P with respect to the angle of the voltage V_R. At time t = 210 ms, the fault is removed and a normal transfer of power from P to R is now expected. Figure 5.20 shows the voltage waveform at busbar P, phase 'a'. The abrupt reduction of the voltage amplitude at the fault inception is clearly observed. The amplitude is also seen to follow an exponential decay trend. Both the sudden amplitude reduction and the exponential decay of the amplitude have already been investigated in the previous studies. The time when the fault is cleared is clearly noticed when the voltage amplitude suddenly returns towards its nominal value. However, the severity of the fault has the effect of conveying the angle V_P to exceed its steady state full load value with respect of V_R. As the generator at busbar P attempts to recover its steady

state operating conditions, its own dynamics move the rotor into an oscillatory status. These oscillations follows the transfer of power in the system which result in power swings between the generators.

The measured frequency at busbar P, phase 'a', is shown in Figure 5.21. The sudden fault to earth results in a positive excursion of the frequency. That is, the reduction of voltage results in a shortage of the exported power from the generator at bus P, which is manifested as an acceleration transient of its own rotor. Because of the time of initialization of the measuring algorithm, the displayed measured frequency only shows a fraction of the rotor acceleration. It is seen that this effect shortly settles down.

When the fault is cleared, at time t = 210 ms, the amplitude of the voltage is taken back to its nominal value. Correspondingly, the generator at P faces an overloading condition. It is noticed from Figure 5.20, that at this time, the voltage waveform exhibits a clear swing of its phase. Hence, the measured frequency as shown in Figure 5.21, displays a dip in its trajectory.

Due to the duration of the fault, the angle between P and R has become so large that synchronism is lost and a pole slip condition results. Figure 5.21 shows a pair of pole slip events occurring at time t = 890 ms and at t = 1150 ms. From the trajectory of the measured frequency it is noticed that before a pole slip is occurs, the frequency suffers an increasing oscillation about f_o; the second half of the pole slip shows the relieving effects on the system when the angle of the generator at P reaches a motoring condition. Figure 5.22 shows a fraction of the voltage waveform and its in-phase component near the first pole slip occurrence. It is seen that at time t = 870 ms, the input signal lies behind its in-phase component; that is, the rotation of its angular phase is decelerating. At time t = 890, the phase of the input signal gains speed once again just after leaving the first pole slip. Figure 5.23 displays the corresponding frequency as measured during this interval. The same sequence of events occur during the second pole slip.

The effects of the random modulation of the amplitude of the input signal on the performance of the measuring algorithm, will certainly result in oscillations of the measured frequency about a mean value. This problem has been discussed during the previous AM/FM studies. In Figure 5.22 it is seen that the in-phase component accurately crosses the time axis at those times when the input signal crosses the same axis. It is also noticed that the in-phase component undergoes amplitude excursions during the tracking of the input signal. In this case, the use of the Hamming post-filter has attenuated the resulting oscillations as shown by the small ripple in the frequency displayed in Figure 5.23. In this figure is seen that the effect of the amplitude modulation has been removed by the lowpass post-filter. Hence, the measured frequency only manifests the variations of the angular phase of the input signal.

5.2.1.2 Sensitivity of the Algorithm to Travelling Wave Noise

Figure 5.24 depicts a power system configuration which has been used to study the sensitivity of the frequency measuring algorithm to the presence of additive noise, particularly, to travelling wave noise [60]. A 100 km transmission line connects two generators at buses P and Q. The generators have a short circuit level of 0.3 GVA and 0.5 GVA, respectively. Although the short circuit levels in the current simulation are rather low, these levels will permit to observe severe travelling waves along the system. It should be mentioned here, that the conditions in the current simulation were not created by a electromechanical model and no deviation of the fundamental frequency should be expected.

In this simulation, phase 'a' was faulted with zero fault resistance; the location of the fault is at 85 km away from busbar P. It will be seen in Appendix 9 that the 'a' phase lies closest to ground for the single circuit, 400 kV, vertical configuration considered. The inception of the fault occurs at t = 60 ms. The voltage waveforms as observed at busbar P are displayed in Figure 5.25. The contamination produced by the travelling wave noise at the time of the fault is shown on the waveforms of phases 'b' and 'c'. The effects of the first odd harmonics on the voltage waveforms

are clearly shown. The faulted phase exhibits the worst scenario: an abrupt reduction of its amplitude followed by an exponential decaying high frequency noise imposed over the main frequency component.

Figure 5.26 displays measurements of the frequency taken at each one of the phases at busbar P. In this figure, the initialization process of the algorithm is shown to follow different trajectories according to the information supplied by the individual phase. It is seen that by time t = 57 ms, the frequency of the three phases has reached the 50 Hz steady value just before the fault inception at t = 60 ms. The frequency measured at phase 'a' is seen to undergo the most severe effects of the fault. Figure 5.27 shows the voltage of phase 'a' taken after the Hamming lowpass pre-filter together with its in-phase component. The sudden cut of the voltage waveform at the fault inception is attenuated by the lowpass filter. The presence of the high frequency noise following the fault is also averaged by this filter and results in a signal driven by the fundamental component but with a decelerating phase. In this figure, it is seen that the amplitude excursion of the in-phase component loses track of the filtered input signal. This Figure also shows, that at time t = 75 ms the phase of the input signal has been stretched. During the transient in the amplitude of phase 'a', the amplitude of the in-phase component is seen to undergo a pair of excursions attempting to gain track of the input signal. From the numeric data generated by the computer model during the simulation, it can be shown that the filtered input signal crosses the time axis at times other than at every 10 ms, thus, the resulting frequency also displays this decelerating effect.

It was already mentioned that the current study case was not simulated by using an electromechanical model, hence the underlying frequency of the power system remains at 50 Hz throughout the simulation. On the other hand, the measured frequency taken at busbar P clearly shows the variations of the rotation of the angular phase of the input signal. It was seen in Figure 5.26, that the measurement of frequency taken at phases 'b' and 'c', exhibited different trajectories as compared to the frequency taken at phase 'a'. The different traces described by the single phase frequency measurements, confirm that the measured frequency corresponds

to the speed of rotation of the angular phase of the input signal.

5.2.2 Evaluation of the Algorithm's Performance Using EMTP Simulations

The modelling of power system conditions by using the electromagnetic transient program (EMTP) [6], provides significant observation facilities of the modelled processes. Particular benefits are achieved from the use of this program package concerning the display of parameters of the modelled power system. These parameters can be observed as the simulation of a complicated power system is taking place.

One of the most relevant features of the EMTP is that it can simulate the cases of power systems undergoing realistic frequency changing conditions with high accuracy. A significant facility from EMTP simulations is that the dynamic model of voltage regulators and speed governing systems can be included at the programming stage. During the simulation of systems including synchronous generators, some of the most important parameters to be observed are the instantaneous value of the angle and speed of the generator rotor. Concerning the performance of the new frequency measurement algorithm, this facility will allow to evaluate the ability to track rapid variations of the power system frequency under simulation. These studies will permit the comparison of the algorithm's performance against the rotor speed of the modelled generator.

The use of the EMTP to model a synchronous machine is very strict and inflexible concerning parameters of a particular model. Different cases of synchronous machines have been studied. However, the available literature does not provide enough information related to the dynamic parameters of a particular machine for a 50 Hz power system simulation by using the EMTP. The simulation studies presented in this section correspond to the use of two particular machines. In the different study cases presented in this section, the model of an automatic voltage regulator and of a speed governing system have been included in order to observe the influence of the dynamics of these devices on the evolution of the rotor speed

and frequency. In these studies, the trajectory of the generator rotor is taken from data generated by the EMTP application. The frequency displayed in the following studies is measured at the generator terminal voltage, phase 'a'. The sampling frequency in all cases is 4 kHz. Due to the computational limitations when dealing with the immense amount of data generated from the EMTP simulations, the results coming out from the different simulations, have a duration of 2.4 seconds only. In theses studies, a one-cycle lowpass Hamming filter is used in the frequency measurement algorithm to pre-filter the signal under observation, and another similar filter is used to smooth the frequency estimates.

5.2.2.1 Single Machine Load Change

The dynamics of a simple power system are investigated in this section. A 75 MVA generator is connected to, initially, a load of 40.72 MVA. The power system configuration is shown in Figure 5.29. The case of two load changing conditions are presented in this section. In both simulations, the speeder motor in the governor has been disabled and hence the new loading condition results in a new steady state system frequency below the nominal. Parameters of the power system used in the simulations are included in Appendix 10. These study cases are intended to show the dynamic performance of the frequency measurement algorithm when a single generating unit system undergoes a load changing condition.

In the first simulation, an additional load of 15 MVA is connected to the generator. The switch is closed at time t = 15.205 s. The generator terminal voltage was processed by the algorithm and the resulting frequency is shown in Figure 5.30. The rotor speed, collected from the EMTP output data, is also displayed in the same figure. When the additional load is connected, the measured frequency shows a depression which is not exhibited by the rotor speed. Figure 5.31 shows a fraction of the waveform of the generator terminal voltage and its in-phase component at the time of the application of the additional load. For clarity, the quadrature component of the input signal is not displayed in this figure. The application of the load produces a small reduction of the amplitude of the terminal voltage. At time t =

15.212 s, the input signal is seen to lie behind its in-phase component (broken line) for a short time. However, as it is shown in Figure 5.30, the transient in the measured frequency produced during this time clearly shows a deceleration of the angular phase of the input signal. When the switch is closed, the variation of the power output is accompanied by a rapid change in the angle spanned between the generator terminal voltage vector and the armature internal electromotive force (emf) vector; the variation in the angle is due to the sudden increase in the armature current in the generator when the extra load is connected. The new loading condition is responsible for the transient deceleration of the rotation of the angle. On the other hand, the inertia time constant of the generator prevents the rotor speed to undergo the fast transient exhibited by the measured frequency. Following this transient, the measured frequency accurately follows the trajectory of the rotor speed.

The case of an additional load of 40% of the machine's rating is displayed in Figure 5.32. The additional load is connected at time t = 15.205 s. For the same initial conditions in the single generator power system as given during the previous experiment, the effects of the additional load now result in a larger transient in the measured frequency. Although the effects of the application of the additional load are manifested in the amplitude of the terminal voltage in the form of an amplitude modulation process, it is seen in Figure 5.33 that the new loading condition produces a small disturbance in the tracking performance of the in-phase component with respect of the input signal. Now, the additional load produces a larger transient in the measured frequency.

Figure 5.34 shows the trajectories of the rotor speed from the two load changing condition cases. The effects of the application of the additional load are reflected in the initial rate of change of the rotor speed. The measured frequency during both simulations is shown in Figure 5.35. Apart from the transient produced during the change of load, the measured frequency closely follows the rotor speed with a constant group delay of 37.5 ms.

5.2.2.2 Separation of a Single Generating Unit from the Grid

Figure 5.36 shows a single generator connected to the main system via a short transmission line. The generating unit has a small rating and it is supplying a local load equal to the rating of the machine with a power factor of 0.9 lag. The generator's infeed is 70% of the load. The remaining 30% of the load is infeed by the infinite bus. Thus, the generator retains a 30% of available spinning reserve. The inertia time constant of the machine is 4.64 [kW s/kVA]. Apart from the 400 kV, 10 miles transmission line, the configuration of the power system used in the current study case is basically the same as that used in the previous section. Details of the transmission line used in the current simulation are included in Appendix 11.

At time t = 15.004 s, the connection to the infinite bus is removed and the generating unit becomes isolated, thus taking up the total load. The trend of the rotor speed as the generator encounters the overload is shown in Figure 5.37. The frequency measured from the generator terminal voltage is also displayed in this figure. Following the separation, the terminal voltage exhibits a sudden amplitude reduction as shown in Figure 5.38. The separation from the grid results in a sudden change of the generator into a full export condition. The effects of the overload in the amplitude of the terminal voltage are seen in this figure. To appreciate the tracking ability of the in-phase component, two cycles of the pre-fault period are shown in the figure. Following the separation, it is seen that the input signal lies behind its in-phase component. As explained in the previous study case, the sudden change in the power output of the generator at the time of the separation, results in a transient deceleration in the rotation of the angle between the terminal voltage and the internal emf vector.

In order to confirm this transient, the measurement of frequency was performed at the three phases during the transient period following the fault inception. Figure 5.39 shows the trajectory of the frequency measured at the three phases. Some differences in the trajectory of the individual single phase frequency measurement are noticed. It should be mentioned that, due to restrictions of the EMTP, the switches connecting the generator transformer with the transmission line can be opened only when the phase voltage goes through a zero crossing. It can be shown from the

generator terminal voltage generated by the EMTP program that phase 'c' crosses the time axis before phases 'a' and 'b'. As shown in Figure 5.39, the differences in the trace of the measured frequency at any of the phases at the terminal voltage, reflects the variations of the armature phase current following the fault inception. Since the system remains balanced throughout the simulation, it is seen from this figure that the frequency measured at the three phases, converges into a single trajectory following the transient period. The same figure also shows that, apart from the group delay of the frequency measurement algorithm, the measured frequency accurately follows the trend of the generator rotor speed.

5.2.2.3 Separation of Two Interconnected Generators from the Grid

The cases of two generating units becoming isolated from a main system will be used to study the behaviour of the frequency of a islanded power system. A typical condition can be depicted when the generators have different time inertia constants since the dynamics of the islanded system will be driven by these constants and by the magnitude of the attempted overload. The most severe case will be a lack of spinning reserve energy of the isolated generating units, Then, the system frequency will be seen to fall without any means to arrest its decay. A more interesting case would be presented if there is enough reserve capacity in the islanded system for assisting the system during the overload. In that case, the different inertia constants and the individual dynamics of the remaining generating units would produce a power swing among the islanded generators and a rapid time varying system's frequency.

Two cases are presented in this section. In both simulations, the islanded system consists of two synchronous machines with similar ratings but different inertia time constants. The rating of the machines is relatively small as compared to modern generators. However, these studies are of particular importance since they show the rapid dynamic behaviour of these small machines and the application of a high speed frequency measurement algorithm.

5.2.2.3.1 Local Load Study Case

In this study case, the two generators are supplying a local load via a transmission line; the load is connected to the main system via a short transmission line. Figure 5.40 shows the power system configuration. The inertia time constants of the machines located at buses SEND 1 and SEND 2, are, 3.5 and 4.64, respectively. The rating of the generators is 750 MVA and 600 MVA, in the same order. The second generator is formed by eight machines rating 75 MVA each. The 75 MVA machine was used during the previous single generator study cases. The parameters of the power system configuration used for the current experiment are included in Appendix 12.

In the present study, the two machines take up a load rated at 100% of the total system's rating at the time of the separation. During the pre-fault conditions, the infinite bus is supplying 46.67% of the load. The generator at SEND 1 is supplying 22.22% of the load and the second generator supplies the remaining 31.11%. The combined generating reserve capacity of the islanded system is 47% of the total system's rating. At time t = 15 s, the system becomes isolated and the generators take up the total load.

The rotor speed of the generator at bus SEND 1 is shown in Figure 5.41 together with the frequency measured at the same bus. The frequency shown in this figure corresponds to the machine with an inertia time constant of 3.5 [kW s/kVA], thus, it is expected that its rotor speed will exhibit rapid oscillations as compared to the machine at SEND 2. The transient of the measured frequency following the fault inception is clearly seen in this figure. It was shown in the previous study case, that the transient in the measured frequency appearing at the fault inception corresponds to variations in the angular phase of the input signal. The frequency measured taken at the generator terminal voltage at busbar SEND 2 is shown in Figure 5.42. The frequency also exhibits a similar transient following the fault. The proximity of the load to this generator is responsible for the larger transient in the frequency.

When the system becomes separated from the grid, the two generators are moved into a full power export condition. Figure 5.43 shows the trace of the rotor speed of the generators in the islanded system. The effects of the new loading condition are appreciated in the initial decaying trace of the rotor speed of the generators. Note that since the generating unit at SEND 2 possesses a higher inertia constant, a shorter excursion of its rotor speed should be expected. However, the fault has occurred close to this generator and so the initial rate of decay of its rotor speed immediately reflects the impact of the sudden application of the full load following the separation from the grid. The frequency measured by the algorithm at both ends of the islanded system is shown in Figure 5.44. This figure shows the frequency oscillations resulting from power swings between the isolated generators.

5.2.2.3.2 Remote Load Study Case

The system configuration used to study the separation from the grid of two interconnected machines supplying a remote load is shown in Figure 5.45. Two generators are connected to a common busbar via transmission line sections. The generators are located 42 miles and 87 miles away from the load, respectively. The generators are loaded to 477.88 MW and to 336.2 MW, in the same order, whereas the infinite bus infeed is 291 MW. The system becomes separated from the infinite bus at time t = 15.015 s. The combined available spinning reserve is 400 MW which exceeds the 291 MW infeed by the grid. Thus, the frequency of system will recover after the fault. It is aimed in the current experiment to measure the frequency at the remote end bus and compare the results against the frequency measured at the generating side

The rotor speed of the generator at SEND 1 is displayed in Figure 5.46 together with the frequency measured from the terminal voltage of the generator at that bus. The rotor speed of the generator SEND 2 and the frequency measured from its terminal voltage are shown in Figure 5.47. In this simulation the load is closer to the generator SEND 1, and so the initial depression in the measured frequency, at the fault inception, is seen to be 0.5 Hz deeper than the dip of the frequency

measured at bus SEND 2. It is also noticed that the initial rate of decay of the frequency of the generator SEND 1 is faster than the decay of the machine at SEND 2 since the inertia time constant is smaller in the former generator. The initial rate of decay of the frequency measured at busbar SEND 2 follows a linear path due to its inertia time constant. In this simulation, the available capacity reserve on the generating side exceeds the magnitude of the overloading, and so the excursion of the frequency of both generators does not fall as much as the frequency of the generators shown in the previous study. As shown in Figure 5.48, the power swing between the generators in the present simulation now takes place near the bottom of the frequency excursions when the generators have taken up the complete overloading. In the previous study, both generators took up the overload immediately after the separation from the grid. This figure clearly shows the different trajectories spanned by the initial rate of decay of the rotor speed of the generators.

The frequency measured at the common busbar is shown in Figure 5.49 together with the frequency measured at the generating side of the system. It is seen that the frequency measured at the load busbar exhibits a deeper transient excursion as compared to the transient of the frequencies measured at the other end of the system. When the system becomes separated from the grid, the voltage vector at the load busbar reflects the severity of the new load changing condition. The amplitude of this voltage vector is abruptly reduced and the redistribution of the power in the islanded system results in a rapid rotation of this voltage vector with respect to the voltage vectors at the other ends of the system. The sudden rotation of the angular phase of the voltage vector at the load busbar is responsible for the large transient in the frequency measured at this point. It is also noticed in Figure 5.49, that the frequency measured at the load bus follows the average trend of the frequencies measured at the other ends of the islanded system. This last point reflects the fact that the frequency measured at a particular node along a power system will exhibit a unique trajectory which corresponds to the average of the frequency of the rotating vectors arriving at that node.

5.3 Summary

The different studies have shown that the measuring algorithm reflects the rate of change, or velocity, of the angular phase of the signal under observation. During the first set of studies, it was shown that sudden variations in the amplitude of the input signal are interpreted by the frequency calculation algorithm as variations in the velocity of the phase of the signal, thus producing oscillations in the frequency estimates. It was shown that the weighted one-step predictor used to compensate the gain of the orthogonal filters promoted better estimates of the frequency as compared to the delay predictor algorithm. It was also shown that the mean value of the oscillations of the frequency corresponded to the reference frequency driving the fundamental component of the signal, and so the oscillations can be removed by a lowpass filter without disturbing the accuracy of the measurements.

The effects of noise components on the algorithm's performance were investigated. The presence of noise falling within the sidelobes of the frequency response of the orthogonal filters, results in erroneous frequency estimates. A one-cycle lowpass Hamming pre-filter is used in the frequency measuring algorithm to remove noise components from the observed signal before they can disturb the frequency estimation process. It was shown that the pre-filter is capable of removing the effects of harmonics for drifts of the fundamental frequency down to 47 Hz. For practical power system applications, a protective scheme will be prompted for a system frequency below 49.5 Hz.

The response of the frequency measurement algorithm was tested for reliability and accuracy by using a set of realistic power system conditions simulated by using the EMTP. From the initial studies on dynamic conditions, it was shown that the occurrence of load changing conditions resulted in a transient in the measured frequency which is not observed in generator rotor speed. The new loading condition results in a modulation of the generator terminal voltage in amplitude and in phase by the impact of the new condition while a redistribution of power takes place. The modulation of the phase of the voltage is due to a variation in the angle between this vector and the generator's internal emf. The rapid change in the angle is responsible for the transient in the measured frequency. During these simulations, the rotor

speed was taken from the data generated by the EMTP simulation and provides a reference for the measured frequency. Apart from the transient, the measured frequency closely follows the trace of the rotor speed and confirms the reliable operation and accuracy of the algorithm.

The last part of the current experimental investigation was devoted to the simulation of a small power system becoming detached from a main system. The results from the last two experiments concerning the separation of two interconnected generators from the grid, have shown that the new frequency measurement algorithm can track relatively fast frequency variations. In the first experiment, this particular feature in the algorithm has allowed to measure the frequency at both ends of the generating side where it was compared with the rotor speed of the generators as produced by the EMTP. In the second experiment, the load is connected at the remote end of the islanded power system. The algorithm has allowed to measure the frequency at the remote end of the system where no reference is available. It was shown that the frequency measured at that the load busbar corresponds to the average of the frequency of the vectors arriving at that point in the system. This last experiment may be indicative of the case of a consuming centre located far away from the generating units. For a substation located at the remote load busbar, an accurate and fast measurement of the local frequency is critical for the correct dispatch of power.

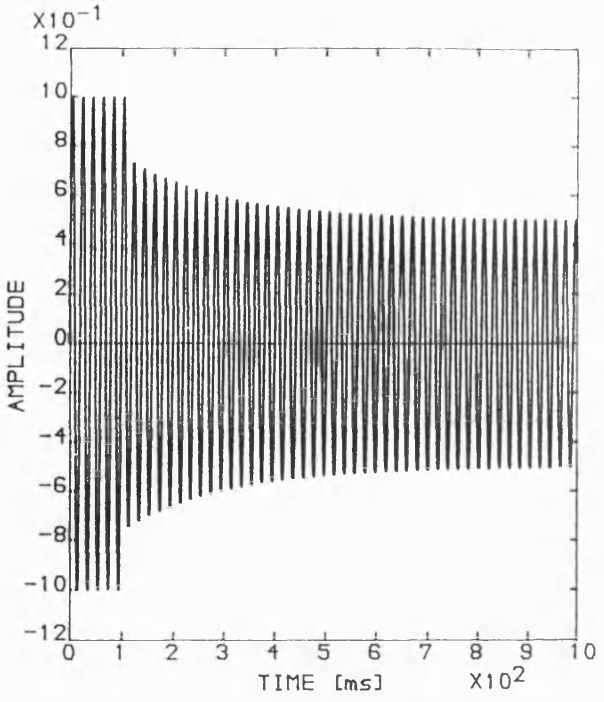

Figure 5.1 Test signal with exponential decaying amplitude and frequency modulation.

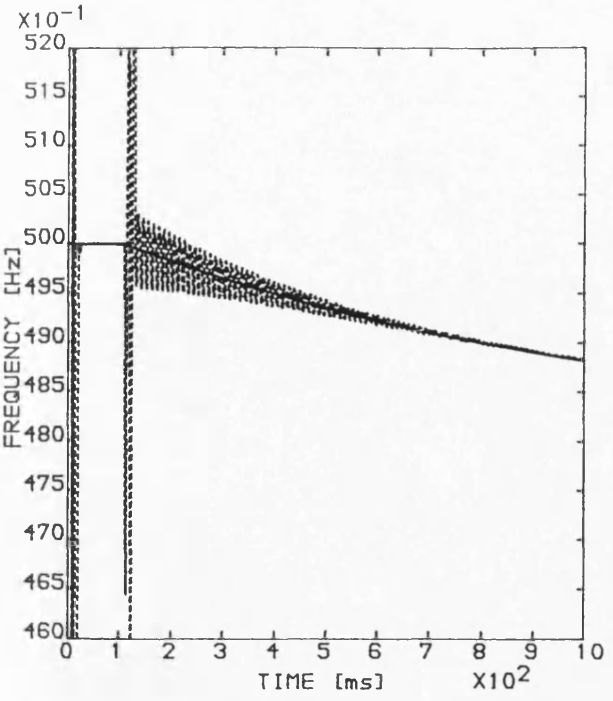

Figure 5.2 Reference frequency (solid line) and delay predictor frequency (broken line).

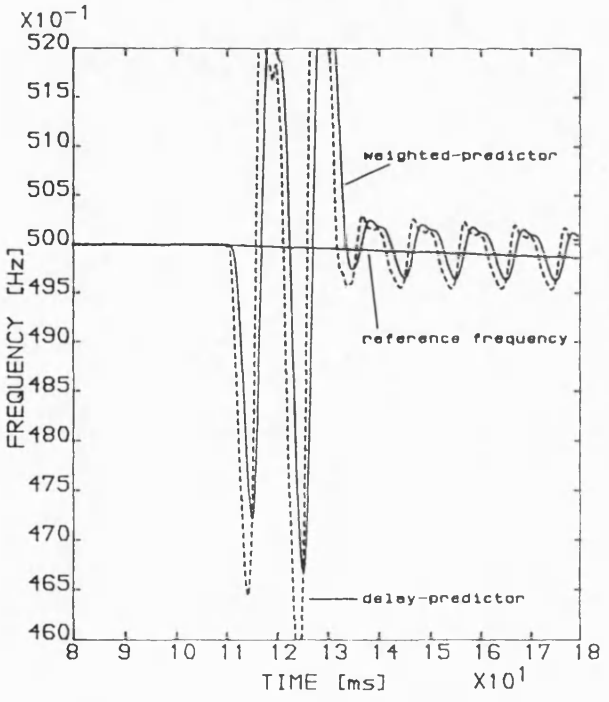

Figure 5.3 Reference frequency, delay predictor frequency and weighted predictor frequency.

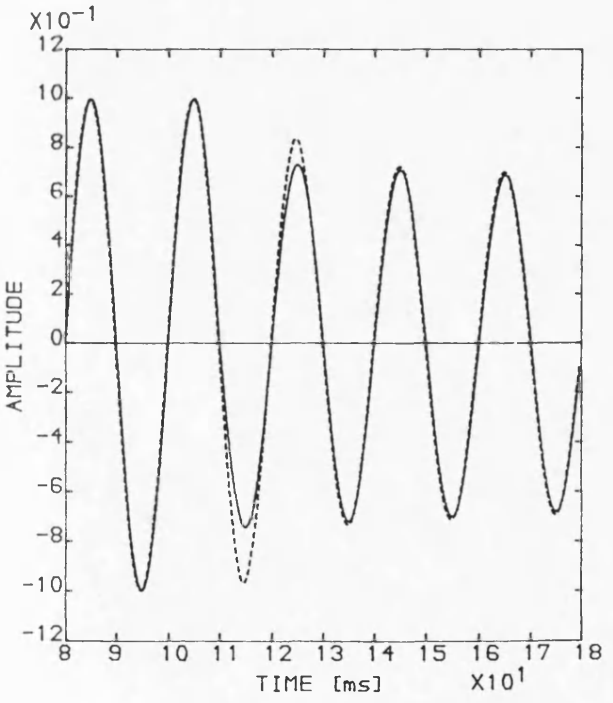

Figure 5.4 Input signal (solid line) and its in-phase component (broken line) near the fault inception.

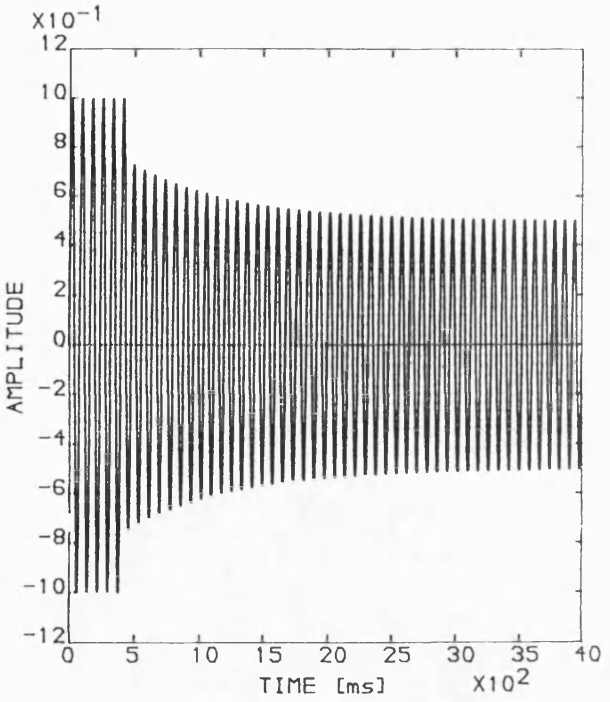

Figure 5.5 Test signal with exponential decaying amplitude modulation and constant frequency.

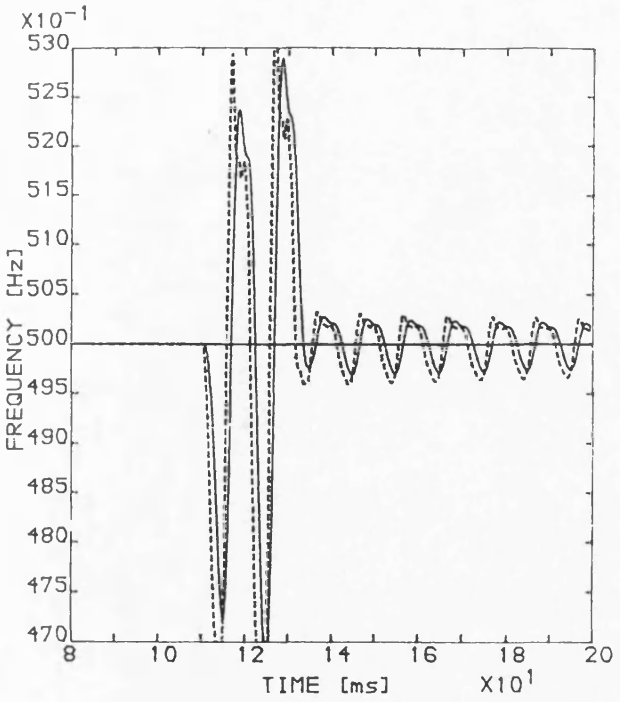

Figure 5.6 Weighted predictor frequency (solid line) and delay predictor frequency (broken line) compared with 50 Hz.

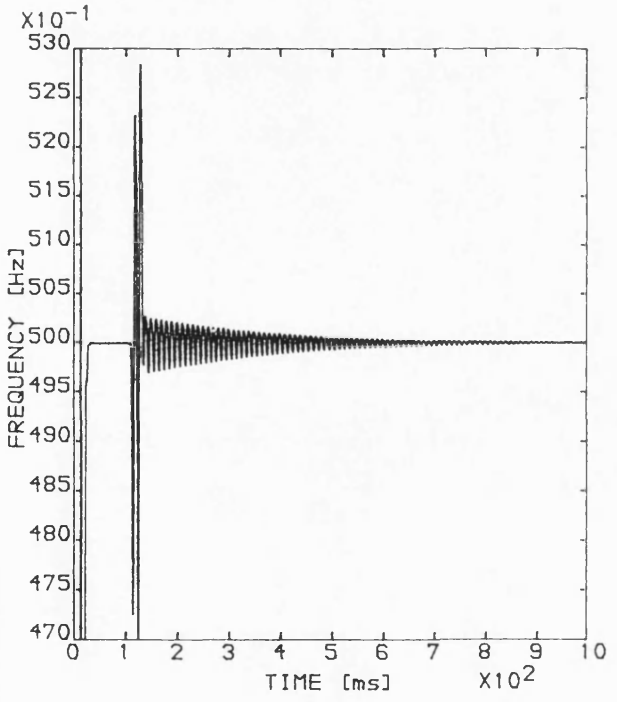

Figure 5.7 Measured frequency using the weighted predictor.

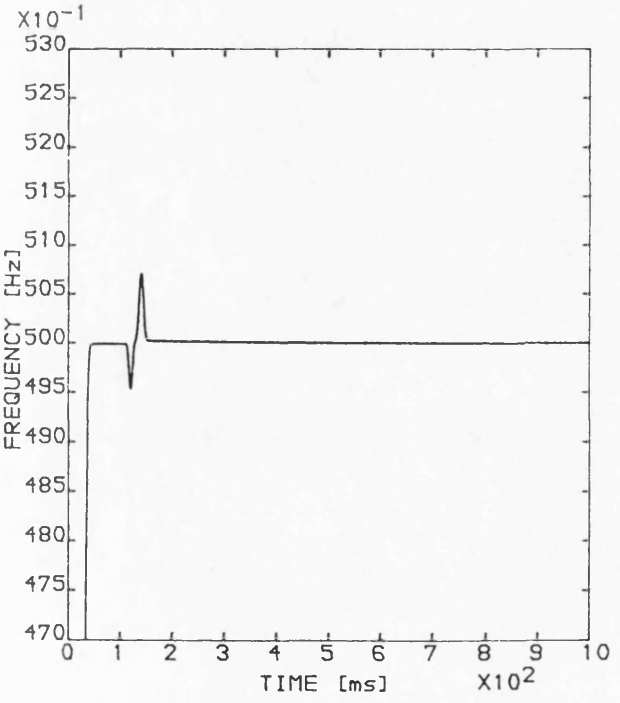

Figure 5.8 One-cycle lowpass Hamming filter following the weighted frequency.

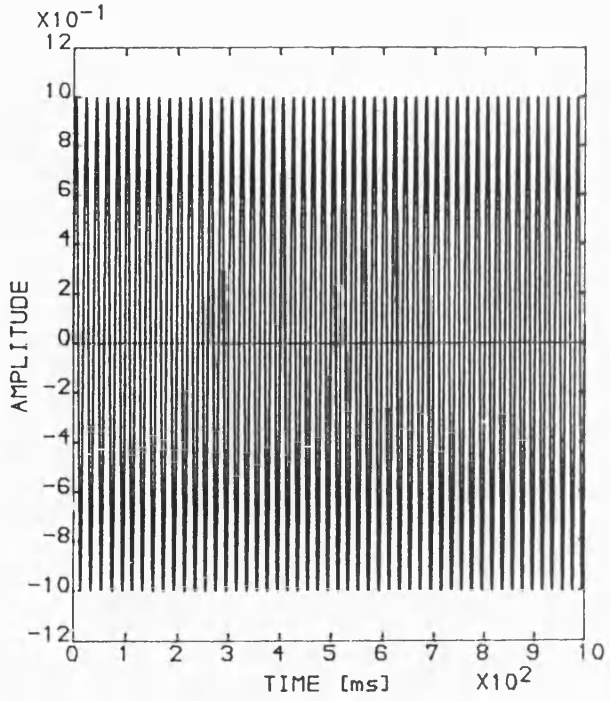

Figure 5.9 Test signal with constant amplitude and sine modulated frequency.

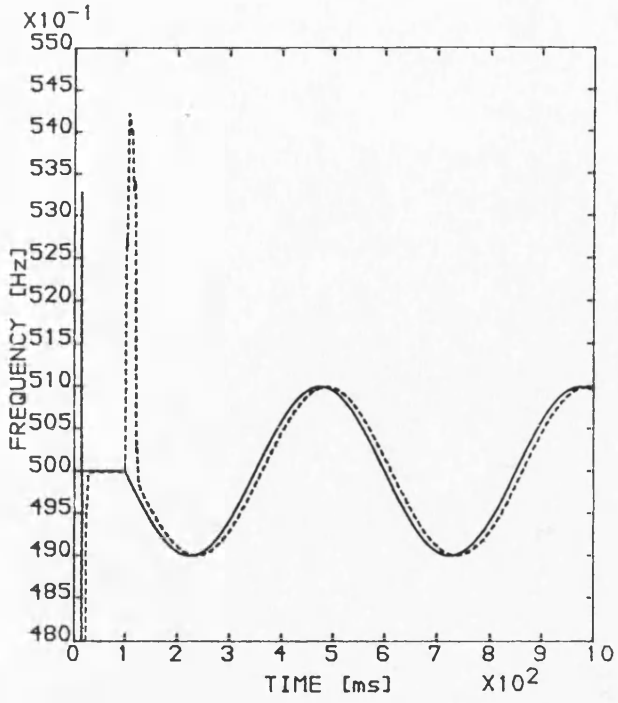

Figure 5.10 Reference frequency (solid line) and weighted predictor frequency (broken line).

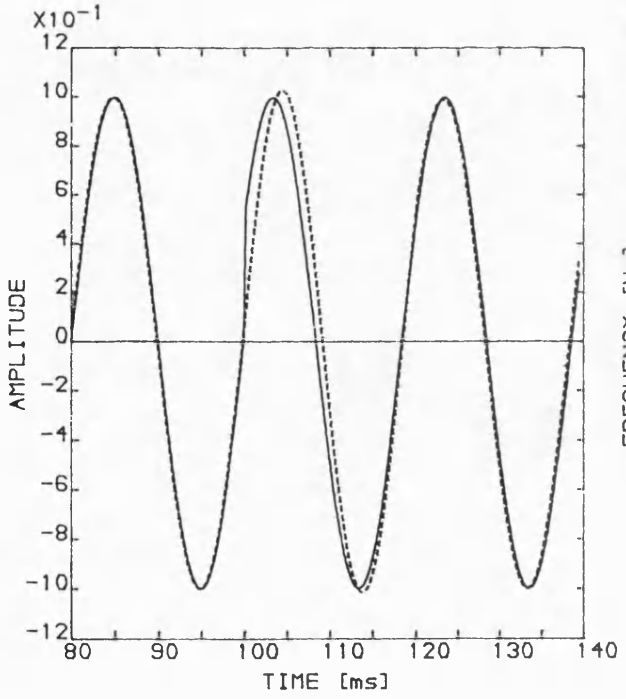

Figure 5.11 Test signal (solid line) and its in-phase component (broken line) at the time when the frequency modulation starts.

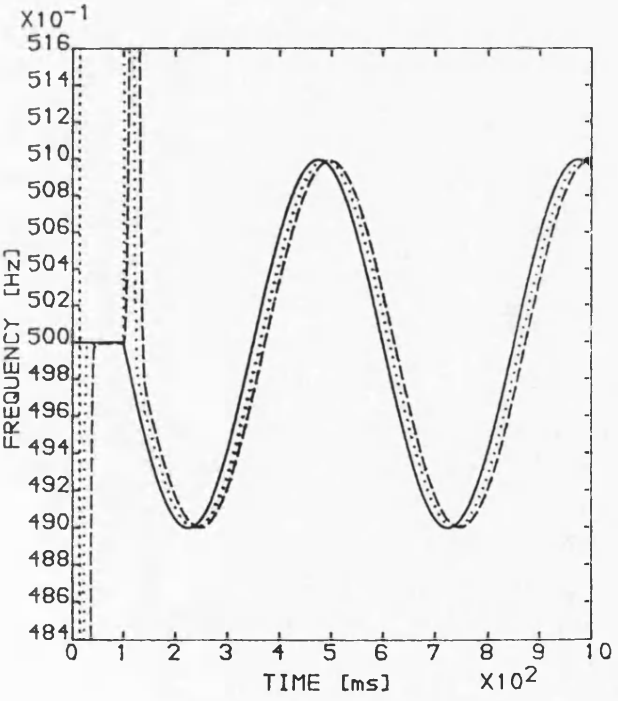

Figure 5.12 Reference frequency (solid line), weighted frequency (dotted line) and Hamming frequency (broken line).

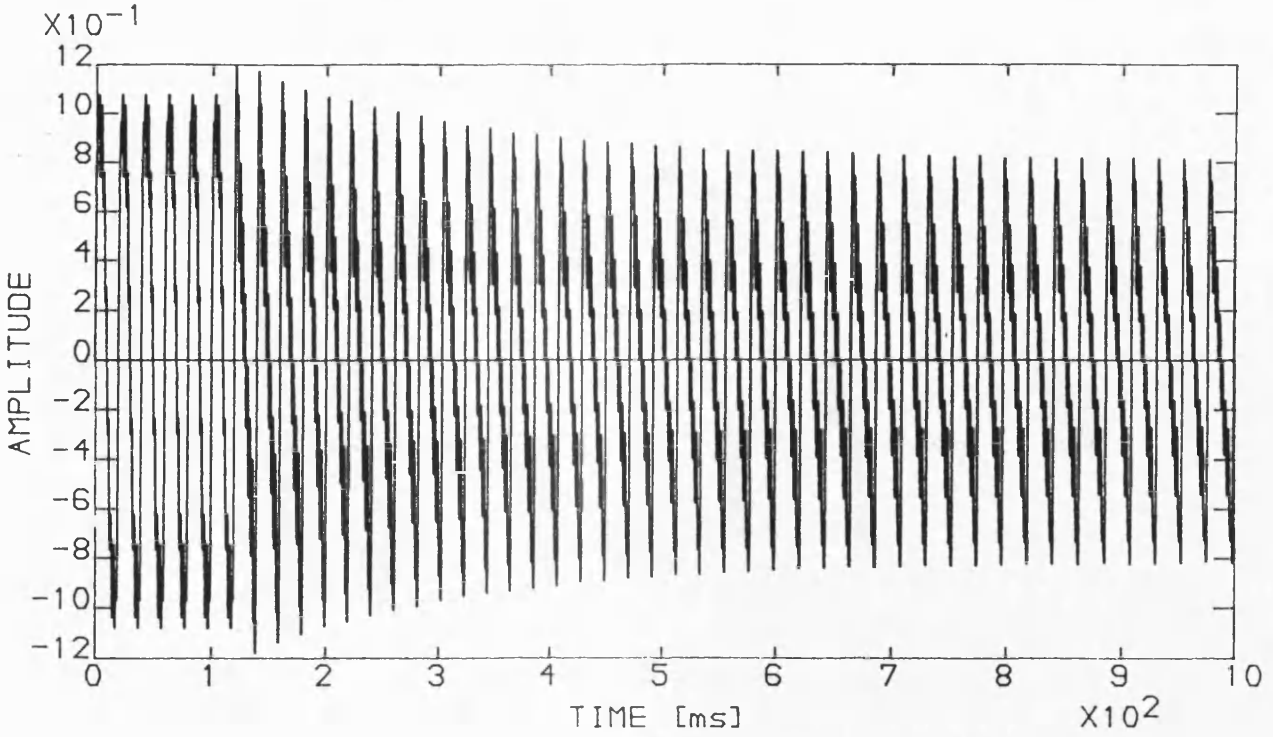

Figure 5.13 Test signal corrupted by harmonics with exponential decaying amplitude and frequency.

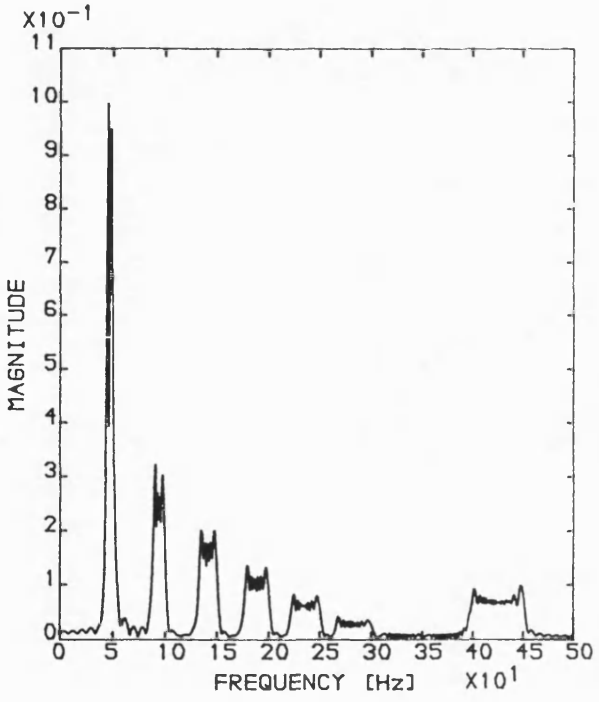

Figure 5.14 Discrete time Fourier Transform of the test signal.

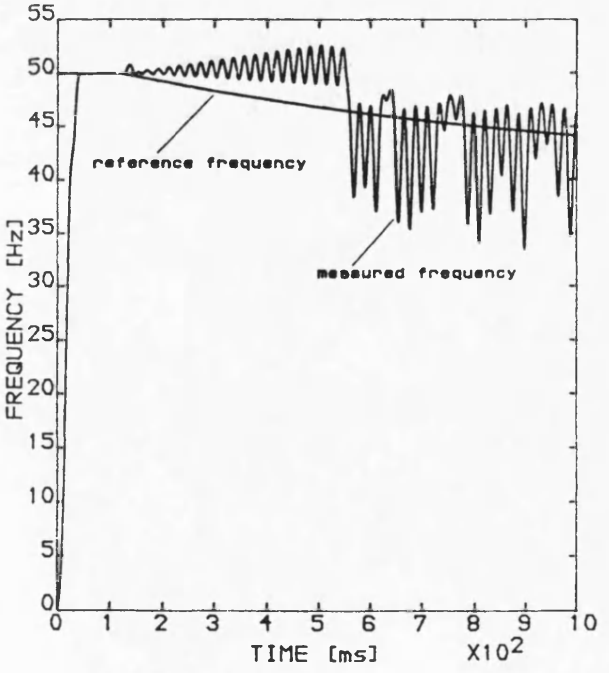

Figure 5.15 Reference and measured frequencies.

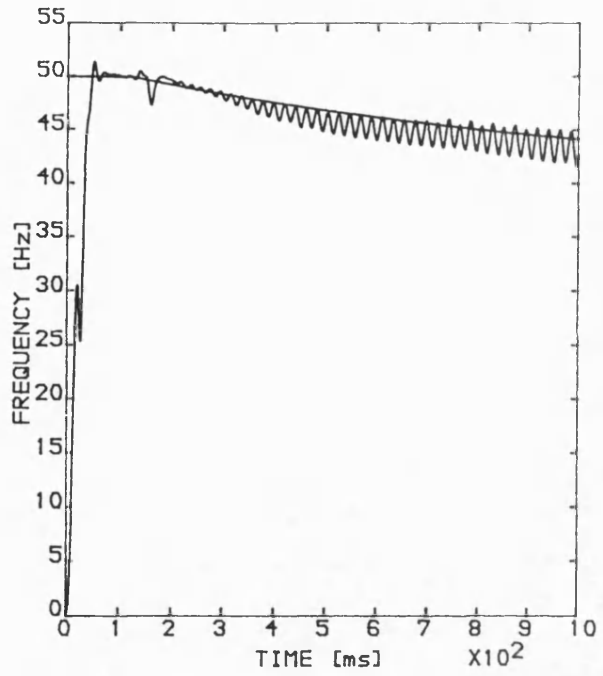

Figure 5.16 Reference and measured frequencies. A 10-order ALE pre-filter is used to enhance the fundamental component.

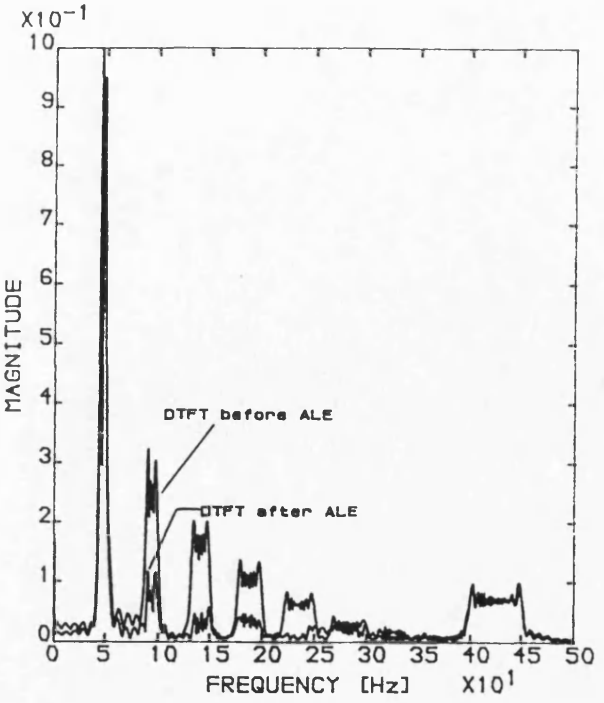

Figure 5.17 Discrete time Fourier Transform of the test signal, before and after the ALE pre-filter.

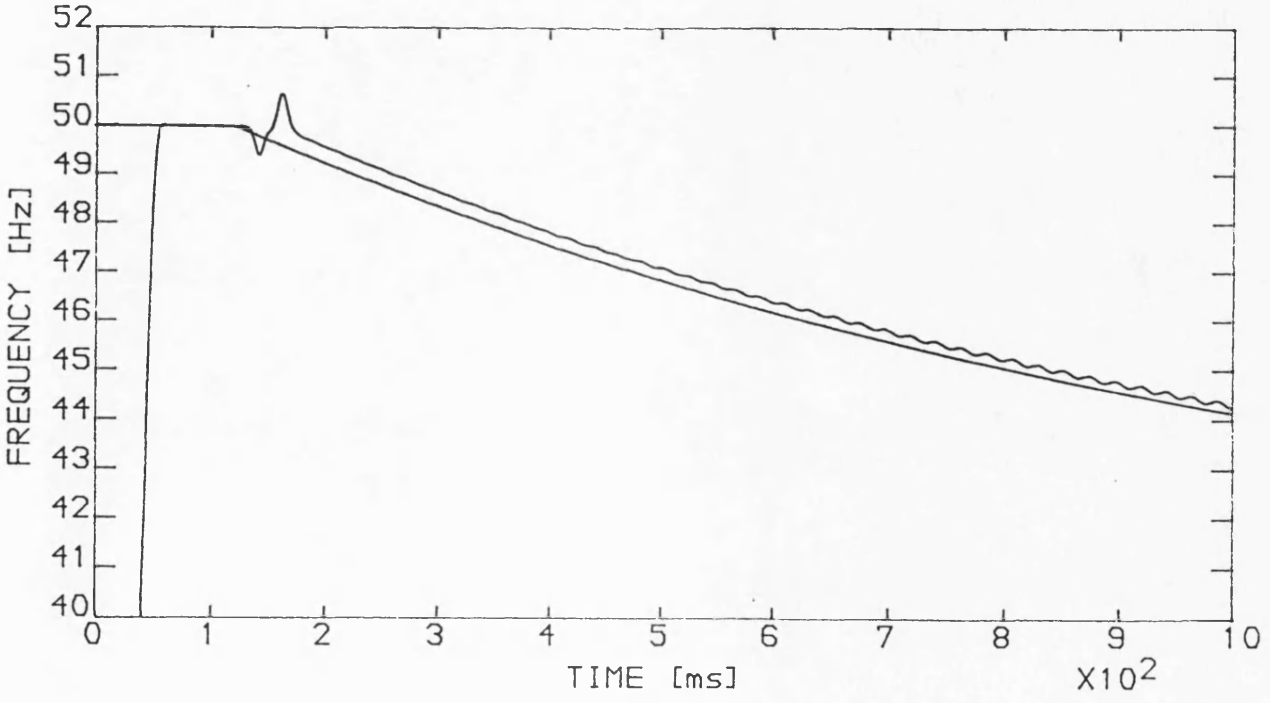

Figure 5.18 Reference and measured frequency. A one-cycle lowpass Hamming filter is used to pre-filter the test signal.

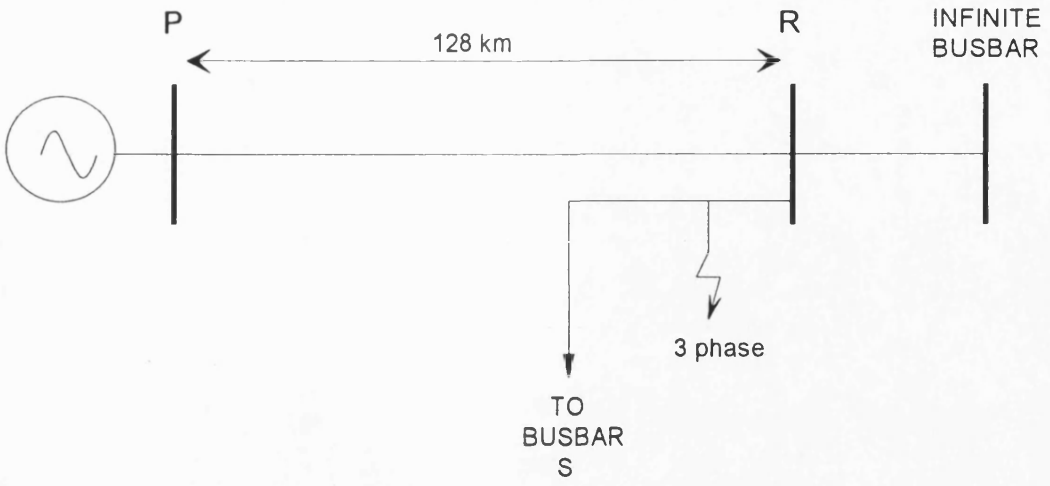

Figure 5.19 400 kV configuration system used to study the performance of the measuring algorithm during a power swing condition.

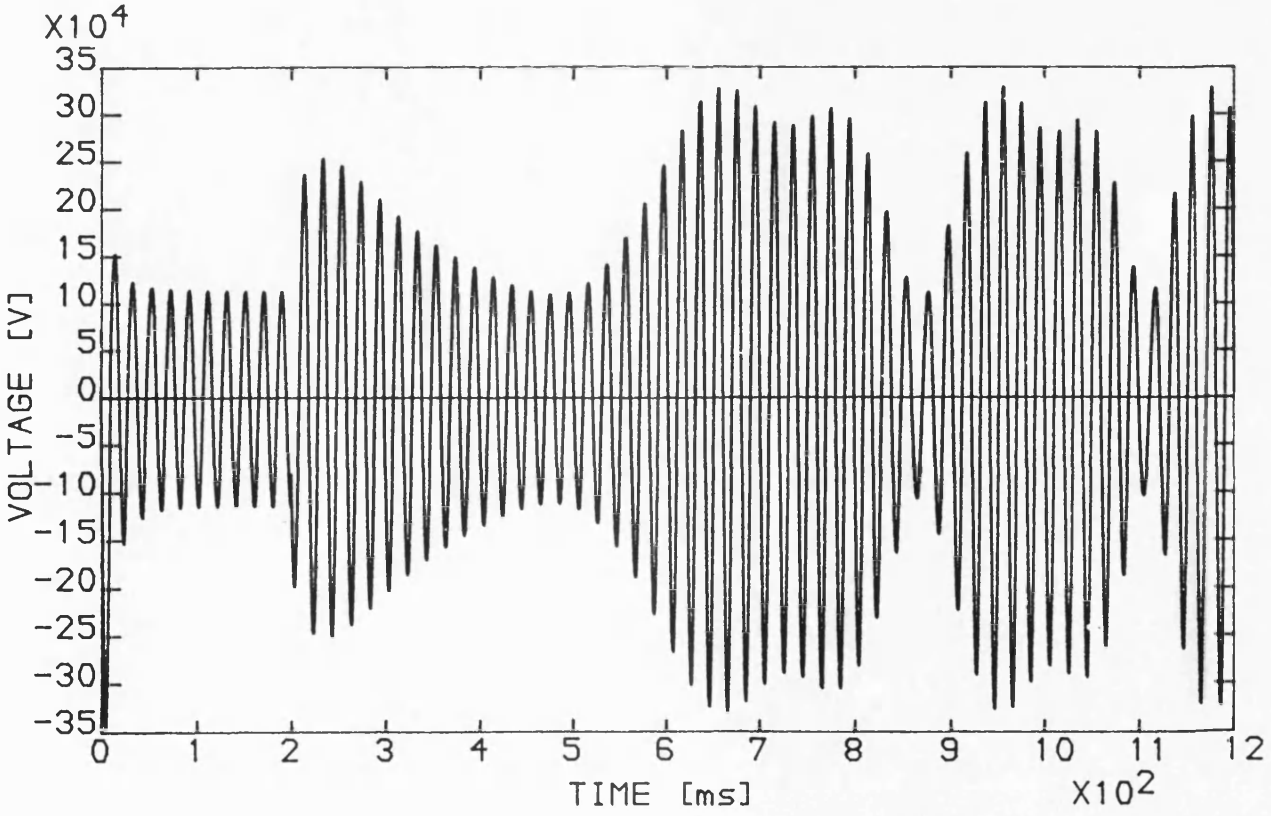

Figure 5.20 Voltage waveform at bus P, phase 'a'.

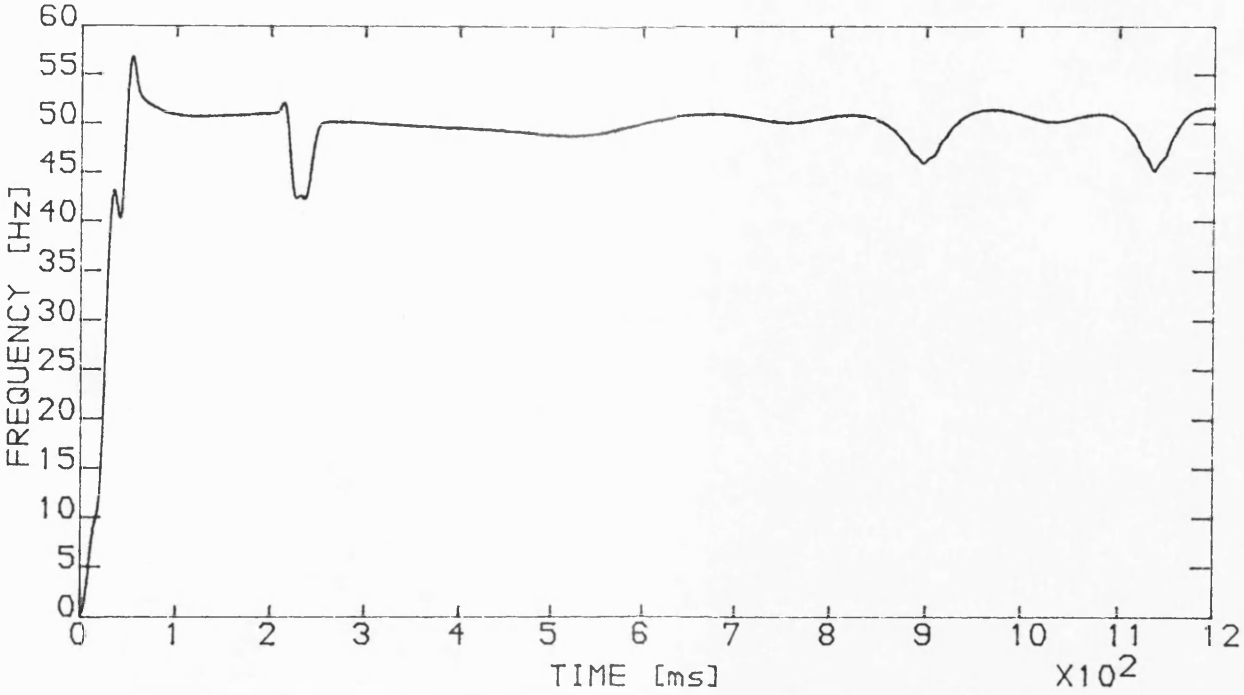

Figure 5.21 Frequency measured at bus P, phase 'a'.

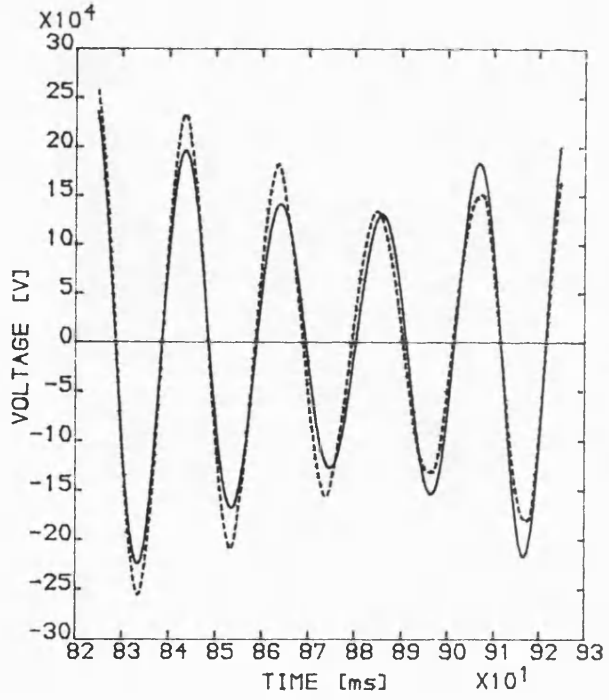

Figure 5.22 Input signal (solid line) and its in-phase component (broken line) at the time of the first pole slip.

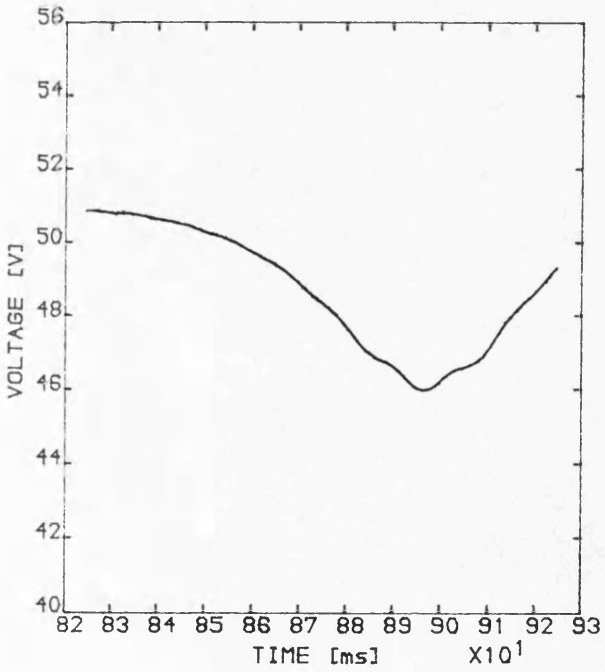

Figure 5.23 Frequency measured at the time of the first pole slip.

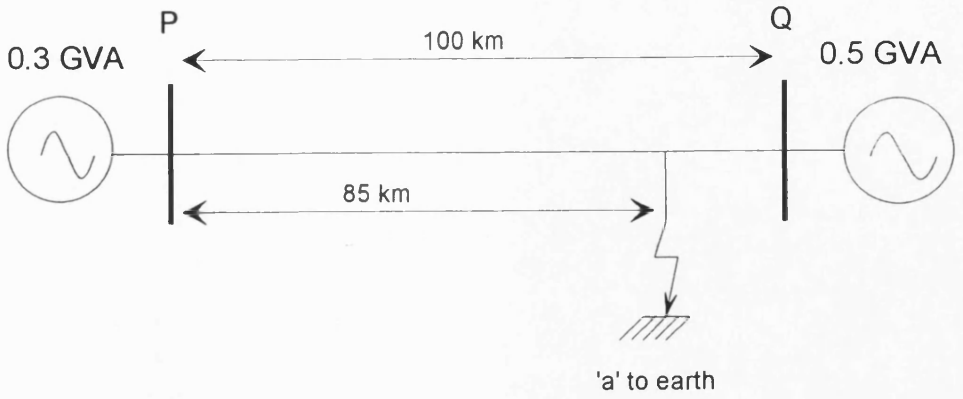

Figure 5.24 Power system configuration used to study the influence of additive noise on the measuring algorithm's performance.

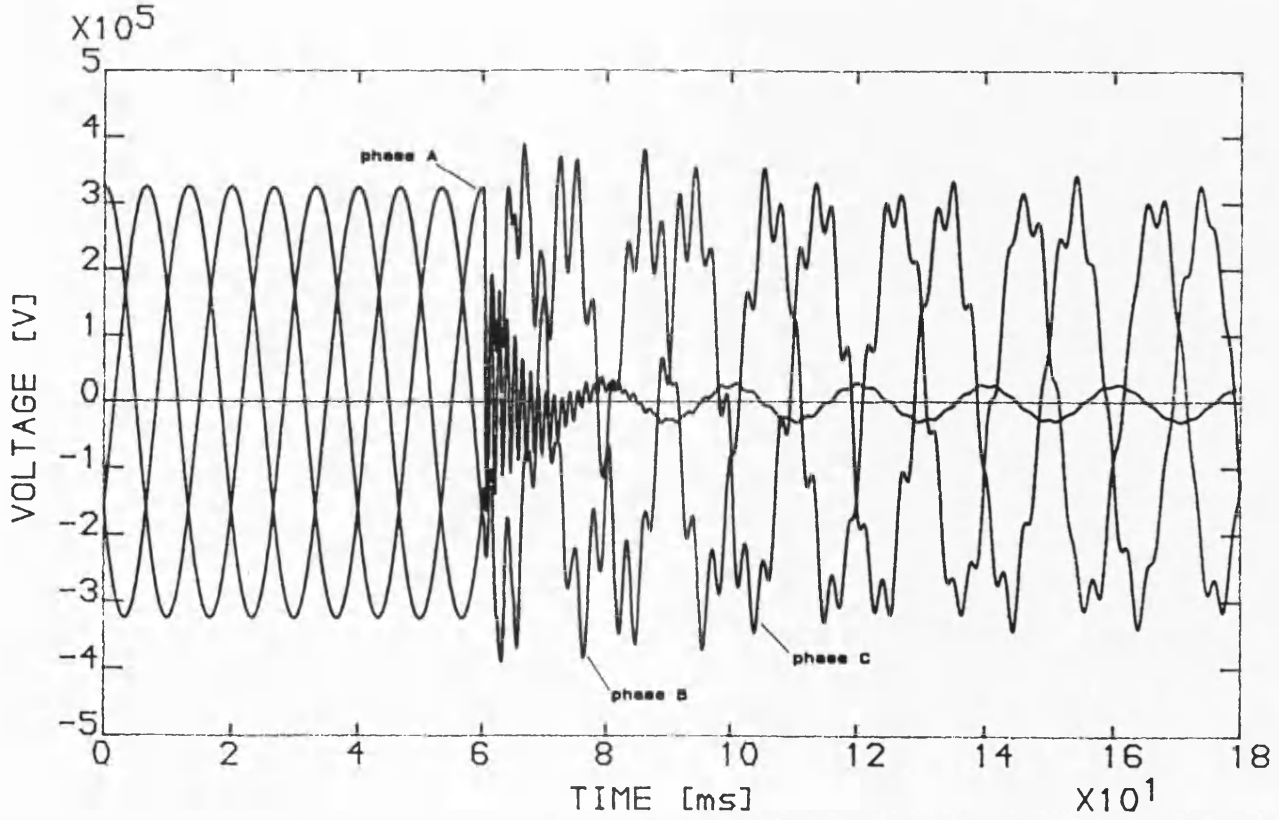

Figure 5.25 Voltage waveforms observed at bus P, phases 'a', 'b' and 'c'.

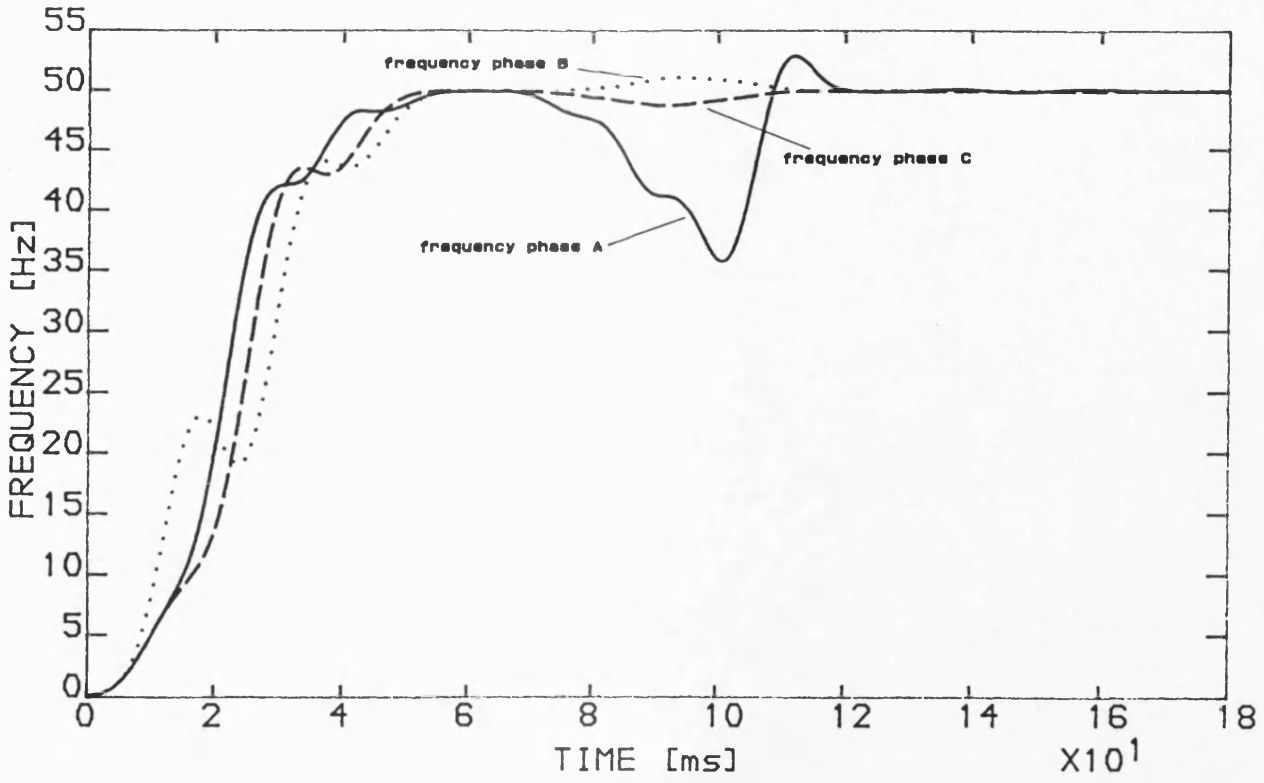

Figure 5.26 Frequency measured at bus P, phases 'a', 'b' and 'c'.

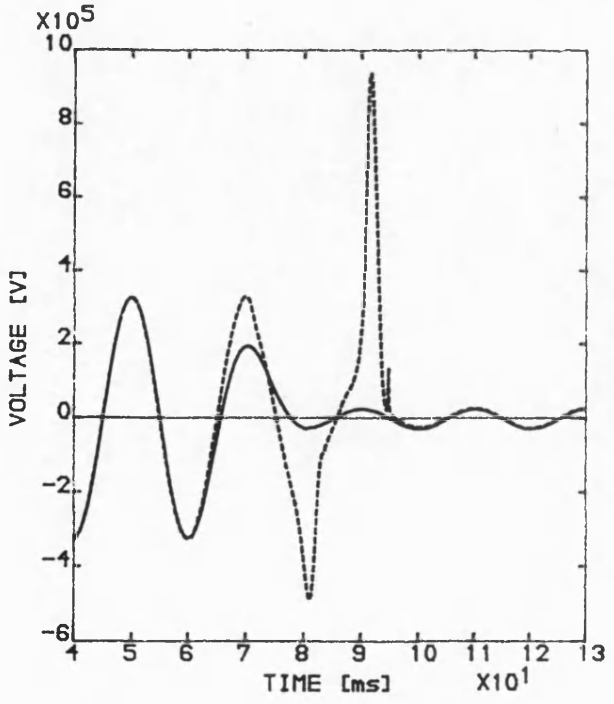

Figure 5.27 Voltage waveform, phase 'a' (solid line) and its in-phase component (broken line) at the fault inception.

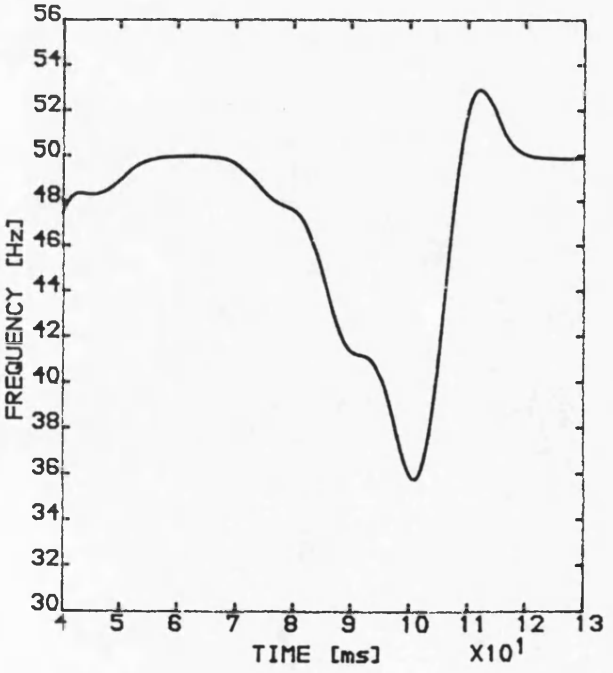

Figure 5.28 Measured frequency of Figure 5.27.

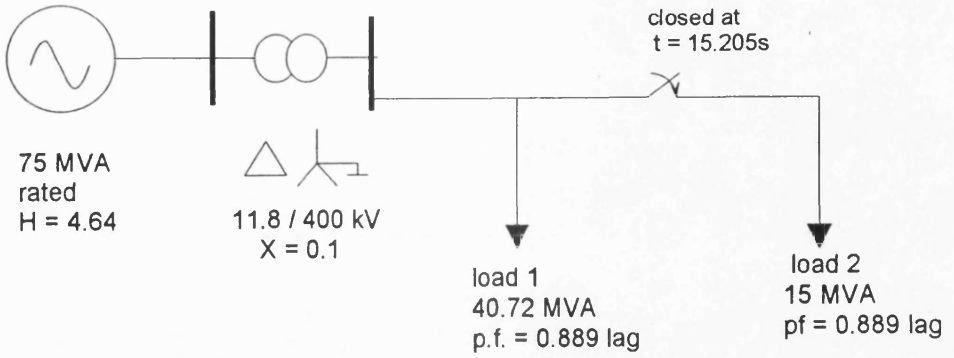

Figure 5.29 Single machine power system configuration used for the study of load changing conditions.

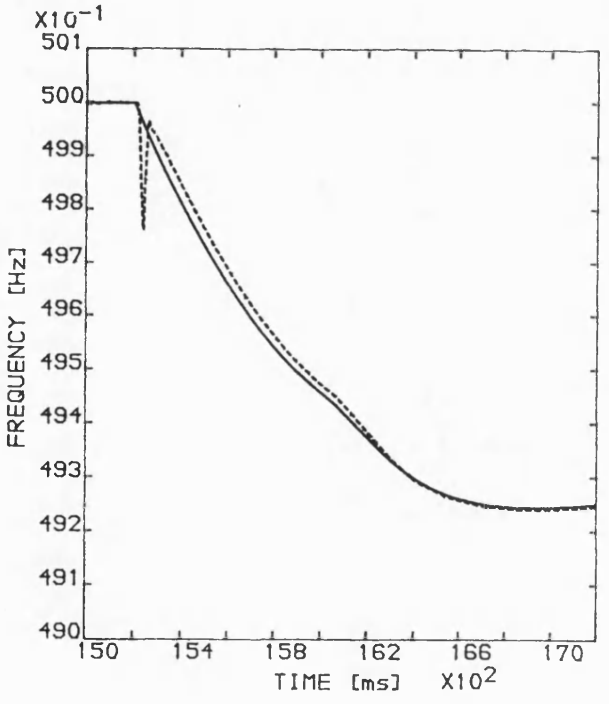

Figure 5.30 Rotor speed (solid line) and measured frequency (broken line) during the 20% additional load case.

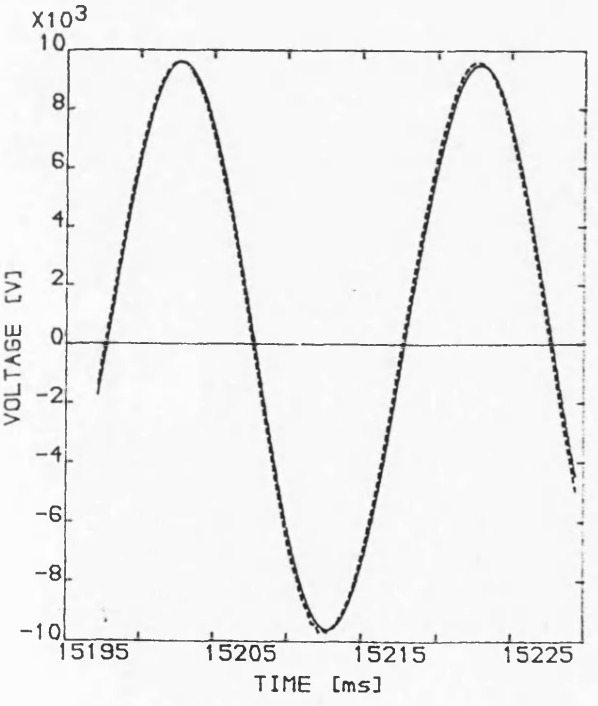

Figure 5.31 Input signal (solid line) and its in-phase component (broken line) during the application of the additional load.

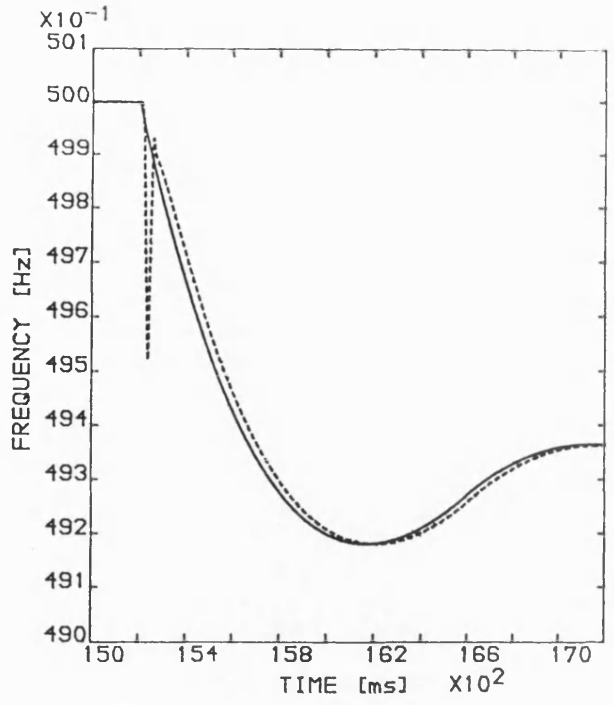

Figure 5.32 Rotor speed (solid line) and measured frequency (broken line) during the 40% additional load case.

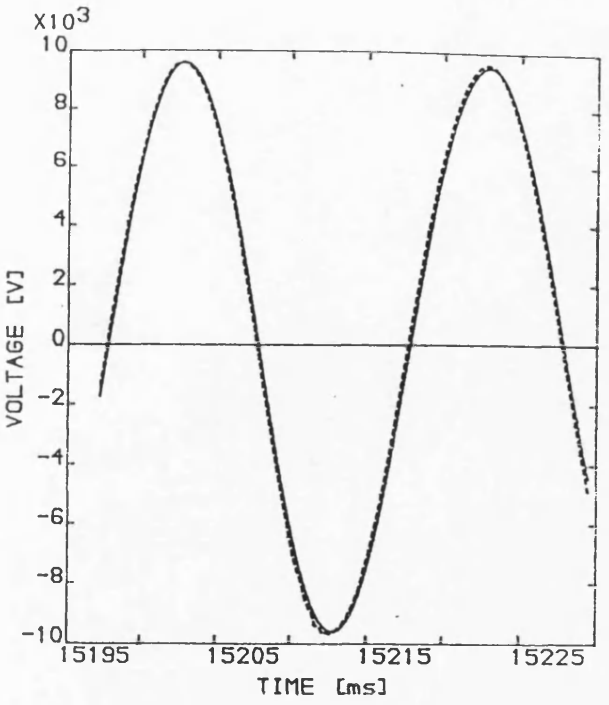

Figure 5.33 Input signal (solid line) and its in-phase component (broken line) during the application of the additional load.

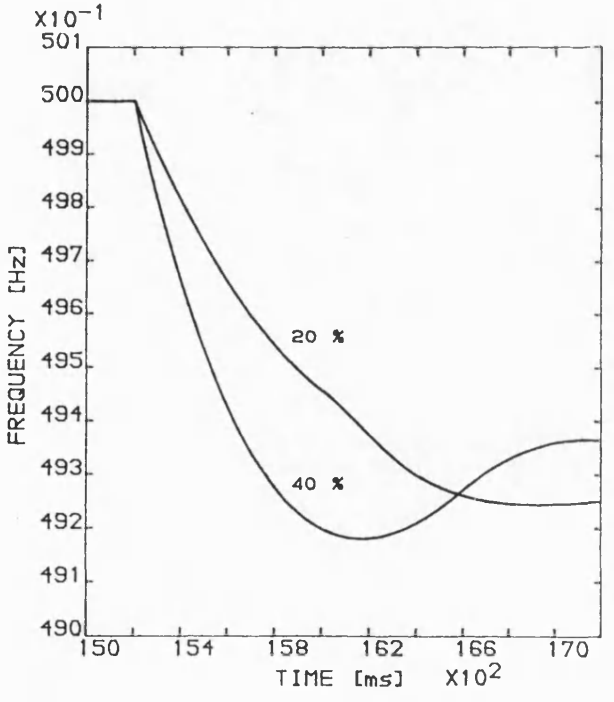

Figure 5.34 Rotor speed during the 20% and 40% changes of load.

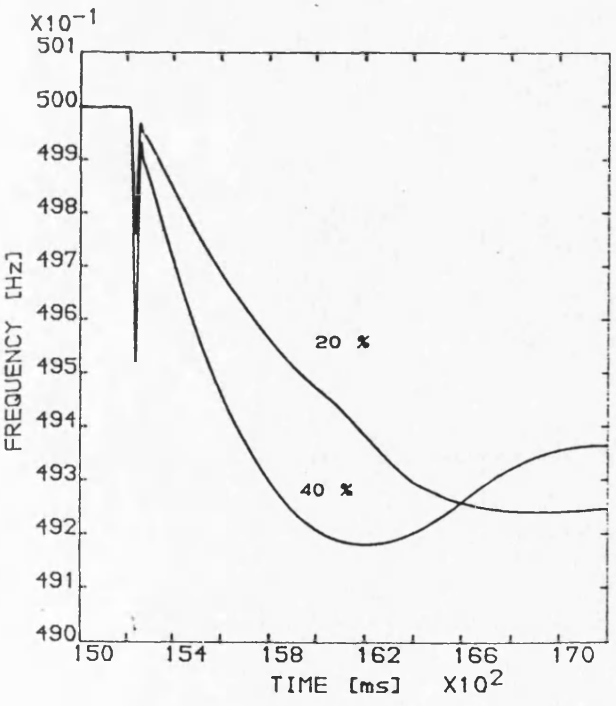

5.35 Measured Frequency during the 20% and 40% changes of load.

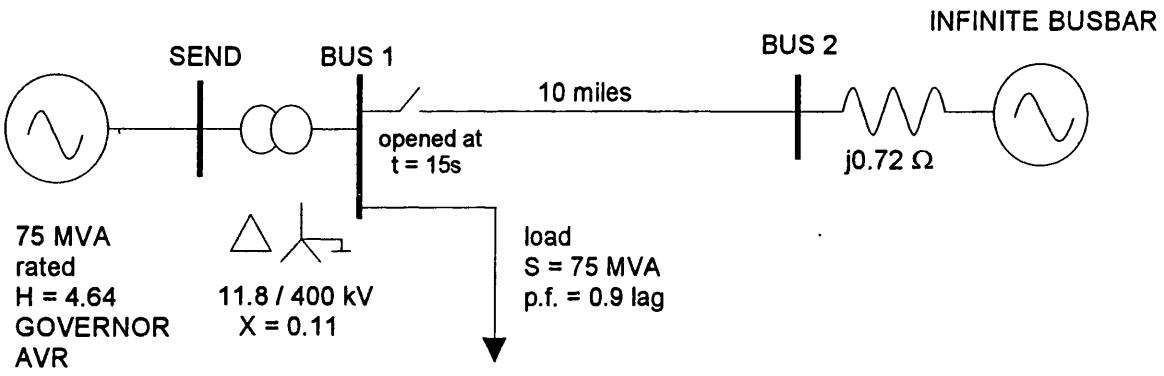

Figure 5.36 System configuration used for the study of the separation of a single machine from the grid.

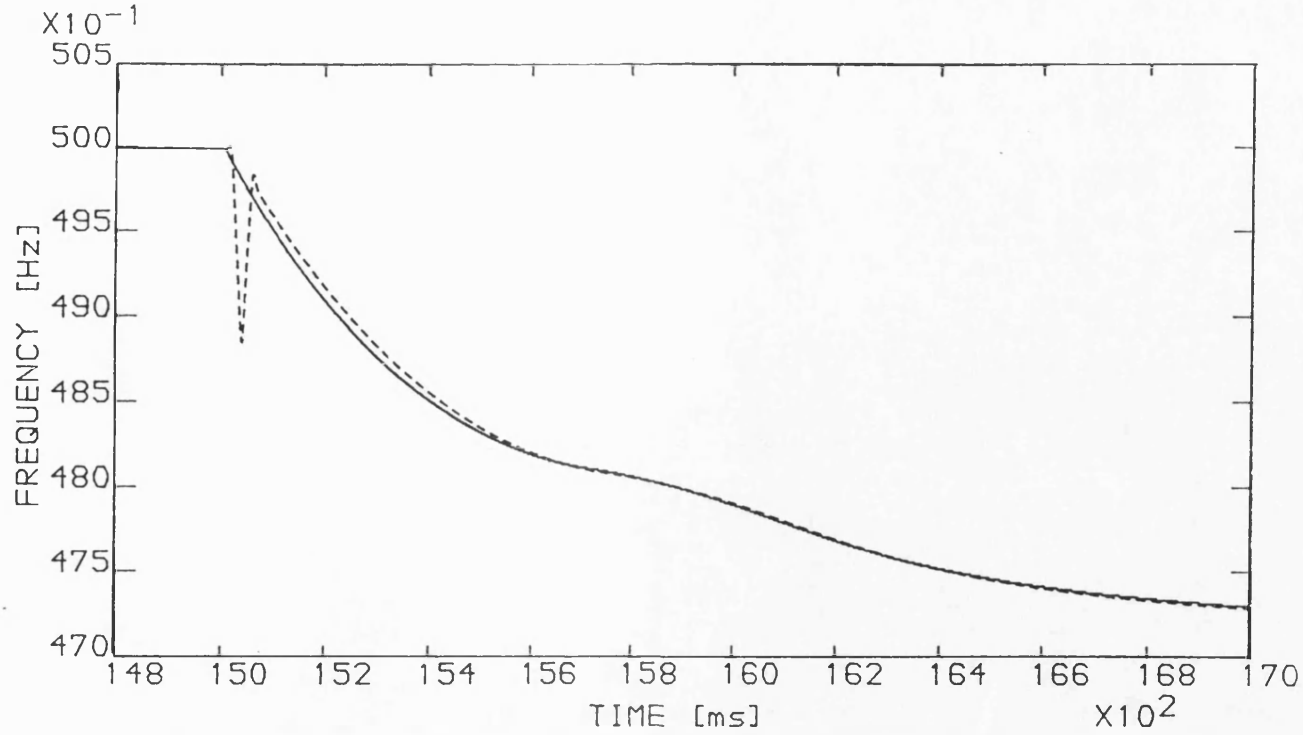

Figure 5.37 Rotor speed (solid line) and measured frequency from the generator terminal voltage, phase 'a' (broken line), following the separation of the generating unit from the grid.

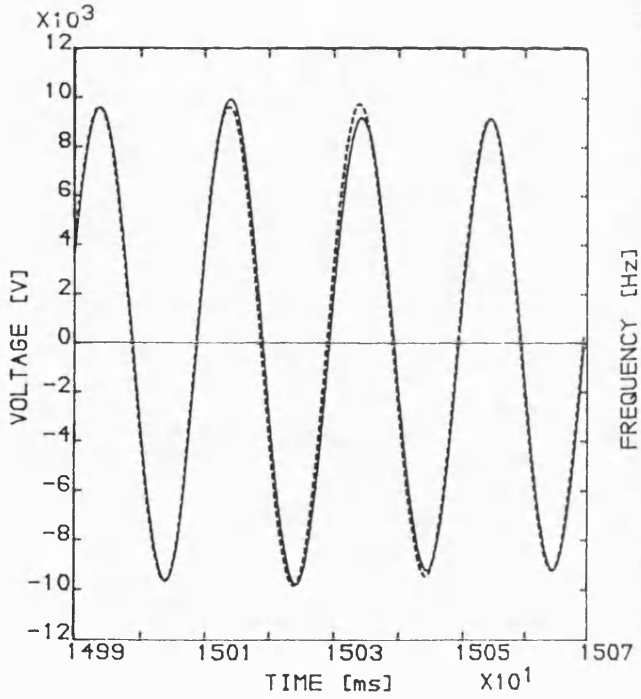

Figure 5.38 Terminal voltage waveform, phase 'a' (solid line) and its in-phase component (broken line) during the time of the separation.

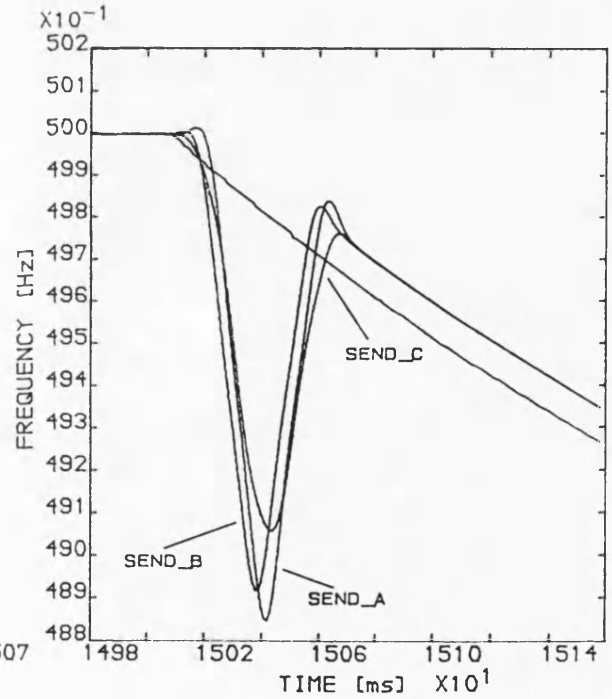

Figure 5.39 Rotor speed and the measured frequency for each of the three phases at the terminal voltage side.

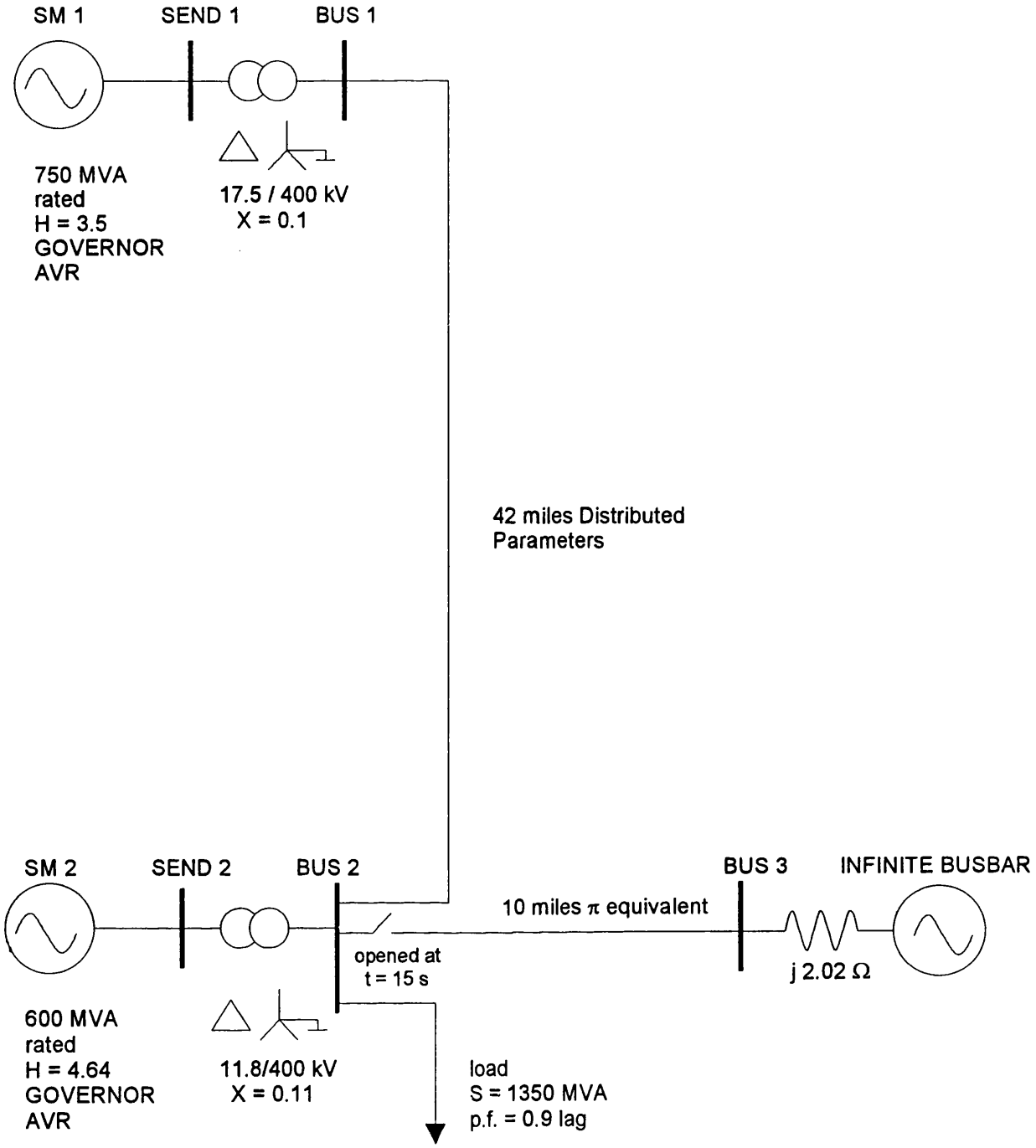

Figure 5.40 System configuration used to study the separation from the grid of two interconnected generators supplying a local load.

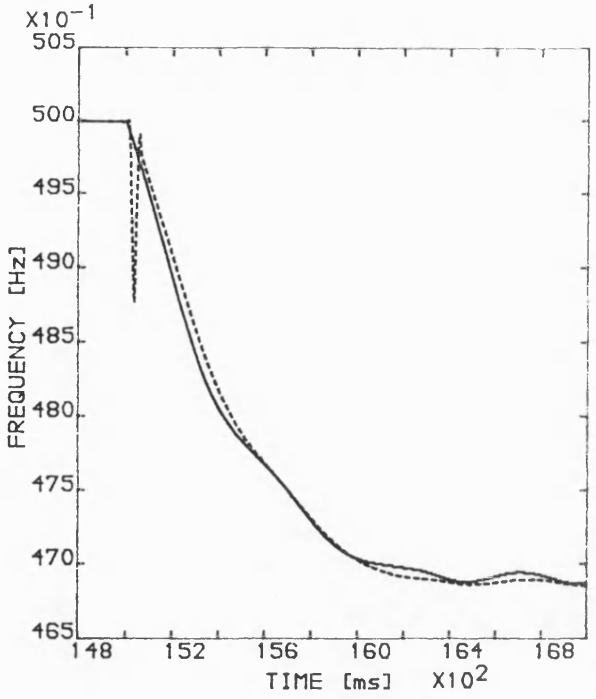

Figure 5.41 Rotor speed (solid line) and the frequency measured at bus SEND 1 (broken line).

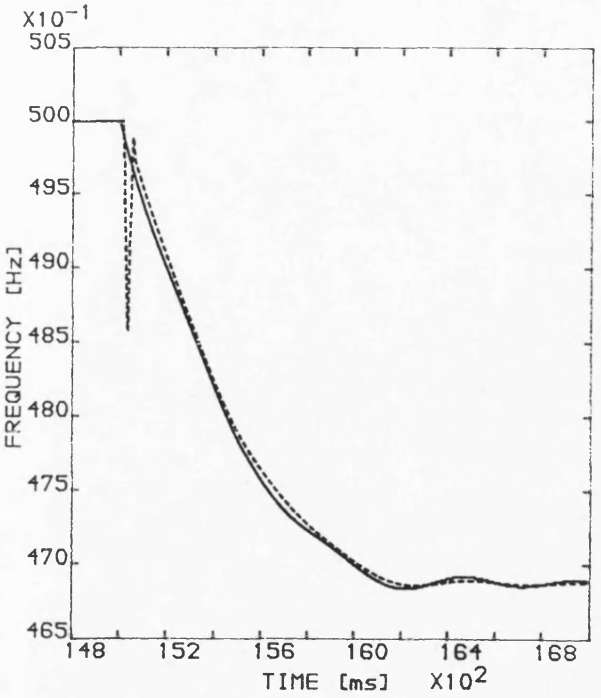

Figure 5.42 Rotor speed (solid line) and the frequency measured at bus SEND 2 (broken line).

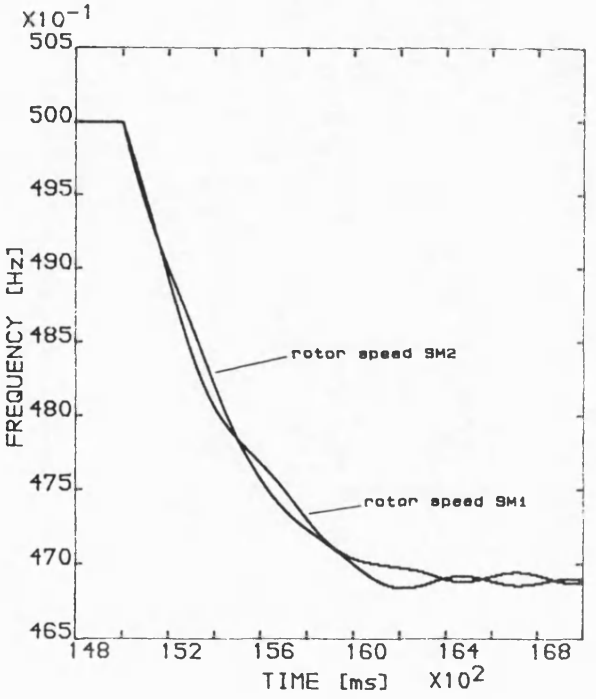

Figure 5.43 Rotor speed of the generators at SEND 1 and at SEND 2.

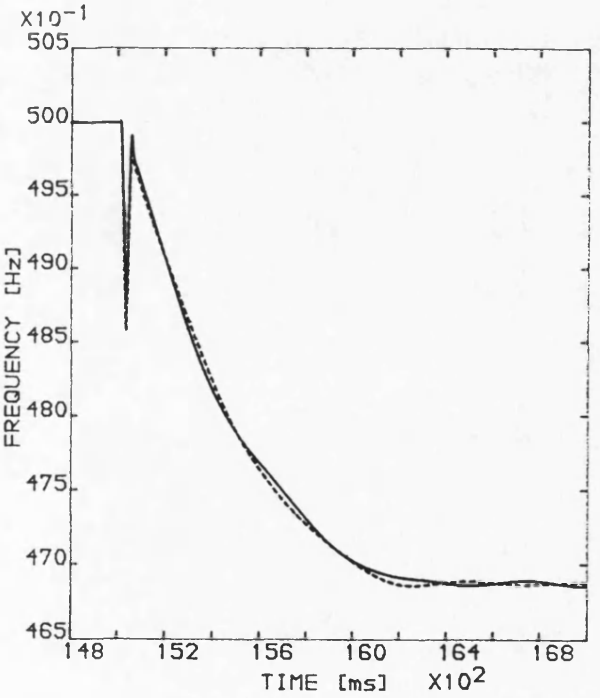

Figure 5.44 Frequency measured at buses SEND 1 (solid line) and at SEND 2 (broken line).

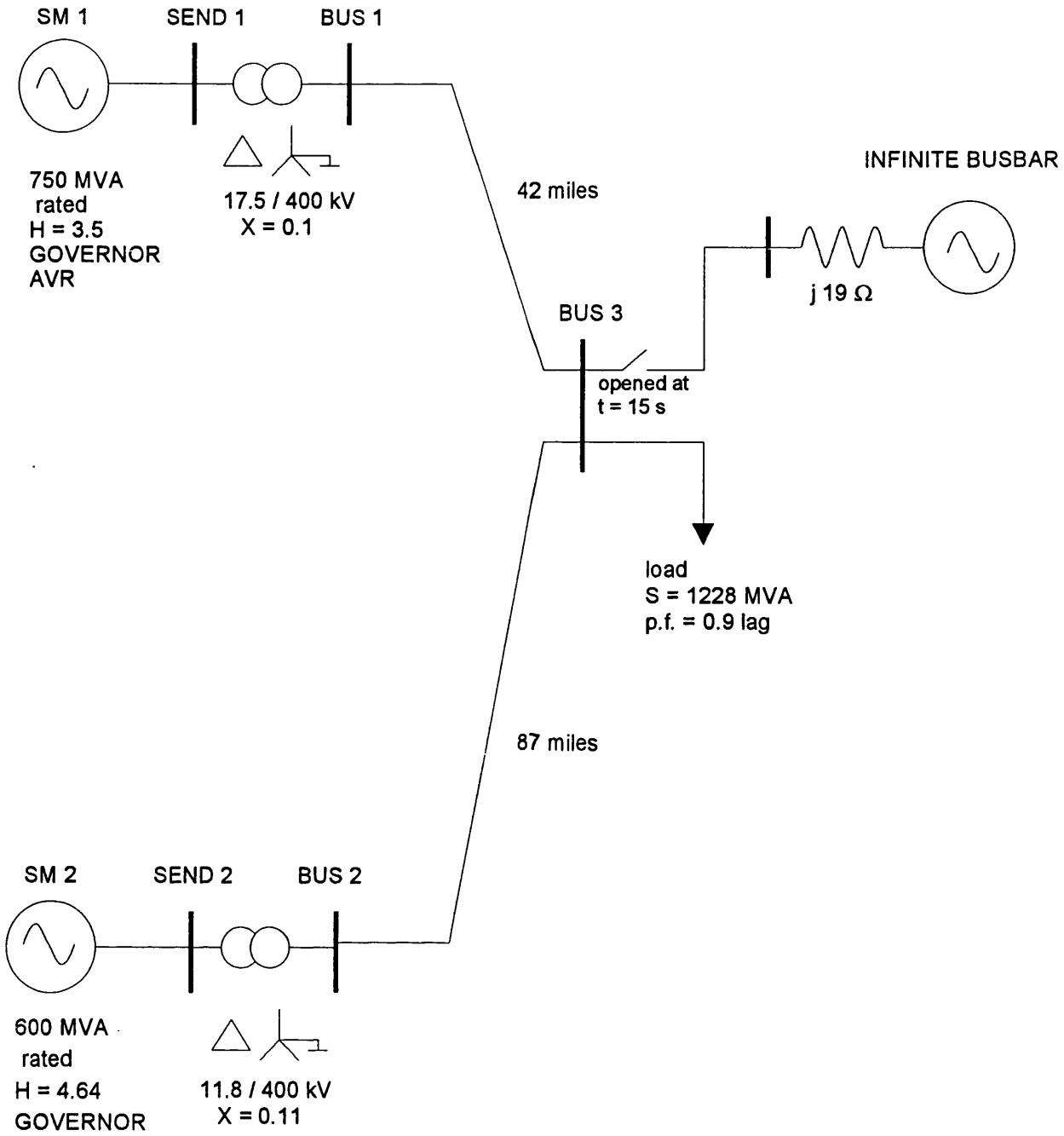

Figure 5.45 System configuration used to study the separation from the grid of two interconnected generators supplying a load at the remote end.

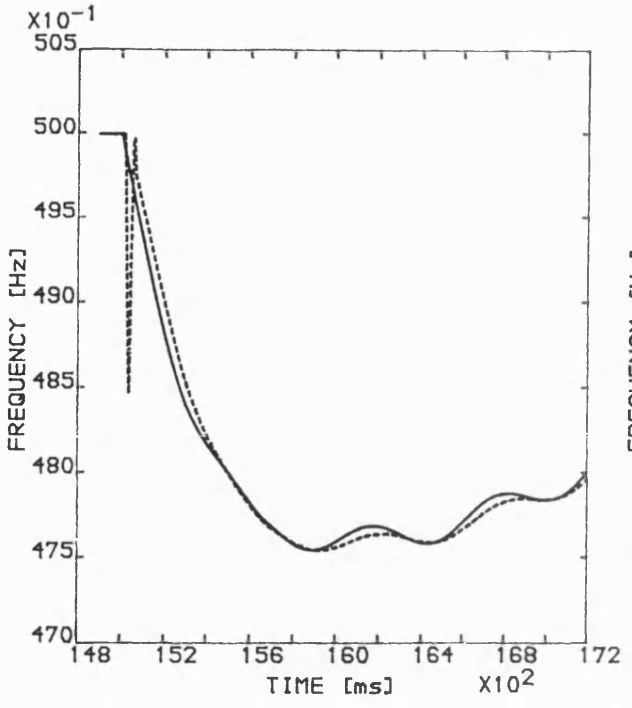

Figure 5.46 Rotor speed (solid line) and the frequency measured at bus SEND 1 (broken line).

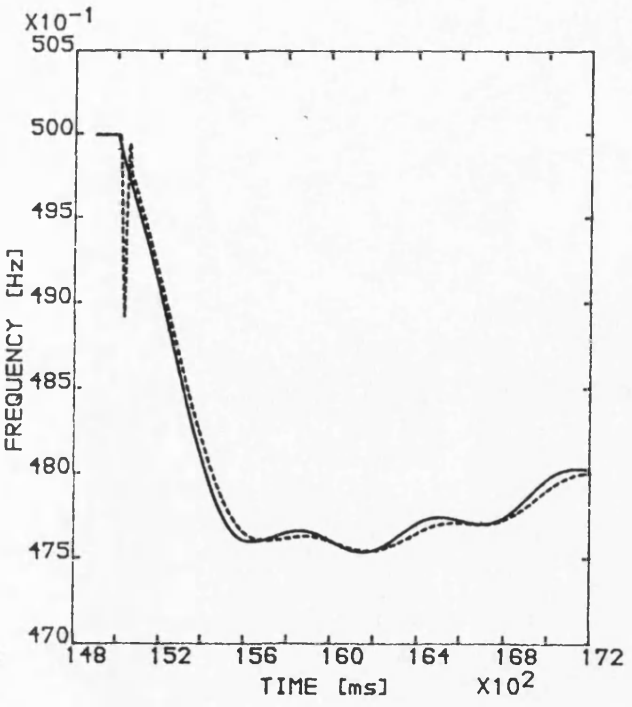

Figure 5.47 Rotor speed (solid line) and the frequency measured at bus SEND 2 (broken line).

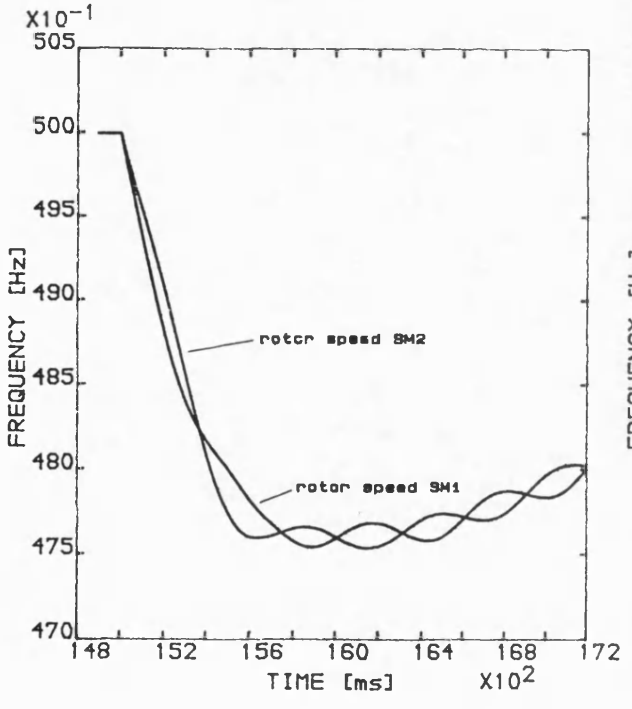

Figure 5.48 Rotor speed of the generators at SEND 1 and at SEND 2.

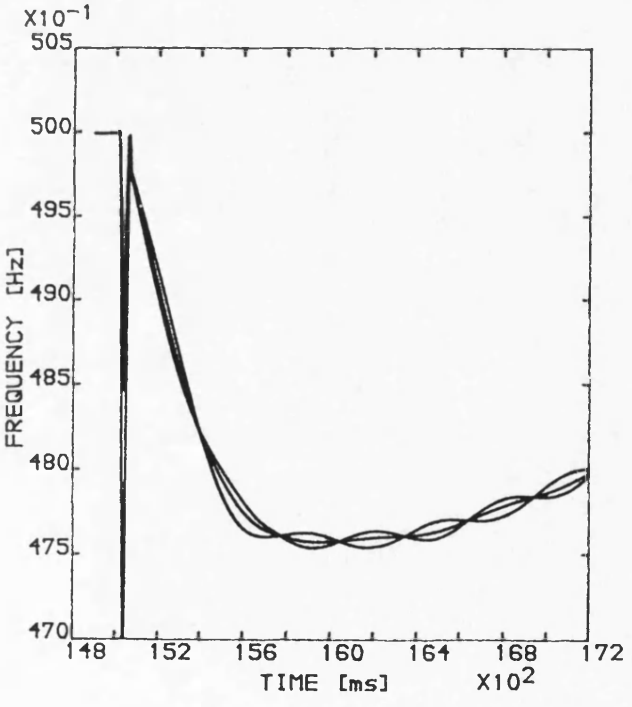

Figure 5.49 Frequency measured at buses SEND 1, SEND 2 and BUS 3.

CHAPTER 6

FREQUENCY MEASUREMENT FROM A POSITIVE PHASE SEQUENCE VOLTAGE VECTOR

The use of the frequency measuring algorithm for power system applications, will often have to deal with unbalanced conditions of the three phases system. The loss of one or more phases during a serious fault can cause such a situation. In this case, the magnitude of the phases and the angular displacement among the phases no longer correspond to a symmetrical system. Under these circumstances, the single-phase frequency measurement cannot function and is potentially dangerous if the correct operation of a power system depends on the correct measurement of frequency. On the other hand, the measurement of frequency can be accomplished from the positive phase sequence vector which is formed from the orthogonal components of the three phases of the observed system. In fact, during the most demanding conditions, the positive phase sequence vector is generally present so the reliability of the frequency measurements will remain undisturbed.

The measurement of frequency from a positive phase sequence vector, denoted as PPS frequency, has been developed and is presented in this Chapter. The input signals to the algorithm can be either voltage or current signals, but for most of the practical applications of the algorithm, voltage signals instead of current signals will be used to form the PPS vector. The in-phase and quadrature components of a PPS vector are obtained from the orthogonal decomposition of each one of the three phases of the input signal. Frequency estimates calculated from the orthogonal components of the PPS vector, correspond to the rotational speed of this vector provided that its orthogonal components are not corrupted by non fundamental frequency components. In this Chapter, the structure of the PPS frequency measurement algorithm will be firstly discussed. Secondly, a set of studies is presented where the performance of the PPS frequency measurement algorithm is ascertained. There is a particular interest on the observation of the performance of the PPS algorithm with respect of the single phase frequency measurement

algorithm. Thus, the group of simulations presented in this chapter follows the same cases presented in the previous Chapter. The performance of the filter when the three phase input signal does not comply with a symmetrical system is also investigated.

6.1 Measuring Frequency From a PPS Voltage Vector

From a system formed by the span of three vectors, **A**, **B**, and **C**, the positive phase sequence vector V_{PPS} of the system is given as:

$$V_{PPS} = \frac{1}{3}[V_A + e^{j\frac{2\pi}{3}} V_B + e^{j\frac{4\pi}{3}} V_C] \qquad (6.1)$$

where

$$e^{j\frac{2\pi}{3}} = \cos(\frac{2\pi}{3}) + j\sin(\frac{2\pi}{3}) \qquad (6.2.a)$$

$$e^{j\frac{4\pi}{3}} = \cos(\frac{2\pi}{3}) - j\sin(\frac{2\pi}{3}) \qquad (6.2.b)$$

The spatial decomposition of the vectors **A**, **B** and **C** is given as:

$$V_A = \sqrt{V_{A_i}^2 + V_{A_q}^2} \quad \tan^{-1}[V_{A_q} / V_{A_i}] \qquad (6.3.a)$$

$$V_B = \sqrt{V_{B_i}^2 + V_{B_q}^2} \quad \tan^{-1}[V_{B_q} / V_{B_i}] \qquad (6.3.b)$$

$$V_C = \sqrt{V_{C_i}^2 + V_{C_q}^2} \quad \tan^{-1}[V_{C_q} / V_{C_i}] \qquad (6.3.c)$$

The subscripts i and q denote the in-phase and quadrature components of the vectors, respectively. Equation (6.3) assumes that the orthogonal decomposition of the vectors **A**, **B** and **C** has been already accomplished. From equations (6.1) and (6.3), the orthogonal components of PPS vector are expressed as:

$$V_{PPS_i} = \frac{1}{3}\left\{V_{A_i} + \cos(2\pi/3)[V_{B_i} + V_{C_i}] + \sin(2\pi/3)[V_{C_q} - V_{B_q}]\right\} \qquad (6.4.a)$$

$$V_{PPS_q} = \frac{j}{3}\left\{V_{A_q} + \cos(2\pi/3)[V_{B_q} + V_{C_q}] + \sin(2\pi/3)[V_{B_i} - V_{C_i}]\right\} \qquad (6.4.b)$$

The development of the PPS frequency measurement algorithm is essentially based on the strategy followed in the single phase frequency measurement algorithm. A diagram of the structure of the PPS frequency measurement algorithm is given in Figure 6.1. The orthogonal components of the PPS vector are produced by using the orthogonal FIR filters. The outputs of these filters are compensated for the gain of their frequency response with respect of the running frequency. Then, new frequency estimates are calculated by the following equation:

$$f(n) = \frac{V_{PPS_q}(n)V_{PPS_i}(n-1) - V_{PPS_q}(n-1)V_{PPS_i}(n)}{2\pi/f_s\left(V^2_{PPS_i}(n) + V^2_{PPS_q}(n)\right)} \qquad (6.5)$$

Equation (6.5) is based on a one-sample backwards differentiation process. Details on the formation of the variables used in equation (6.5) are given in Appendix 13.

6.2.1 PPS Frequency of Amplitude/Frequency Modulated Signals

A three phase signal, with its amplitude and frequency being modulated by an exponential decaying pattern, is used as the input signal for the PPS frequency algorithm. The amplitude and frequency modulation processes are started at time t = 110 ms. The parameters of the input signal are the same as those used in the AM/FM study presented in the last Chapter and described in Figure 5.1. In the current simulation, the amplitude and phase angle of the phases of the input signal correspond to a symmetrical system. As it was described in the previous Chapter, the reference frequency of the input signal is given in equation (5.3).

The PPS frequency measured from this input vector is displayed in Figure 6.2 together with the reference frequency. The PPS frequency is seen to follow the track of the reference frequency. Figure 6.3 shows a closer view of the waveform of the

three phases of the input signal about time t = 110 ms. The steep reduction of the amplitude is seen to produce a greater effect on phases 'b' and 'c' than on phase 'a'. This figure shows that the angular phase of each one of the three components of the input signal has been stretched by the simulated fault. This phase stretching effect is more evident in phases 'b' and 'c'. The measured frequency from the PPS vector exhibits the effects of the variations in the angular phase of the orthogonal components of the three phase input signal. As a result of this effect, a transient excursion of the measured PPS frequency is created, as shown in Figure 6.2. The same figure also shows a second overshoot of the measured PPS frequency going above the reference frequency. This positive excursion results from the speeding up transient of the orthogonal components attempting to gain track of the input signal after the phase stretching transient.

Figure 6.4 displays the frequency measured from a PPS vector when one of the phases of the input signal is set to zero. In this case, phase 'a' has been set to zero. Apart from the magnitude of the overshoot of the frequency at the time of the fault, which is bigger than in the three phases case, the PPS measured frequency accurately follows the reference frequency. In the following experiment, phases 'a' and 'b' have been set zero, as shown in Figure 6.5. Now, the PPS frequency measurement corresponds to the frequency of phase 'c' alone. A comparison among the last three figures renders no difference in the trace of the measurement of frequency when the PPS vector is disturbed by the lost of one or two phases in the input signal.

The frequency measured from a PPS vector formed by a signal with an exponential decaying amplitude but constant frequency, is displayed in Figure 6.6. The parameters of the amplitude modulation pattern are the same as those given in the preceding simulation. A comparison of the measured PPS frequency against the single phase frequency measurement shown in Figure 5.8 in the last Chapter, reveals that both frequency estimates accurately follow the 50 Hz frequency of the input signal. It is noticed that the PPS frequency exhibits an overshoot at the time of the fault which is higher than the overshoot of the single phase frequency. In fact, the

magnitude of the PPS frequency is equal to the overshoot of the PPS frequency presented in the previous study case shown in Figure 6.2. This effect is entirely due to the sudden reduction of the amplitude at time $t = 110$ ms.

The PPS frequency measurement algorithm was tested against an input signal with constant amplitude but with a frequency modulated by a sinusoidal process. The period of the sine frequency modulation process is 2 Hz, and the maximum excursion of the fundamental frequency of the input signal is 1 Hz about 50 Hz. The input signal exhibits symmetrical conditions in the three phases. The effects of the frequency modulation process are started at time $t = 100$ ms. Figure 6.7 shows the PPS frequency measured in this study. It can be seen that the PPS frequency follows the oscillatory nature of the fundamental frequency without lost of accuracy. As pointed out in Chapter 5, the sudden starting of the frequency modulation process in this simulation, produces a shorter period of the phase of the input signal. This effect is clearly shown in Figure 5.11 with respect of phase 'a'. Similar effects are produced in the other two phases. Thus, the PPS measured frequency also shows this angular phase transient following the time of the fault. Following the transient, the PPS frequency is seen to accurately follow the reference frequency. This experiment shows the ability of the PPS frequency measurement algorithm to track rapid variations of the frequency of the input signal.

6.2.2 PPS Frequency of Signals Corrupted by Additive Noise

The presence of non fundamental frequency components in the observed signal has been discussed in the preceding chapters with respect of their influence on the single phase frequency measurement algorithm. In this study case, a three phase input signal corrupted by harmonics of the fundamental is used to ascertain the performance of the PPS frequency measurement algorithm. The fundamental frequency of the input signal is drifted away by an exponential decaying pattern, so its harmonics are proportionally falling into the frequency response of the orthogonal filters. In Chapter 5, a one-cycle lowpass Hamming filter was used to pre-filter the input signal for the single phase frequency measurement. As shown in Figure 6.1,

the pre-filtering stage uses similar lowpass filters on the three phases of the input signal before their arrival to the orthogonal decomposition stage.

Figure 6.8.a shows the PPS frequency measurement of a symmetrical three phases signal being corrupted by the first nine harmonics of the fundamental. The levels of the harmonics are the same as those given in section 5.1.2 of the last Chapter. The waveform of the signal, like the waveform displayed in Figure 5.13, is the same for each one of the three phases of the input signal. In the current study, the PPS frequency is compared against the single phase frequency measurement. The traces of both frequencies are displayed in Figure 6.8.a by a broken line and by a solid line, respectively. It is seen that the PPS frequency is less affected by the presence of the harmonics as compared to the single phase frequency measurement. The fact is that the presence of the harmonics is equally experienced by each one of the phases of the input signal, particularly when the fundamental frequency has fallen below 47 Hz. The symmetrical distribution of the angular displacement among the three phases of this particular input signal is the responsible for the cancellation of the effects of the harmonics in the formation of the PPS vector. It can be said that the PPS frequency measurement approaches the average in time and space of the three individual single phase frequency measurements. In order to provide a better understanding, the same experiment was repeated, but this time, the Hamming pre-filter was removed from the PPS frequency measurement structure. The results from this experiment showed that the resulting measured frequency is greatly affected by the harmonics intruding the frequency response of the orthogonal filters. That is, the formation of the PPS vector conveys information which does not correspond to the fundamental frequency of the input signal. It should not be necessary to report the results of this particular study since the previous reasoning should be sufficient.

In the following two experiments, the performance of the PPS frequency measurement is assessed for the case of an unsymmetrical components three phase input signal. Extremely demanding conditions can be expected from the use of the PPS frequency measurement algorithm for its application in power systems concerning the fact that unbalanced systems are likely to be observed. The

occurrence of a severe fault in the power system will certainly create such conditions. However, a simple monitoring structure for applications in power system protection schemes, may involve the use of transducers and signal conditioning devices exhibiting different gain and phase delay among themselves.

In the next two studies, the input signal has been designed to undergoing a change in the magnitude of the three phases and a change in the angular displacement among the phases. In the first instance, Figure 6.8.b shows the waveform of the three phases of an input signal corrupted by harmonics, where the amplitude of the phases has been modified: phase 'a' is set to 100%, phase 'b' to 50% and phase 'c' to 10%. In this simulation, the angular displacement among the phases of the input signal remains undisturbed. The PPS frequency measured from this input signal is displayed in Figure 6.8.c together with the reference frequency of the input signal. The effect of the intrusion of the second harmonic in the frequency estimates can be appreciated when the fundamental frequency falls below 47 Hz. Even when the angular displacement among the phases corresponds to a symmetrical set, the higher energy contents of harmonic noise of phase 'a' limits the averaging effects of the formation process of the PPS vector.

In the second instance, the same difference in the amplitude of the phases is used. In this case, however, the phases show a different angular displacement among themselves: phase 'a' = +30°, phase 'b' = 0° and phase 'c' = 5° In Figure 6.8.d are shown the waveforms of the three phases. The PPS frequency measured from this input signal is shown in Figure 6.8.e. This frequency exhibits a ripple below 47 Hz with a similar magnitude but with a different phase as compared to the frequency shown in Figure 6.8.c. The effects of the different angular displacement are appreciated at the bottom of this figure which show a PPS frequency with a different phase as compared to the PPS frequency shown at the bottom of Figure 6.8.c.

The results of this study show that the PPS frequency will be insensitive to harmonic noise provided that the three phases of the input signal corresponds to a symmetrical phase system. This requirement is far away from real power system applications.

However, the PPS frequency measurement has shown to cope well with the influence of harmonics noise up to 47 Hz.

6.3 Power System Simulations

It is aimed in this section, to ascertain the performance of the PPS frequency measurement algorithm for its application in power system frequency measurements. The set of power system simulations used in the last Chapter will be used in the present section in order to provide a direct form of comparison of the performance of the PPS frequency algorithm against the results obtained during the assessment of the performance of the single phase frequency measurement algorithm.

6.3.1.1 Power Swing Study Case

It has been reported in the last Chapter, the ability of the single phase frequency measurement algorithm to describe the rapid change of the frequency of a system during the occurrence of power swing conditions. The present study case discusses the results of the measurement of frequency from the PPS voltage vector. The system configuration used in the present study is depicted in Figure 5.19. The three phases of the generator terminal voltage at busbar P, are taken as the input signal to form the PPS voltage vector. In this simulation, the phases of the input signal correspond to a symmetrical vector. Thus, the voltage waveforms of the three phases follow the same waveform pattern shown in Figure 5.20.

The frequency measurement from the PPS voltage vector is shown in Figure 6.9. The vertical axis in this figure has been bounded between 40 and 60 Hz to enhance the results. It is seen that the PPS frequency follows the same trace described by the single phase frequency measurement showed in Figure 5.21. It is also appreciated that the PPS frequency measurement is smoother as shown at the time of the clearance of the fault and also at each one of the pole slip events. This smoothing effect is produced during the formation of the PPS vector and results from the change in the amplitude and angular phase of each one of the phase components of

the input signal. It is noticed that the PPS frequency clearly reflects the behaviour of the power system frequency observed at busbar P. That is, the occurrence of a fault at a given point along the system and its consequences on the remaining elements of the system, can be described in a very consistent way by the measurement of the PPS frequency.

6.3.1.2 Induced Travelling Wave Noise Study Case

The simulation of a severe unbalanced system was presented in Chapter five during the study case of induced travelling wave noise. The system configuration used for this instance is depicted in Figure 5.24. As a result of the single phase to earth fault close to the remote end of the system, the two healthy phases at bus P show the induced travelling wave noise imposed on their respective waveforms. From Figure 5.25, it is seen that the frequency contents of the imposed noise are mainly dominated by the odd harmonics of the fundamental. As pointed out in Chapter 5, the current simulation does not correspond to an electromechanical simulation, hence the system's frequency is not expected to change. From the results of the single phase frequency measurement, it was shown in the last Chapter the effects of the fault on the three phases of the terminal voltage of the generator at bus P, that is, the rotational speed of the angular phase of the three phase components showed an stretching effect following the fault inception. The corresponding frequency measurements displayed a negative dip in the frequency trace of phases 'a' and 'c', whereas phase 'b' suffered an opposite effect.

For the present study, the results of the measurement of frequency from the PPS voltage vector taken at busbar P are shown in Figure 6.10. It is noticed that the PPS frequency does not follow the average trend of the single phase frequency measurements as displayed in Figure 5.26. In fact, the PPS frequency exhibits a very small undershoot at the fault inception compared to the transients produced in the single phase frequency measurements. Particular attention is drawn to the next overshoot of the PPS frequency, shown in Figure 6.10 about time t = 90 ms, which does not to correspond to the combination of the single phase frequency

measurements. This positive excursion of the PPS frequency is due to frequency trace described by the healthy phases 'b' and 'c' whose amplitude is higher than the amplitude of the faulty phase 'a'. It can be noticed from Figure 6.10, that the starting point of the overshoot of the PPS frequency corresponds to the time when the frequency of phase 'b' is recovering from the fault as shown in Figure 5.26. It is also seen in Figure 6.10, that the PPS frequency displays a second step in the positive excursion about time t = 100 ms which exactly corresponds to the time when the frequency of phase 'a', as shown in Figure 5.26, is also recovering from the fault.

From the results obtained in this study case, it can be seen that the measurement of frequency of the PPS voltage vector reflects, in a closer way, the genuine change in the system during the fault conditions.

6.3.2 Power System Simulations with the EMTP

The simulation of different power system conditions by using the EMTP and the measurements of frequency from a single phase voltage signal have already been discussed in Chapter 5. The trace of the rotor speed of the generating units in the EMTP simulations provided a direct means of reference for ascertaining the performance of the frequency measurement algorithm. The same collection of simulations will be used in this section to investigate the measurement of frequency from a PPS voltage vector.

6.3.2.1 Simulation of Load Changing Conditions

In this study, an additional load is connected to a small generating unit. This study case corresponds to the system configuration given in Figure 5.29. Initially, the machine is loaded to 40.72 MVA. The machine is assisted by a speed governor system and by an automatic voltage regulator. In the cases presented in this section, symmetrical conditions will prevail. The measurement of the frequency of the PPS voltage vector is carried out at the generator terminal voltage.

In the first instance, an additional load is 15 MVA which corresponds to a 20% of the generator's rating is connected to the generator terminals. The switch connecting the generator with the load is closed at time t = 15.205 s. In Figure 6.11 are shown the generator rotor speed as taken from the EMTP results and the PPS frequency measured from the three phases input signal at the generator terminal voltage. After the transient following the fault inception, this figure shows the PPS frequency following the rapid decline of the rotor speed. The PPS frequency is compared against the single phase frequency measurement (broken line) in Figure 6.12. The single phase frequency measurement shown in broken line in this figure corresponds to the simulation shown in Figure 5.30 discussed in Chapter 5. Both frequencies describe a slightly different trace during this transient, *i.e*: the PPS frequency follows the combined trend of the frequency of the three phases. It is seen in Figure 6.12, that after the transient, the PPS frequency and the single phase frequency follow the same course.

A similar performance of the PPS frequency measurement is observed for an additional load of 40 % of the generator's rating. Figure 6.13 displays the trace of the PPS frequency measured during the two load changing simulations. The trace of the PPS frequency closely follows the trace of the rotor speed in both cases.

6.3.2.2 Separation of a Single Generating Unit from the Grid

In this simulation, a small rating machine is disconnected from the utility. The configuration of the system used for the current study was given in Figure 5.26 in the last Chapter. At the fault inception, the machine takes up a load equal to its full rating. In this study case, the measurement of the frequency of the PPS voltage vector has been carried out at both the low voltage and at the high voltage sides of the generator transformer. The different effects of the resulting overload at the time of the separation are shown in Figures 6.14 and 6.15, for the measurements of frequency at the generator terminal voltage and at the high voltage side of the generator transformer, respectively.

The transient of the PPS frequency observed at the high voltage side of the transformer, clearly reflects the impact of the fault on the rotational speed of the PPS vector. The abrupt change onto a full export condition results in a transient in the rotation of the angular phase of the PPS voltage vector at this node which is followed by the rotational speed of the generator. In Figure 6.16 are displayed the traces of the PPS frequency measured at both sides of the generator transformer. Due to the redistribution of power in the isolated generating unit, it is noticed that the magnitude of the frequency transient is proportional to the magnitude of the fault; the solid line corresponds to the frequency of the PPS vector observed at the transformer low voltage side.

The PPS measured frequency and the single phase frequency measured from the three phases at the generator terminal voltage are shown in Figure 6.17. The PPS measured frequency is shown by a broken line. It is seen that the PPS frequency follows the average trend of the single phase frequencies. This figure illustrates the time of separation of each one of the phases and the resulting transient in the single phase frequency measurements observed during the fault event.

6.3.2.3 Separation of Two Interconnected Generators from the Grid

The measurement of frequency of the PPS voltage vector during the separation of two interconnected machines from the grid is presented in this section. Two different study cases are presented in this section. The machines used in the simulations have a similar rating but a different inertia time constant. Both machines are assisted by speed governing system and by an automatic voltage regulator.

6.3.2.3.1 Local Load Study Case

This study case presents two generating units supplying a local load, and so the effects of the separation are expected to produce a severe impact on the behaviour of the islanded system. The configuration of the system used for this study is shown in Figure 5.40. A transmission line with a length of 42 miles connects both

generators. The machine at the far end is rated at 750 MVA and the second generator, connected at the load bus, is rated at 600 MVA. Initially, the infinite busbar infeed is 46.67% of the load, whereas the generators at buses SEND 1 and at SEND 2 are supplying 22.27% and 31.11% of the load, respectively. At the time of the separation the two machines take up a load equal to the total rating of the machines. Thus, the available reserve capacity of the generators during the pre-fault conditions will be consumed to overcome the overloading at the time of the separation.

The results from the measurement of the frequency of the PPS voltage vector at both ends of the separated system are shown in Figures 6.18 and 6.19. The change in the rotor speed of both generators is also shown in these figures. It is seen that the PPS measured frequency follows the track of the rotor speed in both cases. A comparison against the results from the measurement of frequency from a single phase can be made from Figure 5.44. The only difference between the PPS frequency and the single phase frequency measurements appears at the time of the fault inception when the PPS frequency exhibits a shorter transient. This effect results from the combined variations of the angular phase of the components of the input signal as it was already discussed in the previous study case. The subsequent power swings between the isolated generators are clearly shown by the trace of the PPS frequency measured at both ends of the system as shown in Figure 6.20.

6.3.2.3.2 Remote Load Study Case

The system configuration used for the present study is taken from Figure 5.40 in Chapter five. In this simulation, two generators are connected to an infinite source by two relatively large transmission lines. The load is located at the node where the two generators are connected with the grid. This study case is intended to observe the measurement of frequency of the PPS voltage vector formed at the terminal voltage of both generators and also, at the remote load busbar during the time when the system becomes separated from the infinite busbar. The details of this simulation have already been discussed in Chapter five.

For the present study, the results of the measurement of frequency of the PPS voltage vector are displayed in figures 6.21, 6.22 and 6.23. In Figure 6.21, the PPS frequency measured at bus SEND 1 is seen to follow the generator rotor speed very closely following the fault. The initial rate of decay of system's frequency is clearly shown by the PPS frequency. Figure 6.23 shows the power swings between the generators following the separation from the utility.

The frequency measured from the PPS voltage vector formed at the load busbar is shown in Figure 6.23. This figure shows the effects of the proximity of the overload on the transient of the rotational speed of the PPS voltage vector. It was shown in the previous paragraph, that the PPS frequency measured at each one of the generating units revealed the change of the power transfer between the two machines following the separation. The frequency of the PPS voltage vector at the load busbar shows now an almost linear trace. In this figure, it is shown that the PPS frequency at the load busbar follows the average of the PPS frequency measured at the other ends of the islanded system.

This study case shows the reliability of the measurement of frequency from a PPS voltage vector for its use in underfrequency and load shedding scheme applications at a substation located far away from a generating centre. In such a case, the local load is being supplied by a power vector rotating at the frequency of the PPS voltage vector which is following the variations of the average transfer of power in the system.

6.4 Summary

The formation of a PPS vector is accomplished by the contribution of the orthogonal components of each of the phase components of the input signal vector. The magnitude of the PPS vector is proportional to the combined magnitude of the phase components, whereas the rotational speed of the PPS vector is proportional to the variation in time of the phase velocity of the phase components. This basic theory has supported the investigation of the measurement of frequency of a PPS vector in

this Chapter.

In the first study cases presented in this Chapter, the influence of amplitude modulation processes on the performance of the PPS frequency measurement algorithm was investigated. It has been observed that sudden changes in the amplitude of the three phases input signal resulted in transient oscillations of the measured PPS frequency which were not reflected by the trace of the reference frequency. These abrupt amplitude changes are entirely due to the progress of the simulation. However, the waveform of the input signal during the occurrence of these transients, has shown the nature of the transient in the angular phase of the phase components of the input signal. It has been shown that the transient exhibited by the PPS frequency corresponds to the variation of the angular phase of the input signal. The results presented at this stage, showed consistency with the results obtained from the single phase frequency measurement presented in the previous Chapter.

The measurement of the frequency of a PPS vector has shown to be insensitive to the case of a three phase signals with symmetrical phase components, as long as the magnitude of the components and the angular displacement among them do not vary in time. It has been shown that individual variations of these parameters will produce a change in the trace of the PPS frequency which will be modified by the contribution of the remaining phase components.

The study of the influence of harmonic noise on the frequency calculations has also been presented. For the case of an input signal with symmetrical components, the formation of the PPS vector removed the influence of the harmonics on the calculation of frequency. Although the amount of harmonics present in this simulation is unrealistic, the complimentary studies have shown that the frequency measurement algorithm can produce accurate estimates even when the fundamental frequency falls down to 47 Hz.

During the different power system condition cases presented in the second part of

this Chapter, it has been seen that the frequency measurement of a PPS voltage vector follows the trace of the frequency of single phase input signals provided that the input signal has symmetrical components. Otherwise, the single phase frequency measurements do not reflect the real variations of the frequency of the system. It has been reported that, during unbalanced conditions, the estimates of frequency from a single phase resulted in different values according to the observed phase component. On the other hand, it has been shown that the frequency of the PPS voltage vector follows the real track of the system's frequency.

The investigation conducted with power system conditions simulated by EMTP models has shown the reliability of the frequency measurement algorithm for the measurement of frequency from a PPS voltage vector. It was shown that the measurement of frequency from single phase input signals does not reflect the real variations of the system's frequency. On the conduction of the EMTP experiments, balanced network conditions were observed. Hence, the PPS frequency measurement has shown a close agreement with the results from the single phase frequency measurement. From the last study case related to the measurement of frequency at the remote load busbar in a separated power system, the measurement of frequency from the PPS voltage vector taken at the load bus has shown that the rotational speed of the load voltage vector corresponds to the average of the rotations of the voltage vectors at the other end of the system.

This Chapter has presented an exhaustive set of study cases on the performance of the PPS frequency measurement algorithm which confirms that the algorithm is able to be used for power system frequency measurements.

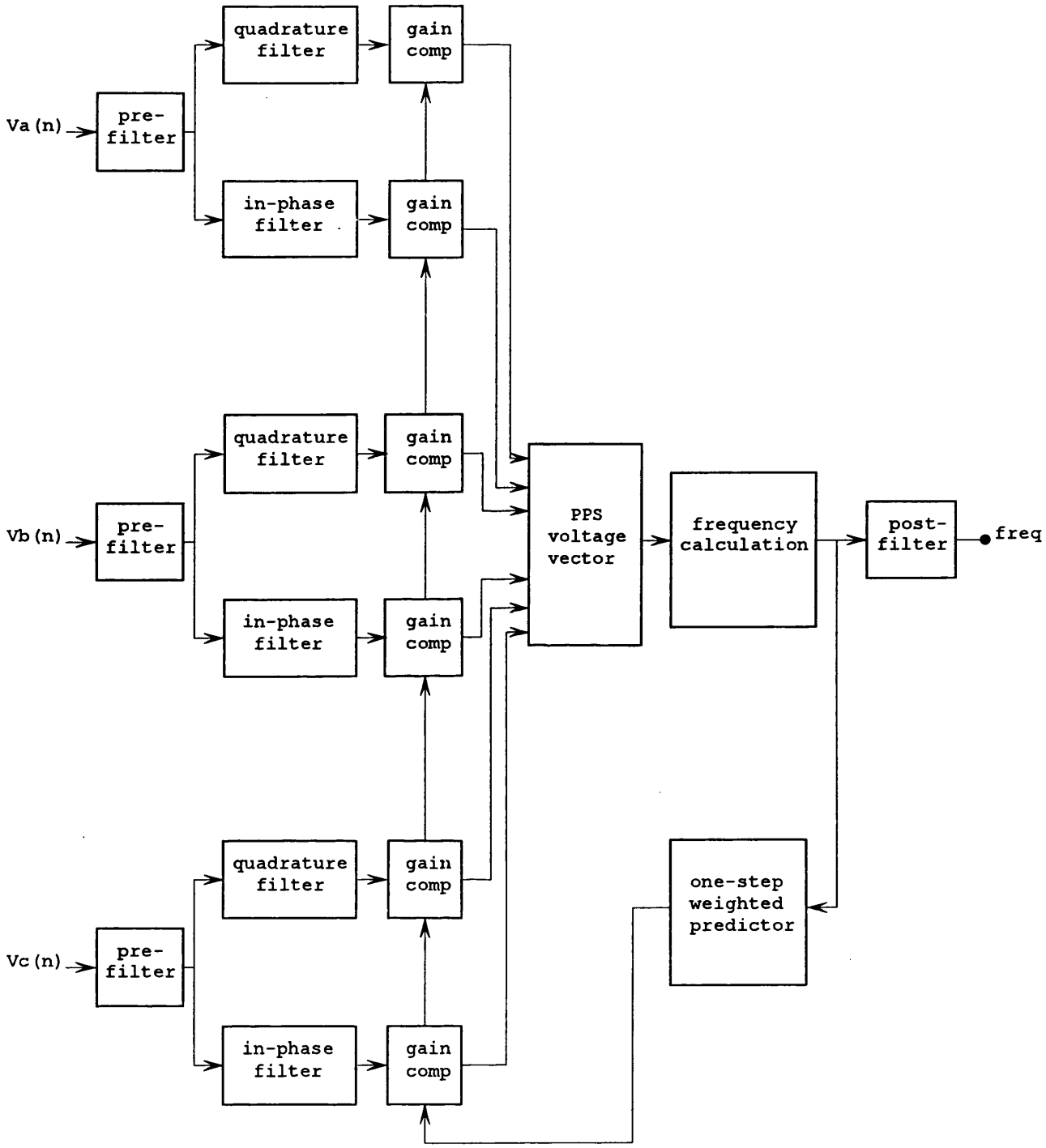

Figure 6.1. Structure of the algorithm for the measurement of frequency from a Positive Phase Sequence voltage vector.

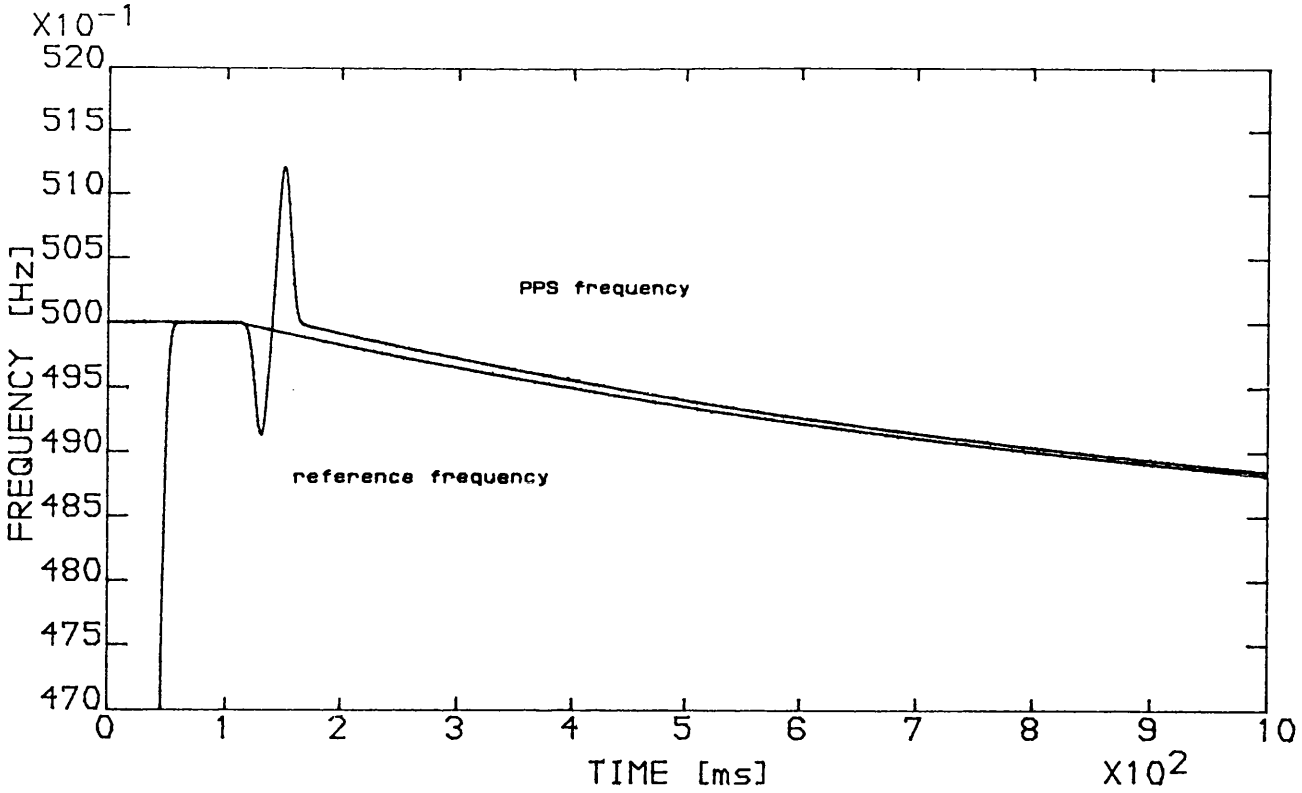

Figure 6.2. Frequency measured from the PPS vector of a signal with exponential decaying amplitude and frequency.

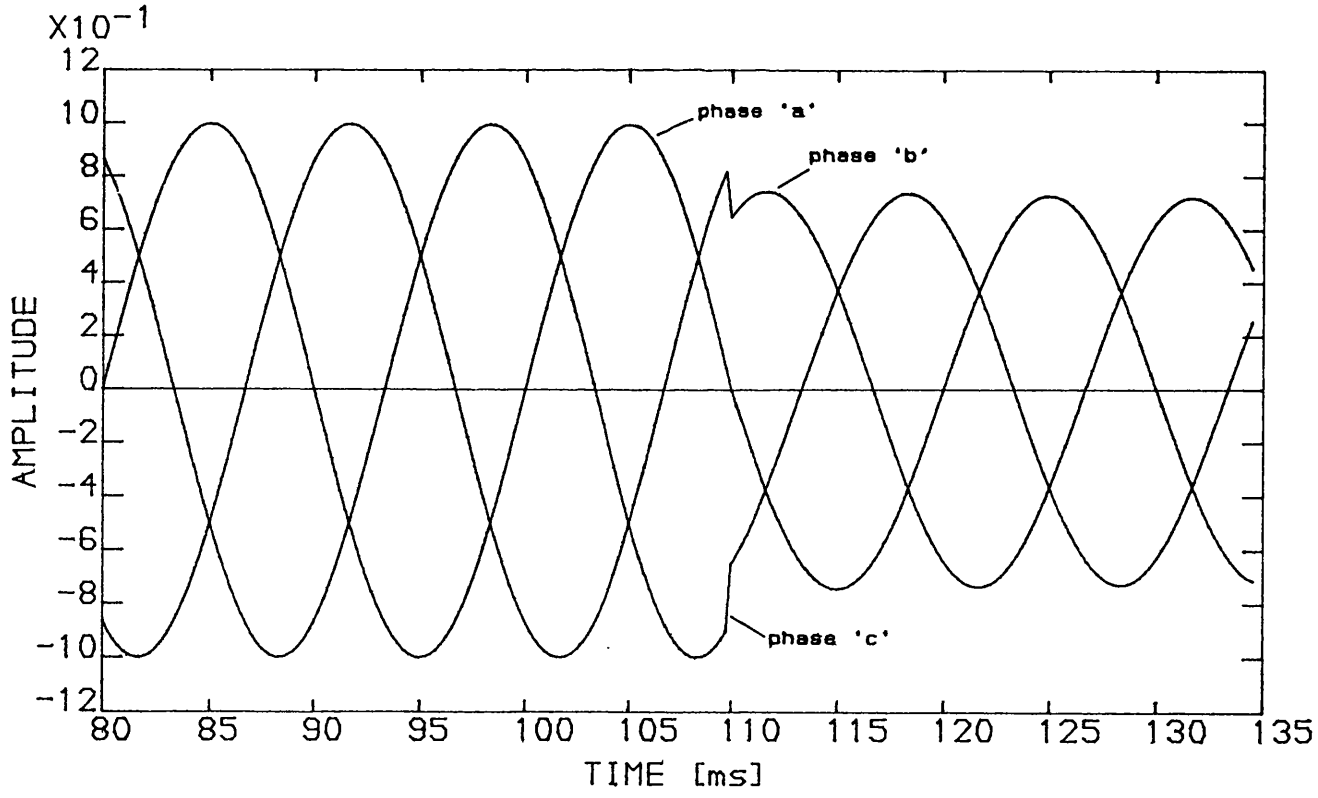

Figure 6.3. The three phases of the input signal about the time of the fault.

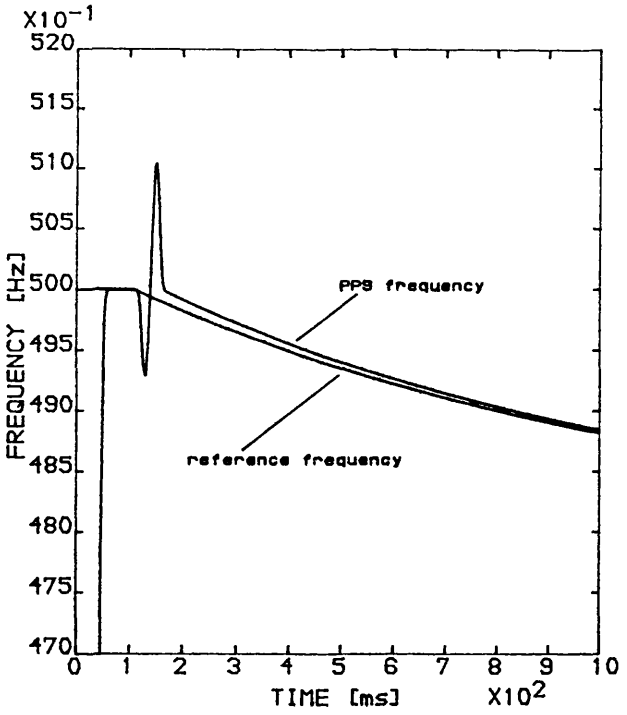

Figure 6.4. Frequency measured from the PPS vector formed by phases 'b' and 'c' only.

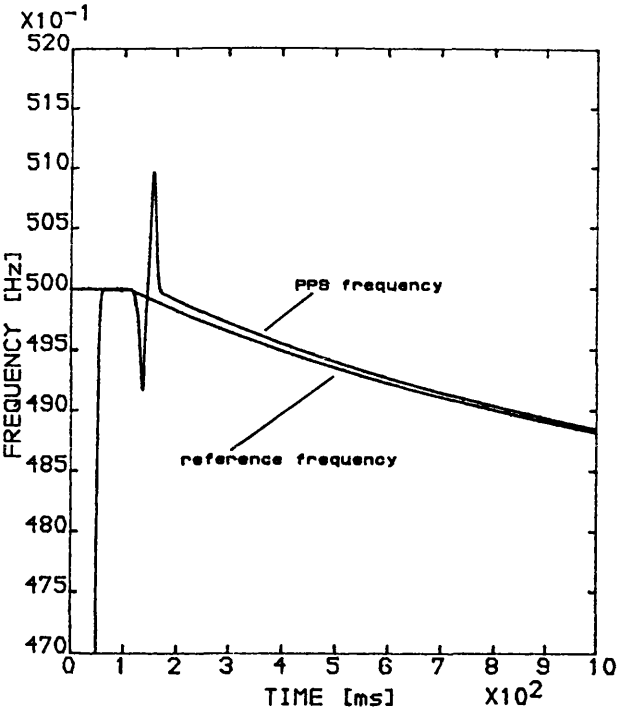

Figure 6.5. Frequency measured from the PPS vector formed by phase 'c' only.

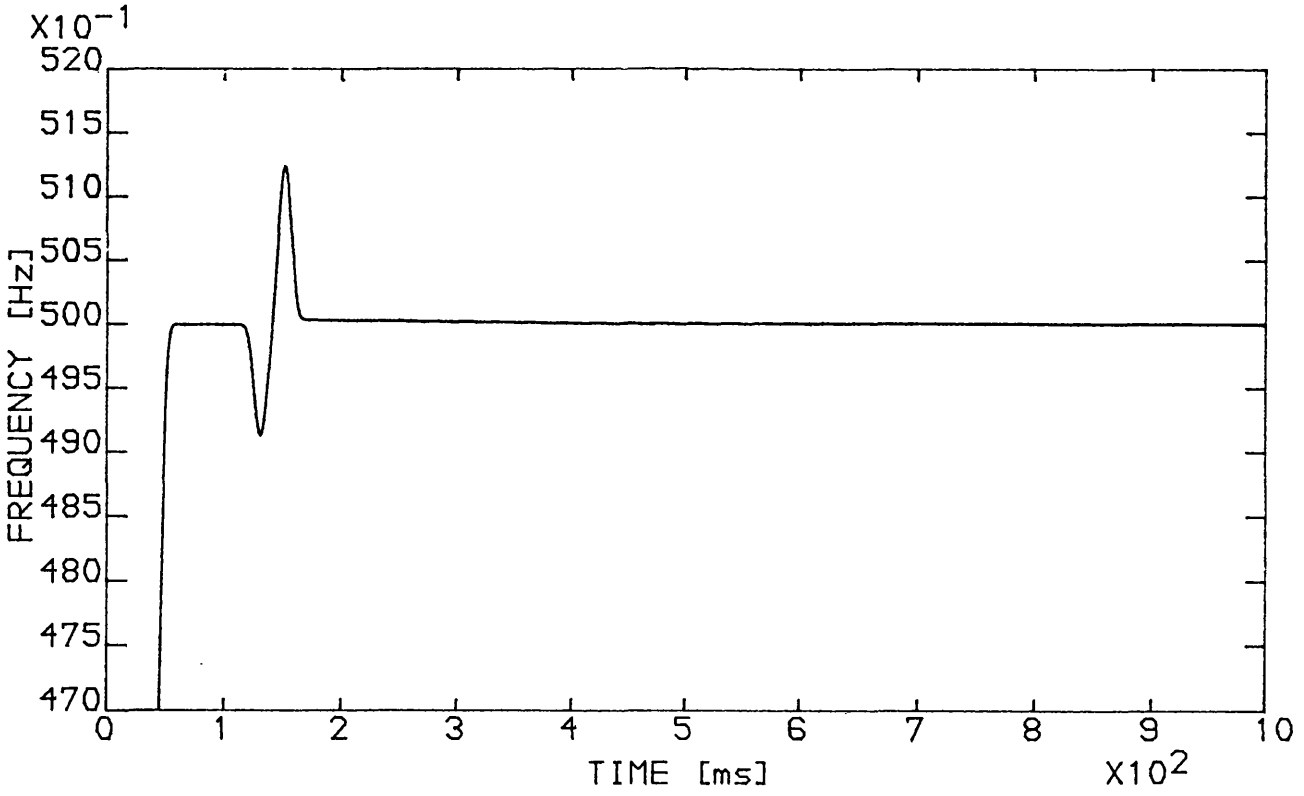

Figure 6.6. PPS measured frequency of a signal with exponential decaying amplitude and constant frequency.

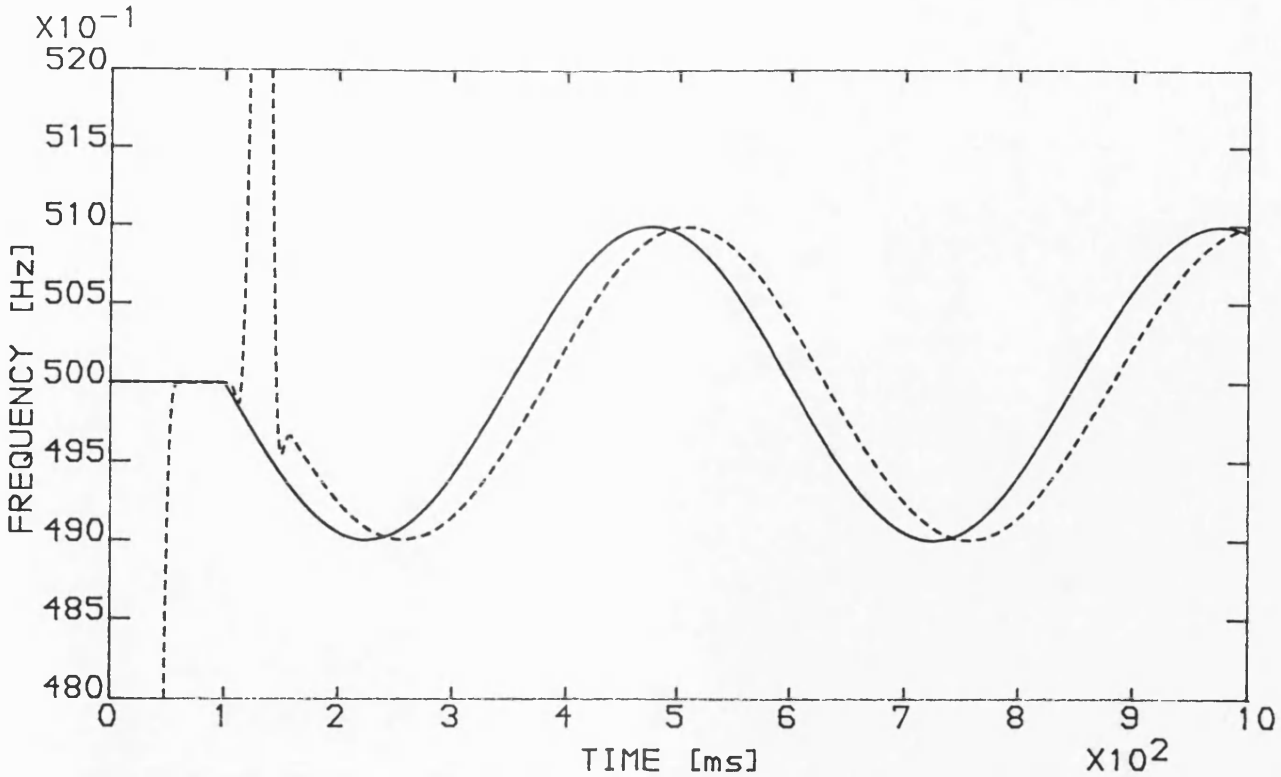

Figure 6.7. Frequency measured (broken line) from the PPS vector of a signal with constant amplitude and sine modulated frequency. The reference frequency is shown in solid line.

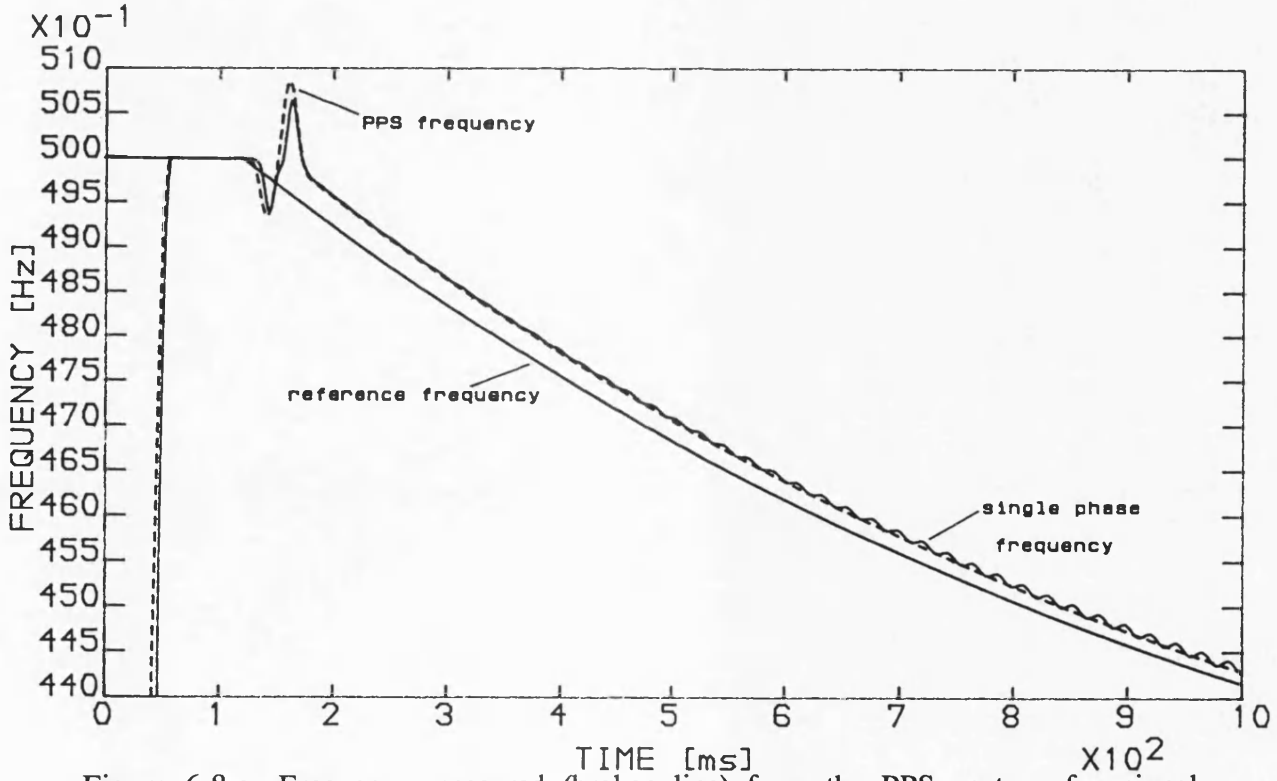

Figure 6.8.a. Frequency measured (broken line) from the PPS vector of a signal corrupted by harmonics. The single phase frequency measurement is also shown in solid line.

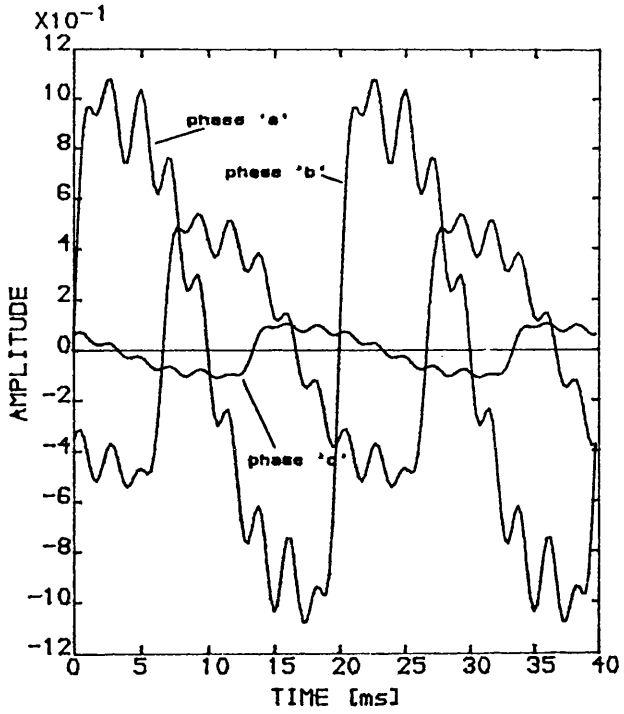

Figure 6.8.b. Input signal corrupted by harmonics. Its phase components exhibit equal phase displacement but different amplitude.

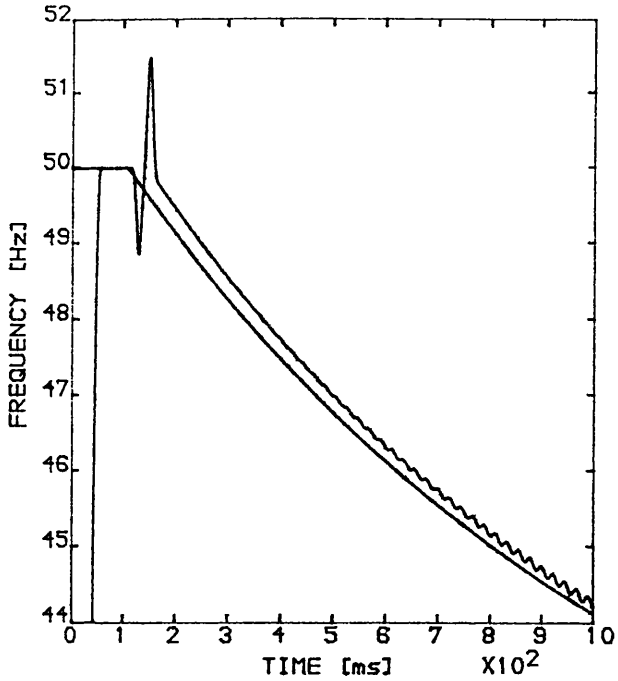

Figure 6.8.c. Reference frequency and the PPS frequency measured from the signal shown in Figure 6.8.b.

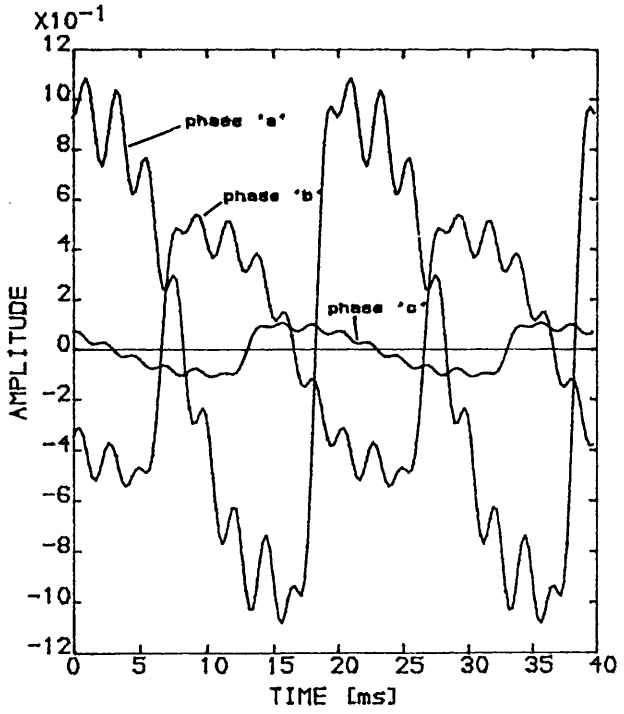

Figure 6.8.d. The phase components of the input signal shown in Figure 6.8.b have been set to a different phase shift.

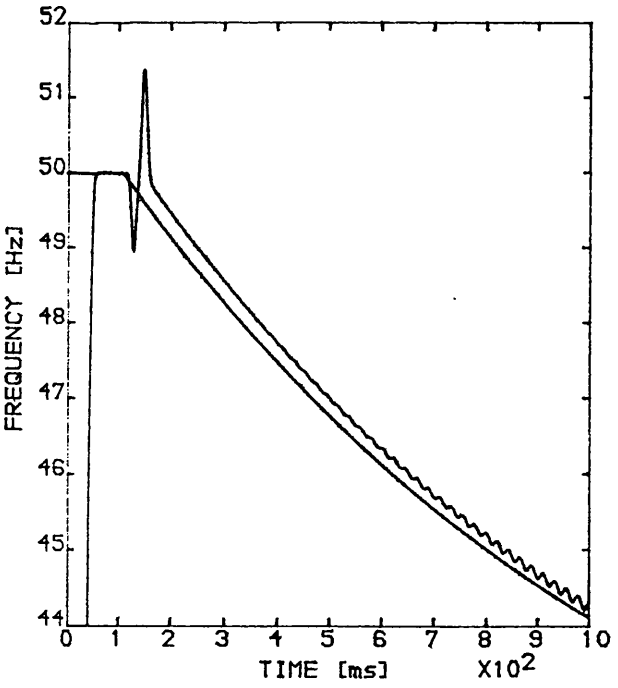

Figure 6.8.e. Reference frequency and the PPS frequency measured from the signal shown in Figure 6.8.d.

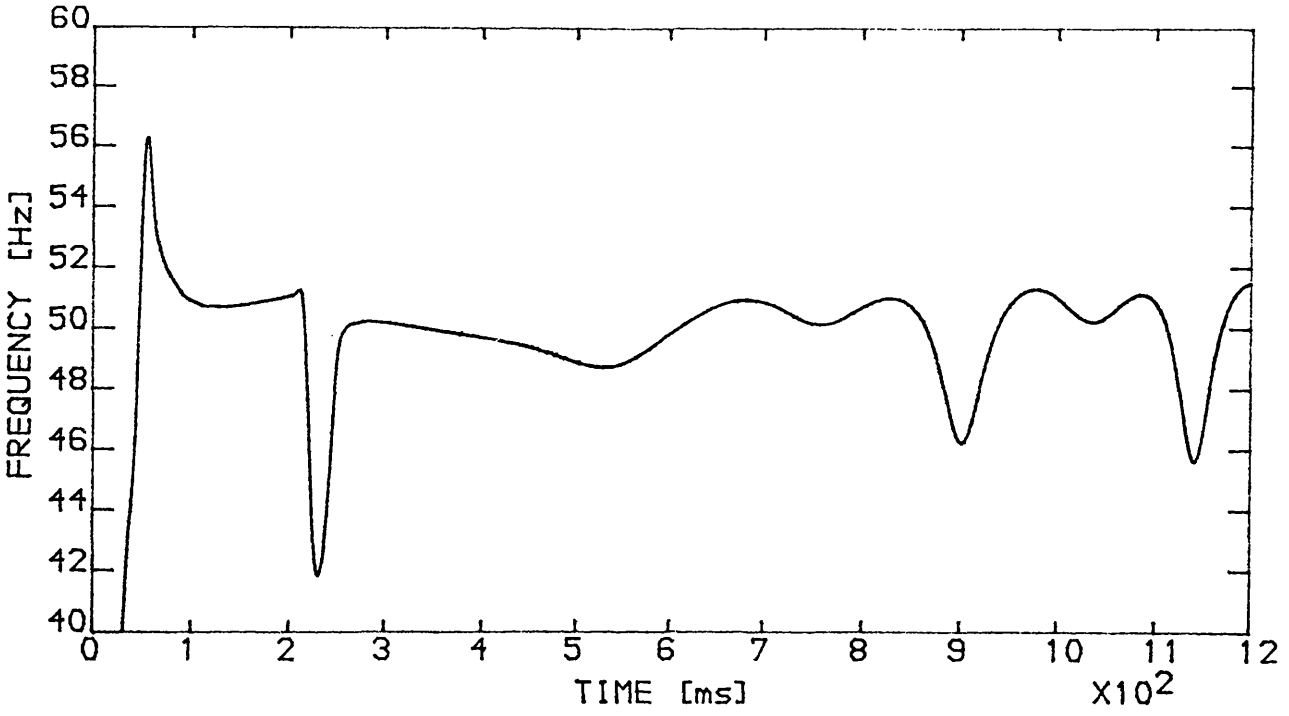

Figure 6.9. Frequency measured from the PPS voltage vector at bus P during the power swing study case.

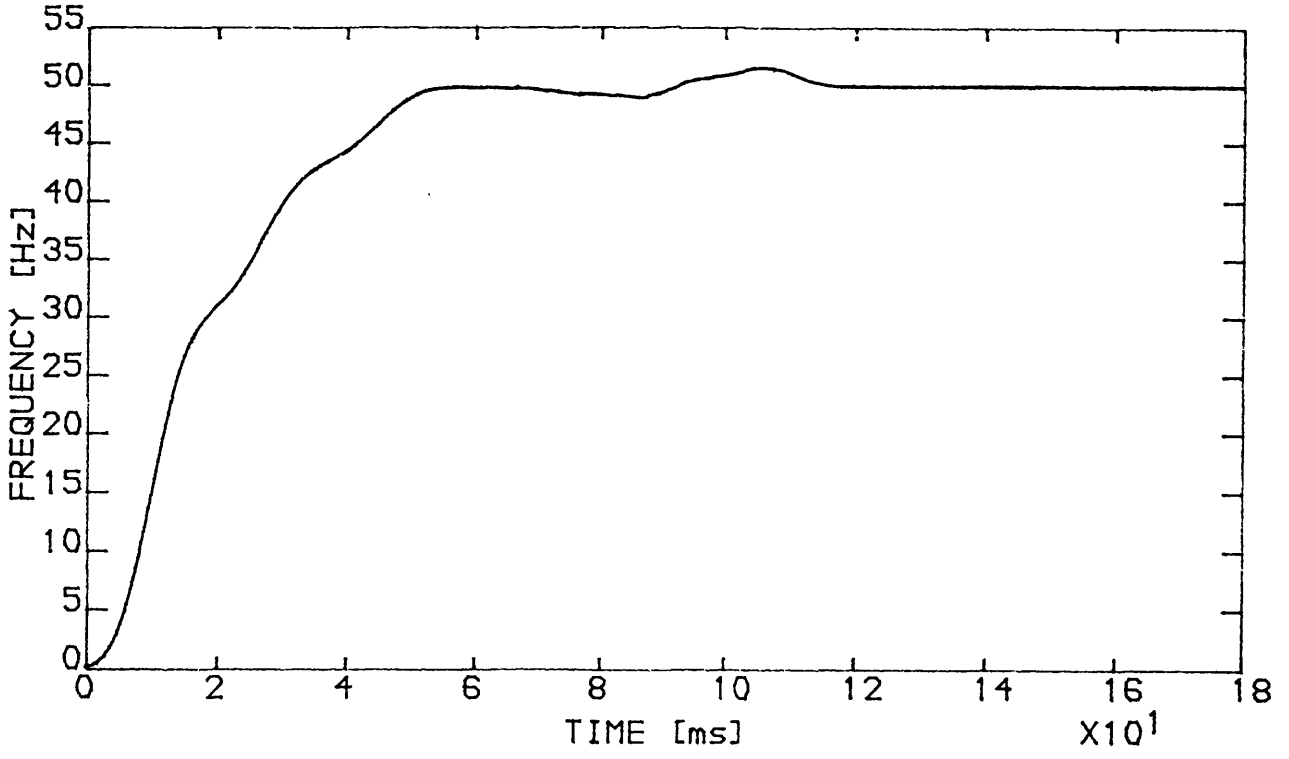

Figure 6.10. Frequency measured from the PPS voltage vector at bus P during the induced travelling wave noise study case.

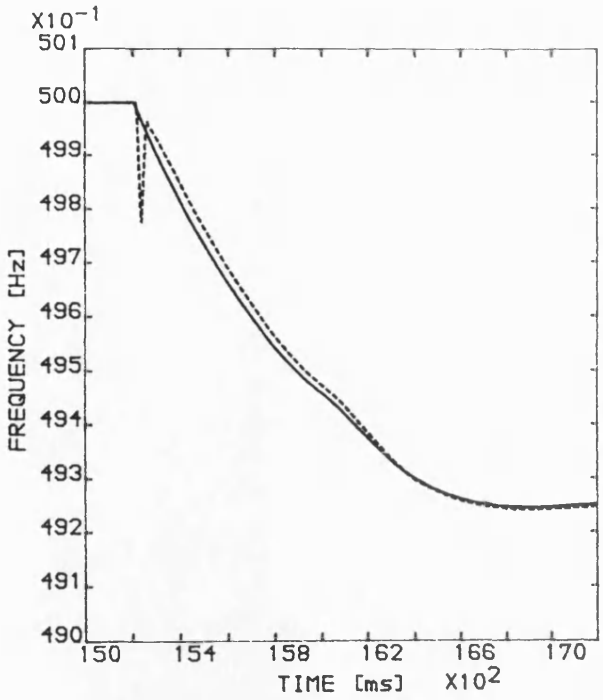

Figure 6.11. Rotor speed (solid line) and the PPS measured frequency (broken line) during the 20% load change.

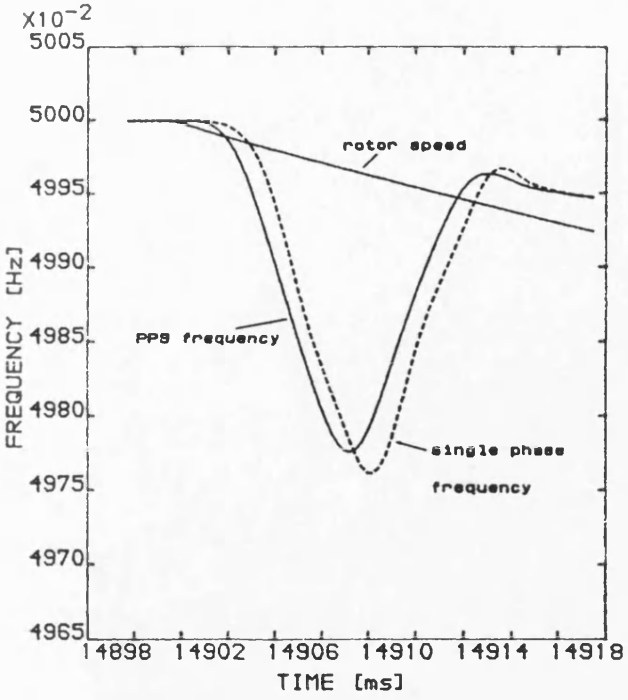

Figure 6.12. Single phase frequency measurement at phase 'a' (broken line), and the PPS frequency during the transient in the 20% additional load case.

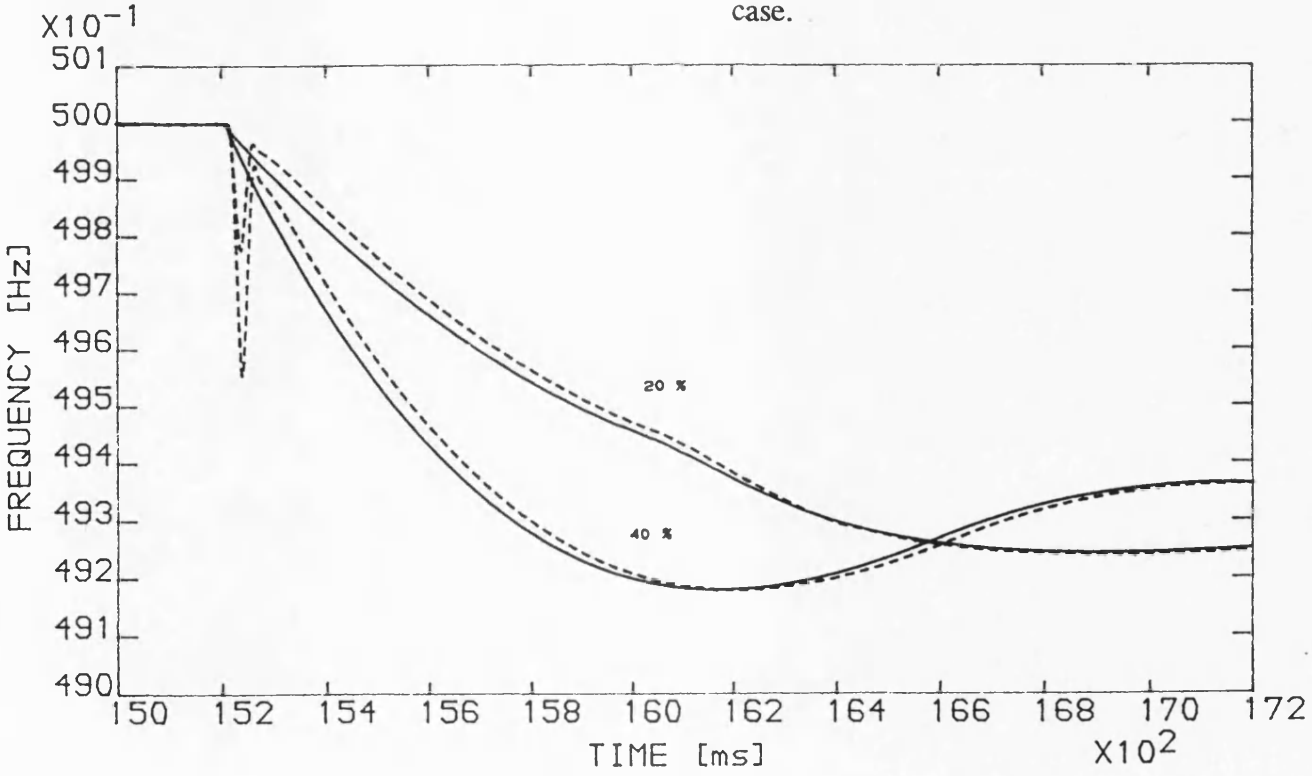

Figure 6.13. Rotor speed (solid line) during the two additional load cases. The PPS measured frequency is shown in broken line.

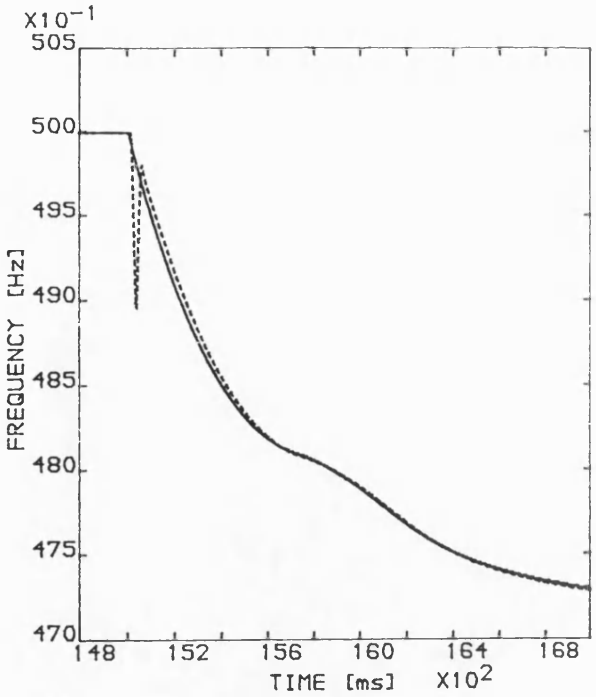

Figure 6.14. Rotor speed (solid line) and the frequency measured (broken line) from the PPS vector at the generator terminal voltage.

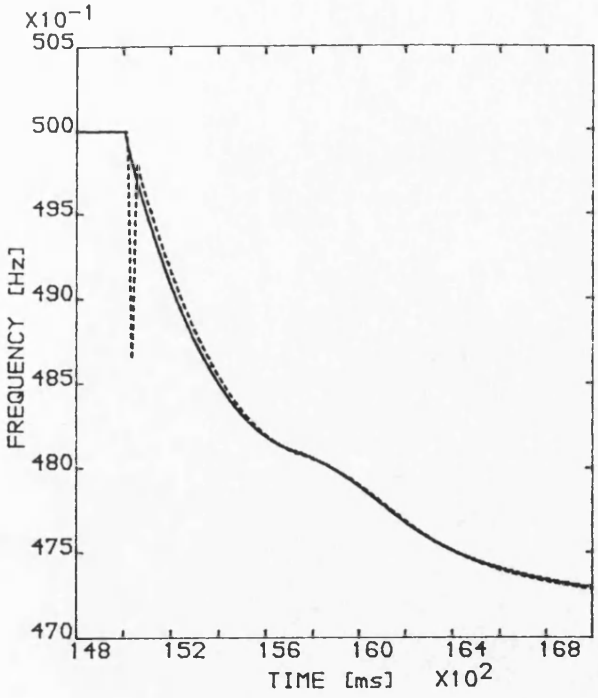

Figure 6.15. Rotor speed (solid line) and the PPS frequency (broken line) measured at bus BUS 1.

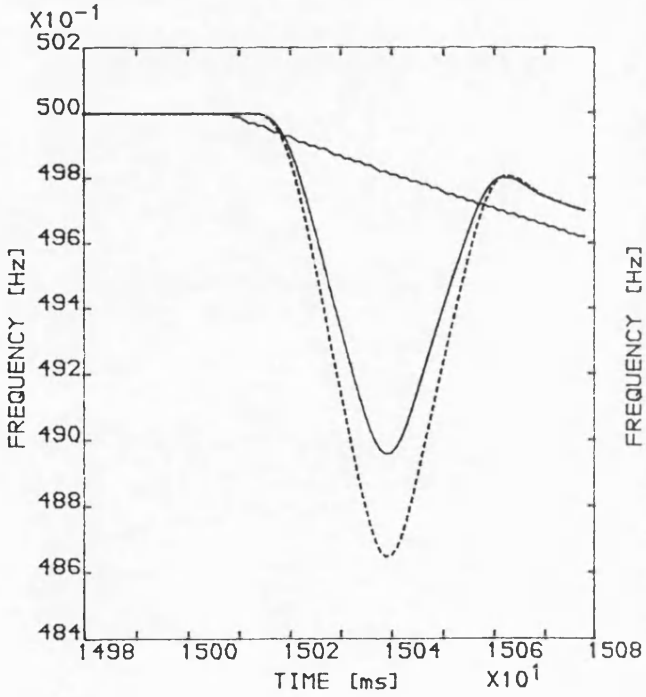

Figure 6.16. Frequency measured from the PPS vector at bus SEND (solid line) and at bus BUS 1 (broken line) during the fault inception.

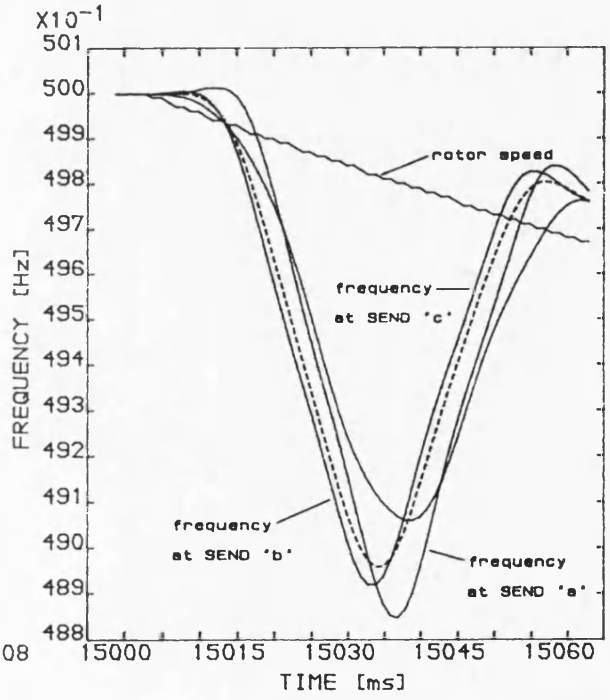

Figure 6.17. The PPS frequency (broken line) and the single phase frequency measurements at bus SEND.

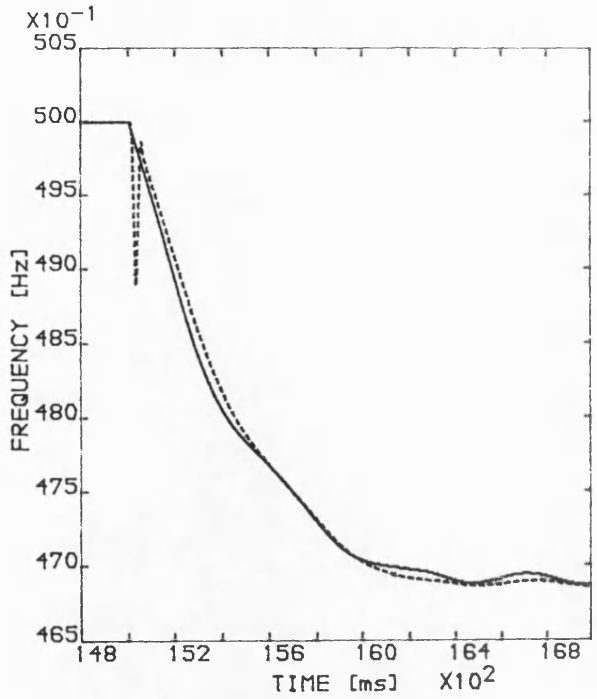

Figure 6.18. Rotor speed (solid line) and the PPS frequency (broken line) measured at bus SEND 1.

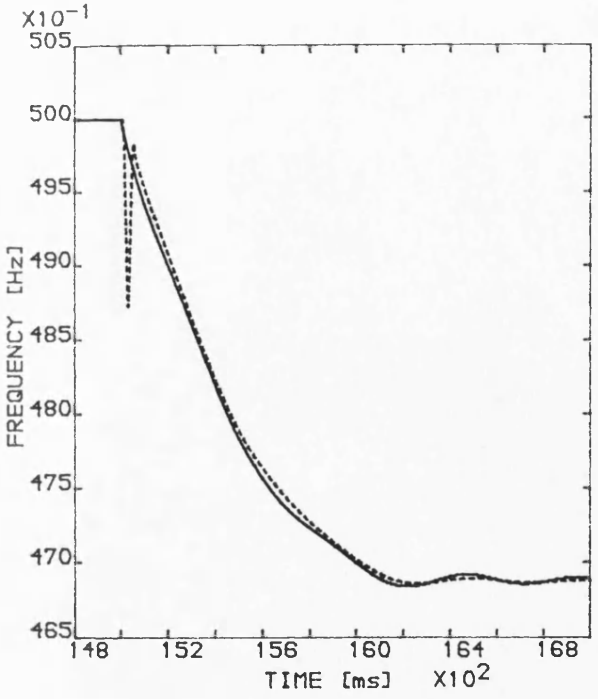

Figure 6.19. Rotor speed (solid line) and the PPS frequency (broken line) measured at bus SEND 2.

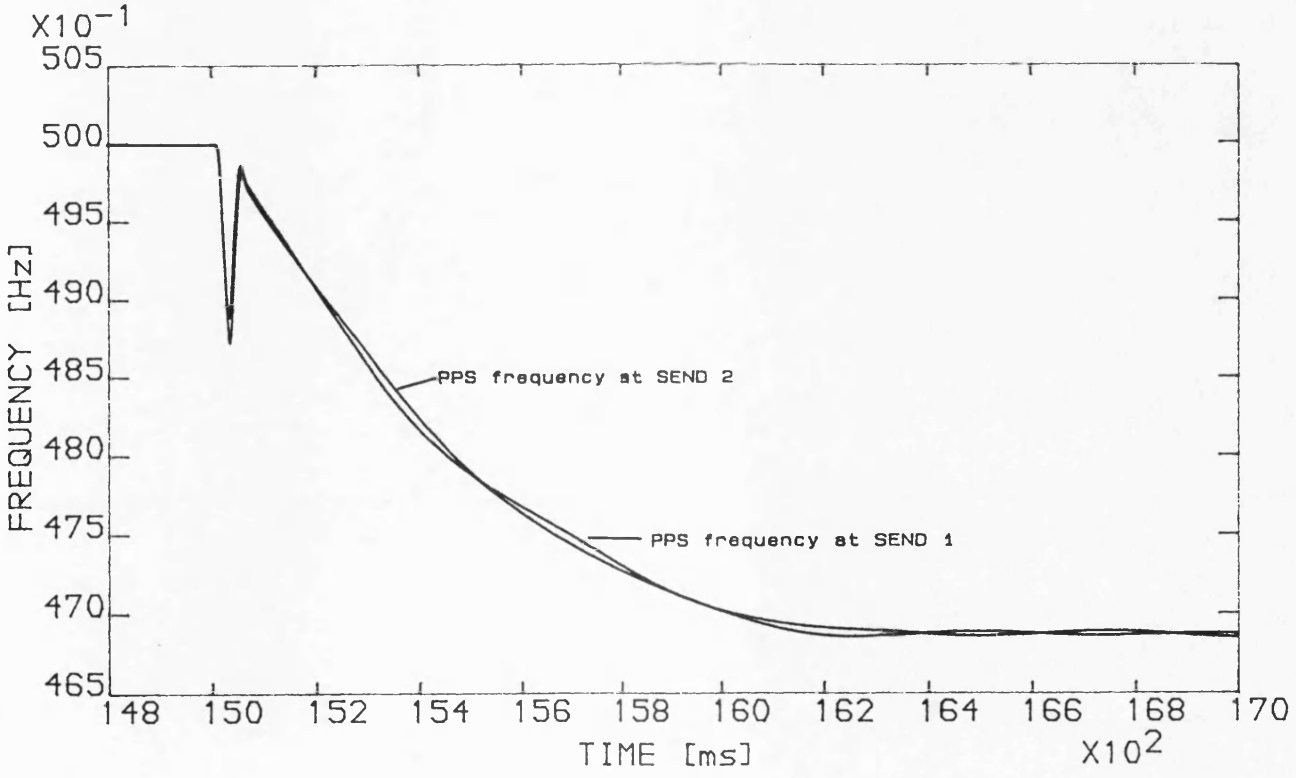

Figure 6.20. PPS frequency measured at buses SEND 1 and SEND 2.

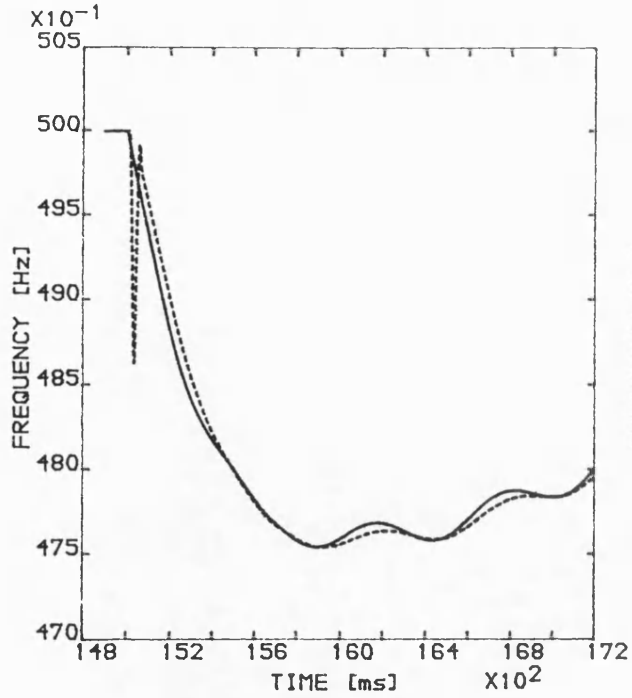

Figure 6.21. Rotor speed (solid line) and the PPS frequency (broken line) measured at bus SEND 1.

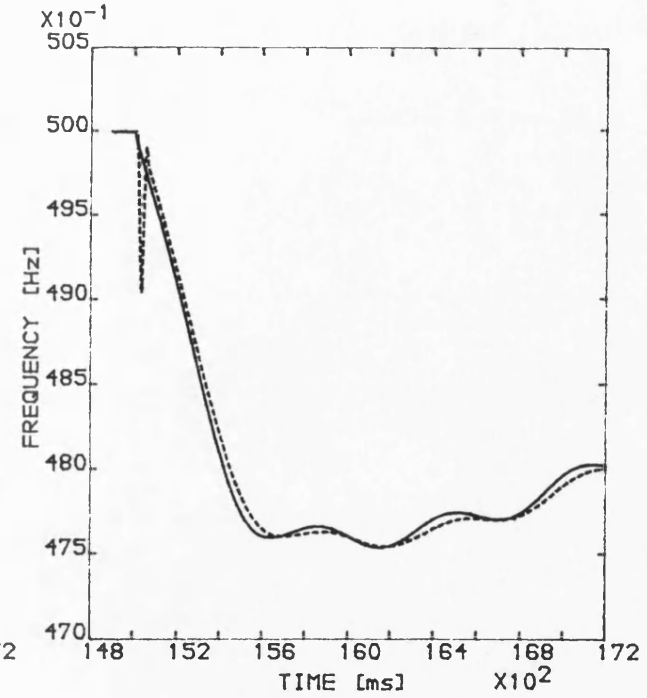

Figure 6.22. Rotor speed (solid line) and the PPS frequency (broken line) measured at bus SEND 2.

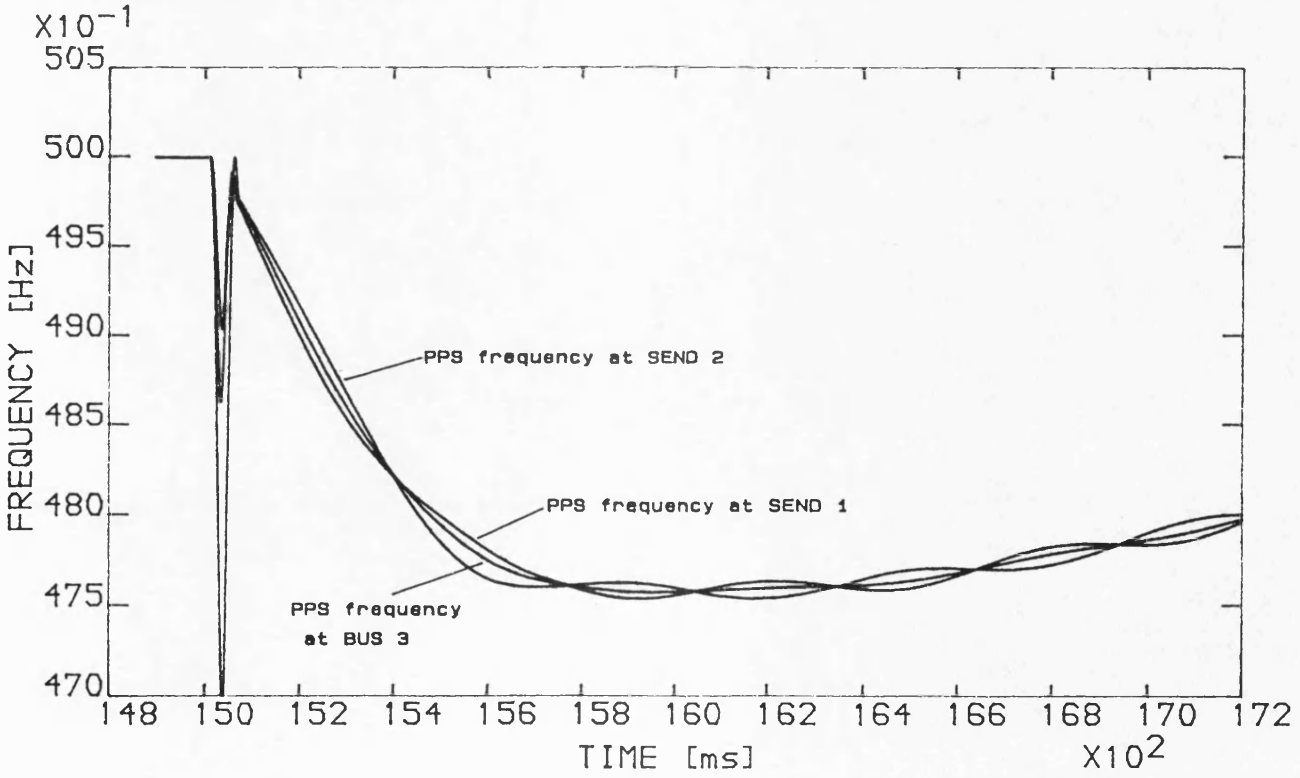

Figure 6.23. PPS frequency measured at buses SEND 1, SEND 2 and BUS 3.

CHAPTER 7

DIGITAL BASED IMPLEMENTATION OF THE NEW ALGORITHM

The implementation of the frequency measurement algorithm on a digital signal processing board has been motivated by the results from the investigation of the performance of the algorithm, in particular, the studies conducted on computer model based power system conditions. The digital implementation of the frequency measurement algorithm is presented in this Chapter. The requirements of the implementation of the algorithm on a digital signal processing board, such as the dynamic range, the quantization noise sensitivity and the operating rates of the algorithm, will be addressed in the first section. Secondly, the development of software and signal conditioning to implement the frequency measurement algorithm on a digital signal processing (DSP) board will be discussed. The last part of the Chapter will be devoted to present the results from an experimental investigation conducted on a micromachine rig. The micromachine system has been developed to represent a large generating unit connected to a large source network by a relatively large transmission line. The model system is capable of adequately representing the response to a transient disturbance, and so it is the ideal system to assess the performance of the DSP based frequency measurement algorithm under realistic conditions.

7.1 Implementation of the Algorithm on a Digital Signal Processing Board

The digital implementation of the new frequency measurement algorithm is motivated by its potential use in on-line power system frequency measurement applications. These applications, and the numerical nature of the algorithm which requires an intensive use of high precision arithmetic, have provided the justification for the implementation of the algorithm on a digital signal processing board.

The first stage in the digital implementation of the algorithm is concerned with the assessment of the quantization noise sensitivity of the algorithm. This noise is due

to the process of sampling and quantizing a continuous time signal. The quantization noise figure will define the dynamic range of the algorithm. These two parameters denote a compromise between accuracy and fast evaluation times in the frequency measurement algorithm, and they will determine its optimum operating rate for a particular DSP board. The results of this evaluation will be presented in this section. A summary of the main features of the DSP board chosen for the implementation of the algorithm will be presented at the end of the current section.

7.1.1 Dynamic Range and Quantization Noise

Different quantization noise sources can be identified throughout the frequency measurement algorithm. An outline of the digital implementation of the frequency measurement algorithm is shown in Figure 7.1. This diagram will be used to assess the dynamic range and quantization noise sensitivity of the algorithm. The main sources of quantization error within the measurement algorithm are: the FIR orthogonal and Hamming filters, the one-step predictor at the adaptive compensation stage and the frequency calculation operations.

Errors from a digital implemented FIR filter are mainly due to the sensitivity of the filter to a coefficient quantization process. It can be shown for the majority of applications that the frequency response of a FIR filter will be preserved if the representation of its coefficients is performed with floating point arithmetic and a wordlength representation of 32 bits [61]. In the current digital implementation, the realization of the FIR filters is direct, that is: the multiplication product operation of two b-bit numbers is represented by a 2-b-bit number, so there is no truncation error, whereas the summation of the products is represented by a b-bit number. In this case, however, the roundoff noise has a zero mean and a variance given as: $\sigma^2 = 2^{-(2b-1)}/12$, where one bit is used for the sign representation. Concerning the implementation of the adaptive one-step predictor, its realization is based on a moving average filter, and so the error from quantization noise is due to the multiplication products and to the summation of products. Since the one-step predictor is formed by the quotient of the product of the magnitude times the

frequency divided by the expected value of the frequency, then, the additional source of quantization noise is due to division operation of two b-bit numbers where the result is also a b-bit number, so the error has the same variance as given before.

From Figure 7.1, it is seen that the external sources of quantization error are found in the signal conditioning stage, particularly in the analogue to digital (A/D) converter. The main source of error will be caused by the truncation and roundoff noise resulting by the integer representation of the quantized signal by a n-bit number. It is practice to use zener limiting diodes in the signal conditioning stage to prevent over-voltages damaging the rest of the instrument. Quantization errors at this stage will be produced by clamping of the input voltage signal.

In order to determine the overall dynamic range of the frequency measurement algorithm, a computer program has been developed to simulate the effects of different lengths of the integer representation of the A/D converter with respect to the amplitude of the input signal. This test will show the smallest level of the input signal data that can be processed by the complete algorithm without being obscured by quantization noise produced within the algorithm. This test consists of applying an input signal $x_{in}(t)$ with constant frequency to the system and adjusting the gain the input amplifier to different levels, whereas the A/D converter is set to a given integer length. The effects of the noise on the performance of the algorithm will be reflected on the accuracy of the measured frequency. This computer test has been performed using the VAX-FORTRAN, version 5.0, computer language in a micro-VAX computer. A single precision arithmetic, which corresponds to a digital representation of 32-bits floating point number, has been used during the test. The computer program incorporates an A/D converter subroutine with a sampling frequency of 4 k-samples/second. The coefficient length of the different FIR filters in the measurement algorithm is given in Figure 7.1.

Table 7.1 shows the results of the test. The variance of the estimated frequency with respect to a fixed frequency in the input signal, has been evaluated as a function of the number of bits of the A/D converter and the amplitude of the input signal. It

should be noticed that the variance figures given in this table represent the sensitivity of the complete frequency measurement algorithm, starting from the A/D converter and including the frequency lowpass post-filter stage. Three different lengths of the A/D converter resolution have been used in this test, while the amplitude of the input signal has been set to 100%, 10% and 1%, respectively.

FREQUENCY [Hz]	A/D RESOLUTION (bits)	VARIANCE		
		INPUT 100%	INPUT 10%	INPUT 1%
52.0	12	0.3997 E-6	0.2042 E-4	0.5285 E-3
	14	0.9849 E-7	0.6229 E-6	0.1638 E-3
	16	0.8436 E-7	0.1045 E-6	0.1096 E-5
51.0	12	0.2257 E-6	0.1318 E-4	0.2050 E-2
	14	0.7187 E-7	0.5840 E-6	0.9062 E-4
	16	0.7840 E-7	0.1070 E-6	0.6215 E-5
50.0	12	0.1398 E-7	0.1353 E-7	0.1221 E-7
	14	0.1173 E-7	0.1443 E-7	0.1392 E-7
	16	0.1314 E-7	0.1385 E-7	0.1365 E-7
49.0	12	0.2052 E-6	0.1718 E-4	0.1200 E-3
	14	0.4465 E-7	0.7161 E-6	0.4482 E-4
	16	0.4107 E-7	0.9193 E-7	0.5810 E-5
48.0	12	0.6610 E-7	0.2425 E-5	0.8004 E-3
	14	0.3352 E-7	0.7171 E-6	0.2069 E-4
	16	0.2948 E-7	0.3954 E-7	0.4232 E-5
47.0	12	0.7038 E-7	0.2157 E-4	0.7672 E-3
	14	0.3649 E-7	0.3199 E-6	0.1245 E-3
	16	0.2761 E-7	0.4120 E-7	0.1975 E-5

Table 7.1. Variance of the estimated frequency as a function of the A/D converter resolution and the amplitude of the input signal.

From Table 7.1, it can be seen that the variance of the measured frequency when the input signal frequency is 50 Hz, exhibits the smallest level in the table regardless of the A/D converter resolution or the input signal amplitude. At other frequencies, the smallest variance will be achieved by using an A/D converter resolution of 16 bits. Using a 16 bits A/D converter, a maximum variance of 0.6215 E-5 has been found for a input signal frequency of 51 Hz and a signal amplitude of 1%. Since the standard deviation approaches the square root of the variance for a white noise sequence, in this case, the quantization noise, the maximum error in the frequency measurement when using a 16 bits A/D converter and an input signal level of 1%, should be $\pm$ 0.0025 Hz about the real frequency. Thus, the use of a 16 bits A/D converter gives adequate dynamic range for the algorithm by minimizing its sensitivity to noise quantization errors.

7.1.2 Digital Signal Processing Board Characteristics

Approximately, 800 arithmetic and logical operations are required to implement the frequency measurement algorithm on a microprocessor board. This figure accounts for single precision arithmetic and logical operations, assuming that not all of which will be executed in one instruction cycle. For an operational overhead of 30%, which will include those operations taking two or more cycles to execute, the number of operations will rise to 1040 operations. For a sampling rate of 4 k-samples/second, an instruction cycle rate of 2.4×10^{-7} s will be required, that is, a single instruction execution time of 240 ns.

As a result of the requirements of the dynamic range and the operational rates for the digital implementation of the frequency measurement algorithm, the PC/31 TMS320C31 board from Loughborough Sound Images has been selected for the current implementation. From now on, this board will be denoted as the PC/C31 board. The main features of the PC/C31 board are:

- a 33 MHz, 32 bit floating point digital signal processor TMS320C31.
- a dual port random access memory (DP-RAM), which provides a direct interface between the board and a PC computer; the length of the port is 2

k-bytes with a wordlength of 16 bits.

- a dual channel I/O module sited on the PC/C31 board. The channels, denoted as A and B, have an A/D and a D/A converters with a resolution of 16 bits. The conversion rate of the module is programmable.
- a programmable timer module for pacing the sampling rate of the I/O converter.
- the PC/C31 board can be plugged into a slot in a PC, IBM compatible computer.

The main features of the TMS320C31 digital signal processor are:

- 60 ns single cycle instruction execution time
- 32 bit instruction and data words, 24 bit addresses
- 40/32 bit floating point/integer multiplier and ALU
- parallel multiplier and sum instructions in a single cycle

7.2 Software Development and Signal Conditioning

This section presents the software package which has been developed to implement the frequency measurement algorithm on the PC/31 board. The software package includes the measurement of frequency for both the single phase and the PPS voltage vector applications. In the present section, the main attributes of the software package will be discussed. The particular implementation of the software for the single phase and for the PPS frequency measurement algorithm will be addressed in the second part of this section.

It should be mentioned here, that for the DSP based implementation of both the single phase and the PPS vector frequency measurement algorithm, the structure of the program has been split in two main parts: a personal computer (PC) resident program which is aimed to provide an interface between the user and the frequency measurement algorithm implemented on an executable code for the TMS320C31 cpu. A set of interface libraries has been purchased along with the PC/31 board. These libraries allow the TMS320C31 executable code to be loaded and executed from the

user's PC resident program. Communication between the PC resident program and the executable code is achieved through a dual port random access memory (DP-RAM).

Three main facilities have been developed in the PC resident program which will allow the user to get most of the advantages of the PC/C31 board: to run a frequency measurement process, either the single phase or the PPS frequency measurement algorithm, to have access to a data file management and display on screen the measured frequency and the voltage waveform from which it has been taken the measurement of frequency. The PC resident program has been developed using the C++ language, version 7 from Microsoft. The structure of the PC resident program is the same for either the single phase frequency measurement of the PPS voltage vector measurement. A personal computer, IBM compatible with a 80-386 cpu, has been used for the realization of the present experimental investigation. The PC/C31 board has been plugged into the computer. Connection of the computer with the signal conditioning board is achieved by a coaxial cable.

The frequency measurement algorithm has been implemented in an executable code form for the TMS320C31. The Texas Instruments assembler language was used for those sections of the executable code where operations involving a direct access to the PC/C31 cpu memory are required, and with the Texas Instruments C language to implement the less demanding tasks in the program. The main attributes of the TMS320C31 executable code are: to configure the I/O module sited on the PC/C31 board for a particular sampling rate, to execute the frequency measurement algorithm from data taken by the I/O module, and to send the results from a frequency measurement process to the PC resident program through the DP-RAM. When the PC resident program is started, the TMS320C31 executable code is loaded in the board's memory map. The next step in the PC program will get the TMS320C31 code running. The process of frequency measurement is started as soon as the executable code is loaded. Thus, a continuous measurement of the frequency of the signal sampled by the I/O module is conducted at all times. On a user request, the PC resident program will prompt the executable code to divert the results of the

most recent frequency measurements to the PC in order to be displayed on the screen. It should be mentioned that both the frequency measurement results and the input voltage waveform are sent to the PC resident program via the DP-RAM buffer. The record process can be paced in three different rates: 0.25 ms, *i.e*: at the same sampling frequency rate, 1 ms, and 5 ms. Note that the measurement of frequency is being executed at a sampling frequency of 4 kHz, whereas the pacing rates will command the executable code to "sample" the frequency results and the input voltage waveform before they are sent to the PC resident program. Thus, the different pacing rates will allow the user to vary the length of the observation records from 1.25 s, to 5 s and to 10 s, respectively.

The main structure of the TMS320C31 executable code is shown in Figure 7.2. The same structure has been followed for the implementation of the frequency measurement algorithm for either a single phase input signal or a PPS vector input signal. Differences related to either application are concentrated in the Interrupt Service Routine (ISR) block shown at the bottom of the flow chart in Figure 7.2. These differences will be addressed later on.

When the PC resident program is started, the PC/C31 cpu executable code is loaded into the TMS320C31 memory map. In the first block shown in Figure 7.2, the executable code sets the registers and memory map of the PC/C31 cpu while an interrupt vector is set to point to the address of the ISR in the TMS320C31 memory. In the second block, the coefficients of the impulse response of the orthogonal and Hamming filters are written in the PC/C31 cpu memory. A "look-up-table" with the gain of the frequency response of the orthogonal filters is also written at this stage. In the next block, the configuration of the I/O and the programmable timer modules takes place. Channel A on the I/O module is configured for sampling a voltage input signal into the PC/C31 cpu program, whereas channel B is configured as a D/A converter in order to output a voltage signal corresponding to the estimated frequency. This voltage output signal has been set to a ratio of 1V/1Hz, with a resolution of 2^{-15} bits, with a range of $\pm$ 3.3 V peak. When the executable code has been loaded, the timer module is initialized to pace the sampling process of the I/O

module at a rate of 4 k samples per second. As shown in Figure 7.2, the TMS320C31 cpu's interrupt register is enabled in the next stage. The next block shows an infinite "while" loop which will be interrupted by the TMS320C31 cpu in order to respond to the completion of an A/D conversion on channel A. The last block of the diagram shows the Interrupt Service Routine. This routine will be accessed by the PC/C31 cpu each time an interrupt from the A/D converter is invoked.

7.2.1 Software Development of the Single Phase Frequency Measurement Algorithm

Figure 7.3 shows an outline of the single phase frequency measurement algorithm. The input to the Signal Conditioning Board is a voltage signal $v_{in}(t)$. From now on, the voltage input signals to the equipment will be denoted by the extension (t) in order to indicate their continuous time nature. On the other hand, discrete time signals will be denoted by $[n]$. The isolating transformer steps down the input voltage from 200 V to 3 V. The input signal $v_{in}(t)$ is lowpass filtered by a fourth order Butterworth anti-aliasing analogue filter. The cut-off frequency of this analogue filter is 300 Hz. Two second order Sallen and Key amplifiers are set in cascade to implement this filter. A "back-to-back" zener diode configuration precedes the analogue filter for limiting the voltage signal to $\pm$ 3.3 V. The Signal Conditioning Board is connected to the A/D converter on the PC/C31 board by a coaxial cable. Further details of the Signal Conditioning Board are given in Appendix 14.

As shown in Figure 7.3, the Interrupt Service Routine (ISR) is located at the inner core of the block denoting the PC/C31 board. The A/D converter on channel A, is paced by the timer module. Every time an A/D conversion is finished, the ISR is invoked by the PC/C31 cpu. The first task to be performed by the ISR is an integer to floating point conversion carried out on the data coming out from the A/D converter. The floating point voltage signal $v[n]$ is then convolved with a one-cycle Hamming lowpass filter before the orthogonal decomposition stage takes place. With

the exception of the frequency calculation block, the arithmetic operations related to the other blocks within the Interrupt Service Routine have been implemented with assembler language since the access to the coefficients of the filters and to the frequency gain "look-up-table" is critical as far as the number of the TMS320C31 cpu instructions per cycle is concerned. The estimated frequency $f[n]$ is used to drive the output D/A converter on channel B. As shown in Figure 7.3, the input signal $v[n]$ is sent to the DP-RAM Management Routine together with the estimated frequency $f[n]$ where these signals will be processed by the PC resident program before being displayed on the PC screen.

The DP-RAM Management Routine provides an interface between the PC/C31 cpu and the PC resident program. The pacing rate at which the voltage signal and the estimated frequency signals are sent to the PC resident program is controlled by this routine. It was pointed out at the beginning of the section, that the length of the DP-RAM is 2 k-bytes. In the present implementation, the DP-RAM memory map has been split in two parts: the frequency results and samples from the voltage signal are stored in the upper half part and in the lower half part of the memory, respectively. The PC resident program can command the DP-RAM routine to pace the recording process at three different rates: 0.25 ms, 5 ms and 20 ms. Since the length of the DP-RAM is 2 k-bytes, then, the length of the record will be 250 ms, 1 s and 5 s, respectively. However, the PC resident program has been programmed to repeat the acquisition process for up to five times. Thus, for a pacing rate of 0.25 ms, the maximum record buffer length will be 1.25 s, whereas for a rate of 1.0 ms, the length will be 5 s. The last pacing rate is repeated twice only, thus, the record is 10 s. For a different application, the length of the record buffer can be easily adjusted.

7.2.2 Software Development of the PPS Frequency Measurement Algorithm

Figure 7.4 shows the schematic diagram followed during the implementation of the PPS frequency measurement algorithm on a DSP board. The implementation of the PPS algorithm has been complicated because only two channels have been purchased with I/O module board. In order to overcome this problem, a multiplexing procedure

has been implemented to sample phases 'a' and 'b' with the same A/D converter on channel A, whereas phase 'c' is sampled by the A/D on channel B. Two sampling/hold stages have been used to accomplish the multiplexing requirement. As seen in Figure 7.4, the first stage is located on the Signal Conditioning board, whereas the second stage is performed in the I/O module. From the same figure it is seen that the Interrupt Service Routine for the PPS application has been divided in two parts. In fact, the rate of operation of this routine is 8 kHz, *i.e*: twice the signal sampling rate. Figure 7.5.a can be used to explain this point. It can be seen that the A/D converter on channel A is connected to the analogue multiplexer, whereas the D/A on the same channel is used to set the multiplexer address value. A zero voltage output at the D/A terminal will set the multiplexer address to *00*, then, the input voltage from phase 'a' is accessed; phase 'b' will be accessed when the address is set to *01*. It can be realized that the pacing times for driving the sample/hold and the multiplexer circuits on the Signal Conditioning Board are critical for the correct operation of the PPS frequency measurement algorithm.

A timing diagram is shown in Figure 7.5.b. It can be seen that the clock of the timer module has been set to 8 kHz, hence, the Interrupt Service Routine will be prompted at every 0.125 ms. It was already mentioned that the ISR has been split in two parts. These two parts will be accessed alternatively by the TMS320C31 executable code. The first part of the ISR will be carried out during the first cycle of the timer, and the second part will be carried out during the next timer cycle. In this way, each part of the ISR will be executed at every 0.25 ms.

The first ISR cycle will be started at the raising edge of the timer clock pulse. It can be seen from the timing diagram, that the output of the D/A converter on channel A is already set to a high level, thus phase 'b' is read by the A/D converter on channel A and phase 'c' is read on channel B. When the A/D conversion in both channels is finished, the ISR is invoked by the TMS320C31 code and the first cycle is started. The first step in the cycle is to set the D/A on channel B to a low level, so the multiplexer now points to phase 'a' which will be read in the second cycle of the ISR. This change of the address of the multiplexer provides enough time for

phase a' at the multiplexer output to settle down before the second cycle is started. In fact, the output of the D/A converter is used to provide a synchronism pulse to coordinate the activities between the multiplexer and the A/D converter on channel A. In the next step of the first cycle, the incoming samples $v_b[n]$ and $v_c[n]$ are convolved with the orthogonal filters. The calculation of the one-step predictor is also carried out in this cycle. The resulting one-step estimate of the frequency will be used during this first cycle to scale the orthogonal components of phases 'b' and 'c' to the running frequency. The same one-step frequency will be used in the next ISR cycle to scale the orthogonal components of phase 'a'. Then, the scaled values of the three phases will be used for the calculation of the PPS voltage vector.

During the second cycle, the Interrupt Service Routine reads a sample from phase 'a' which is already the input to the A/D converter on channel A. Before processing the sample from phase 'a', the interrupt routine firstly sets the output of the D/A converter on channel A (the synchronism pulse) to a high level, so the multiplexer now points to phase 'b' before the next first cycle is started. In the second ISR cycle, phase 'a' is convolved with the orthogonal filters. Now, the orthogonal components from the three phases are processed all together to form the PPS voltage vector. As shown at the bottom of Figure 7.4, the calculation of the frequency from the PPS voltage vector is performed during the second cycle and the frequency estimate is sent to the DP-RAM management routine. The results will be displayed by the PC resident program.

It can be noticed from the timing diagram in Figure 7.5.b that the analogue multiplexer is triggered by the rising edge of the synchronism pulse, and that the first monostable is also driven by the same pulse for a duration of 10 μs, while the second monostable is triggered by the falling edge of the first monostable. Hence, the three phases are sampled by the S/H circuits when the second monostable is triggered. That is, during the second cycle of the ISR the three phases are sampled at the same time. Hence, the effective sampling frequency is 4 kHZ. It should be mentioned that the time constant in the first monostable has been set to 10 μs in order to square the output of the D/A converter because the rising edge of this pulse

is flattened by the time constant of the anti-aliasing filter on the D/A converter output. Otherwise, different triggering times will be observed. The second monostable then is triggered by a perfect squared pulse. An alternative solution to this problem can be afforded by using an external timing source to pace both the TMS320C31 cpu and the I/O module on the PC/C31 board. However, the implementation of this solution will impose the use of a similar triggering configuration where the main restrictions would come from the temperature drift stability of the frequency generator and the time stability of the circuits. Thus, the configuration proposed in Figure 7.5.a has been chosen for the current implementation.

As a result of the present limitation imposed by the lack of a third A/D converter, the division in two cycles of the Interrupt Service Routine has rendered a very restricted timing diagram. For the current PPS frequency measurement application, the number of tasks to be performed in each one of the cycles has been increased. This problem and the fact that the operational rate is 0.125 ms, have lead to the implementation of a PPS frequency measurement algorithm where the Hamming lowpass pre-filtering stage has not been included. It should be mentioned here, that the execution of a floating point division operation by the TMS320C31 is achieved in 30 cycles. If a Hamming lowpass pre-filter were used, then, the input signals from the three phases will have to be scaled in gain at 50 HZ, therefore, the corresponding scaling operation of the three phases will be impossible to execute given the restricted operating conditions. The total group delay in the DSP-based implementation of the PPS frequency measurement algorithm is 27.5 ms

7.3 Experimental Investigation Using a Micromachine Based Model System

Following the implementation of the frequency measurement algorithm on a DSP board it was sought to challenge the performance of the DSP based algorithm with input signals related to more realistic conditions of power system frequency transients. A model power system, incorporating a micromachine, was developed in the School of Electronic and Electrical Engineering of the University of Bath [62].

This power system model has been used in the present experimental investigation in order to show the abilities of the measurement equipment. A brief description of the power system model used for this investigation is presented in this section. The most relevant part of the section is that associated with the results obtained on conducting a series of tests with the micromachine rig where the DSP based algorithm has been used. A discussion on the results from these tests is also presented.

7.3.1 Power System Model

The power model system was originally developed for the study of power system transient and dynamic stability conditions where disturbances can be produced in a controlled manner. The micromachine system is modelled on a section of the United Kingdom 400 kV network. The system is formed by a single machine connected, through a transformer and transmission line to an infinite busbar; a large network with constant voltage and phase is assumed to be represented by the infinite busbar. The network chosen in this model power system is associated with Pembroke Power Station in South Wales. Briefly, this model represents a large capacity generating unit centre situated remotely from the load centre. Figure 7.6 shows an outline of the power system model. Four turbogenerator units, each rated at 500 MW are connected to the 400 kV station busbars through their own step up generator-transformers. The station is connected to the UK grid system via a two double circuit transmission lines.

The power system model is intended to achieve the same per unit quantities of the Pembroke system, thus it is capable of representing real time power system transient conditions similar to the performance of the Pembroke system. The system model basically consists of a micromachine and a transmission line model, and it can be synchronized onto the mains supply. A fault throwing equipment was developed to allow the simulation of one of the most onerous transient conditions: the occurrence of a 3 phase fault close to the loaded machine. A brief description of the elements of the power system model will be given next. Further details of the parameters of the generator, the generator-transformer and the transmission line model are given

in Appendix 15.

1) Prime Mover. The prime mover at Pembroke is formed by three stage, axial flow, steam turbines with a rated speed of 3000 rpm. In the model system, a dc machine is used to model the prime mover. This machine is separately excited by a single phase 200 V thyristor bridge rectifier unit. In the power system model, the action of a speed governor has not been considered, instead, the principle of constant torque during a transient period is adopted.

2) Generator. Each one of the generators at Pembroke station is rated at 500 MW, with a line voltage of 22 kV and a rated power factor of 0.8. The inertia time constant of the generators is 4.44 p.u. In this system model, it has been assumed that the four generators at Pembroke form an identical plant, operating in parallel. On this assumption, a micromachine having the same parameters in per unit quantities, expressed to the total MVA rating, will be capable to model the combined dynamics of the four generators. On the other hand, the micromachine is rated at 3 kVA, 0.8 power factor and 230 V line voltage with the stator winding star connected, while its synchronous speed is 1500 rpm at a system frequency of 50 Hz. The high inertia constant of the generators has been achieved by using a flywheel attached to the micromachine shaft. To achieve transient conditions similar to the generators at Pembroke, the winding resistances in the micromachine stator windings were kept low by increasing the slot depth. An external time constant regulator was connected to the rotor windings to provide the correct rotor time constant. Slip rings were used to connect the external regulator with the rotor windings in order to improve the signal to noise ratio and to provide the correct transient and subtransient time constants. In this way, the rotor current is controlled by reducing the effective resistance and thus increasing the time constant.

3) Electrical Network. The base quantities of 3.45 kVA and 206 V for the model system were determined during the design of the micromachine. The concept of an infinite busbar at the end of the transmission line model, having an ideal zero source impedance, and constant voltage and phase, was approximated by using a high

capacity supply. A separate distribution transformer fed from the high voltage distribution network was used for this purpose. The rating of the transformer is 330 kVA, 10.75 kV/311 V. The transformer is connected to the 6.6 kV distribution network, so by using a 5% tap, the transformer provides a secondary line voltage of 200 V. The secondary winding is star connected with the power system model.

4) Transmission Line. For practical purposes, it has been assumed that the two double circuit transmission lines in the Pembroke system have identical length, and that three line impedances are symmetrical, so the transmission line is modelled by three isolated single phase π equivalent networks. Although this approximation neglects the effects of mutual and self inductances of the three phase line, this assumption remains valid for the present experimental investigation. Due to the high voltage rating and to the 70 miles length of the transmission line, the effects of the shunt capacitance of the line have been included in the equivalent line model. Details of the transmission line in the model system are included in Appendix 15.

5) Fault Throwing Equipment. For the type of disturbances considered for the power system model during the studies in transient stability, the most severe condition will be given if the generator is operating at full load and a three phase solid fault occurs in the transmission line close to the generator transformer. This fault will move the generator into a minimum energy transfer condition where its rotor will be undergo a maximum acceleration. A fault throwing equipment was developed to produce this type of disturbance. Semiconductor devices are used in the fault throwing equipment to carry the fault current for a period of up to 200 ms duration. The fault is fed from both the machine and the infinite busbar so the thrower equipment was designed to withstand currents up to 300 A.

7.3.2 Initial Assessment of the Technique's Performance

In order to evaluate the performance of the DSP based frequency measurement equipment, two groups of tests were conducted. Initially, input signals with constant frequency were used. During this study, the TMS320C31 executable code was

programmed to generate the test signals. The frequencies of the signals for this test are: 47.5 Hz, 50.0 Hz and 52.5 Hz. Figure 7.7 shows the results of the measurement of the frequency of the test signals by using the DSP based technique.

A second group of tests was carried out to appreciate the conditions prevailing under steady state conditions in the micromachine system. Figure 7.8 shows the results of the single phase frequency measurement taken from the generator terminal voltage, phase 'a', under steady state conditions. The peak to peak variation of the measured frequency is 0.01 Hz. It should mentioned here, that during normal operating conditions, the mean value of the measured frequency throughout the experimental investigation was observed to vary within relatively short times. In all the observed cases, the maximum deviation of the frequency was less than 0.1% about 50 Hz. The results from this study also showed that a significant amount of additive noise was imposed on the voltage waveform taken at the generator terminals. The main frequency components of the noise are the odd harmonics of the fundamental frequency produced in the micromachine alternator and also high frequency components generated by nearby power electronic devices. This study constitutes an arduous test for the frequency measurement algorithm since the voltage waveform was more distorted than would be expected on a real power system.

The results from this initial group of tests show the correct operation of the new frequency measurement technique after its implementation on a DSP board. The results also confirm the accuracy of the technique predicted by the investigation conducted on power system computer simulations.

7.3.3 The Applied Disturbance

The type of power system problems which have motivated the development of the power system model, is related to the investigation of the performance of the system during transient stability conditions. A three phase fault on the system side of the generator-transformer with the generator at full load was chosen as the applied disturbance. The fault is followed by full system recovery. This fault is considered

the most severe for the type of power system represented by the present model. As a result of the fault, the micromachine will be swinging against the mains supply. The power system conditions created by this type of disturbance represent an ideal test for the frequency measurement equipment.

The next sections will present a group of tests conducted with the micromachine system. The tests basically consist of applying the fault when the machine is loaded at 1.0 p.u. and at 0.75 p.u. An alternative group of tests has been achieved by changing the duration of the fault. For the current set of tests, the duration times of 70 ms and 120 ms have been used.

The initial rate of change of frequency at the fault inception and the subsequent power swings are determined by the initial conditions in the power system model. Information on the initial conditions is important to assess the response of the system to a particular disturbance. In Table 7.2 and 7.3 are shown the initial values of the system quantities for the generator loaded at 1.0 p.u. and at 0.75 p.u., respectively.

P_t Terminal power	2.4 kW
pf power factor	0.98
V_t Terminal voltage	196 V
I_a Current	8.6 A
V_b Infinite busbar voltage	190 V
I_f Field current	3.2 A
δ Load angle	59°

Table 7.2. Initial conditions for a full loaded generator.

P_t Terminal power	1.8 kW
pf power factor	0.98
V_t Terminal voltage	196 V
I_a Current	7.5 A
V_b Infinite busbar voltage	190 V
I_f Field current	2.8 A
δ Load angle	45°

Table 7.3. Initial conditions for a generator loaded at 0.75 p.u.

Although the fault throwing equipment allows repeatable fault conditions, in conducting the system model studies, care was taken to ensure that the system was operating with stable loaded conditions and that the settings of the fault thrower were the same before any experiment was executed. It should be mentioned here, that the thrower equipment does not synchronize the trigger of the fault with the recording process of the measured frequency conducted on the PC/C31 board. Instead, both the fault throwing and the frequency recording processes have to be started by the user. This problem will result in the frequency measurement records being captured at slightly different times. It will be seen throughout the results obtained in the current experimental investigation that the difference in times from one test to another does not affect the validity of the results.

7.3.4 Single Phase Frequency Measurement

This section presents the results of the experimental investigation conducted on the micromachine system where the DSP based technique has been applied to a single phase voltage input signal. The results presented in this section were taken with the micromachine synchronized onto the distribution network mains supply. The measurement of frequency was conducted both at the generator terminal voltage and at the ac tachogenerator. Since the tachogenerator is operating at a minimum energy transfer condition at all times, it is expected that its frequency will follow the trace

of the rotor speed of the generator. On this assumption, the concept of "mechanical frequency" will be used to denote the rotor speed of the generator. Correspondingly, the frequency measured at the generator terminals will be denoted as the "electrical frequency" of the generator.

The structure of the DSP based single phase frequency measurement technique has been addressed earlier in the present Chapter and an outline of the implemented technique was presented in Figure 7.3. On conducting the present investigation, the measurement of frequency was initially carried out at the generator terminal voltage, phase 'a'. The measurement of frequency is then performed at the tachogenerator terminal voltage, phase 'a'. Throughout the investigation, the sampling frequency of the measurement equipment is 4 kHz.

7.3.4.1 Generator Load = 1.0 p.u. Fault = 120 ms

In the present study case, a three phase fault was applied at the station busbar for a period of 120 ms while the generator was loaded at 1.0 p.u. The frequency measured at the generator terminals, phase 'a', is shown in Figure 7.9. The steady state conditions preceding the fault inception are clearly observed. At the fault inception, the measured frequency undergoes an abrupt positive transient excursion. The nature of this transient in the measured frequency was discussed in Chapters 5 and 6 where it was explained in terms of the redistribution of power in the system. The same conclusion can be reached from the behaviour of the measured frequency in the current study case: the sudden change of the operating conditions of the generator onto a minimum export condition, results in a rapid rotation of the angle between the generator terminal voltage vector and the internal induced emf vector.

Figure 7.9 shows the trace of the measured frequency returning back towards the system's frequency. At time t = 300 ms, the frequency is seen to follow a ramp. This ramp corresponds to the trace of the rotor speed which is accelerating when the generator is moved into the minimum export condition following the fault inception. Due to the large inertia constant of the generator and to the relatively short duration

of the fault, the micromachine does not loss synchronism with the utility.

When the fault is cleared, the generator is prompted to export at full rate. Under this new condition, the angle of the terminal voltage vector is suddenly forced to rotate opposite to the rotor rotation. Hence, the angle of the terminal voltage is moved in advance of the internal induced electromotive (emf) voltage vector. The consequence of the change of the angle is a sudden dip of the electrical frequency. The initial rate of change of the frequency decline is driven by the magnitude of the load and by the inertia time constant of the generator. As the time progresses, a power swing between the machine and the mains supply takes place. The trace of the measured frequency during the power swings correctly describes the direction of the power transfer between the micromachine and the infinite busbar.

In Figure 7.10 is shown the generator terminal voltage waveform, phase 'a', observed during the disturbance. It is seen that the 3-phase fault severely affects the voltage waveform which results in a rapid positive excursion of the measured frequency. The effects of the fault when the generator is full loaded are reflected on the terminal voltage waveform. An exponential decaying dc component is added to the terminal voltage at the fault inception. At the time of the fault, a dc component in the armature current is created to maintain the steady state value of the magnetic flux linkage between the rotor field and the armature winding. The initial amplitude of the dc voltage component at the generator terminals is proportional to the initial conditions before the fault and to the point on wave of the armature current where the fault is applied. Hence, different amplitudes of the dc component should be observed in the phase components of the three phase system at the generator terminal voltage. The time constant of the exponential decaying component in the armature current is determined by the value of the armature resistance. It should be noticed that the frequency response of the orthogonal filters exhibit a zero at dc frequencies, and so the dc component in the terminal voltage will not affect the frequency estimates. In the case of zero-crossing based frequency measurement technique, the dc component will mask the estimates of frequency.

The relatively long duration of the fault allows observation of the point where the transient in the measured frequency has disappeared. In Figure 7.11, the transient in the frequency created at the fault inception, settles down about time t = 300 ms. It can be seen that at this time, the frequency follows a ramp which is deviating from 50 Hz. Such a deviation can be explained in terms of the trajectory of the rotor speed. It was mentioned before that a constant input torque was adopted on developing the prime mover in the power system model. The type of applied disturbance means that the only power exported by the generator during the fault are heating losses only. Hence, the load angle between the electromagnetic and the mechanical torques is almost zero, while the voltage vector at the generator terminals is in-phase with the internal emf vector. Therefore, after the transient, the electrical frequency will follow the trajectory of the rotor speed (mechanical frequency). As a result of this coupling of angles and frequencies, the electrical frequency is seen to follow the speeding up of the rotor speed.

Due to the constant input torque, neither the mechanical nor the electrical frequencies will return to the synchronous frequency unless the fault is removed before the generator losses synchronism with the utility. Figures 7.10 and 7.11, clearly show the time when the fault is removed. The rapid dynamics of the AVR are reflected on the amplitude modulation effects observed in the terminal voltage waveform. However, the change onto a full load condition prevents the terminal voltage to return towards its steady state level. Instead, the angle of the phase of the terminal voltage is stretched as shown in Figure 7.10 at time 355 ms. Figure 7.11 shows the trajectory of the electrical frequency which exactly correspond to the variations in the angular phase of the input signal as shown in Figure 7.10. Apart from the group delay of the frequency measurement algorithm, it can be concluded that the trace of the measured frequency follows the variations in time of the velocity of the phase of the input signal and correctly describes the dynamical response of the machine to the disturbance.

A decaying oscillatory component imposed on the trace of the frequency is shown in Figure 7.9 at time t = 450 ms. The nonlinear response of the dc prime mover

during the disturbance is responsible for this oscillatory component.

From Figure 7.11, it can be observed the transient of the measured frequency when the fault is removed. It will be shown later during the experiments conducted on the tachogenerator terminals, that the electrical frequency follows the direction of the flow of power between the machine and the mains supply during the subsequent power swing period. In terms of the electromagnetic torque at the generator air gap, it can be seen that at the time when the fault is cleared, the rotation of the electromagnetic torque during the power swings is retarded by the power flowing from the mains supply. It was pointed out earlier, that the rotor speed started an accelerating process at the fault inception and the constant input torque in the prime mover had promoted the constant deviation of the rotor speed from 50 Hz. When the fault is removed the change back to the full load condition suddenly applies a braking torque to the generator shaft and the electromagnetic torque provides the means to slow down the rotor speed. The oscillations in the flow of power pushing forwards and backwards between the generator and the utility during the power swing, correspond to the dynamic response of the generator. If the fault had been removed at an earlier stage, the rotor speed would increase for a shorter time, hence, the change onto a full load condition would had resulted in smaller deviations of the frequency from 50 Hz during the power swing.

7.3.4.2 Generator Load = 1.0 p.u. Fault = 70 ms

The duration of the fault has been reduced to 70 ms in this study case. The frequency measured during this test is shown in Figure 7.12. A small negative excursion of the frequency is shown at the fault inception. In particular, this small dip is related to the point on wave of the input signal where the fault has occurred. It is noticed that the dip in the frequency corresponds to the application of the 3-phase fault. Apart from this transient in the phase of the signal, the measured frequency is seen to follow the expected trajectory of the electrical frequency of the generator.

Since in the current study case the generator is also loaded at 1.0 p.u. the variations in the frequency are seen to follow the same trace of the frequency measured in the previous study. A comparison between Figures 7.11 and 7.14, reveals that the initial ramp of the frequency is the same in both cases regardless of the small dip of frequency shown in the current study case.

The waveform of the input signal during the present study case is shown in Figure 7.13. The exponential decaying dc voltage component is observed again. This time, the fault is cleared before this component has completely disappeared. The overshoot of the terminal voltage when the fault is removed corresponds to the response of the AVR encountering a full load condition imposed by the fault clearance. A detailed view of the measured frequency during the disturbance is shown in Figure 7.14. It was mentioned at the end of the last study case that a shorter duration of the fault under the same initial conditions, would result in smaller deviations of the frequency from 50 Hz during the subsequent power swings. It can be seen that the 70 ms fault reduces the amount of kinetic rotating energy in the generator gained during the acceleration of the rotor. The braking torque applied to the generator shaft when the fault is cleared, now results in smaller deviations of frequency during the power swing. Figure 7.12 shows that during the power swing period following the fault clearance, the peak to peak variations of the frequency are smaller as compared to the 120 ms fault.

7.3.4.3 Generator Load = 0.75 p.u. Fault = 120 ms

In this study case the generator is loaded at 0.75 p.u. As shown in Figure 7.15, the measured frequency now undergoes a less severe acceleration when the fault is thrown. The effects of a partial loaded generator are shown on the initial rate of the frequency at the fault inception which can be compared against the initial rate of the frequency when the generator is full loaded. Since the generator is partial loaded, the rotor will not accelerate to a maximum level as seen in the first study case. Apart from the transient, the measured frequency in the current study case exhibits a smoother initial rate of change of frequency as compared with the previous case

of a full loaded generator. Figure 7.17 shows a detailed view of the frequency during the disturbance. A comparison of the frequency shown in this figure with the frequency shown in Figure 7.14, shows the different initial rates of change of the frequency at the fault inception. Since in the micromachine model the prime mover is not assisted by a speed governor, the measured frequency is seen to follow an oscillatory ramp after the fault. As explained during the first study case, the voltage vector at the generator terminals is rotating in phase with the internal mmf, thus, after the transient of the electrical frequency at the fault inception, the frequency will be seen to follow the trace of the rotor speed during the acceleration period. Figure 7.17 shows that the maximum excursion of the frequency following the fault inception is 50.4 Hz. As compared with the full load case, this deviation results from a smoother speeding up of the rotor.

In this study case, the amount of the power exported by the generator during the fault (heat losses only), is smaller. Thus, a smaller exponential decaying dc component is created at the fault inception as observed on the voltage waveform shown in Figure 7.16.

When the fault is removed, the generator encounters a 0.75 p.u. load. Hence, the application of the braking torque to the rotor shaft when the fault is removed results in a slower rate of change of the frequency. As shown in Figure 7.17, the initial rate of change of the frequency when the fault is cleared is smoother as compared with the frequency during full load conditions. Since the infinite busbar infeed is now 0.25 p.u., the power swing periods are smaller in amplitude and duration.

7.3.4.4 Generator Load = 0.75 p.u. Fault = 70 ms

As shown in the input signal waveform displayed in Figure 7.19, the fault has been thrown at a different point on wave as compared to the last study case. As shown in the previous cases, the application of the fault results in a transient in the measured frequency. Since the initial loading conditions of a partial loaded generator still prevail in the current study case, then, the ramp of the frequency during the

acceleration period is the same as the ramp of the frequency in the previous case. Figure 7.20 shows the trace of the frequency when the fault is cleared. The frequency shows the rapid recovering process of the generator when the fault is cleared. The load infeed by the infinite busbar and the short duration of the fault result in a very short power swing period.

7.3.5 Single Phase Frequency Measurement Taken at the Tachogenerator Terminals

As pointed out earlier in the present section, it was sought that the frequency measurement conducted on the tachogenerator terminals would provide a point of reference to appreciate the process of change of the mechanical frequency of the micromachine. In the present experimental stage, the same type of tests presented in the previous study cases is now conducted on the tachogenerator terminals.

From the outline of the power system model shown in Figure 7.6, it can be seen that the tachogenerator is linked in parallel to the micromachine shaft. In fact, a flexible tooth-band links both shafts. Care was taken during the construction of the tachogenerator and of its linkage with the micromachine to ensure a one-to-one ratio of speeds. On the assumption that the proposed speed ratio is observed, the frequency of the tachogenerator terminal voltage will correspond to the rotational speed of the generator's shaft. Since no electrical power output is drawn from the tachogenerator terminals, it is expected that its terminal voltage vector will be synchronously rotating with the tachogenerator's rotor. Correspondingly, the application of the 3-phase fault near the generator transformer will not impose an amplitude modulation process on the tachogenerator terminal voltage. Hence, the measured frequency will not exhibit the transients observed during the application of the 3-phase fault.

7.3.5.1 Generator Load = 1.0 p.u. Fault = 120 ms

The frequency measured under the initial conditions given for this study case is

shown in Figure 7.21. During the steady state conditions preceding the fault inception, a periodic component is observed in the tachogenerator frequency. It has been found that this oscillation corresponds to a sine frequency modulation of 20 Hz approximately. It was found that back-lash in the coupling, caused by the tooth-band, was the cause of the periodic component.

Apart from this problem, the results of the measurement of frequency displayed in Figure 7.21 clearly show the impact of the applied fault on the speed of the tachogenerator. It can be seen that the initial rate of change of the mechanical frequency does not follow the step ramp displayed by the electrical frequency taken at the generator terminals. From the conclusions drawn during the first study case, it is seen that the excursion of the mechanical frequency follows the mechanical dynamics of the generator. The inertia time constant of the machine prevents the rotor from following the rapid acceleration exhibited by the transient of the electrical frequency when the fault is applied. It was mentioned earlier, on conducting the measurement of the frequency at the generator terminals, that the sudden change in the voltage waveform resulted in a transient in the electrical frequency at the fault inception time. After the transient, it was seen that, since the angle between the terminal voltage vector and the internal emf was constant in time, then, the trace of the electrical frequency did correspond to the trace of the rotor speed. Hence, both frequencies should travel the same trace during the acceleration of the generator. The mechanical frequency shown in Figure 7.21 confirms the predicted response of the electrical frequency. As shown in Figure 7.21, the peak deviation of the mechanical frequency is 50.5 Hz. This value is equal to the deviation shown by the electrical frequency as shown in Figure 7.11.

When the fault is removed, the mechanical frequency shown in Figure 7.21 reflects the response of the generator when it encounters a full load condition. The remaining trace of the frequency measured at the tachogenerator clearly shows the power swing between the micromachine and the mains supply. The behaviour of the frequency during the power swing corresponds to fluctuations of power between the generator and the mains supply. Under the assumption of constant input torque from

the prime mover, the electromagnetic torque is the only means to slow down the oscillations of the rotor speed following the clearance of the fault and during the power swing. Eventually, the oscillations of the mechanical frequency shown during the power swing period will decrease until a balance between the electromagnetic and the mechanical torques is achieved.

7.3.5.2 Generator Load = 1.0 p.u. Fault = 70 ms

In the present study case the generator is full loaded as in the last case, hence, its response at the fault inception should be the same. In Figure 7.22 is shown the measured frequency taken at the tachogenerator terminals. The initial rate of change of the mechanical frequency during the acceleration process of the generator is equal to rate of change already seen in the last case. Now, however, the shorter duration of the fault has prevented the rotor speed from accelerating for a longer time. Thus, when the fault is removed, the shorter duration of the fault allows the generator to withstand better the effects of the application of the full load. The amount of kinetic energy gained during the acceleration process is smaller as compared with the full loaded generator initial conditions. Therefore, the trace of the mechanical frequency is seen to follow the smaller deviations from 50 Hz during the power swings.

7.3.5.3 Generator Load = 0.75 p.u. Fault = 120 ms

For the initial conditions of this study case, the slope of the rate of change of the mechanical frequency, as shown in Figure 7.23., should be the same as the slope of the rate of change of the electrical frequency observed in Figure 7.15. Although the transient in the electrical frequency masks the initial ramp of the frequency, it was seen in figure 7.17 (the detailed view of the measured frequency), that the electrical frequency did subsequently follow the trajectory of the rotor speed. Now, the mechanical frequency taken at the tachogenerator terminals confirms that observation. Both the mechanical and the electrical frequencies reach a maximum deviation of 50.4 Hz at 120 ms after the fault inception.

The initial conditions in the current study case result in a smoother initial rate of change of the mechanical frequency when the fault is applied. This fact was also observed in the initial rate of change of the electrical frequency. The partial loaded generator initial conditions result in a smoother acceleration of the rotor when the fault is applied. Hence, when the fault is removed the rate of decay of the frequency is slower, and the subsequent deviations of the mechanical frequency are smaller during the power swing.

7.3.5.4 Generator Load = 0.75 p.u. Fault = 70 ms

For this case, shown in Figure 7.24, the mechanical frequency seen at the tachogenerator terminals scarcely reflects the effects of the fault on the micromachine rotor speed. The slope of the initial rate of change of the mechanical frequency during the acceleration period should be equal to slope of the frequency shown in the previous case. However, the 20 Hz periodic component in the tachogenerator waveform masks much of these results. The main indication of the fault are the small power swings following the fault clearance.

7.3.6 Extended Lowpass Post-filtering of the Measured Frequency

The last set of study cases shows the necessity of removing the 20 Hz frequency oscillation from the mechanical frequency. In this section, a three-cycle Hamming lowpass post-filter has been implemented on the DSP based frequency measurement equipment to remove the 20 Hz component from estimates of the mechanical frequency. As pointed out earlier, the high cpu execution time of the digital implementation of the PPS frequency measurement, make it impossible to apply this filter for the PPS application.

The set of initial operating conditions of the power system model observed during the conduction of the experimental tests with the tachogenerator is now repeated for the application of a 3-cycle Hamming post-filter to the single phase frequency measurement equipment. The results from the use of the post-filter on the estimates

of the frequency measured at the tachogenerator terminals have been collected in Figure 7.25. It is seen that the frequency response of this filter effectively removes the 20 Hz periodic component from the mechanical frequency and confirms the nature of the periodic oscillations.

Figure 7.25.a clearly shows the slope of the ramp of the mechanical frequency following the fault inception. Apart from the increased group delay (57.5 ms), from which, 20 ms are due to the 3-cycle Hamming post-filter, the smoothed frequency accurately follows the changes of the response of the micromachine when the fault is applied and when the fault is removed. From the graphics shown in Figure 7.25, the following conclusions can be drawn:

1° The point of the frequency excursion where the fault takes place is clearly observed since the transient observed in the electrical frequency does not mask the current measurements.

2° The effects of the fault on the initial rate of change of the rotor speed are clearly observed. The initial rate of change corresponds to the initial loading conditions and the inertia time constant of the generator.

3° The trajectory of the rotor speed following the clearance of the fault show the amount of kinetic gained during the speeding up of the rotor. For the same initial conditions, a shorter duration of the fault results in shorter oscillations of the frequency about 50 Hz during the power swings.

In order to provide a fair point of reference with respect of the investigation performed on the generator terminals, the 3-cycle post-filter was used during the same study cases. The results from the measurement of frequency of a single phase voltage signal, as taken at the generator terminals, are displayed in Figure 7.26. The results from the set of different initial conditions and fault duration times are presented in Figures 7. 26.a, 7.26.b, 7.26.c and 7.26.d.

The effects of the frequency response of the three-cycles Hamming lowpass filter can be appreciated in the electrical frequency displayed in these figures. The amplitude of the transient of the electrical frequency at the fault inception has been attenuated in all the cases. It is also noticed that the initial rate of change of frequency has also been modified as a result of the frequency response of the post-filter. It is seen that the extreme attenuation of the filter masks the trace of the frequency following the transient which as compared to the one-cycle Hamming post-filter. However, the peak to peak deviations of the electrical frequency during the power swing periods are preserved. A unit gain bandpass of 5 Hz near to dc is required if the oscillations due to the frequency modulation process are to be preserved. This requirement can be achieved by implementing a larger FIR lowpass filter at the expense of a longer group delay.

Figures 7.26.a and 7.26.c provide a point of comparison between the electrical frequency measured when the generator is full and partial loaded. It is seen that the peak deviation of the electrical frequency transient at the fault inception in the latter case corresponds to a 75 % of the former frequency. The same figures also show that the initial rate of change of electrical frequency following the fault inception is different. The frequency response of the post-filter is responsible for the attenuation of the trace of the rapid variations of the electrical frequency, while the same filter preserves the slower variations of the mechanical frequency.

7.3.7 Experimental Investigation with the PPS Frequency Measurement

The structure of the DSP based frequency measurement equipment for its application on the measurement of frequency from a PPS voltage vector is shown in Figure 7.4. The measurement of frequency from a PPS voltage vector has been taken at the generator terminals and at the tachogenerator terminals. On conducting the measurement of frequency from a PPS voltage vector, it is expected to observe the combined variations in the angle phase of the phase components of the input signal, both at the fault inception and at the fault clearance times. As it was pointed out earlier during the discussion on the implementation of the software for the PPS

application, the DSP implemented PPS frequency measurement equipment has not been provided with the one-cycle Hamming lowpass pre-filter. Thus, it should be expected to observe the influence of the harmonic noise on the frequency estimates. It should also be mentioned that in the current PPS frequency measurement implementation, the voltage waveform is not sent to the PC resident program since it is not possible to send the information of the three phases at the same time. The earlier set of studies conducted with the single phase frequency measurement can be used now as a point of reference in order to evaluate the performance of the PPS frequency measurement.

The performance of the PPS frequency measurement equipment was tested using the same type of disturbances used during the evaluation of the single phase frequency measurement. The results from these tests show the correct operation and accuracy of the frequency measurements as predicted during the EMTP experimental investigation. Since the results have confirmed the reliability of the PPS frequency measurement equipment, in this section are presented the results of the measurement of frequency taken at the generator and at the tachogenerator terminals for a full loaded generator and a fault duration of 120 ms only.

7.3.7.1 PPS Frequency Measurements at the Generator Terminals

The initial conditions for this case are: generator loaded at 1.0 p.u. and fault duration = 120 ms. In Figure 7.27 is displayed the frequency measured from the PPS voltage vector formed at the generator terminals. The trajectory of the PPS frequency measured during steady state conditions preceding the fault inception is clearly shown. This initial measurement is used to confirm the correct operation of the PPS frequency measurement algorithm following its implementation on the DSP board. Figure 7.27 shows the combined effect of the 3-phase fault on the three phase components of the PPS voltage vector. The first negative excursion of the PPS frequency clearly shows the results of the application of the fault on the individual phase components. Following this transient, it is seen that the PPS electrical frequency accurately follows the trajectory of the single phase frequency. Since the

fault did not affect the balanced condition of the system, the frequency of the PPS voltage vector accurately describes the effects of the fault in the rapid transient rotation of the internal emf vector as shown by the single phase frequency measurement. After the transient in the PPS frequency, Figure 7.27 shows the PPS frequency following the trajectory of the rotor speed. As soon as the transient in the PPS frequency is finished, the angle between the PPS vector and the internal emf becomes close to zero, and so the angle remains constant in time.

When the fault is removed, the PPS frequency shows the response of the system to the sudden application of the full load. A comparison of the transient of the PPS frequency at the fault clearance with the transient of the single phase frequency renders no difference. During the single frequency measurements it was argued that the removal of the fault produced a rapid variation in the rotation of the angular phase of the input signal. In the current study case, the same effect is present in the three phase components of the PPS voltage vector. Apart from the transient, it can be seen in figure 7.27, that the PPS frequency returns back to the system's frequency in time to encounter the power swing between the machine and the mains supply. It is noticed that, as the power swing progresses, a small ripple is imposed on the PPS frequency. The frequency of this noise component is due to the second harmonic of the fundamental. As shown during the initial assessment of the performance of the frequency measurement algorithm, the presence of harmonics in the input signal produces corrupted estimates of frequency.

7.3.7.2 PPS Frequency Measurements at the Tachogenerator Terminals

The measurement of frequency from a PPS voltage vector is now conducted at the tachogenerator terminals. The measurement of frequency from a PPS voltage vector at the tachogenerator terminals has been the most arduous throughout the experimental investigation as far as the sensitivity to additive noise of the frequency measurement algorithm is concerned. Since symmetrical conditions prevail and no electrical power output is drawn from the tachogenerator terminals, it is expected that the PPS frequency measurements will exhibit the same performance of the single

phase frequency measurements. The initial conditions in the system from the last study case are used now on conducting this investigation.

The PPS frequency during the steady state conditions before the fault is applied is shown in Figure 7.28. The 20 Hz periodic component imposed on the PPS frequency is clearly observed. When the fault is applied, the initial rate of change of the mechanical frequency represented by the PPS voltage vector at the tachogenerator terminals, corresponds to the predicted response of the generator according to the initial conditions. The trajectory of the PPS frequency when the fault is removed, exactly corresponds to the trace of the single phase mechanical frequency. During the power swing period following the clearance of the fault, the presence of the second harmonic is clearly seen on the peak deviations of the frequency. This study case remains the necessity of correctly extracting the fundamental component from noise before the frequency estimation.

7.4 Summary

The implementation of the frequency measurement algorithm on a digital signal processing board has been presented in this Chapter. A computer program was used to ascertain the sensitivity of the overall algorithm to the presence of quantization noise as this noise may be generated within the same algorithm as a result of its digital implementation. The evaluation of the dynamic range figure and the operational rate of the algorithm, resulted in the selection of a 32-bit floating point DSP board. A single instruction execution time of 60 n is guaranteed by the chosen board.

The development of a software package to implement the algorithm on the DSP board, was presented in the second section of this Chapter. A discussion on the main structure of the DSP program was presented with respect to the measurement of frequency from both a single phase input signal and from a PPS vector. The limitations of the implementation of the PPS frequency measurement algorithm were also addressed. The one-cycle Hamming lowpass pre-filter is not used in the PPS

frequency measurement implementation.

An experimental investigation was conducted on a micromachine based power system model and the results of using the DSP based frequency measurement equipment during this experimental stage have been presented later in the Chapter. The realistic power system frequency transients created by this laboratory simulator confirmed the accuracy and fast response of the frequency measurement equipment. The following conclusions have been made from the results obtained during this experimental investigation:

1° In order to account for the influence of the random behaviour of elements inside and outside the frequency measurement equipment such as temperature drifts, long term drift of the parameters of elements such as analogue filters, transformers, power supplies, etc, the accuracy of the algorithm as predicted during the computer modelling simulations, should be decreased by an order of ten times, that is the accuracy of the frequency estimates by using the measurement algorithm implemented on the DSP board is $\pm$ 0.01 Hz.

2° The type of disturbance applied onto the power system model has shown that the system model is capable of representing a realistic set of power system frequency transient conditions. Hence, the experimental investigation represents the most arduous and conclusive series of tests to confirm the accuracy and fast evaluation time of the new frequency measurement algorithm.

3° Measurement of frequency at the generator terminals. The frequency measured at the generator terminals has been denoted as the electrical frequency of the generator. In the different study cases presented, it was seen that the measured frequency did describe the variations of the angular phase of the input signal. For the same initial conditions, it was seen that both the single phase frequency and the PPS frequency showed the same trajectories at the fault inception. The initial transient in the electrical frequency has been shown to correspond to variations in time of the angle of the phase of the observed input signal. Following the transient,

it has been shown that the duration of the fault, for similar initial conditions, resulted in a different response of the generator when the fault is removed. That is, the longer the fault duration, the longer will be the deviations of the frequency from 50 Hz during the power swing following the fault clearance.

The response of the generator when the fault is cleared has been perfectly shown by the measured frequency. Both the single phase and the PPS frequencies follow the same trace on pursuing the variations of the power swing created after the fault release.

4° Frequency measured at the tachogenerator terminals. The performance of the new frequency measurement technique when it is connected to the tachogenerator terminals, has shown the real response of the rotor speed, denoted as "mechanical frequency", during the disturbance. The results from this experimental stage have shown that the initial rate of change of the rotor speed can be masked by the transient observed in the electrical frequency. However, it has been shown that the transient in the electrical frequency corresponds to a real phenomenon which is particularly related to variations of the angle between the voltage vector at the generator terminals and the internal induced emf vector. Hence, for the particular type of disturbances used in this investigation, the transient in the electrical frequency is an accurate indication that a severe disturbance in the power output of the generator has occurred, either due to the change onto minimum power export or the change onto a full load condition.

5° The measurement of frequency from a PPS voltage vector has shown a close agreement with the single phase frequency measurements. From the nature of the PPS voltage vector, it has been possible to observe the combined variations of the angular phase of the phase components of the PPS vector. The PPS frequency measurements have confirmed the fact that the variations of the frequency measured individually at a single phase can undergo a different trace as compared to the trace of the frequency of the other two phases. The effects of harmonics in the PPS frequency have shown the necessity of a lowpass pre-filter to improve the frequency

response of the orthogonal filters.

6° From the results obtained in Chapters 5 and 6, the performance of the new frequency measurement technique was evaluated against computer based models. The results obtained on conducting the experimental investigation presented in this Chapter, have corroborated the correct operation of the new frequency measurement technique implemented on a DSP based board, and also confirm that this technique fulfils the requirements of accuracy and fast evaluation times which are necessary for its use in on-line power system frequency measurement applications.

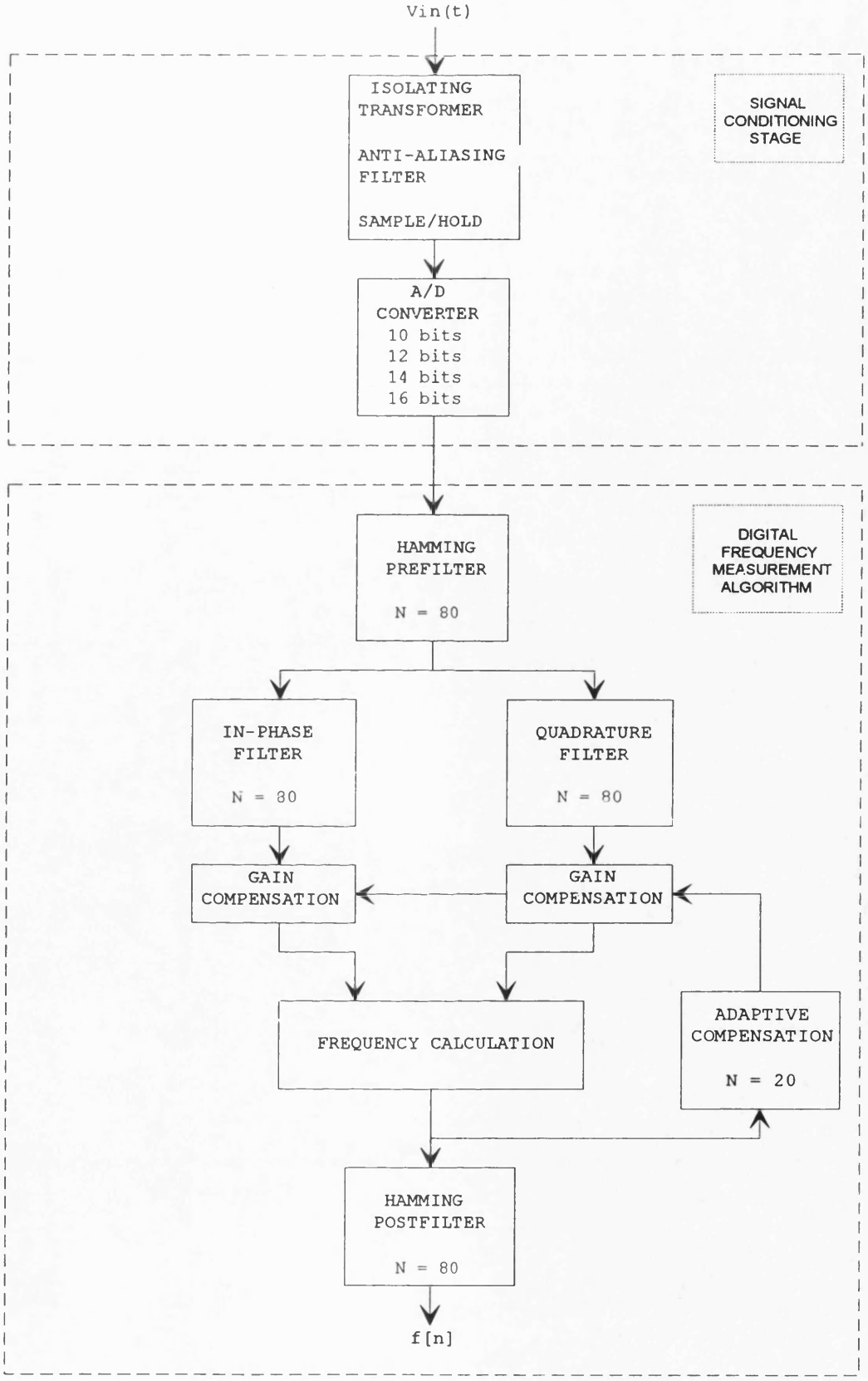

Figure 7.1. Outline of the digital implementation of the frequency measurement algorithm.

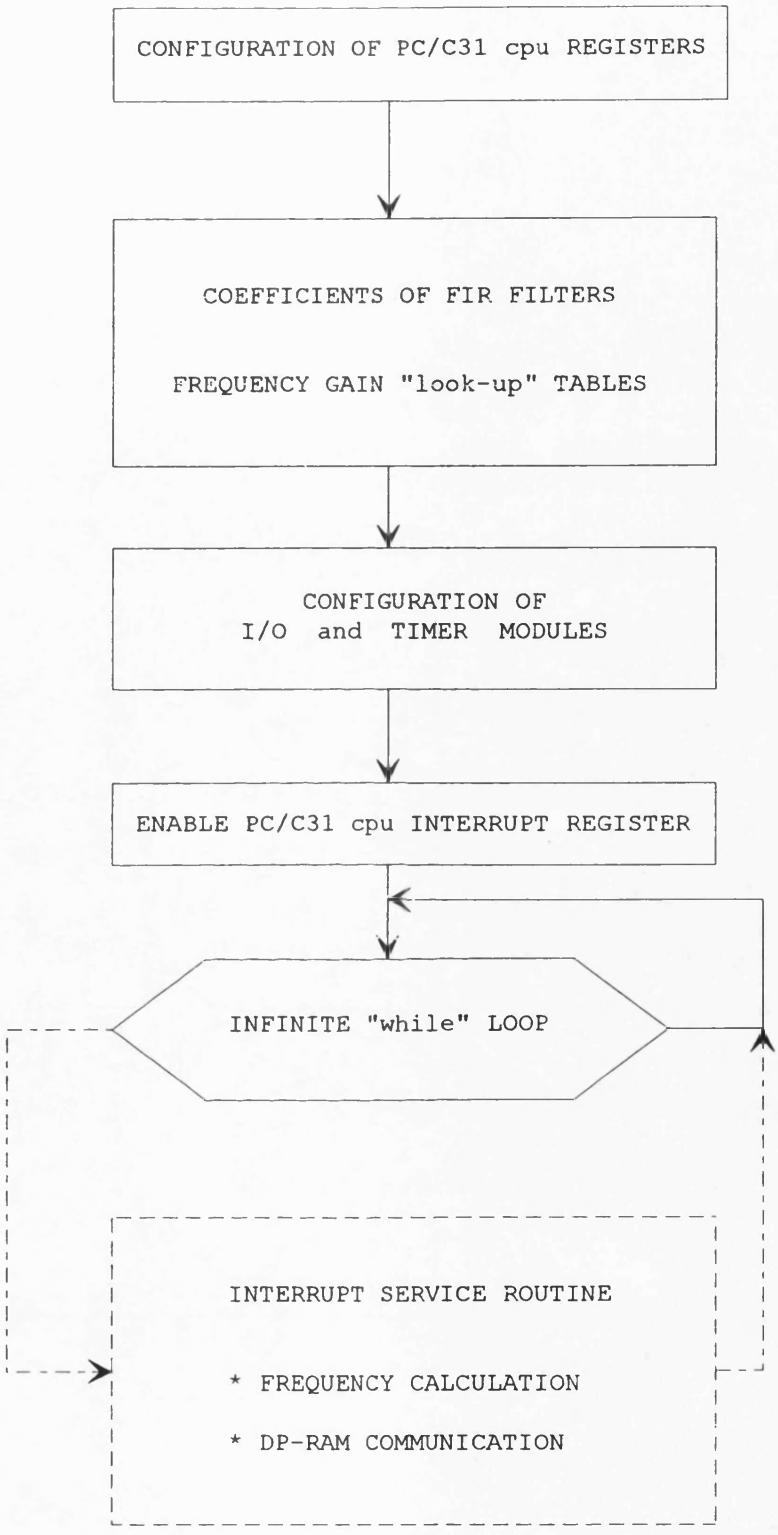

Figure 7.2. Flow chart of the PC/C31 executable code.

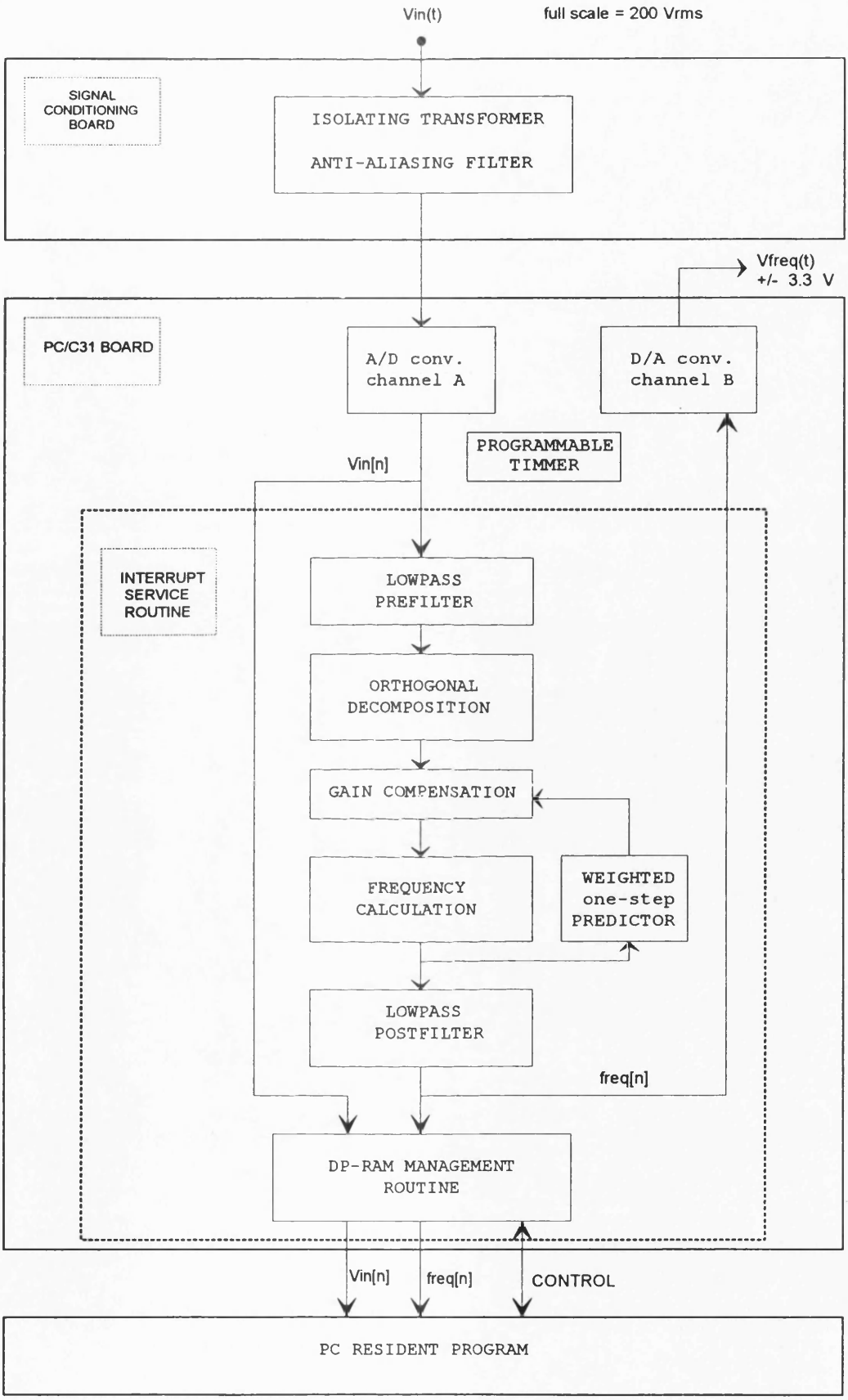

Figure 7.3. Outline of the DSP based single phase frequency measurement algorithm.

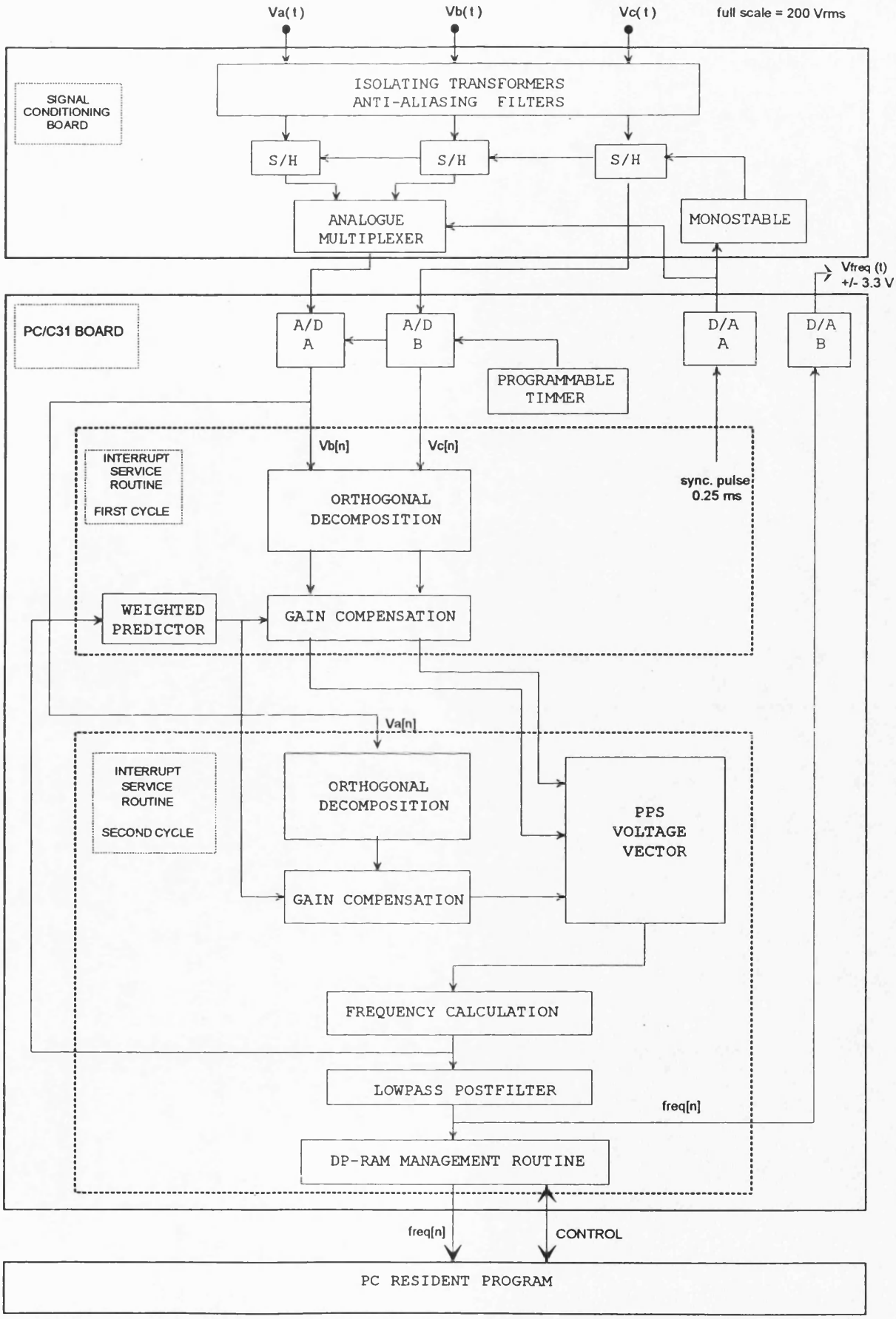

Figure 7.4. Outline of the DSP based PPS frequency measurement algorithm.

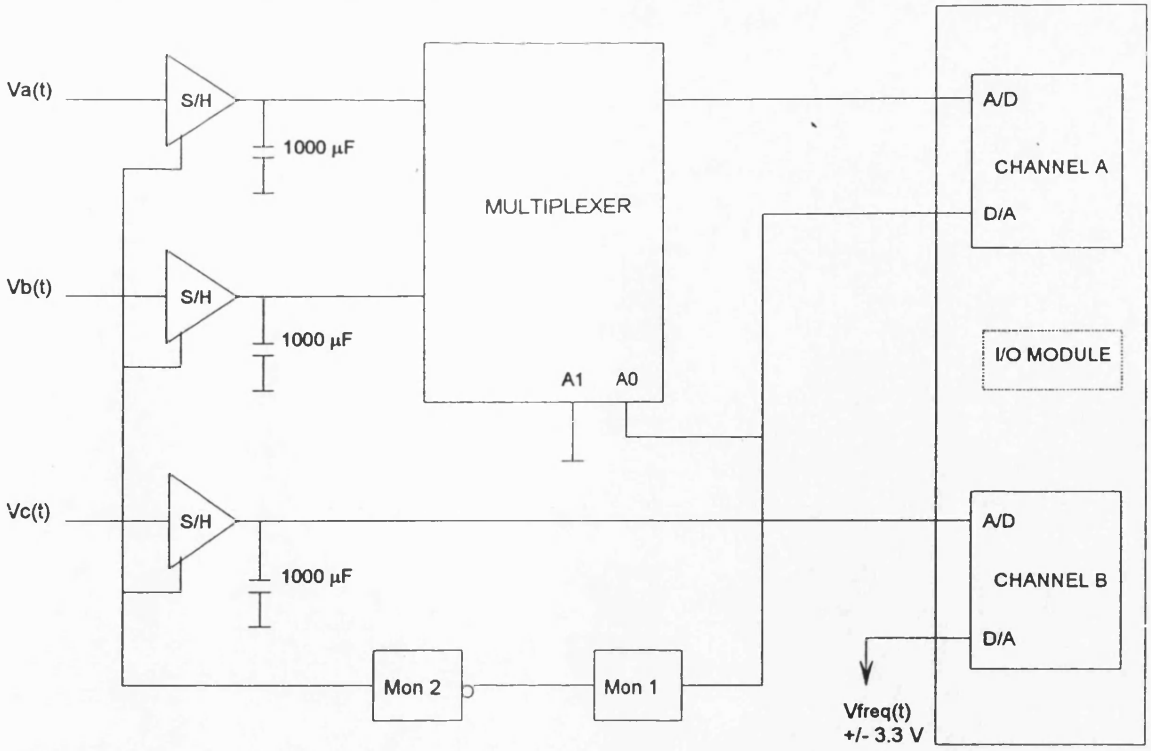

Figure 7.5.a. Using the D/A converter on channel A to drive the multiplexer and the S/H circuits.

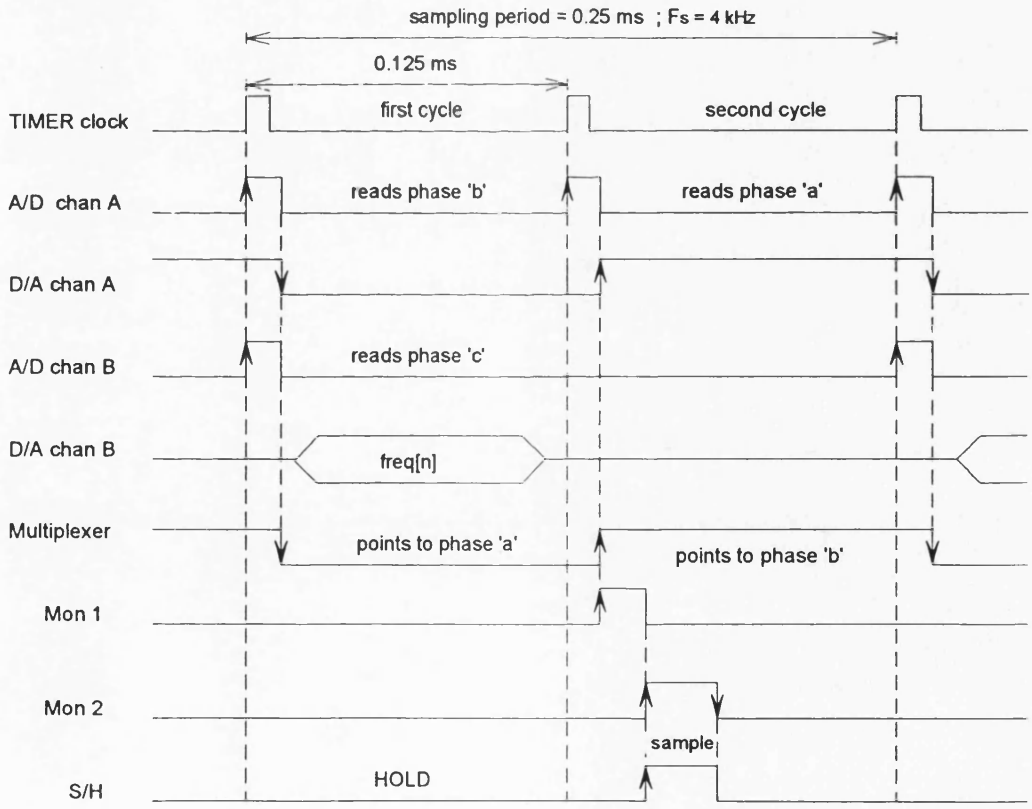

Figure 7.5.b. Timing diagram of the ISR for the PPS frequency measurement process

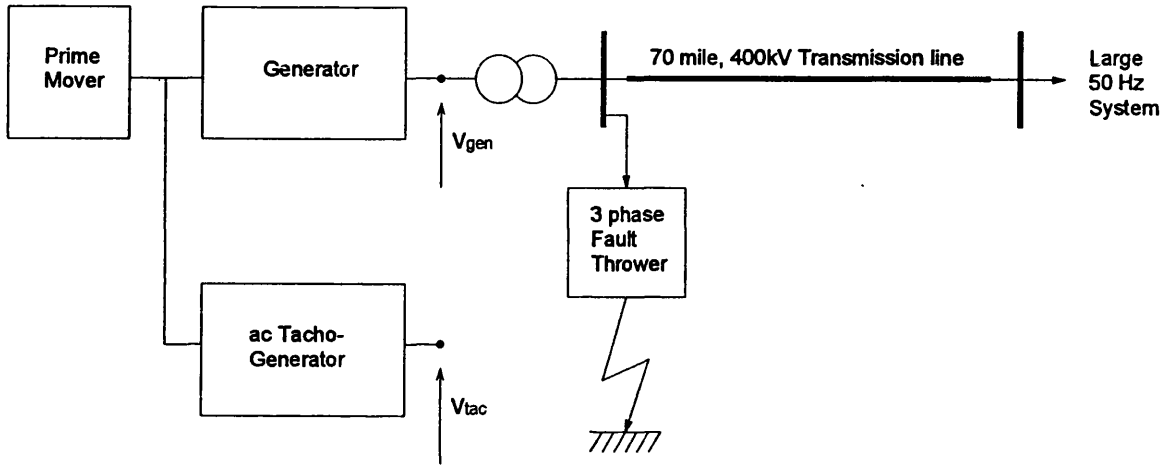

Figure 7.6. Outline of the power system model.

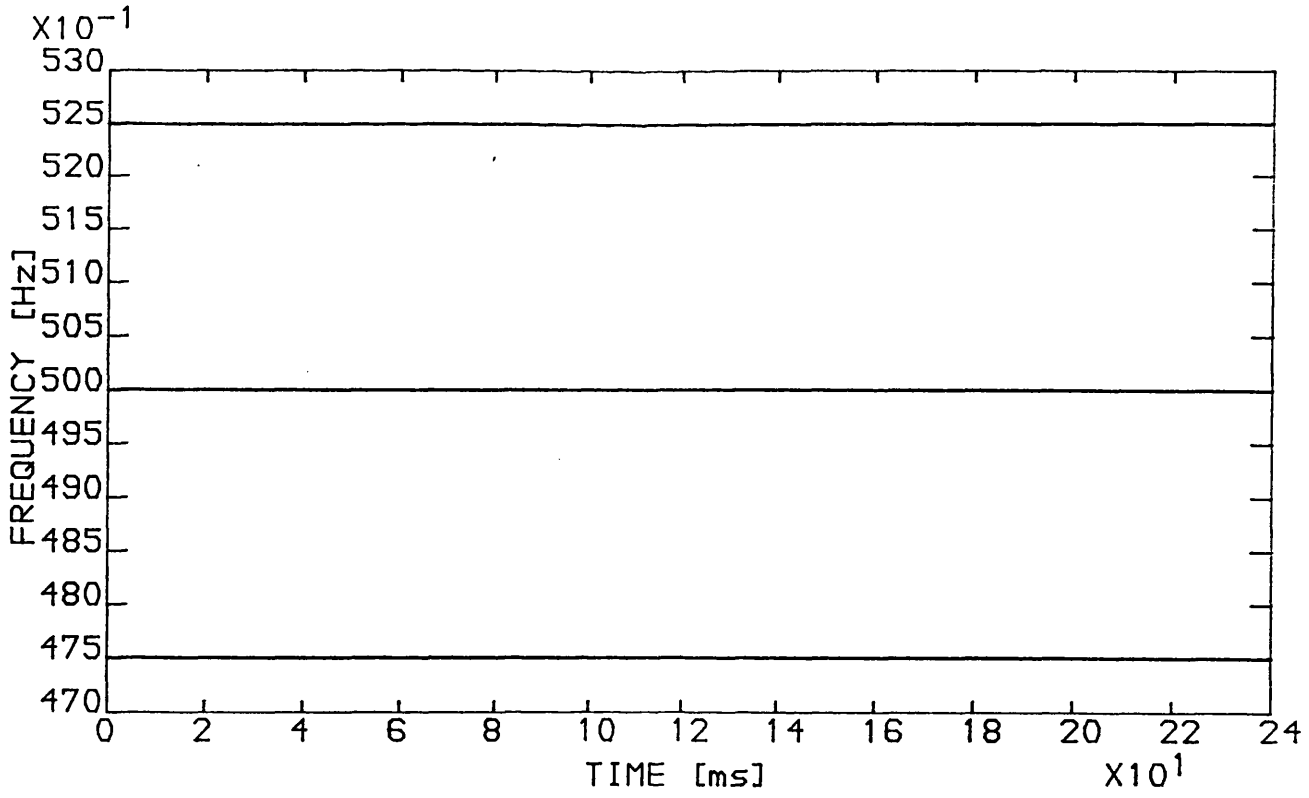

Figure 7.7. Measured frequency of test signals generated by the PC/C31 executable code.

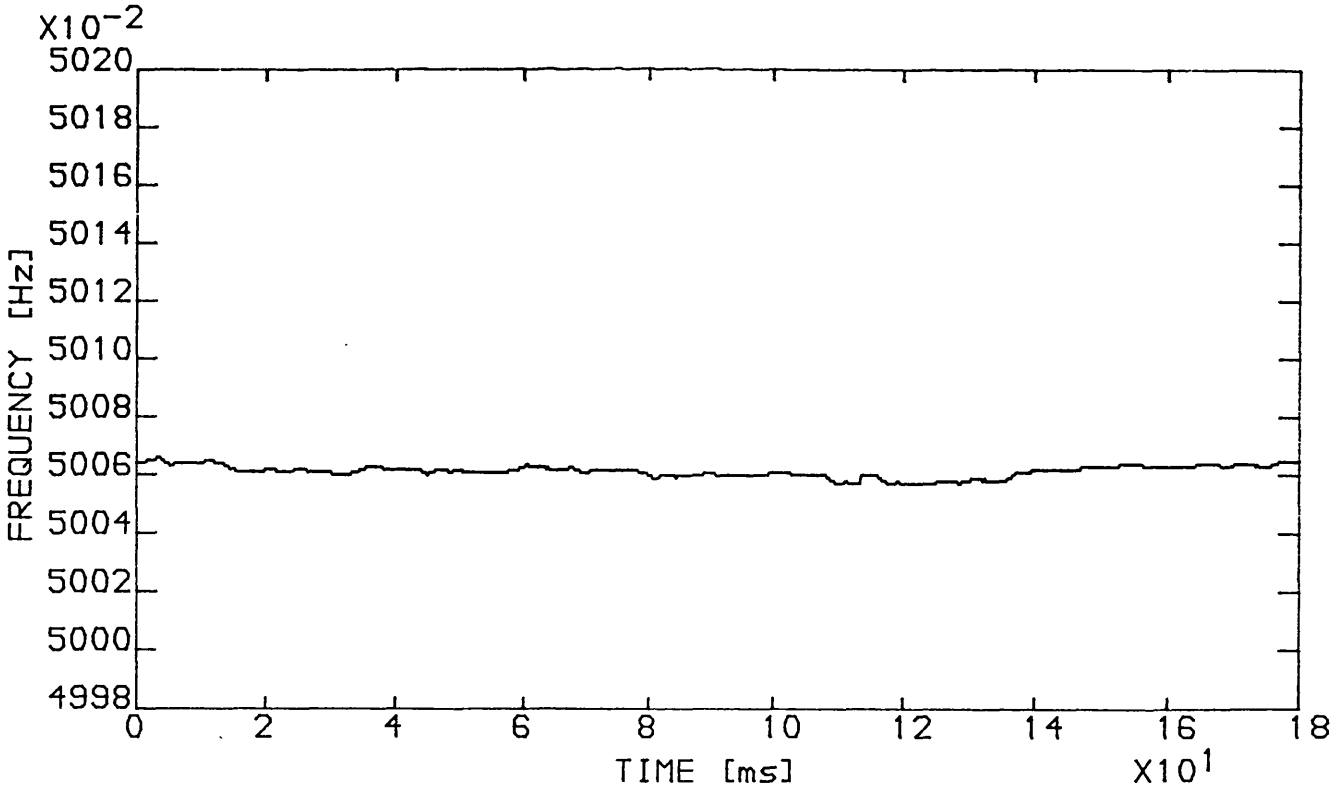

Figure 7.8. Steady state, single phase frequency measurement at the generator terminals.

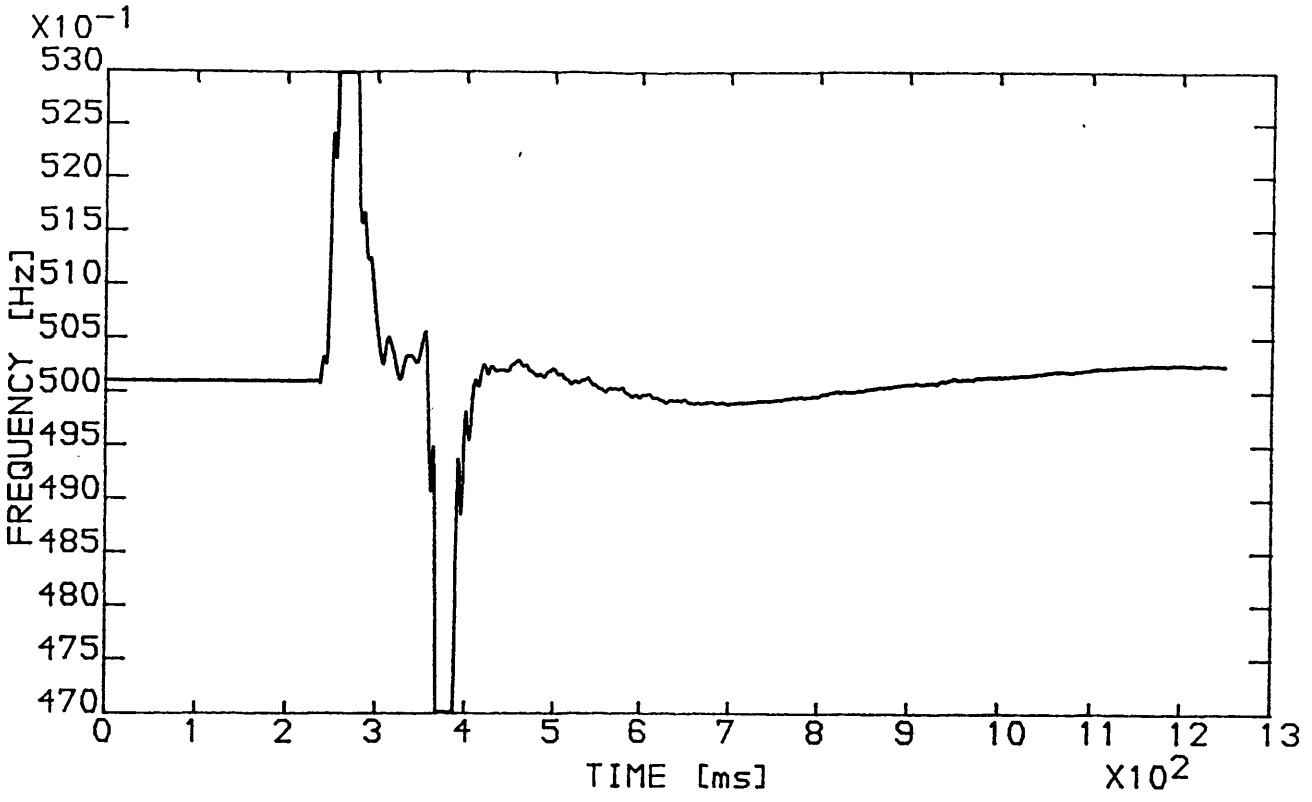

Figure 7.9. Single phase frequency measurement. Generator loaded at 1.0 pu; fault duration = 120 ms.

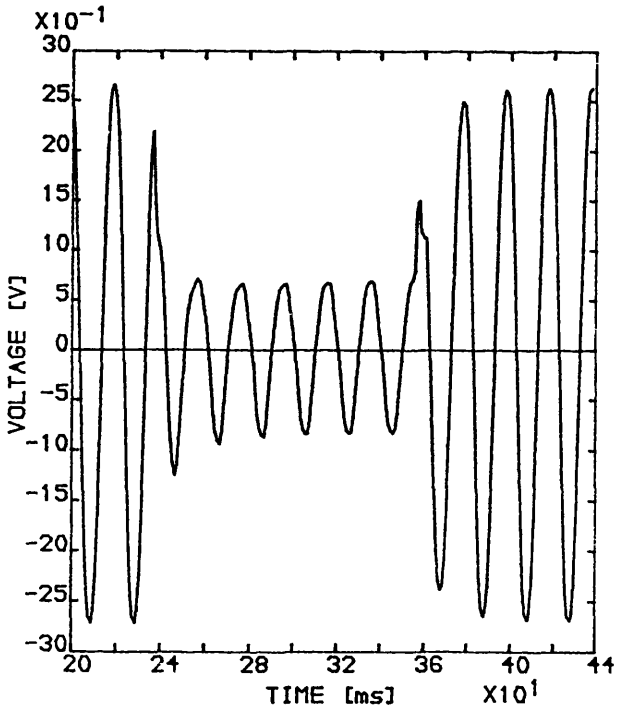

Figure 7.10. Generator terminal voltage waveform, phase 'a', during the disturbance.

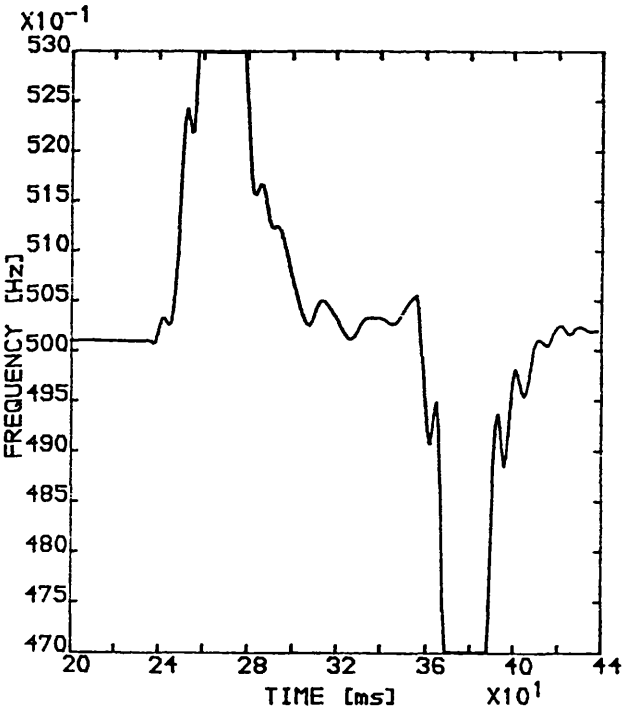

Figure 7.11. Measured frequency during the disturbance.

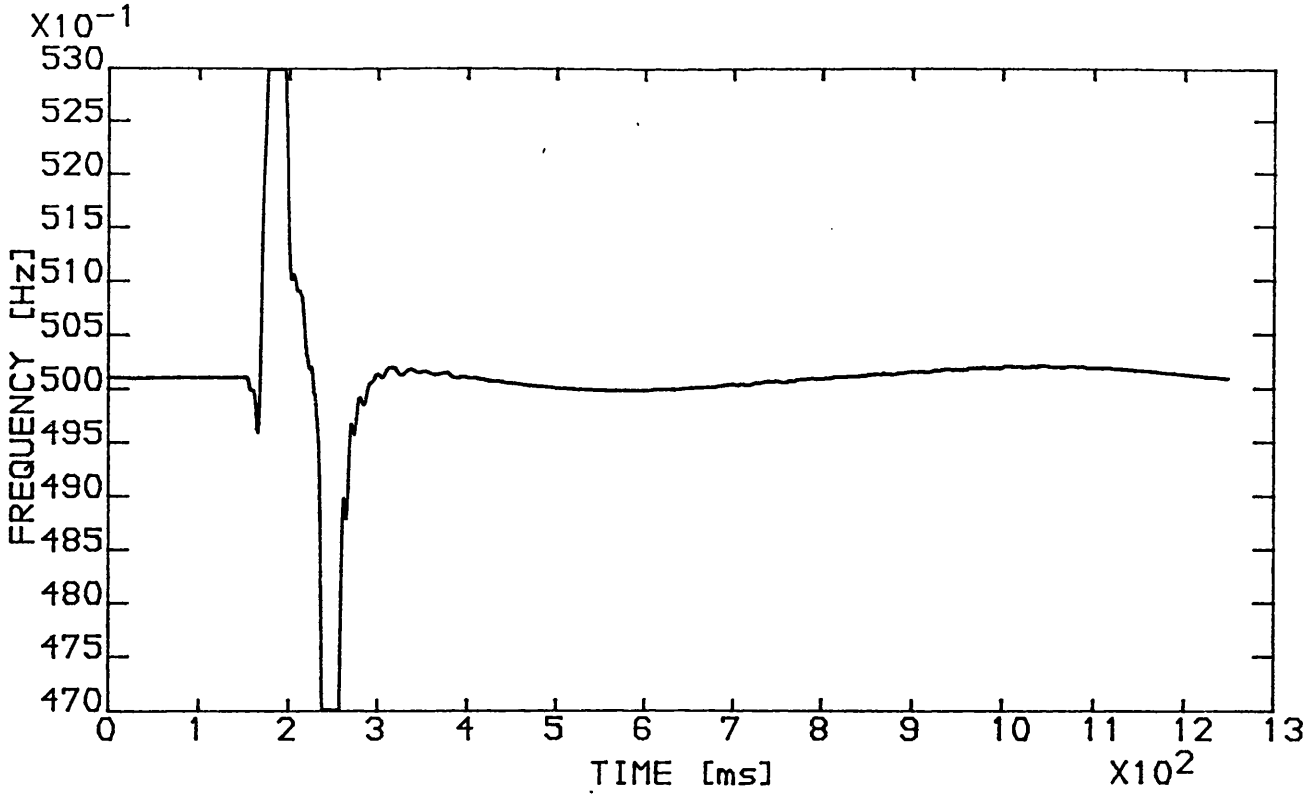

Figure 7.12. Single phase frequency measurement. Generator loaded at 1.0 pu; fault duration = 70 ms.

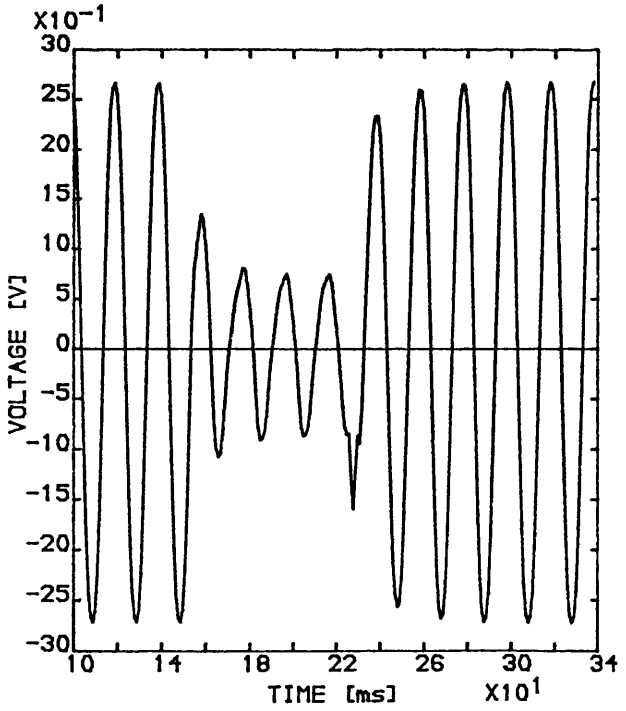

Figure 7.13. Generator terminal voltage waveform, phase 'a', during the disturbance.

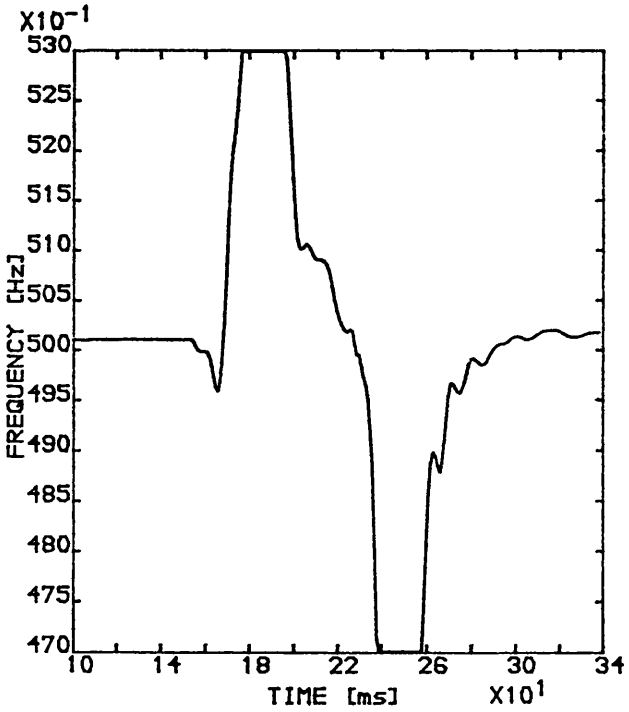

Figure 7.14. Measured frequency during the disturbance.

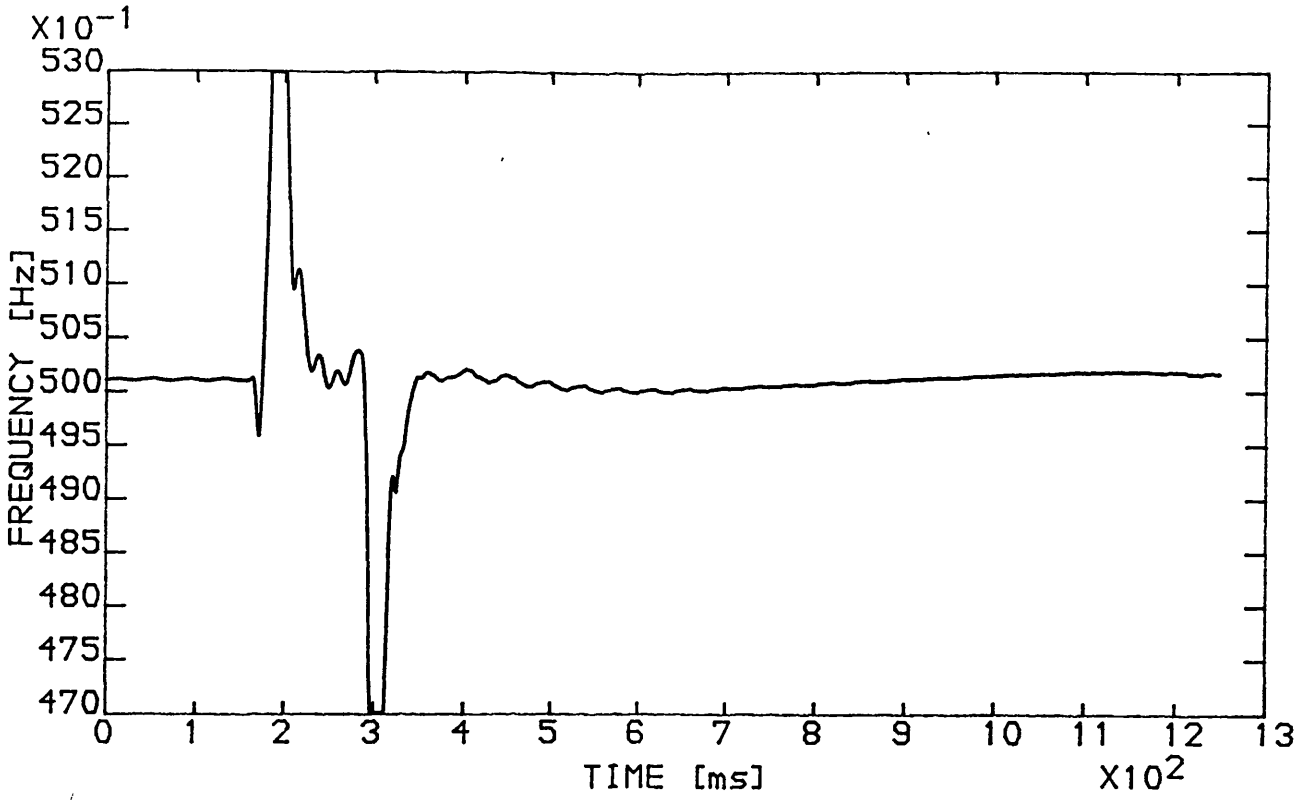

Figure 7.15. Single phase frequency measurement. Generator loaded at 0.75 pu; fault duration = 120 ms.

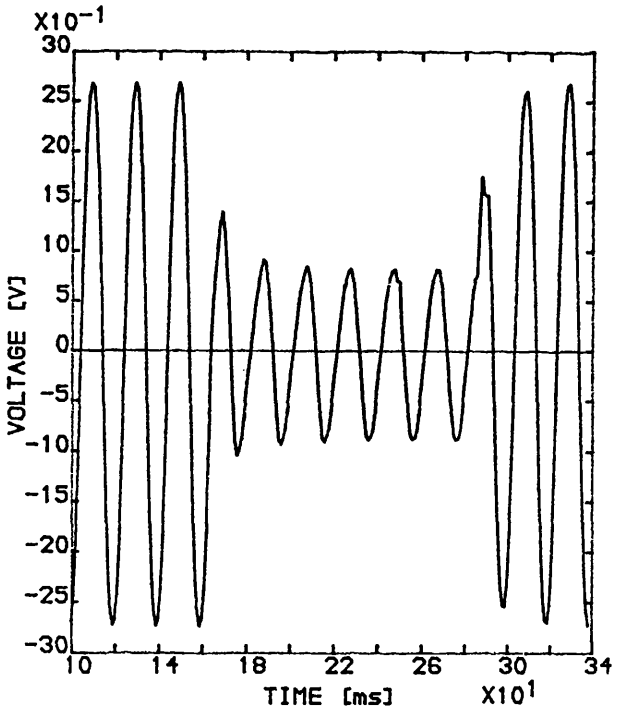

Figure 7.16. Generator terminal voltage waveform, phase 'a', during the disturbance.

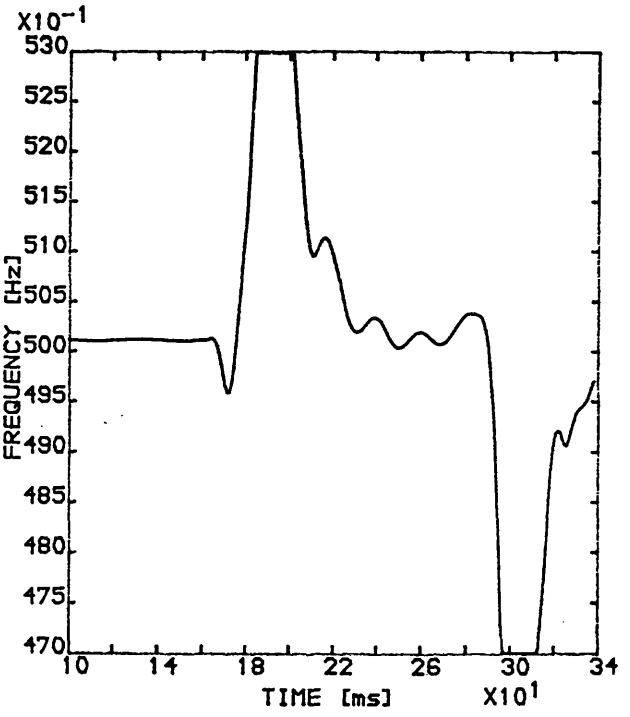

Figure 7.17. Measured frequency during the disturbance.

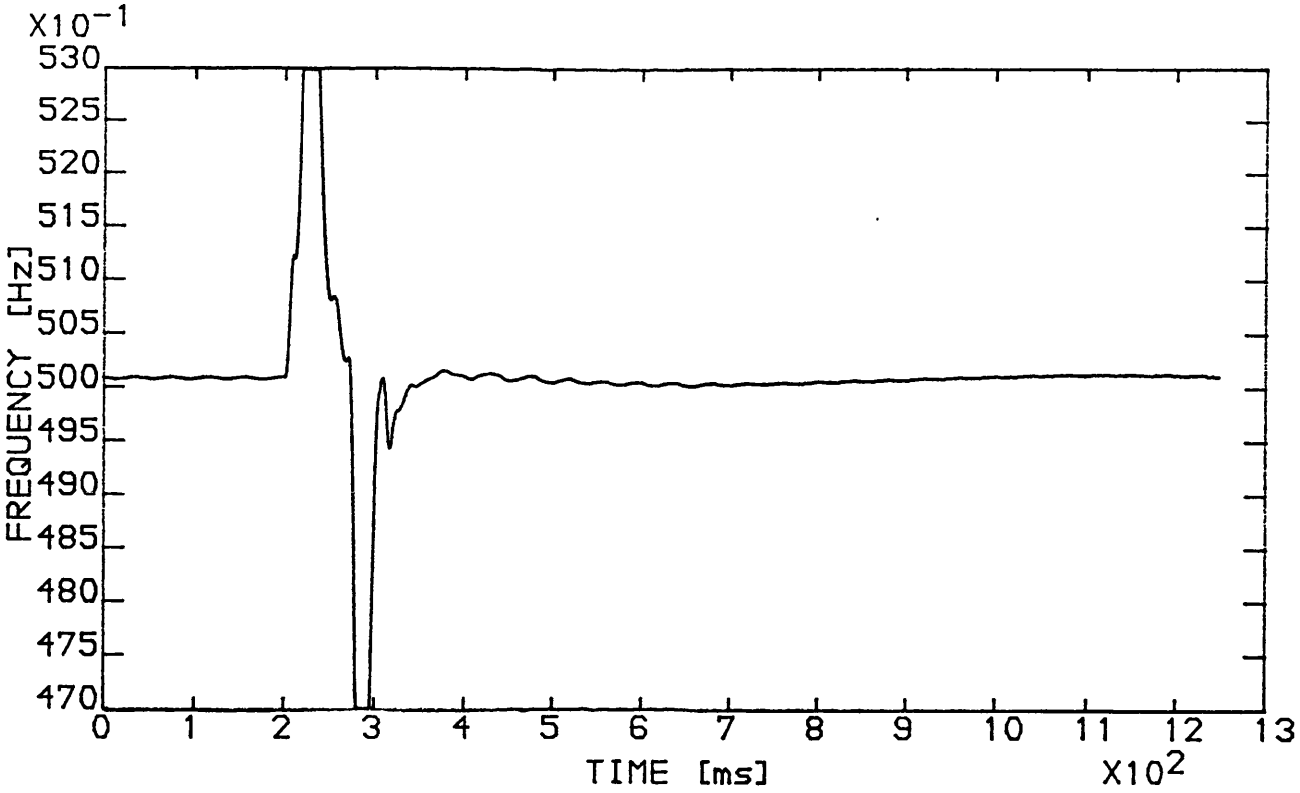

Figure 7.18. Single phase frequency measurement. Generator loaded at 0.75 pu; fault duration = 70 ms.

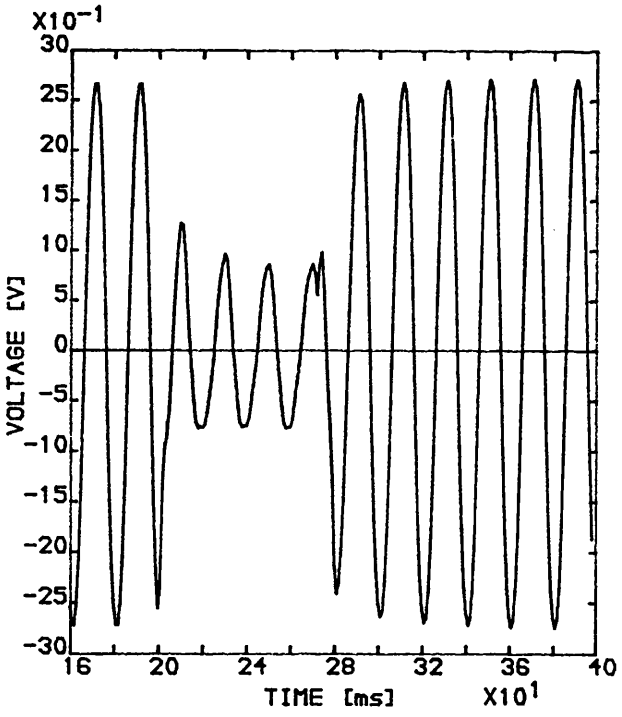

Figure 7.19. Generator terminal voltage waveform, phase 'a', during the disturbance.

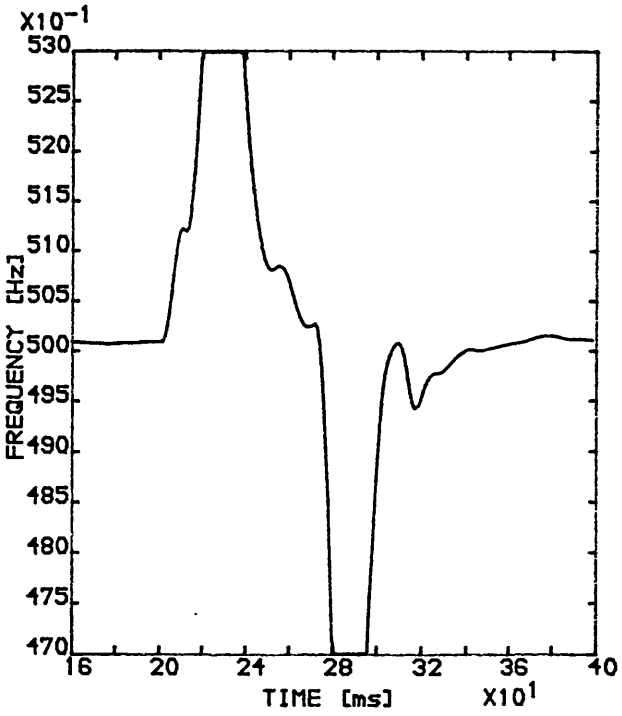

Figure 7.20. Measured frequency during the disturbance.

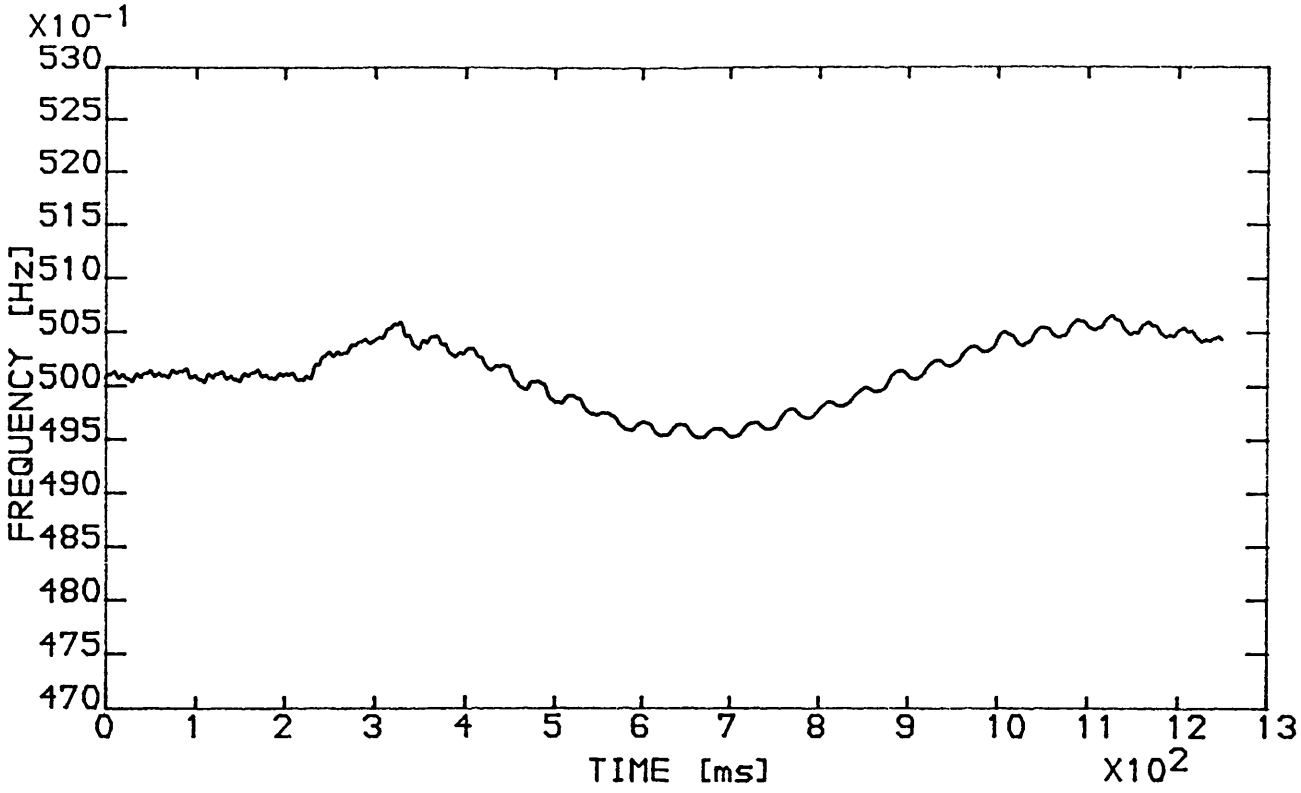

Figure 7.21. Tachogenerator single phase frequency measurement. Generator loaded at 1.0 pu; fault duration = 120 ms.

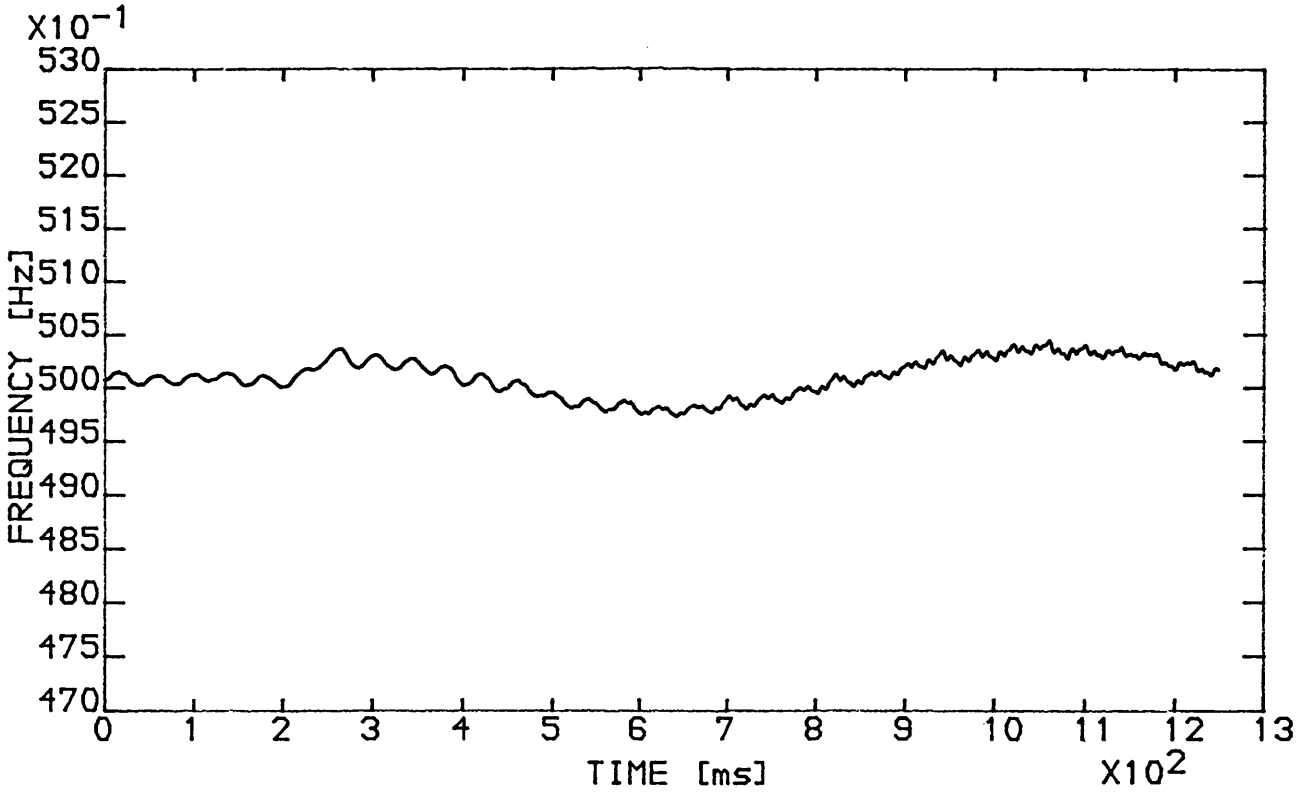

Figure 7.22. Tachogenerator single phase frequency measurement. Generator loaded at 1.0 pu; fault duration = 70 ms.

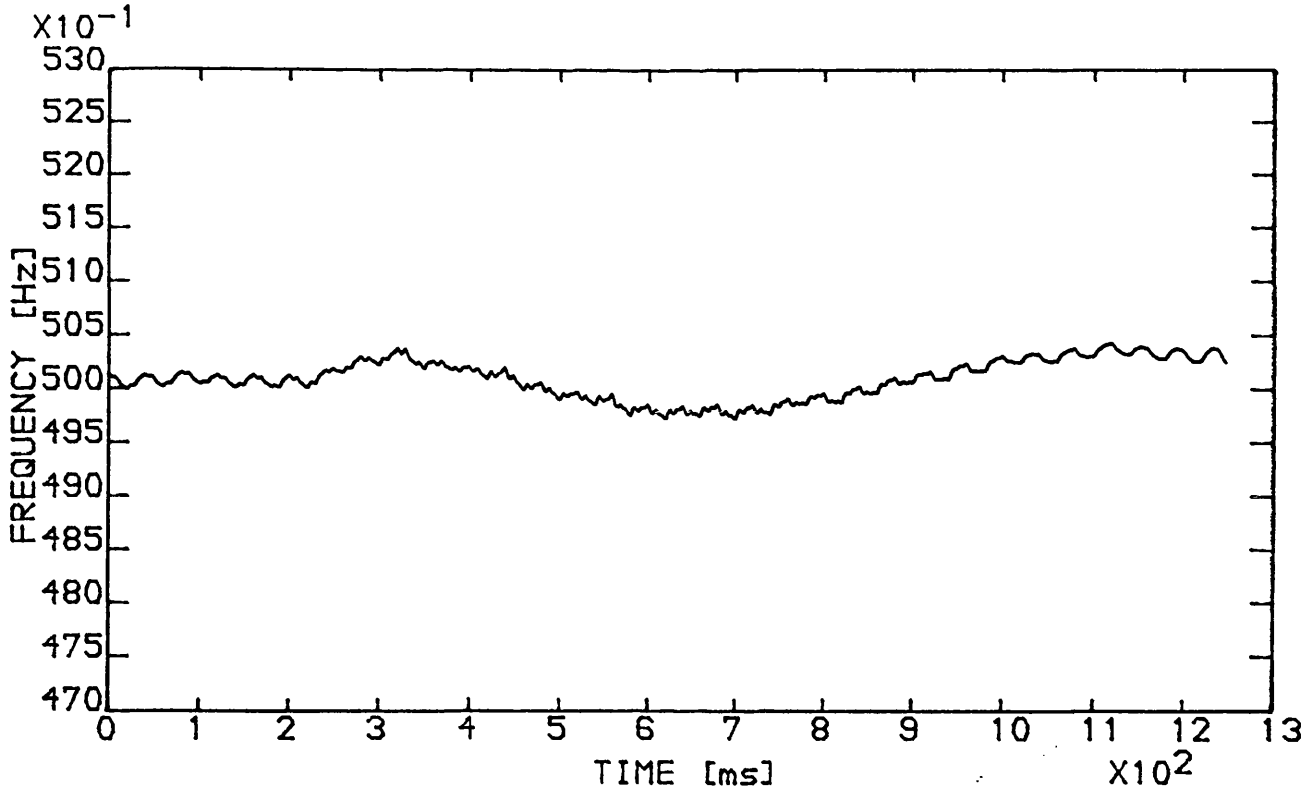

Figure 7.23. Tachogenerator single phase frequency measurement. Generator loaded at 0.75 pu; fault duration = 120 ms.

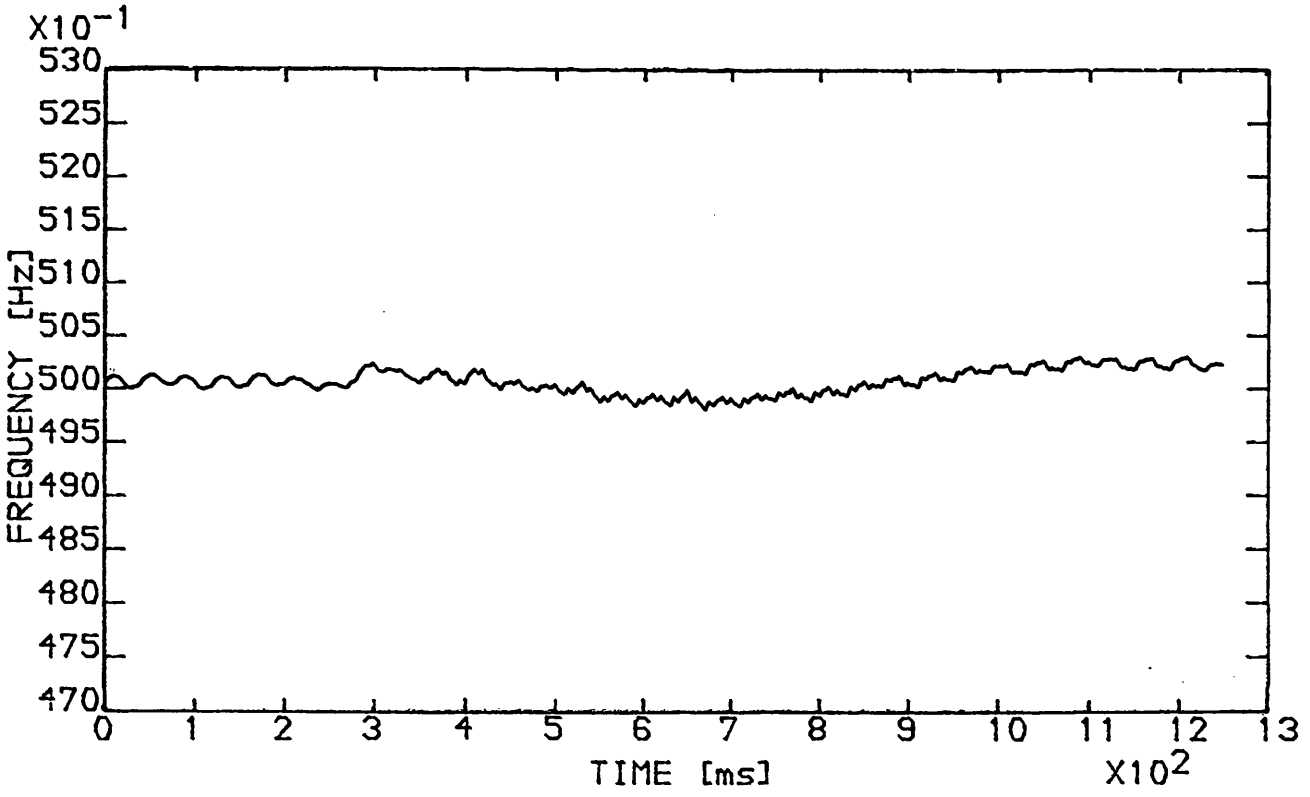

Figure 7.24. Tachogenerator single phase frequency measurement. Generator loaded at 0.75 pu; fault duration = 70 ms.

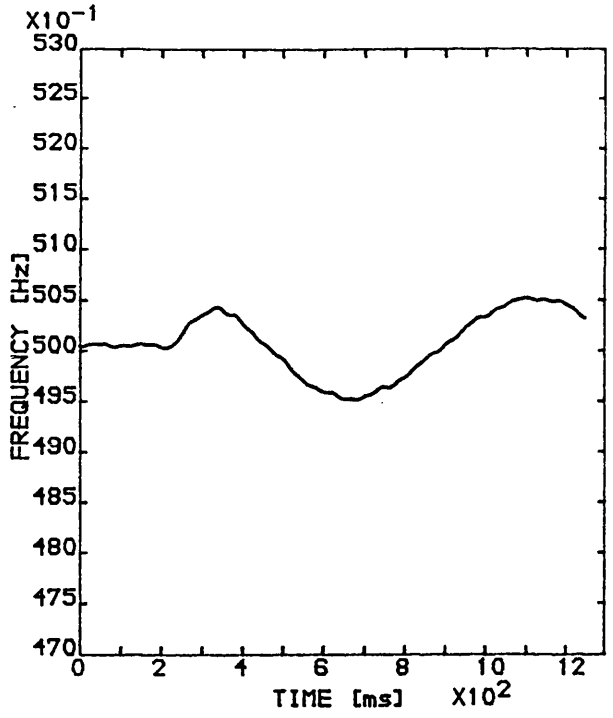

(a) 1.0 pu, 120 ms.

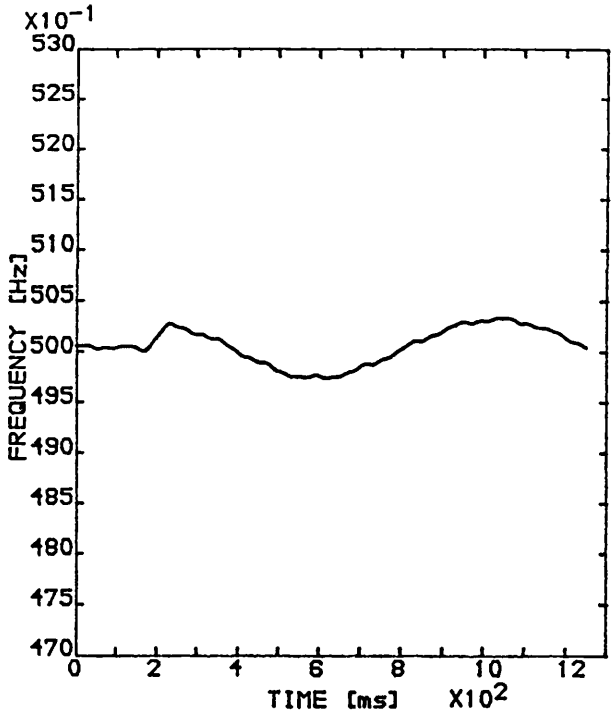

(b) 1.0 pu, 70 ms.

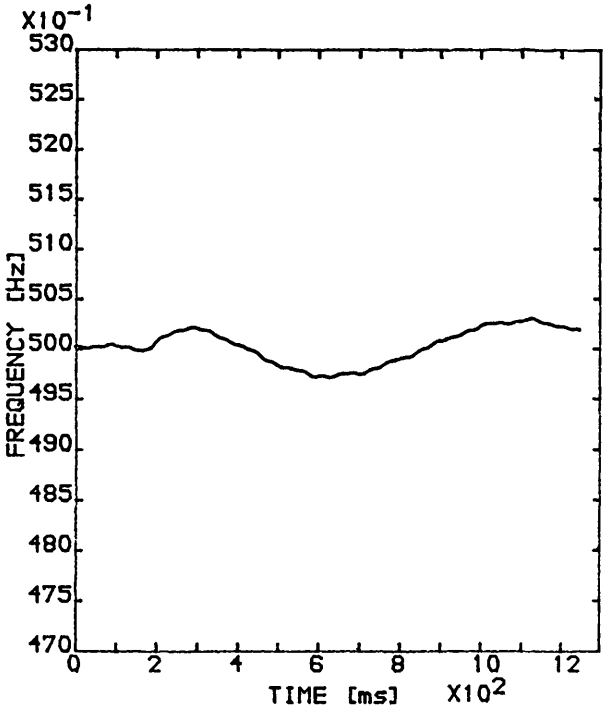

(c) 0.75 pu, 120 ms.

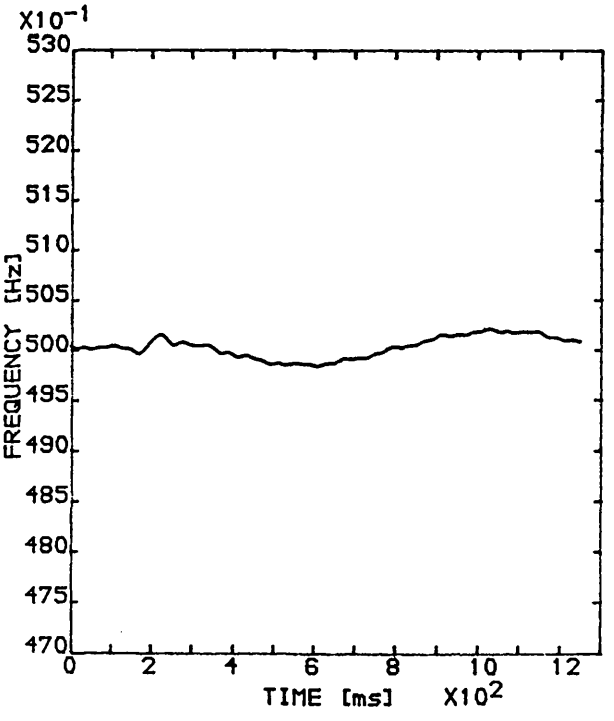

(d) 0.75 pu, 70 ms.

Figure 7. 25. Using a 3-cycle Hamming lowpass filter on the tachogenerator frequency measurements.

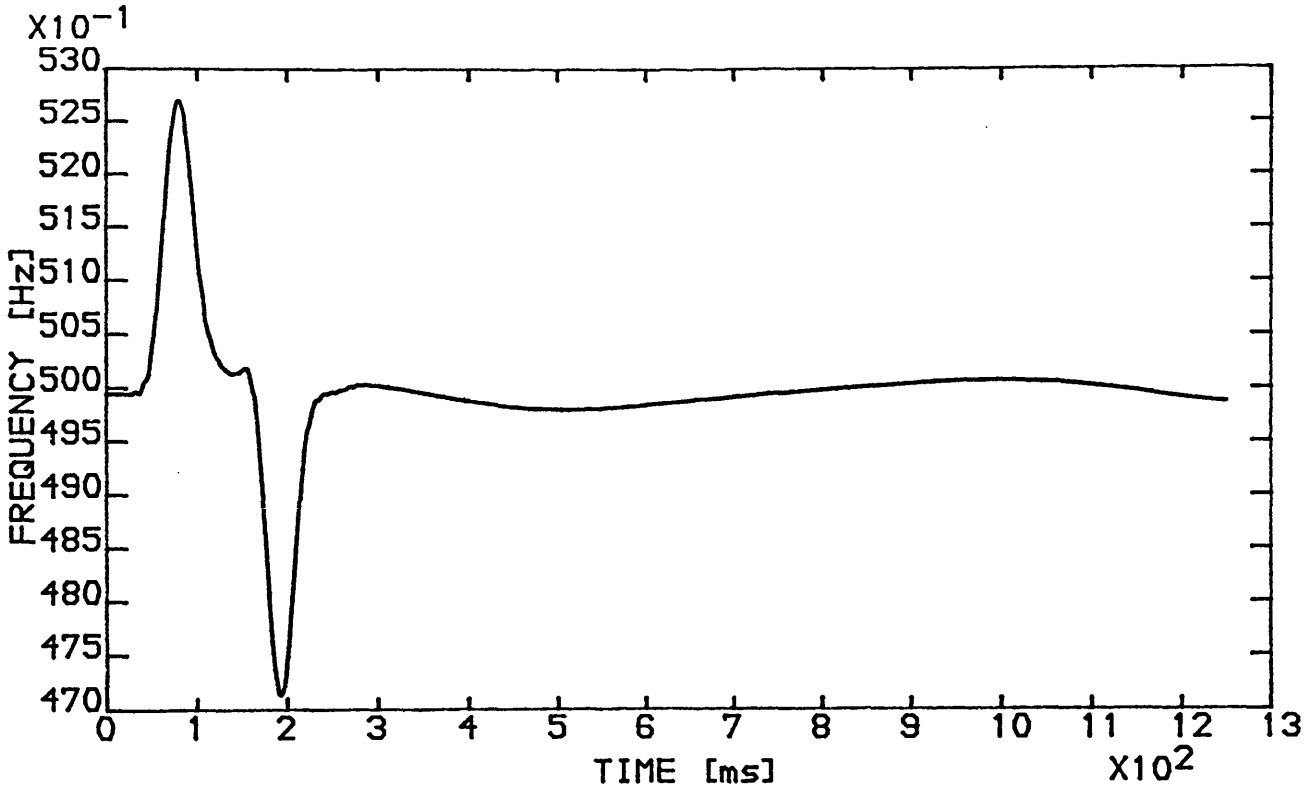

(a) 1.0 pu, 120 ms.

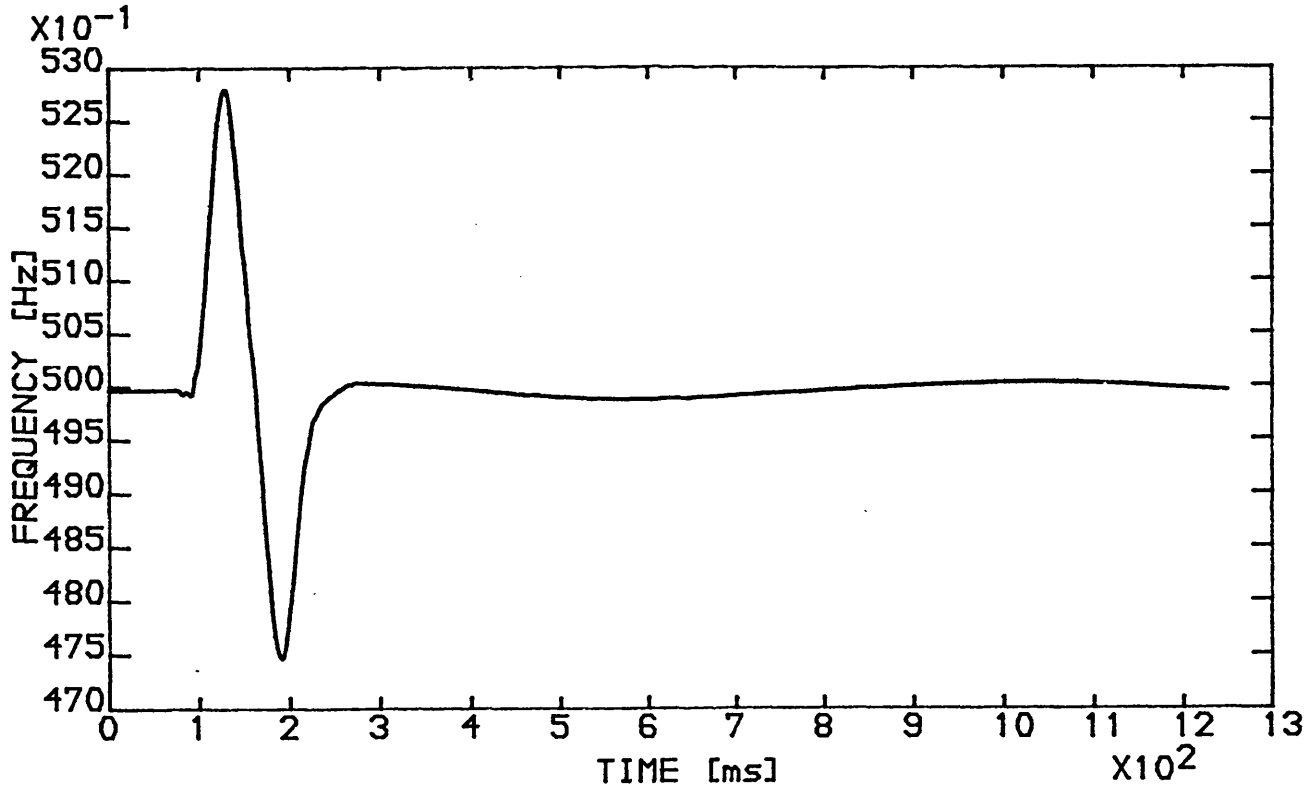

(b) 1.0 pu, 70 ms.

Figure 7.26. Using a 3-cycle Hamming lowpass filter on the generator frequency measurements.

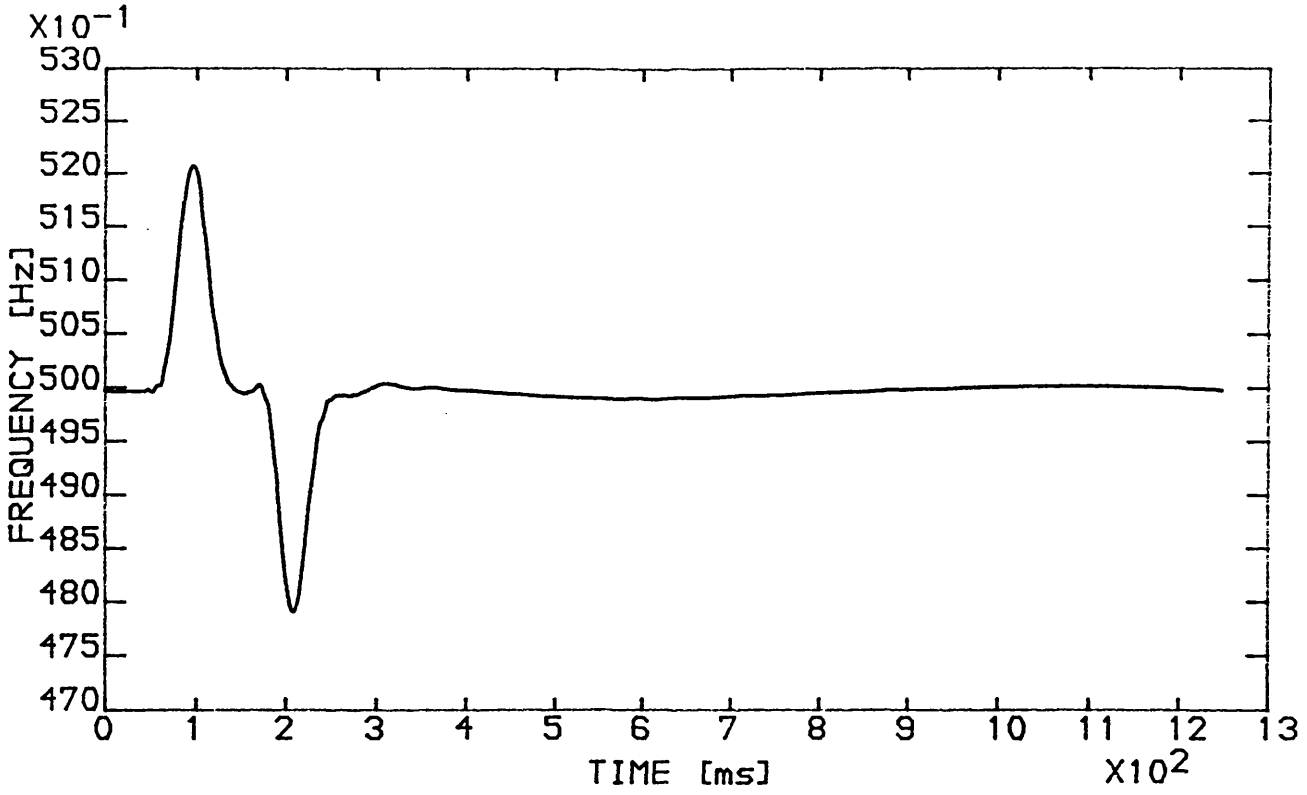

(c) 0.75 pu, 120 ms.

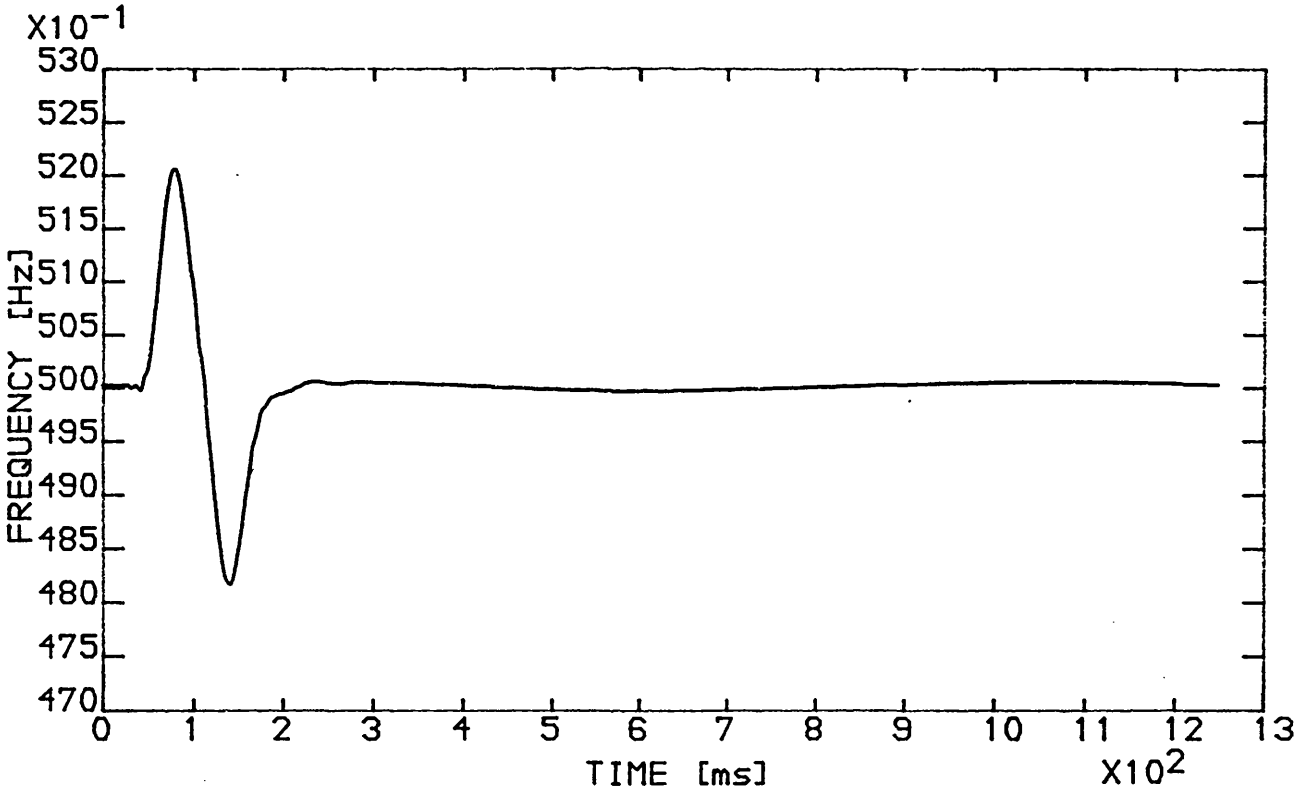

(d) 0.75 pu, 70 ms.

Figure 7.26, (cont.). Generator frequency measurements with a 3-cycle Hamming postfilter

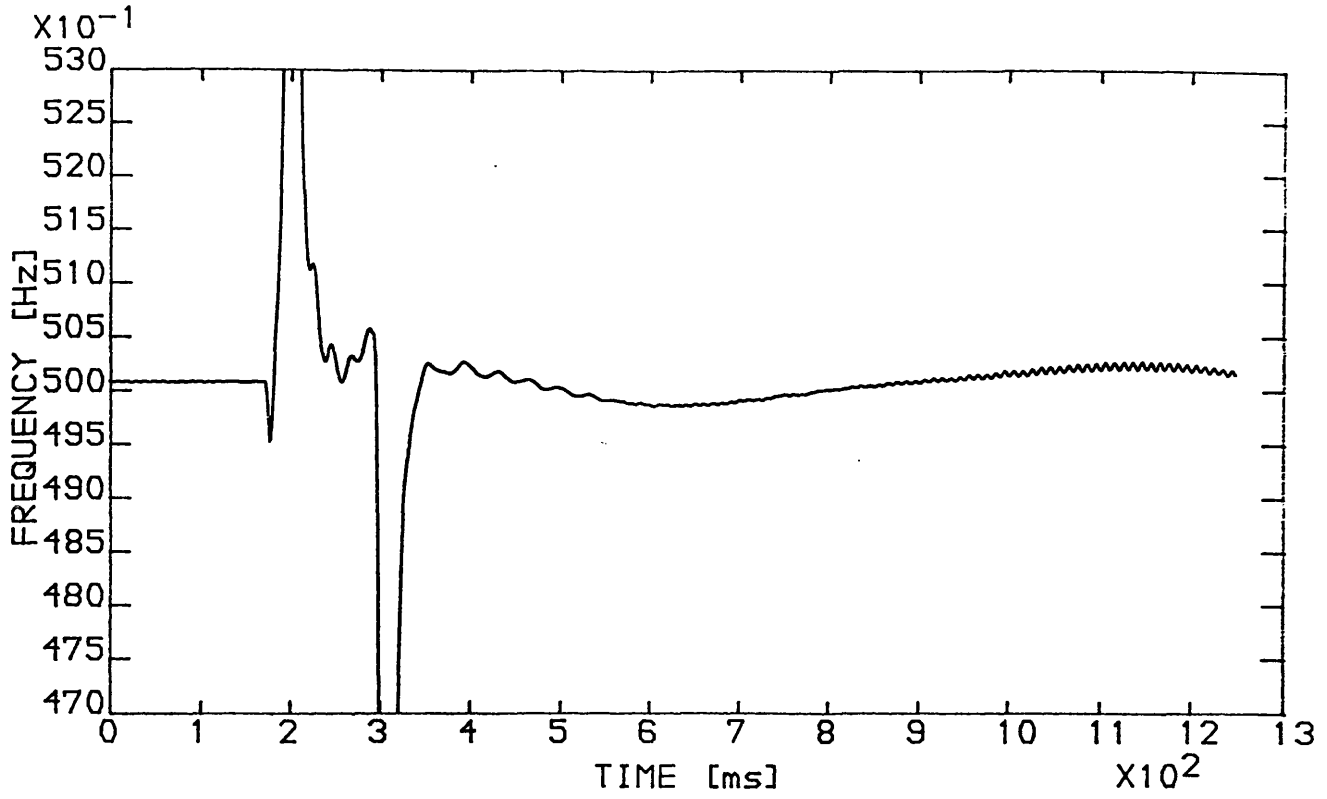

Figure 7.27. PPS frequency measurement at generator terminals. Generator loaded at 1.0 pu, fault duration = 120 ms.

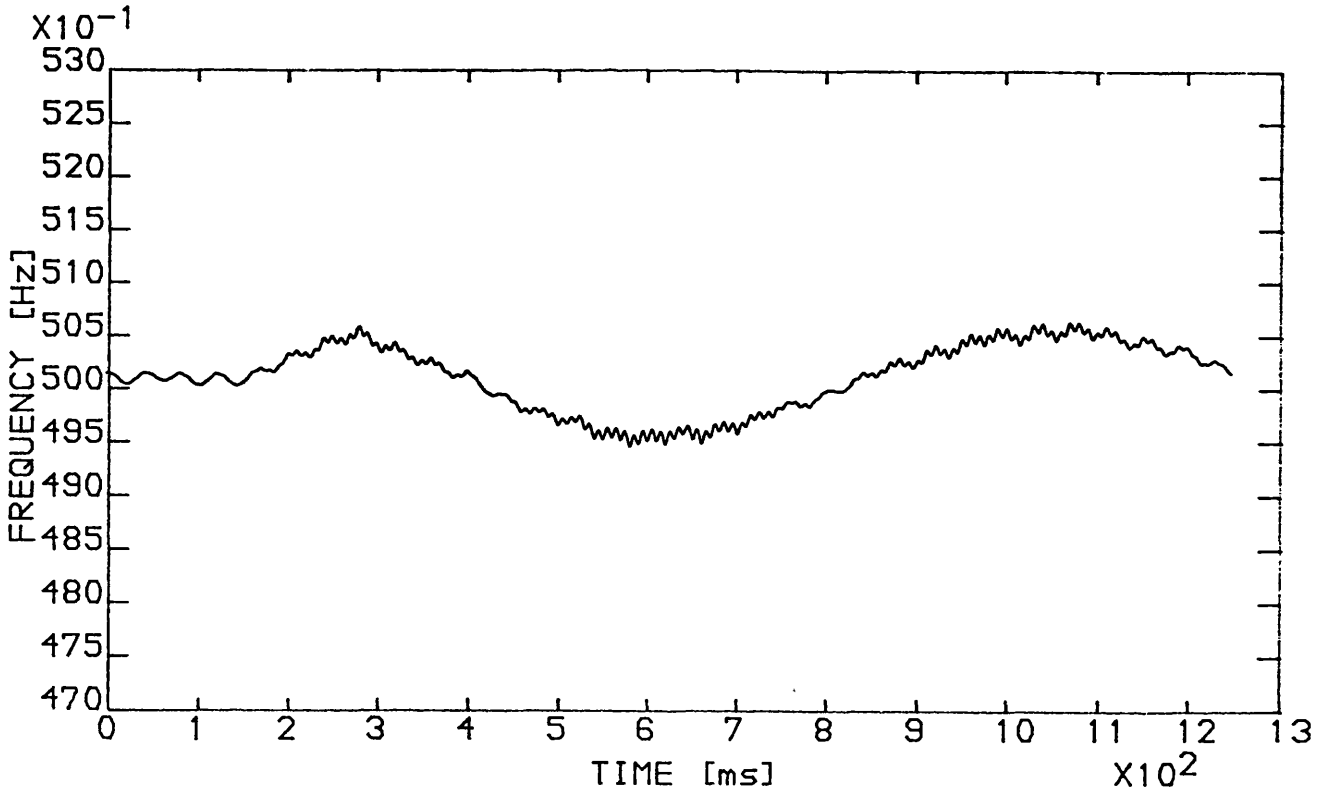

Figure 7.28. PPS frequency measurement at tachogenerator terminals. Generator loaded at 1.0 pu, fault duration = 120 ms.

CHAPTER 8

SUMMARY AND PROPOSALS FOR FURTHER WORK

This Chapter summarizes the work performed in developing a new technique for the measurement of power system frequency. Some conclusions are drawn and proposals are made for further work.

8.1 Summary

The development of a new technique for the measurement of power system frequency by digital means has been presented in this thesis. The technique is shown to be capable of tracking rapid variations of frequency with high accuracy and with a short evaluation time.

8.1.1 Development of the New Power System Frequency Technique

It was shown in the initial Chapters of the thesis, that information on the system's frequency is carried by a single component signal modulated by random amplitude and frequency processes. The signal is immersed in nonstationary broad band noise. For a voltage or a current signal taken at busbar, it was shown that the fundamental component should be extracted from the contaminating noise by an adaptive filter to provide accurate estimates of frequency. A discussion on the amplitude modulation nature of a signal taken at a power system busbar was given in Chapter 2 in relation to the dynamics of a power system. It was seen that the occurrence of severe faults in a power system, which are responsible for variations of the system's frequency, are generally accompanied of variations of the amplitude of the observed signal.

An investigation in the area of signal processing showed that, in the continuous time domain, the definition of the instantaneous frequency (IF) of a signal can be uniquely obtained in terms of the analytic function associated with the signal. The formation

of an analytic signal requires an orthogonal decomposition of the input signal within a unit gain bandpass centred at the signal's frequency. Under this approach, the amplitude and frequency modulation properties of the observed signal are correctly discriminated for an accurate estimation of the signal's frequency. It was shown in Chapter 3, that only recent research in the field of power system frequency measurement has addressed the AM/FM plus additive noise nature of the signal centred at the power system's frequency.

The starting point of the new power system frequency technique was introduced by Moore and Johns [1]. The approach adopted by the initial frequency measurement algorithm was based on the continuous time definition of the IF of a signal. In order to form an approximation to the analytic function associated with the incoming signal, orthogonal finite impulse response filters, with a one-cycle sine and cosine expressions, are used to decompose the input signal into its orthogonal components. The orthogonal components of the input signal are used in the algorithm to calculate the signal's frequency.

The analysis in the frequency domain of the orthogonal filters showed that a correct approximation to the complex representation of the input signal can be achieved if the gain of the filters is compensated for deviations of the fundamental frequency of the input signal. The analysis also showed that the frequency response of the filters provides a 90° phase shift between the orthogonal components irrespective of the frequency and also, that the filters can extract the incoming signal from additive noise within a bandpass centred at the system's frequency. The initial algorithm used a one-step frequency estimator to compensate the gain of the filters for the running frequency; the value of the frequency estimated four samples before was used as the one-step frequency estimate.

From the continuous time formulation of the frequency measurement algorithm, it was assumed that effects of amplitude variations of the incoming signal could be neglected. However, the nature of the discrete time implementation which requires the use of finite impulse response filters invalidated this assumption. It was shown

in Chapter 4, that during the digital convolution of the samples of the incoming signal with the coefficients of the orthogonal filters, variations of the amplitude of the signal resulted in variations of the frequency estimates. An investigation in the area of signal processing rendered a one-step frequency predictor which compensates the gain of the orthogonal filters for variations of amplitude and frequency of the incoming signal; this predictor was denoted as the one-step weighted predictor.

The frequency domain analysis of the algorithm also shown that the presence of non-50 Hz components intruding the frequency sidelobes of the orthogonal filters will corrupt the frequency estimates. It was shown that a one-cycle Hamming lowpass pre-filter is the optimum solution in terms of a short group delay and linear phase response as compared to other filters.

8.1.2 Assessment of the Performance of the Technique

An experimental investigation was conducted to assess the performance of the new frequency measurement algorithm. The initial stage was performed by using known signals. The response of the algorithm for variations of amplitude and frequency in the test signals, showed that the one-step weighted predictor provides an improved minimization of the effects of a time varying amplitude as compared to the four samples delay predictor. It was shown that the remaining effects of the amplitude variations, which are not removed by the predictor, resulted in oscillations in the frequency estimates whose mean value is equal to the real frequency. Hence, a lowpass filter is used to completely remove the effects of amplitude variations in the frequency estimates.

The results from this initial investigation showed that the frequency measurement algorithm exhibited a transient at the time when the waveform of the incoming signal was suddenly changed. It was shown that these variations in the signal's waveform did correspond to variations in time of the angular phase of the signal, and so the transient in the measured frequency is only a consequence of the time variation of the signal's phase. This initial set of tests confirmed the nature of the algorithm: the

IF of a single component signal equals the instantaneous rate of change of its angular phase.

In the second stage of the experimental investigation, the response of the frequency measurement algorithm to rapid changes of the underlying frequency was evaluated. It was shown that the algorithm can track rapid variations of frequency with high accuracy and fast evaluation time. The effects of harmonics when the fundamental frequency drifts from nominal were also investigated. The high energy level of the harmonics used in this investigation represent an arduous test for the frequency measurement algorithm. It was shown that for such high energy level, deviations of the fundamental frequency below 47 Hz resulted in inaccurate frequency estimates. On the assumption that a power system frequency deviation below 49.5 Hz will prompt a protective scheme to account for, the performance of the frequency measurement algorithm is considered to promote accurate frequency measurements for power system applications.

A set of realistic power system conditions, developed by computer modelling, was used to evaluate the reliability and accuracy of the frequency measurement algorithm. The initial tests were performed under dynamic conditions which are intended to be representative of realistic frequency transients in power systems. Particular attention was placed on the performance of the algorithm during the simulation of a small power system encountering an overload condition following its separation from the main system. The use of the EMTP allowed observation of the rotor speed of the generating units in the isolated system during the simulations, and so a reliable point of reference was available to assess the performance of the frequency measurement algorithm. It was shown that the algorithm accurately describes the dynamic response of the elements in the isolated system. The point of measurement of the frequency during these simulations was initially located at the generator terminal voltage. The local measurement of frequency allowed to be observed the rapid variations of the angular phase of the terminal voltage vector at the time when the system was separated from the main supply. The estimated frequency showed that the redistribution of power at the separation time results in

a sudden rotation of the angular phase of the terminal voltage vector with respect of the generator internal emf vector. The new power transfer condition, which the generating unit encounters following the separation from the grid, is responsible for the redistribution of power. During these simulations, the measurement of frequency taken from an electrical vector was denoted as the electrical frequency, while the rotating speed of a generator was denoted as the mechanical frequency. Accordingly, it was shown that the transient of the measured frequency at the separation time did correspond to a variation of the electrical frequency, while the inertia time constant of the generating unit restricted the rotor speed to experience the same rapid phenomenon.

In the last simulation using the EMTP, the frequency measurement point was moved onto the remote end of the isolated system. In this simulation the generating units in the system are connected via transmission lines at the remote end busbar where a load has been placed. The results showed that the electrical frequency measured at the load busbar corresponds to the average of the electrical frequency measured at the generating units at the other end of the system. This particular simulation shows the reliability of the frequency measurement algorithm for its potential use in protective scheme applications at substations located far from a generating centre.

The measurement of frequency from a positive phase sequence voltage vector was also investigated. The formation of the PPS vector is accomplished from the orthogonal components of a three phase voltage input signal. The measurement of frequency from a PPS voltage vector overcomes the potentially dangerous conditions prevailing from the use of single phase frequency measurement during unbalanced power system conditions.

The assessment of performance of the PPS frequency measurement algorithm was executed with the same group of tests used during the evaluation of the single phase frequency measurement. The response of the PPS frequency measurement to unbalanced conditions showed the ability of the algorithm to withstand variations of amplitude or phase among the phase components of the three phase input signal. The

effects of harmonics on the PPS frequency performance were also investigated. For a symmetrical component input signal, the harmonics rendered no effect in the PPS frequency estimates. For the case of unsymmetrical component input signal, it was shown that the harmonics resulted in inaccurate estimates of frequency. To evaluate the performance of the PPS frequency under unbalanced conditions and the presence of harmonics, the high energy level of harmonics used during the evaluation of the single phase frequency measurement was used. The results showed that a deviation of the fundamental frequency below 47 Hz for an unsymmetrical components input signal produced a corrupted frequency measurement.

The simulations with computer based power system conditions showed that the PPS frequency is able to follow the variations of the three phase system at the point of measurement. For the case of induced travelling wave noise it was shown that the unbalanced conditions prevailing during the fault prevented the single phase frequency measurement to describe the electrical frequency of the system. As pointed out in Chapter 5, this particular simulation is not based in an electromechanical model, and so no variations of the simulated system were expected. However, the PPS frequency measurement showed that, at the measurement point, the fault produces a rotation of the angle of the PPS voltage vector which is masked by the single phase frequency measurement. This test confirms the reliability of the PPS frequency measurement for its application in unbalanced power system conditions.

The EMTP simulations of dynamic power system conditions used during the evaluation of the single phase frequency measurement were used to assess the performance of the PPS frequency measurement. For the same type of disturbances, the performance of the PPS frequency measurement showed that the application of severe faults results in variations of the angular phase of the PPS voltage vector at the point of measurement. As a result of these variations, the PPS frequency exhibited a transient following the fault inception.

8.1.3 Digital Implementation of the Technique

The results from the experimental investigation showed the new frequency measurement algorithm to be capable of reliable operation under rapid changing frequency conditions. This quality enables the algorithm to be used for on-line power system frequency measurement. Following the computer based experimental investigation, the frequency measurement algorithm was implemented on a microprocessor based board.

Initially, the quantization noise sensitivity of the algorithm was evaluated to ascertain the operational features of the microprocessor based implementation. It was shown that for a sampling frequency of 4 kHz, an A/D converter with a resolution of 16 bits is required, and so the TMS320C31 digital signal processor (DSP) was selected for the implementation of the algorithm. The main features of this processor are: 32-bit floating point arithmetic operations and 60 ns single instruction execution time. Both the single phase and the PPS frequency measurement algorithms were implemented using this signal processor.

A power system simulator developed in the University of Bath was used to evaluate the correct operation and reliability of the DSP based frequency measurement algorithm. The simulator was developed to model a large generating centre connected to the United Kingdom 400 kV network via a transmission line. The basis of the simulator is a micromachine and a transmission line model which can be synchronized to the mains supply. This model system was developed to promote the study of power system transient conditions, and so it provides the ideal conditions to investigate the performance of the frequency measurement algorithm.

Fault throwing equipment allows a 3-phase fault to be applied near to the full loaded generator which produces swinging of the micromachine against the mains supply. The design of the frequency measurement equipment permitted the measurement of frequency at two points in the system: at the generator terminals and at the terminals of an ac tachogenerator attached to the generator's rotor. This configuration allowed

the measurement of the electrical and mechanical frequency of the system.

Initially, the performance of the single phase frequency measurement was evaluated. The application of the 3-phase fault when the generator is full loaded suddenly moved the generator to a minimum export condition. Hence, the measured electrical frequency showed a transient following the application of the fault. It was shown that the transient in the frequency corresponds to a rapid variation of the angular phase of the generator terminal voltage vector with respect of the generator's internal emf vector. For the same initial conditions, the measurement of the mechanical frequency taken at the tachogenerator terminals confirmed that the rotor speed was unable to undergo the same acceleration of the electrical frequency at the fault inception. The inertia time constant of the generator is the cause of the retardation in the response of the rotor speed. The effects of the duration of the fault in the response of the generator were also investigated. The results from the measurement of the mechanical and electrical frequency showed that the swinging of power between the micromachine and the mains supply following the clearance of the fault, were proportional to the initial loading conditions of the generator and to the duration of the fault.

In the second part of this investigation, the performance of the PPS frequency measurement algorithm implemented on the TMS320C31 board was evaluated. Since balanced system conditions were observed on conducting this investigation, the results from the measurement of frequency from a PPS voltage vector rendered no difference with respect of the single phase frequency measurements. Due to the high execution time of the processor cpu, the implementation of the PPS frequency measurement algorithm did not include the lowpass pre-filter stage. The harmonics generated during the swinging of power following the removal of the fault resulted in corrupted estimates of the PPS frequency.

8.2 Conclusions

From the experimental investigation conducted on computer modelling of dynamic

power system conditions, and on the power system simulator, some conclusions relative to the measurement of frequency with the new frequency measurement technique are drawn:

1° The measurement of electrical frequency taken from an electrical vector signal corresponds to instantaneous variations of the angular phase of the electrical vector. The term instantaneous is used to denote the time varying nature of this phenomenon.

2° Variations of the angle spanned between two rotating vectors will result in different frequency measurements. Hence, only during steady conditions in a power system, will the measurement of local frequency, performed at different nodes along the system, render equal estimates of the system's frequency.

3° During the occurrence of a sudden change in the transfer of power of a generator, rapid variations in the angle between the generator terminal voltage and the internal emf vector result in variations in the electrical frequency, however, the inertia of the generator restricts its mechanical frequency from following the rapid variations of the electrical frequency.

4° It has been shown that the new frequency measurement algorithm is capable of reliable operation under dynamic power system frequency conditions, exhibiting an accuracy of 0.01 Hz and a delay of 37.5 ms.

8.3 Proposals for further work

Further work is recommend in the following areas:

a) Enhancement of the bandpass features of the frequency measurement algorithm. An attempt for improving the bandpass characteristics of the algorithm was performed during this investigation by using a recursive least squares filter. The presence of the second harmonic when the fundamental frequency deviates from

nominal resulted in a limited adaptive scheme which was not able to track the time varying characteristics of the input signal. An improvement to the tracking ability of the filter will be accomplished by developing an adaptive decorrelating algorithm.

Further research on the formation of the orthogonal decomposition of a signal by using a lattice form recursive least squares filter is also recommended. It is known that the lattice form structure provides uncoupling among the filter's stages [47]. The estimation of the current value of the sampled input signal, based on the information from the most recent samples, can be used to project a vector which is orthogonal to the span of the input signal sequence vector. The tracking ability of the recursive least squares line enhancer will thus provide an orthogonal plus bandpass filtering of the incoming signal. An improved complex representation of the fundamental component of the input signal is expected where an adaptive tracking of the fundamental can be accomplished with a reduced group delay.

An alternative solution to the influence of harmonics on the frequency estimation during dynamic changes of the frequency is to adjust the sampling interval of the algorithm to ensure that the number of samples taken during the interval corresponds to the number of coefficients of the orthogonal filters. It was shown that the frequency response of the orthogonal filters highly attenuates frequency components located at the harmonics of the fundamental provided that the number of coefficients of the filters is equal to the ratio between the sampling frequency and the fundamental frequency. An investigation on the suitability of an adaptive interpolating method for its application to power system frequency measurement is recommended. It is also advised a further investigation on the sensitivity of this algorithm to variations of amplitude of the input signal.

b) Application of the new power system frequency measurement technique to load shedding and frequency relaying schemes. The high-speed tracking ability of the frequency measurement algorithm can be applied to load shedding and frequency relaying schemes. An optimum load shedding scheme depends on the accurate estimation of the amount of load to be shed. It is known that the amount of load to

be shed during generating deficiency periods is proportional to the initial rate of change of decline of the frequency of the system. As shown in Chapter 2, in the case of a large system undergoing a period of generating deficiency, the frequency of the system is considered to be equal to the frequency of a single equivalent generating unit located at the centre of inertia of the large system. Hence, variations of the mechanical frequency of the system are used as the basis to calculate the magnitude of the imbalance between generation and demand during a deficiency period.

It was shown in this thesis that the measurement of electrical frequency at the generator terminals during the application of faults disturbing the transfer of power in the system exhibited a transient in the measured frequency which corresponds to variations in the angle between the generator terminal voltage and its internal emf vector. On the other hand, the measurement of the mechanical frequency showed that the generator speed was not able to follow such rapid variations. Different authors [2], [4], [20], [21], have proposed different adaptive schemes to remove the transient variations of the electrical frequency observed on the occurrence of power imbalance conditions. It is known that the local frequency during dynamic power system conditions is unlikely to be same from one point of measurement to another within the same system. However, for load shedding and frequency relaying schemes to be placed at locations far from a generating centre, the measured electrical frequency is the only source of information on the system's frequency.

In order to overcome the problem of the initial transient in the electrical frequency, it is proposed to perform the development of an adaptive method to estimate the underlying mechanical frequency. This method is based on the information carried by the electrical frequency where the inertia time constant of the system can be used to provide a point of reference for the adaptive scheme. At the time when the electrical frequency exhibits a transient, a delayed change in the rotation of the generator rotor is expected. The response time of the rotor speed to a rapid variation of the electrical frequency is thus determined by the inertia time constant of the system. The behaviour of the electrical frequency during a transient caused by a

rapid variation of power transfer in the generator, can be represented as an impulse signal suddenly applied to a lowpass process dominated by the system's inertia time constant. Hence, the output of the adaptive process should equal the expected response of the rotating speed of the generating unit during the disturbance.

APPENDIX 1

Derivation of the instantaneous frequency of a signal

From the analytic signal $z(t)$ associated with the real function $s(t) = a(t)cos[\theta(t)]$, then:

$$z(t) = a(t)e^{j\theta(t)} \qquad (A.1.1)$$

where $\theta(t)$ is given as:

$$\theta(t) = [w_0(t) + \phi] \qquad (A.1.2)$$

The instantaneous frequency (IF) of $s(t)$ is defined as:

$$f_i(t) = \frac{1}{2\pi}\frac{d\theta(t)}{dt} \qquad (A.1.3)$$

The product of $z(t)$ times its complex conjugate $z^*(t)$ yields:

$$z(t)\, z^*(t) = a(t)e^{j\theta(t)}\, a^*(t)e^{-j\theta(t)} \qquad (A.1.4)$$

while the product of the derivative of $z(t)$ times the complex conjugate $z^*(t)$ gives:

$$\frac{dz(t)}{dt}\, z^*(t) = \frac{da(t)}{dt} + ja(t)\frac{d\theta(t)}{dt} \qquad (A.1.5)$$

From equations (A.1.4) and (A.1.5), the IF of $s(t)$ is given as:

$$w_i(t) = \frac{IM[z'(t)z^*(t)]}{|z(t)\, z^*(t)|} \qquad (A.1.6)$$

Since $z(t) = s(t) + j\hat{s}(t)$ and $z^*(t) = s(t) - j\hat{s}(t)$, then, $z'(t) = s'(t) + j\hat{s}'(t)$. From equation (A.1.5), the numerator in equation (A.1.6) can be expressed as:

$$IM[z'(t)\hat{z}*(t)] = \hat{s}'(t)s(t) - \hat{s}(t)s'(t) \qquad (A.1.7)$$

Hence,

$$f_i(t) = \frac{\hat{s}'(t)s(t) - \hat{s}(t)s'(t)}{2\pi\, [s^2(t) + \hat{s}^2(t)]} \qquad (A.1.8)$$

APPENDIX 2

Description of terms of the power dynamics equation

A description of the terms of the power dynamics equation (2.21) is given here:

$$\Delta f^*(t) = \frac{\sigma P^*_{step}}{D_{fv}\sigma + K_M}[1 + A\, e^{-\alpha t} \sin(w_R t + \phi)] \qquad (A.2.1)$$

where:

$\Delta f^*(t)$ = frequency deviation in per unit

P^*_{step} = unity step impulse

H = inertia time constant

σ = governor regulation gain = droop

D = dependence of the load on frequency

F_H = fraction of the power generated by the high pressure turbine

T_R = reheat time constant

and:

$$A = \sqrt{\frac{1 - 2T_R\varsigma w_n + T_R^2 w_n^2}{1 - \varsigma^2}} \qquad (A.2.2)$$

$$2\varsigma w_n = \frac{\sigma D T_R + 2H\sigma + K_M F_H T_R}{2HT_R\sigma} \qquad (A.2.3)$$

$$w_n^2 = \frac{\sigma D + K_M}{2HT_R\sigma} \qquad (A.2.4)$$

$$w_R = w_n\sqrt{1 - \varsigma^2} \qquad (A.2.5)$$

APPENDIX 3

Frequency error due to the discrete approximation

From a signal $x(t) = \sin(w_0 t)$, its orthogonal components are: $x_i(t) = \sin(w_0 t)$ and $x_q(t) = \cos(w_0 t)$. An approximation to the continuous time derivative of the orthogonal components of the signal can be given in terms of one-sample backwards difference equation:

$$x'_i(t) = \frac{x_i(t + \Delta T) - x_i(t - \Delta T)}{2\Delta T} = \frac{-\sin(w_0 t)\,\sin(w_0 \Delta T)}{\Delta T} \qquad (A.3.1.a)$$

$$x'_q(t) = \frac{x_q(t + \Delta T) - x_q(t - \Delta T)}{2\Delta T} = \frac{\cos(w_0 t)\,\sin(w_0 \Delta T)}{\Delta T} \qquad (A.3.1.a)$$

The frequency of $x(t)$ is given as:

$$f = \frac{x_i\, x'_q - x'_i\, x_q}{2\pi\,(x^2_i + x^2_q)} \qquad (A.3.2)$$

Hence, the frequency calculated from equations (A.3.1.a) and (A.3.1.b) yields:

$$f = \frac{\cos^2(w_0 t)\,\sin(w_0 \Delta T) + \sin^2(w_0 t)\,\sin(w_0 \Delta T)}{2\pi \Delta T\,(x^2_i + x^2_q)} \qquad (A.3.3)$$

since $x_i(t) = \sin(w_0 t)$ and $x_q(t) = \cos(w_0 t)$, then, the frequency becomes:

$$f = \frac{\sin(w_0 \Delta T)}{2\pi \Delta T} \qquad (A.3.4)$$

The first two terms in the McLaurin series expansion of $\sin(w_0\, \Delta T)$ are:

$$\sin(w_0 \Delta T) \simeq w_0 \Delta T - \frac{w^3_0 \Delta T^3}{6}$$

$$= 2\pi f_0 \Delta T - \frac{8\pi^3 f_0^3 \Delta T^3}{6} \qquad (A.3.5)$$

Hence, the frequency as given in equation (A.3.4) becomes:

Appendix 3. Frequency error due to the discrete approximation

$$f = f_0 - \frac{2\pi^2 f_0^3 \Delta T^2}{3} \qquad (A.3.6)$$

The term on the right side of equation (A.3.6) results from the difference equation approximation and it should be compensated for during the frequency estimation.

APPENDIX 4

Singularity in the frequency response of the orthogonal filters

The magnitude of the in-phase orthogonal filter, as given in Equation (4.25.a) in Chapter 4, exhibits a singularity in both the numerator and the denominator when the Ω is equal to the fundamental frequency Ω_0. Using the L'Hôpital's rule, then:

$$\lim_{\Omega \to \Omega_0} mag_i(\Omega) = \lim_{\Omega \to \Omega_0} \left\{ \frac{\frac{\delta}{\delta \Omega}[2\cos(\frac{\Omega_0}{2})\sin(\frac{N\Omega}{2})\sin(\frac{\Omega}{2})]}{\cos(\Omega) - \cos(\Omega_0)} \right\} \qquad (A.4.1)$$

$$= \lim_{\Omega \to \Omega_0} \frac{2\cos(\frac{\Omega_0}{2})}{-\sin\Omega} \left[\frac{N}{2} \cos(\frac{N\Omega}{2})\sin(\frac{N\Omega}{2}) + \frac{1}{2} \sin(\frac{N\Omega}{2})\cos(\frac{N\Omega}{2}) \right]$$

At $\Omega = \Omega_0$, then $N\Omega/2 = \pi$ and $\Omega/2 = \pi$. Hence, the magnitude of the filter becomes:

$$\lim_{\Omega \to \Omega_0} mag_i(\Omega) = \frac{N \cos(\frac{\Omega_0}{2})\sin(\frac{\Omega_0}{2})}{\sin(\Omega_0)} \qquad (A.4.2)$$

From the complex form of the sine and cosine terms in the numerator of equation (A.4.2), the magnitude is given as:

$$\lim_{\Omega \to \Omega_0} mag_i(\Omega) = \frac{N\,(e^{j\Omega_0} - e^{-j\Omega_0})}{2\,(e^{j\Omega_0} - e^{-j\Omega_0})} = \frac{N}{2} \qquad (A.4.3)$$

Thus, the response of the in-phase orthogonal filter is equal to half its coefficient length.

A similar procedure can be followed with respect of the frequency response of the quadrature filter. It can be shown that the magnitude of this filter at 50 Hz is the same as the magnitude of the in-phase orthogonal filter.

APPENDIX 5

Expression of the energy envelope *e(t)*

From Equation (4.40) in Chapter 4, the power spectrum of ***de(t)/dt*** is given as:

$$FT\left\{\frac{de(t)}{dt}\right\} = jwU(w) \qquad (A.5.1)$$

where ***FT*** operator denotes the Fourier Transform of the variable.

The power spectrum of a differentiator, expressed in terms of its input and output is given as:

$$S_{inp-out}(w) = S_{inp-inp}H^*(w) \qquad (A.5.2)$$

where the *S* operator is the Fourier Transform of the cross correlation input-output and the autocorrelation input-input of the variables, and $H^*(w)$ is the conjugate expression of the frequency response $H(w)$ of the filter. Equation (A.5.2) can be expressed in terms of the autocorrelation input-input:

$$S_{out-out}(w) = S_{inp-inp}H(w)H^*(w) \qquad (A.5.3)$$

From Equation (A.5.1):

$$S_{out-out}(w) = w^2 S_{inp-inp} \qquad (A.5.4)$$

Since the input to the differentiator is the complex envelope $e(t) = z(t)\, e^{jw_o t}$, then:

$$S_{out-out}(w) = w^2 S_{zz}(w + w_0) = (w - w_o)^2 S_{zz}(w) \qquad (A.5.5)$$

Hence, the expected value of the numerator of ***M*** as given in equation (4.40) in Chapter 4 becomes:

$$E\left\{\left|\frac{de(t)}{dt}\right|^2\right\} = \frac{1}{2\pi}\int_{-\infty}^{\infty} wS_{out-out}(w)dw \qquad (A.5.6)$$

Substitution of Equation (A.5.5) into the right side of Equation (A.5.6) yields:

Appendix 5. Expression of the energy envelope *e(t)*

$$E\left\{\left|\frac{de(t)}{dt}\right|^2\right\} = \frac{1}{2\pi}\int_{-\infty}^{\infty}(w - w_0)^2 S_{zz}(w)dw \qquad (A.5.7)$$

APPENDIX 6

Expression of the angular frequency w_0

From the definition of the analytic signal $z(t)$ associated with the signal $s(t)$, i.e:

$$z(t) = s(t) + j\hat{s}(t) \tag{A.6.1}$$

The power spectrum of $z(t)$ is given as [55]:

$$S_{zz}(w) = 4S_{ss}(w)U(w) \tag{A.6.2}$$

The unit frequency function $U(w)$ is defined as:

$$U(w) = \begin{cases} 1 & for\ 0 \le w \le \pi \\ 0 & for -\pi \le w \le 0 \end{cases} \tag{A.6.3}$$

Substitution of Equation (A.6.3) in Equation (4.43) given in Chapter 4 yields:

$$w_o = \frac{\int_0^{\infty} wS_{ss}(w)dw}{\int_0^{\infty} S_{ss}(w)dw} \tag{A.6.4}$$

The effect of the Hilbert Transform in the analytic signal $z(t)$ is reflected in the unit frequency function shown in Equation (A.6.3).

From the definition of the IF of $s(t)$ as given in Appendix 1, the product $z^*(t)\,dz(t)/dt$ gives:

$$z'(t)z^*(t) = |z(t)|\frac{d|z(t)|}{dt} + jw_0(t)|z(t)|^2 \tag{A.6.5}$$

The expected value of the first term on the right side of the last equation equals zero since for $s(t) = cos(w_0t)$, then, the magnitude of $z(t)$ equals the unity, thus, the derivative of the first term on the right side of Equation (A.6.5) equals zero. On the other hand, the expected value of the next term on the right side of the same equation yields:

Appendix 6. Expression of the angular frequency w_0

$$E\{w_0(t)\ |z(t)|^2\} = \frac{1}{2\pi}\int_{-\infty}^{\infty} wS_{zz}(w)dw \qquad (A.6.6)$$

since $S_{zz}(w) = 4S_{ss}(w)U(w)$ as given in Equation (A.6.2), then, the expected value of the magnitude of $z(t)$ gives:

$$E\{|z(t)|^2\} = \frac{2}{\pi}\int_{0}^{\infty} S_{zz}(w)dw \qquad (A.6.7)$$

Then, Equation (A.6.4) can be expressed as:

$$\frac{\int_{0}^{\infty} wS_{zz}(w)dw}{\int_{0}^{\infty} S_{zz}(w)dw} = \frac{E\{|z(t)|^2\ w_0(t)\}}{E\{|z(t)|^2\}} \qquad (A.6.8)$$

for $s(t) = a(t)\ cos(w_0t)$, then $z^2(t) = a^2(t)$. Hence, the frequency is given as:

$$w_0(t) = \frac{E\{a^2(t)w_0(T)\}}{E\{a^2(T)\}} \qquad (A.6.9)$$

APPENDIX 7

Frequency response of the Hamming lowpass filter

The impulse response of an N coefficients Hamming lowpass filter is given as:

$$h[k] = w_R[k](\alpha + (1 - \alpha)\cos(\frac{2\pi k}{N})) \qquad (A.7.1)$$

where $w_R[k]$ is the unit step rectangular function defined for values of $k > 0$. Since the number of coefficients N of the filter equals $N = f_s/f_0$, then $\cos(2\pi k/N) = \cos(\Omega_0 k)$. The Z Transform of the product of the unit function and the cosine term is given as:

$$Z\{w_r[k]\cos(\Omega_0 k)\} = \frac{1}{2}\left[W_R(ze^{j\Omega_0}) + W_R(ze^{-j\Omega_0})\right] \qquad (A.7.2)$$

where:

$$Z\{w_R[k]\} = \frac{z(1 - z^{-N})}{z - 1} \qquad (A.7.3)$$

hence, Equation (A.7.2) is expressed as:

$$Z\{w_R[k]\cos(\Omega_0 k)\} = \frac{z^2 - z^{-N+2} - z\cos(\Omega_0) + z^{-N-1}\cos(\Omega_0)}{z^2 - 2z\cos(\Omega_0) + 1} \qquad (A.7.4)$$

for $z = e^{j\Omega}$ in the unit circle plane, then, the frequency response of the Hamming lowpass filter is:

$$H(\Omega) = \alpha\frac{\sin(\frac{\Omega N}{2})\ \frac{e^{-j\Omega(N-1)}}{2}}{\Omega/2} - j(1-\alpha)\ \frac{\sin(\frac{\Omega N}{2})[e^{j\Omega} - \cos(\Omega_0)]\ e^{-j\frac{\Omega N}{2}}}{\cos(\Omega) - \cos(\Omega_0)} \qquad (A.7.5)$$

APPENDIX 8

Parameters for power swing study

The system configuration used to study the performance of the frequency measurement algorithm during power swing conditions is shown in Figure 5.19. The parameters used in the simulation [60] are as follows:

LINE

Voltage = 400 kV

$Z_0 = 0.388 + j1.019 \ \Omega/km$

$Z_1 = 0.23 + j0.298 \ \Omega/km$

GENERATING PLANT AT P

Single machine, rating = 600 MVA, 22 kV

H = 4.44 kW s/kVA	$X_l = 0.161 \ \Omega$
$R_a = 0.003 \ \Omega$	$X_q = 2.194 \ \Omega$
$X_d = 2.259 \ \Omega$	$X_{q'} = 0.178 \ \Omega$
$X_{d'} = 0.292 \ \Omega$	
$X_{d''} = 0.184 \ \Omega$	
$T_{d'} = 0.945$ s	$T_{q'} = 0.009$ s
$T_{d''} = 0.020$ s	
$T_a = 0.231$ s	

GENERATOR TRANSFORMER

Rating 600 MVA. 22 kV/432 kV (+2%, -15%)

$Z = 0.0018 + j0.163$ p.u.

APPENDIX 9

400 kV line configuration for travelling wave noise study

The following 400 kV, single circuit line configuration was used in the simulation of travelling wave noise:

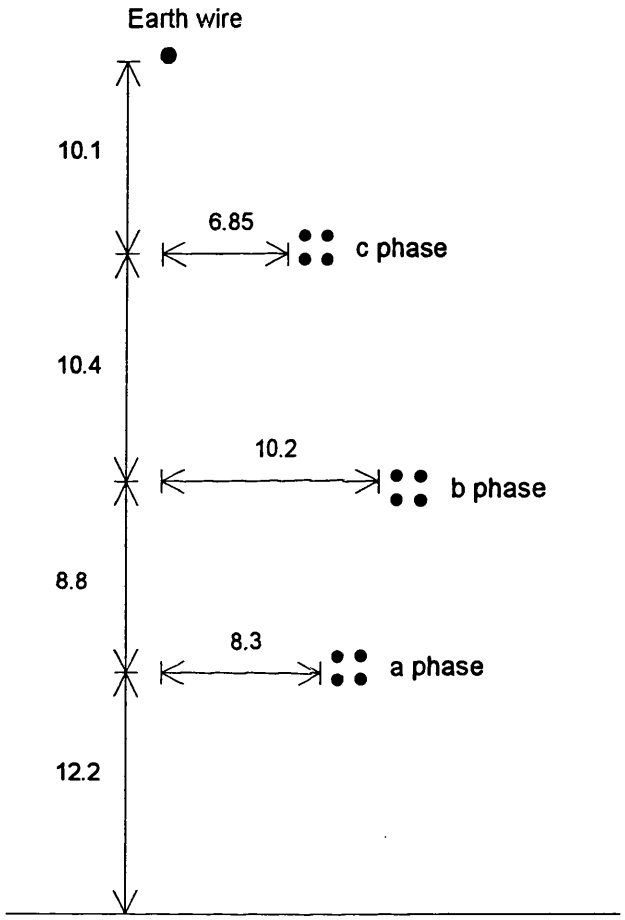

All dimensions in metres.

APPENDIX 10

Parameters for single machine load change study

The single machine power system configuration used for the study of load changing conditions is shown in Figure 5.29. The parameters used in the simulation are as follows:

GENERATING PLANT

Single machine, rating = 60 MW, p.f. = 0.8 lagging, 11.8 kV

H = 4.64 kW s/kVA	X_l = 0.185 Ω
R_a = 1.85E-4 Ω	X_q = 3.53 Ω
X_d = 3.713 Ω	$X_{q'}$ = 0.3527 Ω
$X_{d'}$ = 0.3713 Ω	$X_{q''}$ = 0.2293 Ω
$X_{d''}$ = 0.2413 Ω	
$T_{d'}$ = 8.189 s	$T_{q'}$ = 7.78 s
$T_{d''}$ = 0.03419 s	$T_{q''}$ = 0.1026 s

GENERATOR TRANSFORMER

Rating 75 MVA, 11.8 kV/400 kV

Z = j0.11 p.u.

APPENDIX 11

400 kV line used in the separation of a single machine from grid

The following 400 kV, single line configuration was used for the simulation of the separation of a single machine from the grid:

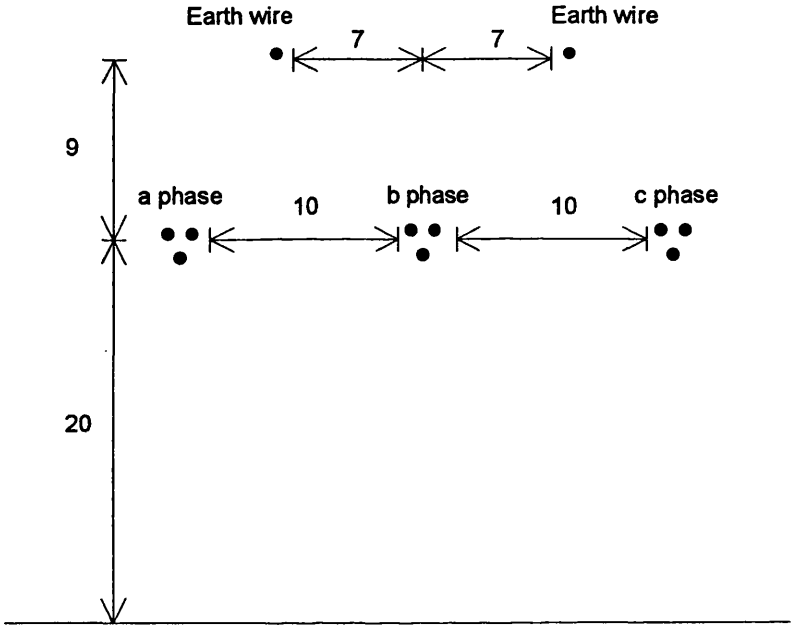

All dimensions in metres.

APPENDIX 12

Parameters for the separation of a system supplying a local load

Figure 5.40 shows the system configuration used to study the separation of two generating units separated from the grid. The parameters used in the simulation are as follows:

10 MILES π EQUIVALENT LINE

The configuration of the line is given in Appendix 11

Voltage = 400 kV

Z_0 = 4.1796 + j16.7801 Ω

Z_1 = 0.40645 + j4.9054 Ω

42 MILES DISTRIBUTED PARAMETERS LINE

The configuration of the line is given in Appendix 11

Voltage = 400 kV

Z_0 = 0.25977 + j1.04289 Ω/km

Z_1 = 0.02405 + j0.29026 Ω/km

GENERATING PLANT AT SEND 1

Single machine, rating = 750MVA, 17.5 kV

H = 3.5 kW s/kVA

R_a = 5.5696E-4 Ω

X_d = 0.71458 Ω

$X_{d'}$ = 0.1820 Ω

$X_{d''}$ = 0.08167 Ω

$T_{d'}$ = 4.0 s

$T_{d''}$ = 0.031 s

X_l = 0.07023 Ω

X_q = 0.71458 Ω

$X_{q'}$ = 0.1820 Ω

$X_{q''}$ = 0.08167 Ω

$T_{q'}$ = 3.9 s

$T_{q''}$ = 0.119 s

GENERATOR TRANSFORMER AT SEND 1

Rating = 750 MVA, 17.5 kV/400 kV

Z = j0.1 p.u.

GENERATING PLANT AT SEND 2

8 machines in parallel, total rating = 600 MVA, 11.8 kV

Single machine parameters correspond to the 75 MVA machine given in Appendix 10.

GENERATOR TRANSFORMER AT SEND 2

Rating = 600 MVA, 11.8 kV/400 kV

Z = j0.11 p.u.

APPENDIX 13

Derivation of parameters for the calculation of the PPS frequency

This Appendix describe the derivation of Equation (6.5) for the calculation of frequency using the orthogonal components of the PPS voltage vector. For the digital implementation of Equation (6.4), the in-phase and quadrature components of the PPS vector are given as:

$$V_{PPS_i}(n) = \frac{\frac{V_{PPS_i}(n)}{G_i} + \frac{V_{PPS_i}(n-1)}{G_i}}{2} \qquad (A.13.1)$$

$$V_{PPS_q}(n) = \frac{\frac{V_{PPS_q}(n)}{G_q} + \frac{V_{PPS_q}(n-1)}{G_q}}{2} \qquad (A.13.2)$$

The continuous time derivative can be approximated by the one-sample backwards algorithm:

$$\frac{dV_{PPS_i}(n)}{dt} = \frac{\frac{V_{PPS_i}(n)}{G_i} - \frac{V_{PPS_i}(n-1)}{G_i}}{1/f_s} \qquad (A.13.3)$$

$$\frac{dV_{PPS_q}(n)}{dt} = \frac{\frac{V_{PPS_q}(n)}{G_q} - \frac{V_{PPS_q}(n-1)}{G_q}}{1/f_s} \qquad (A.13.4)$$

Then, by using the definition of the frequency as given in Equation (A.1.8) in Appendix 1, the frequency calculation from a PPS voltage vector yields:

$$f(n) = \frac{V_{PPS_q}(n)V_{PPS_i}(n-1) - V_{PPS_q}(n-1)V_{PPS_i}(n)}{2\pi/f_s\,(V^2_{PPS_i}(n) + V^2_{PPS_q}(n))} \qquad (A.13.5)$$

which is equal to Equation (6.5) shown in Chapter 6.

APPENDIX 14

Signal conditioning board

A schematic diagram of the fourth order Butterworth anti-aliasing filter is given in the following figure. This filter is preceded by an isolating transformer and a "back-back" zener diode configuration used to step down the input voltage and protect the board from overvoltages, respectively.

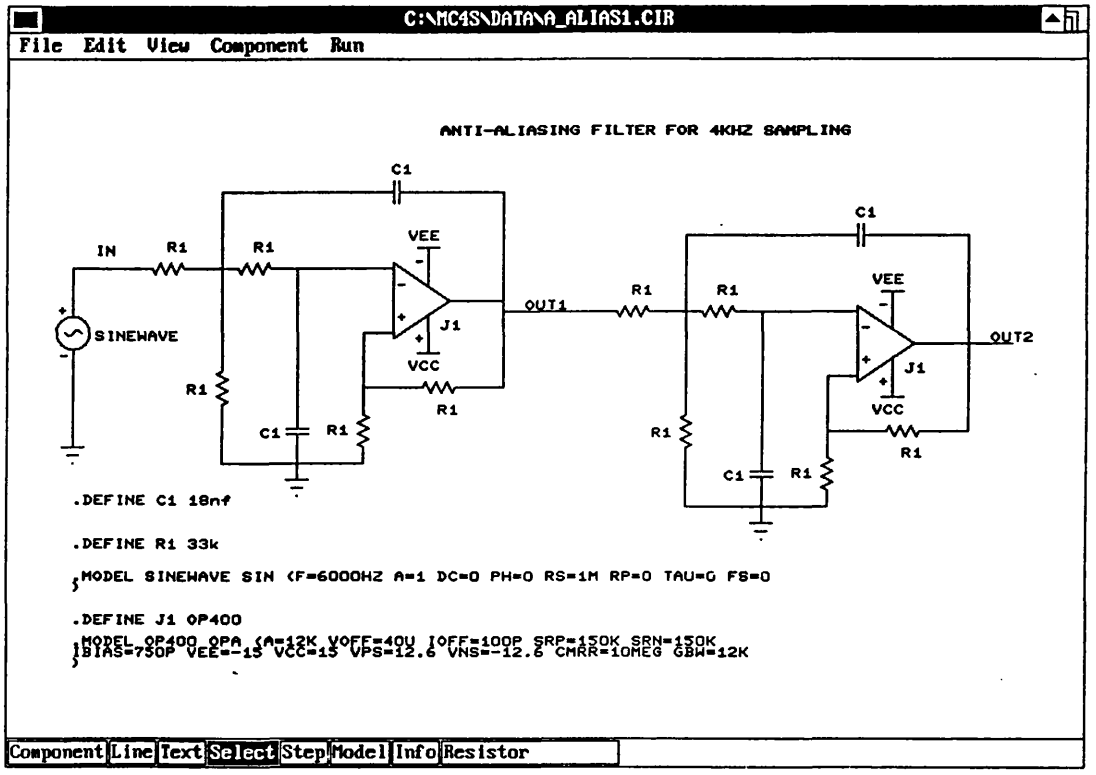

Figure A.14.1. Schematic diagram of the anti-aliasing filter used in the signal conditioning board.

The frequency and phase response of the anti-aliasing filter are shown in Figures A.14.2 and A.14.3, respectively.

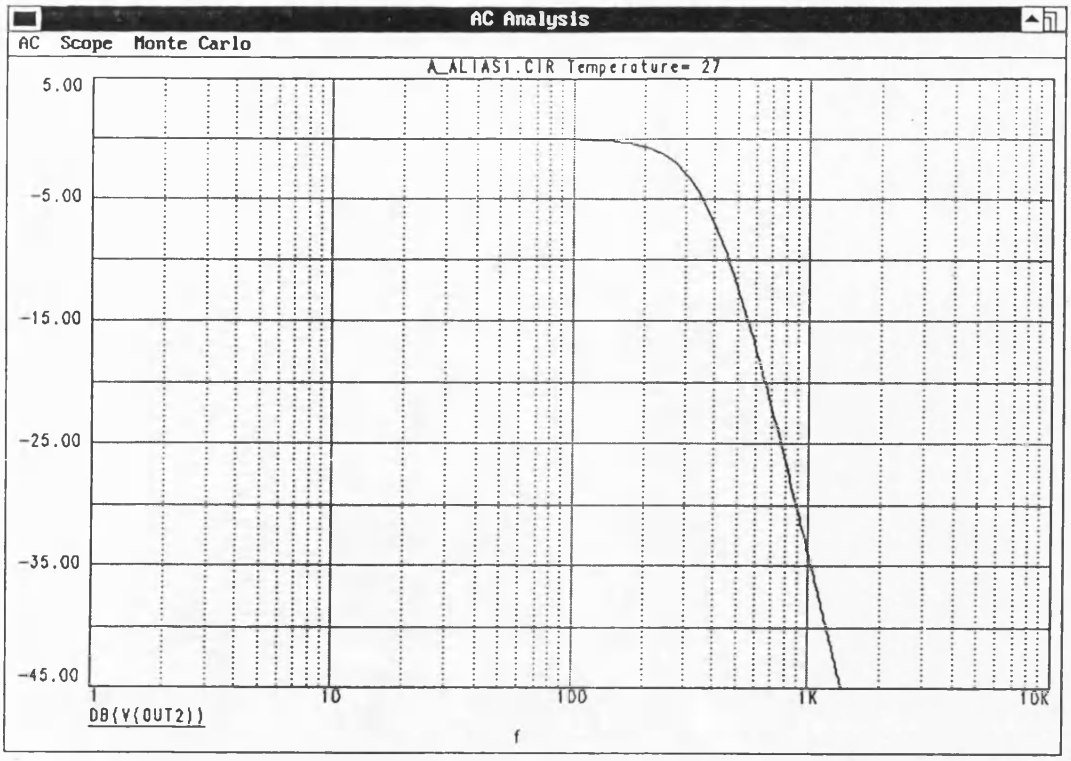

Figure A.14.2. Frequency Response of the anti-aliasing filter.

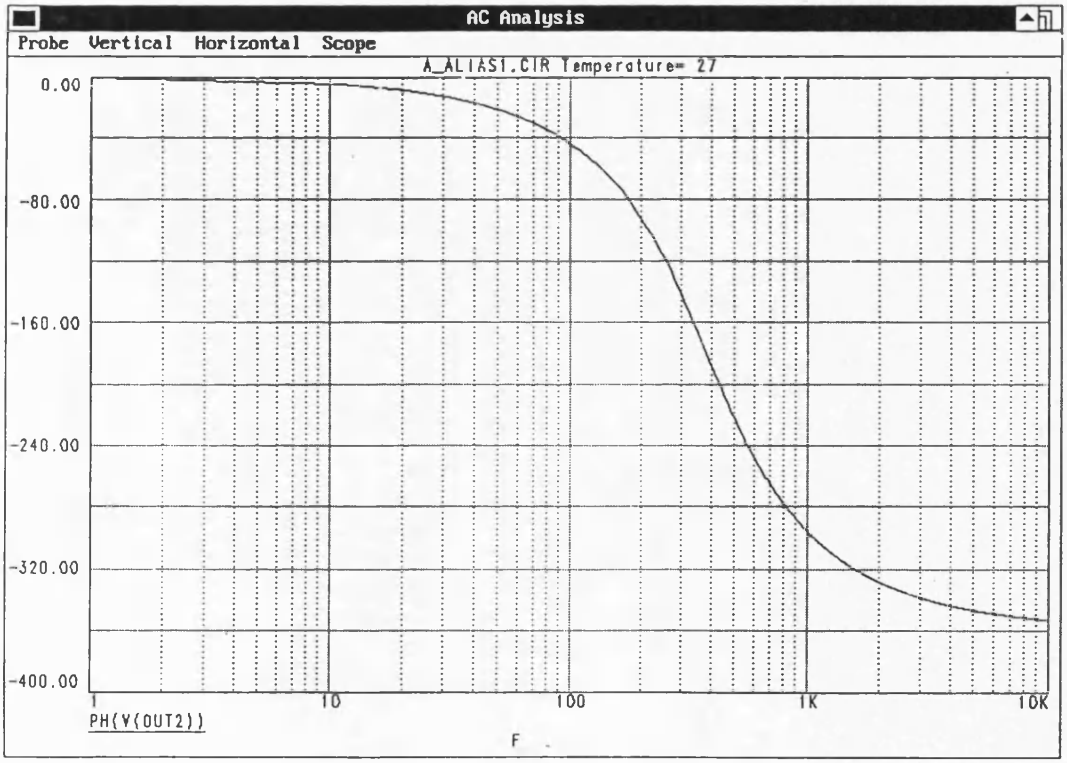

Figure A.14.3. Phase response of the anti-aliasing filter.

APPENDIX 15

Parameters of the simulated power system plant

An outline of the power system model used for the study of power system frequency transients is shown in Figure 7.6. The parameters of the simulator are as follows:

GENERATING PLANT

Four machines. Single rating 500 MW, p.f. = 0.8, 22 kV
Base = 2352 MVA base

H = 4.44 p.u.
S.C.R. = 0.4 p.u.
X_d = 2.8 p.u.
$X_{d'}$ = 0.362 p.u.
$X_{d''}$ = 0.230 p.u.
$T_{do'}$ = 7.3 s
$T_{do''}$ = 0.0314 s

X_q = 2.72 p.u.
$X_{q''}$ = 0.220 p.u.

$T_{qo''}$ = 0.116 s

GENERATOR TRANSFORMER

Base = 600 MVA
Z = 0.005 + j0.16 p.u.

TRANSMISSION LINE

Base = 100 MVA
Resistance = 0.00135 p.u.
Reactance = 0.185 p.u.
Susceptance = 0.735 p.u.

REFERENCES

1. P. J. Moore and A. T. Johns, "A New Approach to Digital Measurement of Power System Frequency", APSCOM 1991, Hong Kong.

2. X. He, Y. Min and Y. Han, "A New Definition and Method of Measurement of Dynamic Frequency in Power Systems", IEE Int. Power Engineering Conference, Singapore, Mar. 1993, pp. 227-232.

3. A.D. Baker, "Power System Response to Frequency Transients", IEEE Winter Power Meeting, Paper 71TP82-PWR, Jan. 1971.

4. M. Yong, H. Shao-bin, H. Ying-duo, G. Yuan-kai and W. Yi,"Analysis of Power-frequency Dynamics and Designation of Under Frequency Load Shedding Scheme in Large Scale Multi-machine Power Systems", IEE Int. Conf. on Advances in Power System Control, Operation and Management, Hong Kong, Nov. 1991, pp. 871-876.

5. M. Gupta, "Definition of Instantaneous Frequency and Frequency Measurability", American Journal of Physics, Vol. 42, Oct. 1974, pp. 840-846.

6. Electro Magnetic Transients Program, DEC VAX Translation. Usage licensed by LEC of K. U. Leuven, Belgium, 1978.

7. D. Gabor,"Theory of Communications", Journal of the IEE, Vol. 93, Part 3, Nov. 1946, pp. 429-441.

8. J. Ville,"Theorie et Applications de la Notion de Signal Analytique", Cables et Transmissions, Vol. 2A(1), Paris, France, Jan. 1948, pp. 61-74.

9. L. Mandel, "Complex Representation of Optical Fields in Coherence Theory", Journal of the Optic Society of America, Vol. 51, No. 5, May 1967, pp. 613-619.

10. A. Papoulis,"Random Modulation: A Review", IEEE Trans. on Acoustics, Speech and Signal Processing, Vol. ASSP-31, No. 1, Feb. 193, pp. 96-105.

11. E. Bedrosian,"A Product Theorem for Hilbert Transforms", IEEE Proc., May 1963, pp. 868-869.

12. I. R. Rabiner and B. Gold, *Theory and Applications of Digital Signal Processing*, Prentice-Hall, Englewood Clifts, N. J., 1975.

13. C. Berthomier,"Instantaneous Frequency and Energy Distribution of a Signal", Signal Processing, North Holland Publishing Company, Vol. 5, No. 1, Jan. 1983, pp. 31-45.

14. P. M. Anderson and M. Mirheydar,"A Low-Order System Frequency Response Model", IEEE Trans. on Power Systems, Vol. 5, No. 3, Aug. 1990, pp. 720-729.

15. P. M. Anderson and M. Mirheydar,"An Adaptive Method for Setting Underfrequency Load Shedding Relays", IEEE Trans. on Power Systems, Vol. 5, No. 2, May 1992, pp. 647-653.

16. M. M. Elkateb and M. F. Dias,"New Proposed Adaptive Frequency Load Shedding Scheme for Cogeneration Plants", IEE Int. Conf. on Power System Protection Development, York, I. K., May 1993, pp. 236-239.

17. M. M. Elkateb and M. F. Dias,"An Adaptive Load Shedding Technique for Industrial Plants Utilizing Local Information", Int. Power Engineering Conference, Singapore, Mar. 1993, pp. 772-777.

18. Z. Rujing and H. Yee,"Electric Power System Dynamics-Modes and Coherent Generators", IEE Int. Conf. on Advances in Power System Control, Operation and Management, Hong Kong, Nov. 1991, pp. 865-870.

19. Central Electricity Generating Board, *Modern Power Station Practice*, Vol. 7, *Operation and Efficiency*, Second Edition, Pergamon Press, Oxford, U.K., 1971.

20. M. S. Baldwin and H. S. Henkel,"Determination of Frequency Decay Rates During Periods of Generation Deficiency", IEEE Trans. on Power Apparatus and Systems, Vol. PAS-95, No. 1, Jan. 1976, pp. 26-36.

21. V. Eckhardt, P. Hipe and G. Hossemann,"Dynamic Measuring of Frequency and Frequency Oscillations in Multiphase Power Systems", IEEE Trans. on Power Delivering, Vol. 4, No. 1, Jan. 1989, pp. 95-102.

22. Ph. Denys, C. Counan, L. Hossenlopp and C. Holweck,"Measurement of Voltage Phase for the French Future Defence Plan Against Loss of Synchronism", IEEE Trans. on Power Delivery, Vol. 7, No. 1, Jan. 1992, pp. 62-69.

23. B. Fox, J. G. Thompson and C. E. Tindall,"Adaptive Control of Load-Shedding Relays Under Generation Loss Conditions", IEE Int. Conf. on Developments in Power System Protection, No. 302, 1988, pp. 259-263.

24. M. M. Elkateb and M. F. Dias,"An Adaptive Load Shedding Technique for Industrial Plants Utilizing Local Information", Int. Power Engineering Conference, Singapore, Mar. 1993, pp. 772-776.

25. V. K. Govindan, M. Vaiyan and C. Velayudham, "A Novel Method for Digital Monitoring of Frequency Deviation in Power Systems", Int. Journal of Electronics, Vol. 56. No. 1, 1984, p. 127.

26. O. P. Malik," Frequency Measurement for Use with a Microprocessor-based Water Turbine Governor", IEEE Trans. on energy Conversion, Vol. 6, No. 3, Sep. 1991, pp. 361-366.

27. A. Mukhatar,"Measurement of Power System Frequency Deviation Using a Microprocessor", Int. Journal of Electronics, Vol. 68, No. 1, 1990, p. 161.

28. S. A. McIlwaine, C. E. Tindall and W. McClay,"Frequency Tracking for Power Control", IEE Proc. on Generation, Transmission and Distribution, Vol. 133, Part C, No. 2, Mar. 1986, pp. 95-98.

29. J. Heydeman and E. N. Lulf,"Microprocessor Based Underfrequency Relaying", IEE Conf. Publication No. 249, Apr. 1985, pp. 24-27

30. C. T. Nguyen,"A New Technique for Rapid Tracking of Frequency Deviations Based on Level Crossings", IEEE Trans. on Power Apparatus and Systems, Vol. PAS-103, No. 8, Aug. 1984, pp. 2230-2237.

31. F. M. Ham and A. A. Girgis,"Measurement of Power Frequency Fluctuations Using the FFT", IEEE Trans. on Industrial Electronics, Vol. IE-32, No. 3, Aug. 185, pp.199-204.

32. A. G. Phadke, J. S. Thorp and M. C. Adamiak,"A New Measurement Technique for Tracking Voltage Phasor, Local System Frequency and the Rate of Change of Frequency", IEEE Trans. on Power Apparatus and Systems, Vol. PAS-102, No. 5, May 1983, pp. 1025-1033.

33. G. Benmouyal,"Design of a Combined Digital Global Differential and Volt/Hertz Relay for Step-up Transformers", IEEE Trans. on Power Delivery, Vol. 6, No. 3, Jul. 1991, pp. 1000-1007.

34. J. S. Thorp, A. G. Phadke, S. Horowitz and M. Begović,"Some Applications of Phasor Measurement to Adaptive Protection", IEEE Trans. on Power Systems, Vol. 3, No. 2, May 1988, pp. 791-798.

35. L. J. Griffiths,"Rapid Measurement of Digital Instantaneous Frequency",

IEEE Trans. on Acoustics, Speech and Signal Processing, Vol. ASSP-23, 1975, pp. 207-222.

36. V. U. Reddy, B. Egardt and T. Kailath,"Optimized Lattice Form Adaptive Line Enhancer for a Sinusoidal Signal in Broad-Band Noise", IEEE Trans. on Circuits and Systems, Vol. CAS-28, No. 6, Jun. 1981, pp. 542-549.

37. M. S. Sachdev and M. Nagpal,"A Recursive Least Error Squares Algorithm for Power System Relaying and Measurement Applications", IEEE Trans. on Power Delivery, Vol. 6, No. 3, Jul. 1991, pp. 1008-1015.

38. J. A. Chambers and A. G. Constantinides,"Frequency Tracking Using Constrained Adaptive Notch Filters Synthesized from Allpass Sections", IEE Proc., Vol. 137, Part F, No. 6, Dec. 1990, pp. 475-481.

39. J. F. Chicharo and T. N. Saing,"Gradient-Based Adaptive IIR Notch Filtering for Frequency Estimation", IEEE Trans. on Acoustics, Speech and Signal Processing, Vol. 38, No. 5, May 1990, pp. 769-777.

40. B. Widrow and J. D. Stearns, *Adaptive Signal Processing*, Prentice-Hall, Englewood Clifts, N. J., 1985.

41. M. S. Sachdev and J. Shen,"A New Digital Technique for Measuring Frequency at a Power System Bus", IEE Conf. Publication 302, 1989, pp. 102-106.

42. I. Kamwa and R. Grondin,"Fast Adaptive Schemes for Tracking Voltage Phasor and Local Frequency in Power Transmission and Distribution Systems", IEEE Trans. on Power Delivery, No. 2, Apr. 1992, pp. 789-795.

43. M. S. Sachdev, H. C. Wood and N. G. Johnson,"Kalman Filtering Applied to Power System Measurements for Relaying", IEEE Trans. on Power

Apparatus and Systems, Vol. PAS-104, No. 12, Dec. 1985, pp. 3565-3573.

44. A. A. Girgis and T. L. D. Hwang,"Optimal Estimation of Voltage Phasors and Frequency Deviation Using Linear and Non-linear Kalman Filtering: Theory and Limitations", IEEE Trans. on Power Apparatus and Systems, Vol. PAS-103, No. 10, Oct. 1984, pp. 2943-2949.

45. A. A. Girgis, W. B. Chang and E. B. Makram,"A Digital Recursive Measurement Scheme for On-line Tracking of Power System Harmonics", IEEE Trans. on Power Delivery, Vol. 6, No. 3, Jul. 1991, pp. 1153-1160.

46. A.A. Girgis and W. L. Peterson,"Adaptive Estimation of Power System Frequency and its Rate of Change for Calculating Sudden Power System Overloads", IEEE Trans. on Power Delivery, Vol. 5, No. 2, Apr. 1990, pp. 585-594.

47. S. Haykin, *Adaptive Filter Theory*, Second Edition., Prentice-Hall Int., Englewood Clifts. N. J., 1991.

48. R. G. Brown and P. Y. C. Hwang, *Introduction to Random Signals and Applied Kalman Filtering*, Second Edition, John Wiley & Sons, 1992.

49. M. M. Begović, P. M. Djurić, S. Dunlap and A. Phadke,"Frequency Tracking in Power Networks in the Presence of Harmonics", IEEE Trans. on Power Delivery, Vol. 8, No. 2, Apr. 1993, pp. 480-486.

50. L. R. Rabiner and R. V. Schafer,"On the Behaviour of Minimax FIR Digital Hilbert Transforms", The Bell Systems Technical Journal, Vol. 53, No. 2, Feb. 1974, pp. 363-390.

51. M. Sun and R. J. Sclabassi,"Discrete-Time Instantaneous Frequency and its Computation", IEEE Trans. on Signal Processing, Vol. 41, No. 5, May

1993, pp. 1867-1879.

52. A. V. Oppenheim and R. V. Shafer, *Discrete-Time Signal Processing*, Prentice-Hall Int., Englewood Clifts, N.J., 1989.

53. B. Boashash,"Estimating and Interpreting the Instantaneous Frequency of a Signal Part 1: Fundamentals. Part 2: Algorithms and Applications", IEEE Proc., Vol. 80, No. 4, Apr. 1992, pp. 520-568.

54. F. Hlawatsch and G. F. Boudreax-Bartels,"Linear and Quadratic Time-Frequency Signal Representations", IEEE Signal Processing Magazine, Apr. 1992, pp. 21-65.

55. P. J. Moore, D. Carranza and A. T, Johns,"Improved Digital Measurement of Power System Frequency", 27th Universities Power Enginerring Conference, University of Bath, U.K., Sep. 1992.

56. E. Kamen, *Introduction to Signals and Systems*, MacMillan Publishing Co., 1987.

57. A. Papoulis. *Probability, Random Variables and Stochastic Process*, 3rd. Ed., McGraw-Hill, 1991.

58. T. Ström,"On Amplitude-weighted Instantaneous Frequency", IEEE Trans. on Acoustics, Speech and Signal Processing, Vol. ASSp-28, No. 4, Aug. 1977, pp. 351-353.

59. M. M. Elkateb,"Machine Fault Analysis for Power System Studies", Internal report, No. MK0101, Power Systems Research Lab., Dept. of Electrical, Electronic and Information engineering, City University, London, 1988.

60. A. T. Johns and A. A. El-Alaily, "New Distance Protective Relay with

Improved Coverage for High-resistance Earth Faults", Proc. IEE, Vol. 124, No. 4, Apr. 1977, pp. 349-355.

61. D. J. DeFatta, J. G. Lucas and W. S. Hodgkiss, *Digital Signal Processing: A System Design Approach*, John Wiley & Sons, 1988.

62. P. J. Burrows and A. R. Daniels,"Digital excitation control of a.c. turbogenerators using a dedicated microprocessor", IEE Proc., Vol. 125, No. 3, Mar. 1978, pp. 237-240.

63. T. H. Mason, P. D. Aylett and F. H. Birch,"Turbo-Generator Performance Under Exceptional Operating Conditions", IEE Proc., Part A, Jan. 1959, pp. 357-380.

PUBLISHED WORK

The following four papers have been published based on the work described in this thesis:

1. P. J. Moore, D. Carranza and A. T. Johns,"Improved Digital Measurement of Power System Frequency", 27th Universities Power Engineering Conference, University of Bath, Sep. 1992.

2. P. J. Moore, R. D. Carranza and A. T. Johns,"Performance of a New High Speed Digital Technique for Measuring Power System Frequency", 5th Int. Conf. on Developments in Power System Protection, IEE, York, Mar. 1993.

3. R. D. Carranza, P. J. Moore and A. T. Johns,"Validity of a Bandpass Plus Orthogonal Decomposition Technique for the Digital Measurement of Power System Frequency", 28th Universities Power Engineering Conference, Straffordshire University, Sep. 1993.

4. P. J. Moore, R. D. Carranza and A. T. Johns,"A New Numeric Technique for High-Speed Evaluation of Power System Frequency", IEE Proc. Gener. Transm. and Distrib., Vol. 141, No. 5, Sep. 1994.

The following paper was presented to the 27th Universities Power Engineering Conference at the University of Bath, 23rd - 25th September 1992.

IMPROVED DIGITAL MEASUREMENT OF POWER SYSTEM FREQUENCY

P J Moore, D Carranza and A T Johns

University of Bath, UK

ABSTRACT

Recently, a novel approach to the measurement of the frequency of a power system by digital means was introduced [1]. The technique decomposes a signal taken from the power system into a pair of orthogonal and bandlimited signals by using two FIR filters. A discrete-time algorithm calculates the instantaneous frequency using the outputs of the filters. Some improvements on the measuring characteristics of the technique have been achieved and are shown in this paper. A study of the time and frequency responses of the filters was performed to define the effects of bandlimiting the input signal and calculating its frequency by the discrete-time algorithm. Correct analytic expressions of the frequency gains of the filters have been found. They are used within a feedback loop in the measuring algorithm for accurately estimating any frequency deviation. In this paper we present the results of these studies and the improvements that have been achieved.

1. INTRODUCTION

Deviations of the frequency from its nominal value are used to indicate the balance status between the mechanic and the electric energies in a power system. Physical disturbances along the power system, such as faulting generation plants, loss of a major tie-line or a sudden overload, severly affect this energy balance which manifests itself as deviations of the frequency. Emergency procedures should be started for correcting such situations as soon as a fault occurs. These procedures depend on the accurate measurement of the power system frequency. A key factor is the time spent to recognize a frequency deviation.

The main relevance of the present technique is its ability to measure rapid changes of frequency within very short evaluation times and to obtain accurate estimates even if the input signal is embedded in time-varying noise which is typical in power system environments. On-line calculations to estimate the frequency of a power system are affected by non-50 Hz components superimposed on the measuring signal. Such components are a combination of harmonics of the fundamental frequency plus bandlimited noise. The statistics of such disturbances during unbalanced situtations are slowly time varying making impractical to base any measuring algorithm on an a priori statistical model. Moreover, disturbances are commonly followed by synchronizing oscillations due to the high mechanical inertias in a power system.

This problem is well established and has been addressed by some other techniques. Their commonest profile is the assumption of some degree of stationarity of the statistics of the signal over a finite period of time. For instance: zero crossing techniques [2], adaptive time intervals of sampling algorithm [3] and least squares error techniques [4]. Recent techniques are based on the theory of adaptive estimation so the fundamental frequency of the signal is recursively tracked [5]. However, the trade-off between evaluation times and accurate measurements remains being non time-cost effective.

In this paper we present the work performed in improving the technique of Moore and Johns [1]. An analysis of the filters frequency response resulted in closed form expressions which are used within a feedback loop to continuously compensate their non flat frequency response for other frequencies different from 50 Hz. This compensation has improved the measurements within the bandwidth of the filters while retaining their orthogonal characteristics. It was also analyzed the effect of the length of the FIR expressions of the filters with respect to their frequency sidelobes because measurements are disturbed by the non linear attenuation of the filters within those frequency intervals. Consequently, a Hamming low pass prefilter was digitally implemented to limit the bandwidth of the input signal within the FIR filters bandwidth to improve the overall measuring system performance in respect of harmonic and high frequency noise.

2. FREQUENCY CALCULATION ALGORITHM

1. Expression of the instantaneous frequency of a signal. Let a continuous time signal x(t) to be taken from a power system data bus, either from voltage or current data. A complex representation of x(t) allows a definition of the instantaneous frequency of x(t). An orthogonal decomposition of x(t) yields:

$$x_s(t) = A \sin(\omega t + \phi) \qquad ...(1)$$

and

$$x_c(t) = A \cos(\omega t + \phi) \qquad ...(2)$$

where A is the amplitude of x(t) and ϕ equals its phase. Differentiating equations (1) and (2) with respect to time gives:

$$\frac{d\, x_s(t)}{dt} = x_s'(t) = 2\pi f A \cos(\omega t + \phi) \qquad ...(3)$$

and

$$\frac{d\, x_c(t)}{dt} = x_c'(t) = -2\pi f A \sin(\omega t + \phi) \qquad ...(4)$$

Manipulating equations (3) and (4) yields:

$$x_s'(t)x_c(t) - x_s(t)x_c'(t) = 2\pi f A^2[\cos^2(\omega t+\phi) + \sin^2(\omega t+\phi)] = 2\pi f A^2 \qquad ...(5)$$

The amplitude A of x(t) may be expressed as the instantaneous magnitude of the orthogonal components, i.e.:

$$A^2 = x_s^2(t) + x_c^2(t) \qquad ...(6)$$

Using (6) and (5) gives:

$$x_s'(t)x_c(t)-x_s(t)x_c'(t) = 2\pi f[x_s^2(t)+x_c^2(t)] \qquad ...(7)$$

finally,

$$f = \frac{x_s'(t)x_c(t) - x_s(t)x_c'(t)}{2\pi[\, x_s^2(t) + x_c^2(t)\,]} \qquad ...(8)$$

2. Orthogonal Decomposition and bandlimiting of the input signal x(t). Two finite impulse response (FIR) bandpass filters, having a linear phase delay of 90° each other, are used to decompose the signal x(t) into two orthogonal bandpass components. These bandpass filters were designed to have a central frequency at freq = f_{sys} = 50 Hz and a bandwidth of 2 f_{sys} such that the narrow bandwidth of the power system signal x(t) is well represented by the complex transformation that these filters provide. Frequency components of x(t) outside the FIR filters bandwidth (0Hz to 100Hz) are attenuated, i.e. : DC and harmonic components of f_{sys}.

The finite time response expressions of the orthogonal filters are:

sine-component : $h_s[kT]=SIN(2\pi kT/N+\pi/N)$ ...(9)

cosine-component: $h_c[kT] = COS(2\pi kT/N+\pi/N)$ ...(10)

where k = 0,1,2,...(N-1) and T = $1/f_s$, f_s = sampling frequency.

The number N of coefficients in the impulse response is proportional to fs and to the nominal power system frequency (f_{sys} = 50 Hz). The factor π/N in the phase argument is used to provide equal gain of both of the filters at freq = f_{sys}. Analysis of the frequency response of equations (9) and (10) shows that such a gain is given by the ratio 2/N, thus, at f_s = 4 kHz and f_{sys} = 50 Hz, then N = 80 and gain = 40.

Figure (1) shows the frequency response of the FIR filters for N = 80. The effect of π/N is shown at freq = 50 Hz. Accurate estimation of the frequency requires a continuous compensation of the gain of the FIR filters when the frequency deviates from 50 Hz. It is seen that the frequency sidelobes of the FIR filters do not provide enough attenuation of frequency components after 100 Hz which appear as disturbances impossed on the frequency estimates. The broken line corresponds to the COSINE filter response. Its high sidelobes cause distorsions during measurements. A Hamming low pass prefilter was implemented to fully attenuate frequencies after 100 Hz.

In [1] there were given approximated expressions for the filters frequency responses which leaded to innacurate estimations under frequency deviations. Using the 'one-side' Z_Transform there were found the analytic expressions of the frequency responses in closed forms:

$$Hs(z) = \frac{z\,SIN(\Omega o/2)(1 - z^{-n})(z + 1)}{z^2 - 2z\,COS(\Omega o) + 1} \quad ...(11)$$

and

$$Hc(z) = \frac{z\,COS(\Omega o/2)(1 - z^{-n})(z - 1)}{z^2 - 2z\,COS(\Omega o) + 1} \quad ...(12)$$

These expressions are convergent if $z = \exp(j\Omega)$, for $\Omega = 2\pi freq/f_s$ and $\Omega o = 2\pi f_{sys}/f_s$. Hence, their magnitudes as functions of frequency are:

$$|Hs(freq)| = \frac{2SIN(\pi f_{sys}/f_s)SIN(\pi freqN/f_s)COS(\pi freq/f_s)}{COS(2\pi freq/f_s) - COS(2\pi f_{sys}/f_s)} \quad ...(13)$$

and

$$|Hc(freq)| = \frac{2COS(\pi f_{sys}/f_s)SIN(\pi freqN/f_s)SIN(\pi freq/f_s)}{COS(2\pi freq/f_s) - COS(2\pi f_{sys}/f_s)} \quad ...(14)$$

Reciprocal expressions of equations (13) and (14) are used within an internal feedback in the algorithm for providing the frequency gain compensation of the filters at the value freq of the measured frequency.

3. Approximation to the derivative of the orthogonal signals. Real time implementation of equation (8) is achieved by using the method of finite backward differences over the output signals of the orthogonal filters: $x_s[nT]$ and $x_c[nT]$, respectively. The current algorithm uses a three point derivative approximation which takes account of the current and the two previous data samples:

$$\frac{d\,x_s[nT]}{dt} = \frac{3x_s[nT] - 4x_s[nT - T] + x_s[nT - 2T]}{2T} \quad ...(15)$$

and

$$\frac{d\,x_c[nT]}{dt} = \frac{3x_c[nT] - 4x_c[nT - T] + x_c[nT - 2T]}{2T} \quad ...(16)$$

where T = $1/f_s$.

Inserting equations (15) and (16) into equation (8) gives:

$$freq = \frac{x_s[n]\left[4x_c[n-1]-x_c[n-2]\right] - x_c[n]\left[4x_s[n-1]-x_s[n-2]\right]}{4\pi G_s G_c\,[\,(x_s[n]/G_s)^2 + (x_c[n]/G_c)^2\,]/f_s} \quad ...(17)$$

However, use of equation (17) leads to an error due to the approximation to the derivative which can be shown to be:

$$error = \frac{4(\pi/f_s)^2 freq^3}{3} - \frac{28 freq(\pi^2 freq^2/f_s^2)^2}{15} \quad ...(18)$$

Equation (17) contains the terms $G_s = 1/H_s(freq)$ and $G_c = 1/H_c(freq)$ to compensate the frequency gain of the filters.

3. FREQUENCY MEASUREMENT RESULTS

The estimation algorithm was implemented using Fortran programming language on a VAX computer. All the operations have been performed in single precision floating arithmetic. Simulation data was generated by in-house designed Fortran programs. The sampling frequency is 4 kHz.

1° Figure (2) shows the response of the measuring algorithm to the application of pure sinusoidal inputs at f_{sys} = 47 Hz, 50 Hz and 53 Hz. The length of the initial transient, 160 samples, corresponds to the total length of the Hamming and the orthogonal filters.

2° In figure (3), the input is a sinusoid signal at 50 Hz corrupted by its first three harmonics and additive bandlimited noise. These components have the following per-unit levels: 0.2, 0.1, 0.05 and 0.2, respectively. Figure (4) shows the improvement afforded by the Hamming prefilter in the sense that it removes frequencies outside the orthogonal filters bandwidth. In figure (5) the input is equal to that in figure (3) except that its central frequency is f_{sys} = 47 Hz. However, here the prefilter is not used in order to show how the zeros of orthogonal filters (see equations (11) and (12)), poorly attenuate harmonic frequencies if f_{sys} is not 50 Hz. In figure (6) the prefilter is used. Note: the ripple noise which still remains in figures (4) and (6) when using the prefilter, can be shown to be produced by noise components located within the bandwidth of the orthogonal filters at the evaluation time.

3° A non realistic situation of abrupt frequency changes is shown in figure (7). The changes range from f_{sys} = 47 Hz to 53 Hz. During this test the amplitude of the input signal is held to 1.0 p.u. free of additive noise.

4° The performance of the algorithm under sudden amplitude changes is shown in figure (8). The changes are relative to parts per unit: 0.8 pu to 0.5 pu to 1.0 pu, while the frequency f_{sys} is held at 50 Hz.

5° In figure (9) is shown the ability of the algorithm to track rapid frequency deviations. The input is frequency modulated at f_m = 2 Hz with a total excursion of 4 Hz about 50 Hz. The ripple curve is the measured frequency while the solid line corresponds to the real instantaneous frequency of the input signal. It is seen that the time delay in the frequency measurement is due to the 160 coefficients length of the prefilter plus the orthogonal filters.

6° Figure (10) shows the algorithm when tracking an exponentially decaying frequency signal = $SIN(2\pi f_{sys} - Df[t + Texp(-t/T)])$ for Df = 0.5 Hz, T = 1 s and f_{sys} = 50 Hz.

CONCLUSIONS

An improved method for measuring the deviation of the frequency of a power system signal has been presented. The orthogonal transformation and filtering of the input signal within a narrow bandpass frequency interval, provides a meaningful complex representation of the input signal such that it allows the instantaneous value of the fundamental frequency to be calculated in the presence of harmonics and additive

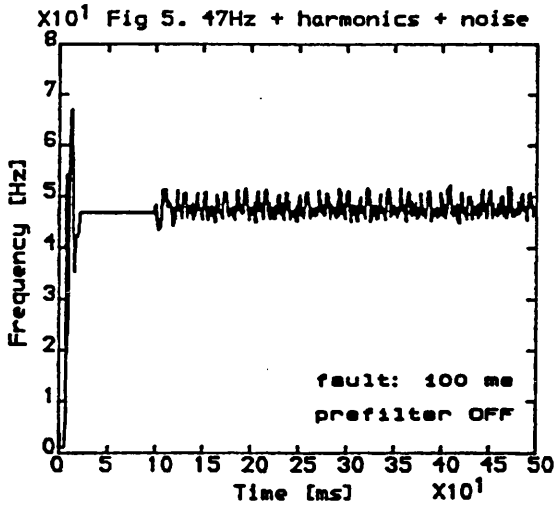
X10¹ Fig 5. 47Hz + harmonics + noise
Frequency [Hz]
Time [ms] X10¹
fault: 100 ms
prefilter OFF

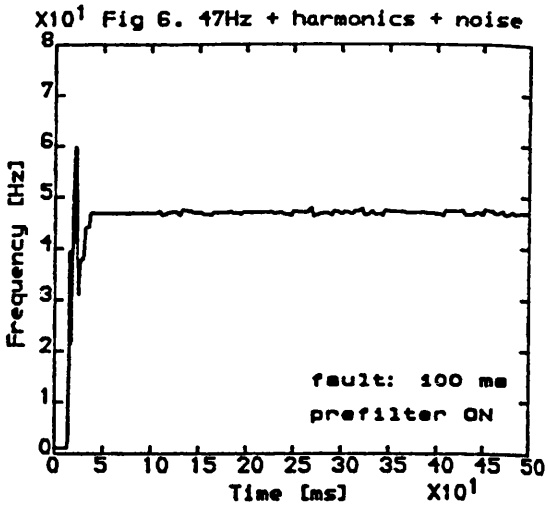
X10¹ Fig 6. 47Hz + harmonics + noise
Frequency [Hz]
Time [ms] X10¹
fault: 100 ms
prefilter ON

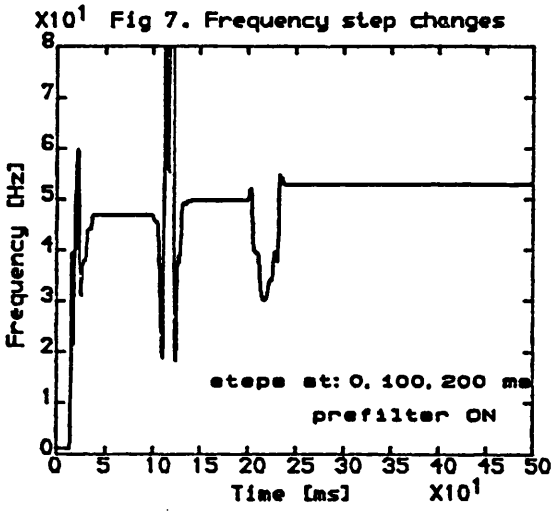
X10¹ Fig 7. Frequency step changes
Frequency [Hz]
Time [ms] X10¹
steps at: 0, 100, 200 ms
prefilter ON

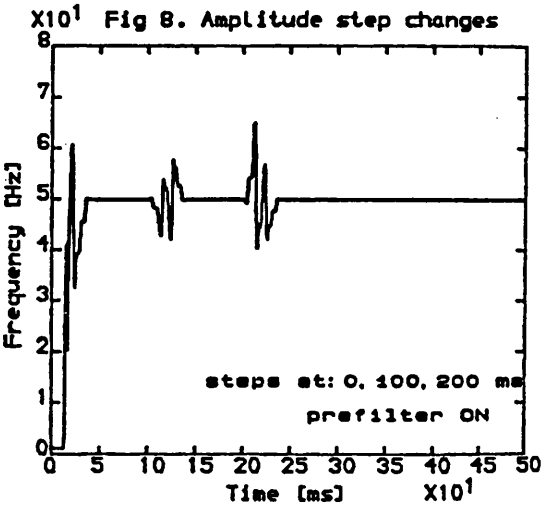
X10¹ Fig 8. Amplitude step changes
Frequency [Hz]
Time [ms] X10¹
steps at: 0, 100, 200 ms
prefilter ON

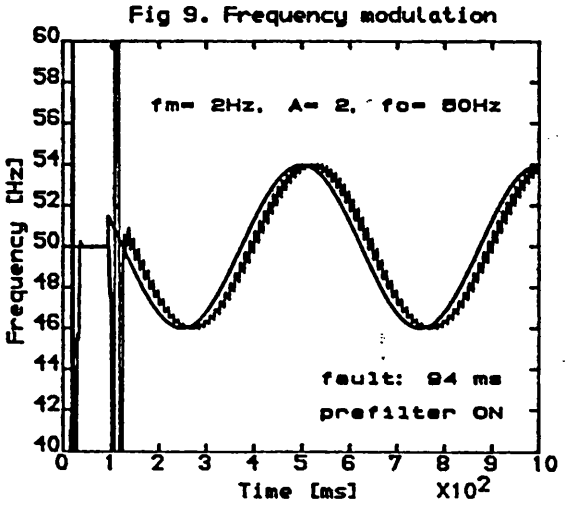
Fig 9. Frequency modulation
Frequency [Hz]
Time [ms] X10²
fm= 2Hz, A= 2, fo= 50Hz
fault: 94 ms
prefilter ON

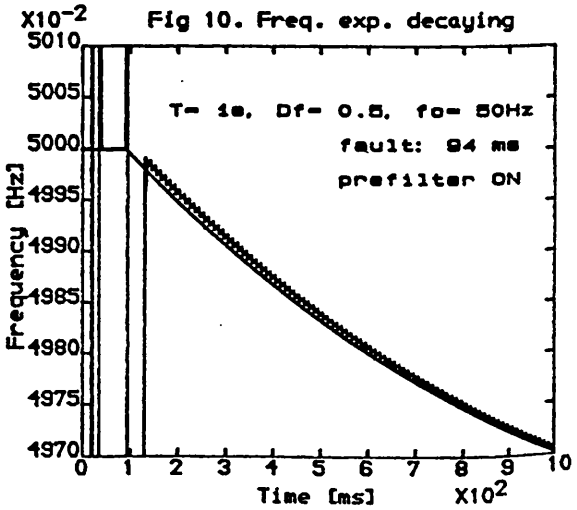
X10⁻² Fig 10. Freq. exp. decaying
Frequency [Hz]
Time [ms] X10²
T= 10, Df= 0.5, fo= 50Hz
fault: 94 ms
prefilter ON

noise. The accuracy of the algorithm has been improved after the analysis of its time and frequency responses. Accordingly, enhancement of the performance of the orthogonal filters within their bandwidth has been performed. The very short evaluation time of this algorithm allows a close tracking of the input signal frequency even when additive distortions are time varying. The real time implementation of this algorithm can be used as the basis of under-frequency relaying or frequency deviation based system load shedding schemes.

ACKNOWLEDGEMENTS

The authors would like to thank the University of Bath for the provision of facilities for this work. The second author woul like to thank CONACYT-Mexico for financial support.

REFERENCES

1. Moore, P.J. and Johns, A.T.,"A New Approach to Digital Measurement of Power System Frequency", APSCOM 1991, Hong Kong.

2. Malik, O.P.,"Frequency Measurement for Use with a Microprocessor-Based Water Turbine Governor", IEEE PAS Winter Meeting, Paper No. 91WM140-4 EC, Feb. 1991.

3. Benmouyal, G.,"An Adaptive Sampling-Interval Generator for Digital Relaying", IEEE PAS Winter Meeting, Paper No. 89WM054-8 PWRD, Jan. 1989.

4. Soliman, S.A. and Christensen, G.S.,"Estimation of Steady State Voltage and Frequency of Power Systems from Digitalized Bus Voltage Samples", Electric Machines and Power Systems, Vol. 19, No. 4, Jul-Aug. 1991, pp. 555-576.

5. Giray, M.M. and Sachdev, M.S.,"Off-Nominal Frequency Measurements in Electric Power Systems", IEEE Trans. on Power Delivery, Vol. 4, No. 3, Jul. 1989, pp. 1573-1578.

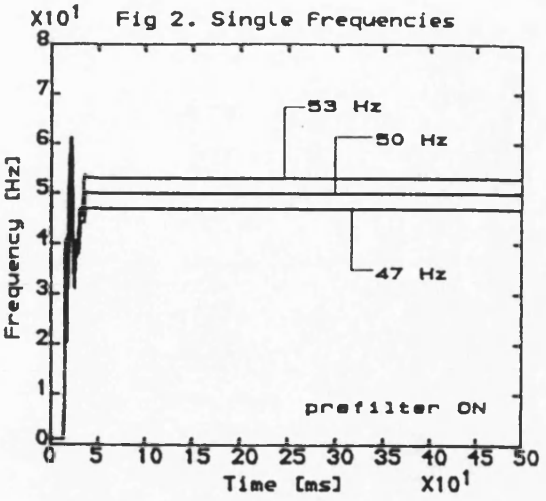

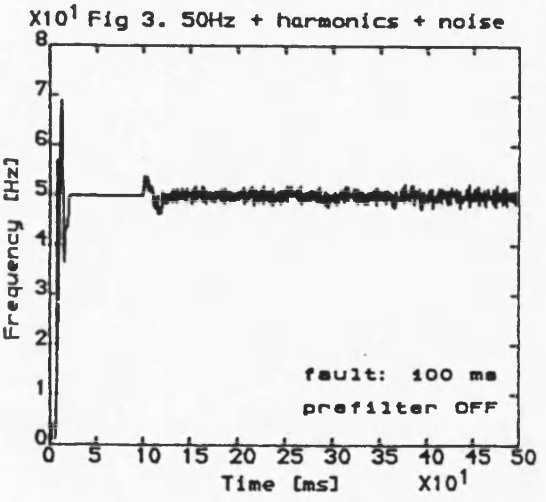

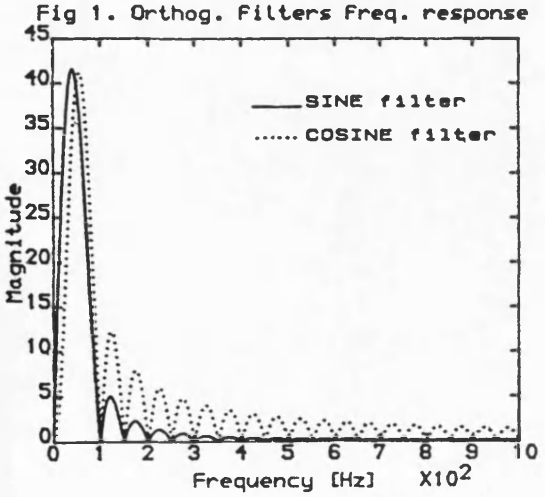

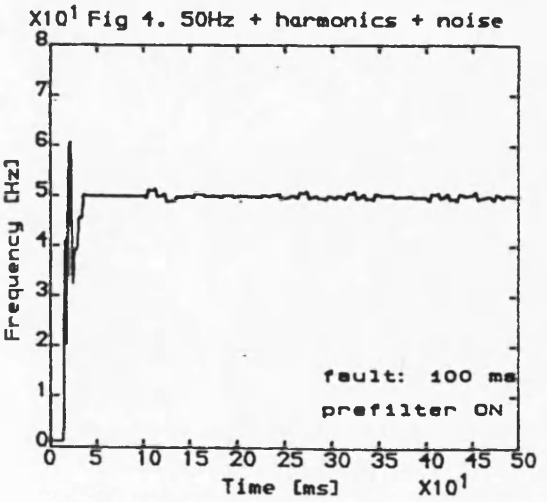

The following paper was presented to the fifth Int. Conf. on Developments in Power System Protection at University of York, 30th March- 1st April 1993

PERFORMANCE OF A NEW HIGH SPEED DIGITAL TECHNIQUE FOR MEASURING POWER SYSTEM FREQUENCY

P J Moore, D Carranza and A T Johns

University of Bath,UK

1. Introduction

If a voltage or current measured at a bus in a power system were composed of only a sinusoid at the fundamental power system frequency, then the measurement of the frequency, whether by digital means or otherwise, would be simple and quickly performed. However, in reality, such measured signals are corrupted with non-50Hz components, such as harmonics and additive broadband noise from time varying sources such as synchronising oscillations and start-up transients. If the period of observation to form an estimate of the frequency is small, then the variation of the disturbances within this period is minimal and the disturbance is termed *wide sense stationary* (WSS).

Currently, much work has been performed in the development of frequency measurement techniques, by digital means, under the assumption that the statistics of the power system remain stationary (i.e. do not vary with time) during the observation period. Zero-crossing algorithms [1,2] show frequency deviations that exponentially approach the true value as the number of cycles considered approach infinity. Adaptation of the sampling interval to ensure correct measurement using a discrete Fourier transform algorithm is possible [3] although it is prone to round off oscillations since the sampling interval should take an integer value. Another approach has been to make assumptions about the power system behaviour using a *a priori* statistics model [4]. Several authors have incorporated least mean squares (LMS) estimation theory using both stationary models [5,6] and adaptive estimation models where the fundamental frequency is tracked without having to know any statistical property in advance [7,8]. However, in all these works, there is a compromise between the accuracy of the frequency measurement and the length of the observation period. Accuracy decreases as the period becomes smaller.

This paper describes the further development of a recently developed technique [9] for the fast and accurate measurement of power system frequency.

2. Instantaneous Frequency

Let $x(t) = s(t) + n(t)$ be a signal, either voltage or current, measured at the power system bus, where $s(t)$ is a narrow-band signal centred at $f_i(t)$ (i.e. the frequency of the power system as a function of time) and $n(t)$ a broad-band signal representing additive noise also with time varying characteristics. It will be shown later that $s(t)$ may be recovered from $x(t)$ by using a narrow-band filter.

Let $s(t)$ be expressed as:

$$s(t) = a(t)\cos(\omega_o t) - b(t)\sin(\omega_o t) \quad (1)$$

thus,

$$s(t) = r(t)\cos[\theta(t)] \quad (2)$$

where $\theta(t) = \omega_o + \varphi(t)$ and $s(t)$ is expressed in terms of $\omega_o = 2\pi f_o$, where f_o is the nominal power system frequency, and two random modulation factors: $r(t) = [a^2(t) + b^2(t)]^{1/2}$ for the amplitude and for the phase, $\varphi(t) = \tan^{-1}[b(t)/a(t)]$. Both $a(t)$ and $b(t)$ are considered to be WSS processes with zero mean. The instantaneous frequency of $s(t)$ is defined as:

$$d\theta(t)/dt \triangleq \omega_i(t) = \omega_o + d\varphi(t)/dt \quad (3)$$

It can be further shown [10,11] that the best estimate of $\omega_i(t)$ is given by:

$$\omega_i(t) = E\{r^2(t)\,\omega_i(t)\}/E\{r^2(t)\} \quad (4)$$

where $E\{y(t)\}$ is the expected, or mean value, of a variable $y(t)$ over some period of time.

3. Frequency Measurement Algorithm

A block diagram of the frequency measurement algorithm, which is a refinement of earlier work [9], is shown in Figure 1. Instrumental to the frequency measurement process is the decomposition of the input signal, $s(t)$, into two orthogonal components. This is achieved by using two finite impulse response bandpass-orthogonal filters, centred at ω_o, which decompose $s(t)$ into two orthogonal components, $s_i(t)$ and $s_r(t)$, by introducing a 90° phase shift between the two derived signals. The frequency domain response of the orthogonal filters ensures that only the narrow band signal $s(t)$, is recovered from the total signal measured at the power system bus; $s_i(t)$ and $s_r(t)$ are bandlimited to 30 - 70Hz. The orthogonal filters have a group delay of 20ms.

The impulse responses of the orthogonal filters are expressed as:

$$h_i[k] = \sin(2\pi k/N + \pi/N)$$

and

$$h_r[k] = \cos(2\pi k/N + \pi/N)$$

where k = 0, 1, 2, ... N-1, and $N = f_s/f_o$, where f_s is

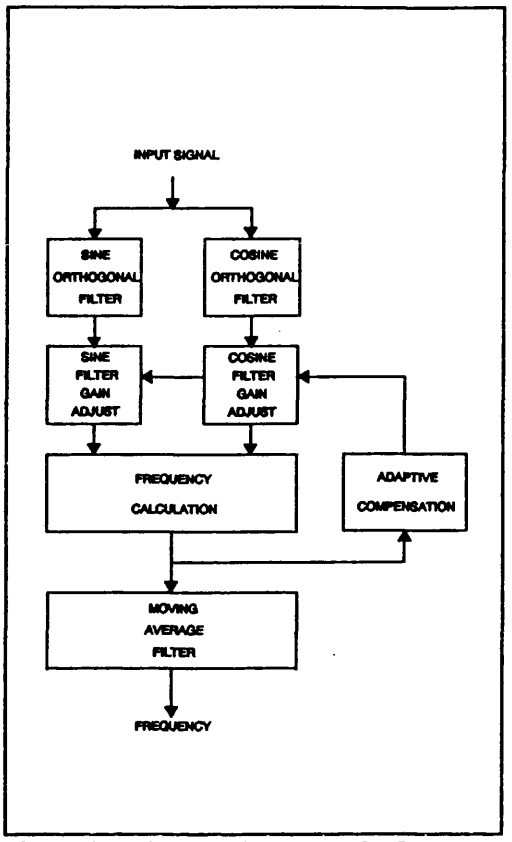

Figure 1 Block Diagram of Frequency Measurement Process

the sampling frequency and f_o is the nominal power system frequency. The outputs of these filters may be described as:

$$s_i[n] = H_i sin(\omega_o n + \gamma)$$
and $$s_r[n] = H_r cos(\omega_o n + \gamma)$$

where H_i and H_r are the frequency gains of the filters and γ is a phase shift corresponding to the filter group delay. Both expressions are given in terms of the discrete time variable [n].

An estimate of the frequency may then be calculated from:

$$f_i[n] = \frac{s_i'[n]s_r[n] - s_i[n]s_r'[n]}{2\pi(s_i^2[n] + s_r^2[n])} \qquad (5)$$

again expressed in terms of the discrete time variable, where $s_i'[n] = d(s_i[n])/dt$. This differentiation in time of $s_i[n]$ and $s_r[n]$ is performed by a two point backward derivative. Due to the approximation in this derivative, a frequency dependent error is introduced but easily compensated for [9]. After evaluation of $f_i[n]$, a moving average filter, having a group delay of 20ms, is applied to the frequency estimates to remove any non-50Hz components not removed by the orthogonal filters. The *adaptive compensation* block in Figure 1 provides an optimum prediction of $f_i[n]$ by implementing Equation 4. This is achieved by using separate moving average filters, each with a group delay of 5ms, for the numerator and denominator of Equation 4, Note that the numerator of Equation 5 corresponds to the term, $r^2(t)\omega_i(t)$, of Equation 4, and the term, $(s_i^2[n]+s_r^2[n])$, in the denominator of Equation 5 corresponds to the term, $r^2(t)$, in the denominator of Equation 4. This predicted value of $f_i[n]$ is used to adjust the gain of the orthogonal filters to ensure unity gain when the fundamental frequency in $s(t)$ deviates from f_o. The gain adjustments are achieved by using highly accurate, Z-transform derived analytic expressions for the orthogonal filter gains.

4. Simulation Results

Computer simulation results are shown for an implementation of the algorithm written in FORTRAN using single precision arithmetic. Under steady state conditions the nominal power system frequency is 50Hz. The sampling frequency is assumed to 8kHz in all the results. Differing power system frequencies and sampling frequencies may be accommodated by the appropriate modification to the algorithm. It is assumed that the measured signal from the power system bus is ideally sampled.

Figure 2 shows a power system waveform where, after an initial 4 cycles of steady state, the frequency and amplitude both decay exponentially. In the period 80-1000 ms, the amplitude decays from 1p.u. to 0.5 p.u. and the frequency decays from 50 to 44Hz. The output from the frequency measurement algorithm is shown in Figure 3 together with the reference frequency used to program the power system waveform simulation. The measured frequency curve shows an initial start-up transient which corresponds to the delays inherent in the algorithm. After this initial transient, the measured frequency is seen to accurately follow the reference frequency with a delay of 22.5ms.

Figure 4 shows the voltage measured at one end of a single circuit transmission line where a severe power swing is occurring which results in pole slips at approximately 850ms and 1100ms. Figure 5 shows the measured frequency which is observed to behave in a relatively smooth manner except at the pole slips where the frequency suddenly drops and then recovers.

Figure 6 shows a sound phase voltage waveform when an adjacent phase has been subject to a single phase to earth fault. The fault occurs at 60ms and the distortion on the voltage is due to travelling wave noise which is not harmonically related to the fundamental power system frequency. Figure 7 shows the measured frequency where, after the intial start-up transient, the algorithm settles down to a smooth evaluation of the frequency. Close examination of Figure 6 will reveal a

slight change in phase of the waveform immediately after the point of fault. This manifests itself as a slight drop in frequency in the period 60 - 100ms. Note that the travelling wave distortion has little effect on the measured frequency.

5. Conclusions

An algorithm for the digital evaluation of power system frequency has been presented. The algorithm calculates the instantaneous frequency of a narrow band representation of the measured signal which may be either voltage or current. Digital filters are used to band-limit the measured signal and also to perform an orthogonalisation process which is required for the frequency evaluation. Finally a moving average filter is used to further filter the frequency estimates.

Under simulated tests, the algorithm gives highly accurate and fast evaluation of the power system frequency. The results show that the algorithm is stable under dynamic power system conditions yet is unaffected by fast transients.

Applications for this algorithm include load shedding schemes where a fast response time is required and as a basis for rate of change of frequency measurement.

6. Further Work

Future work on this project includes the implementation of the algorithm on a TMS320C30 microprocessor to form part of a load shedding scheme.

7. Acknowledgements

The authors would like to thank the University of Bath for provision of facilities and kind permission to publish this work. The second author would like to thank CONACYT-Mexico for financial support.

8. References

1. Malik O.P. et al, "Frequency measurement for use with a microprocessor-based turbine governor", Paper no. 91WM140-4EC, IEEE PAS Winter Meeting, New York, Feb 1991.
2. McIlwaine S.A., Tindall C.E. and McClay W., "Frequency tracking for power system control", Proc IEE, Vol 133, Part C, No. 2, March 1986, pp 95-98.
3. Benmouyal G., "Design of a combined global differential and volt/hertz relay for step-up transformers", IEEE Trans on Power Delivery, July 1991, pp 1000-1007.
4. Giray M.M. and Sachdev M.S., "Off nominal frequency measurements in electric power systems", IEEE Trans on Power Delivery, Vol. 4, No. 3, July 1989, pp 1573-1578.
5. Girgis A.A. and Hwang D., "Optimal estimation of voltage phasors and frequency deviations using linear and non-linear Kalman filtering. Theory and Limitations.", IEEE Trans on PAS, Vol PAS 103, N0. 10, Oct 1084, pp 2943-2949.
6. Sachdev M.S., Wood H.C. and Johnson N., "Kalman filtering applied to power system measurements for relaying", IEEE Trans. on PAS, Vol 104, No. 2, Dec 1985, pp 3565-3573.
7. Girgis A.A. and Peterson L.W., "Adaptive estimation of power system frequency deviation and its rate of deviation for calculating sudden power system overloads", IEEE Trans. on Power Delivery, Vol. 3, No. 2, April 1990, pp 585-594.
8. Kamwa I. and Grondin R., "Fast adaptive schemes for tracking voltage phasor and local frequency in power transmission and distribution systems", IEEE Trans on Power delivery, Vol. 7, No. 2, April 1992, pp 789-795.
9. Moore P.J. and Johns A.T., "A new approach to digital measurement of power system frequency", APSCOM 1991, Hong Kong.
10. Gabor D., "Theory of communications", J IEE, Vol. 93, Part 3, Nov 1946, pp 429-441.
11. Strōm, T., "On amplitude-weighted instantaneous frequencies", IEEE Trans. on Acoustics, Speech and Signal Processing, Vol. ASSP-25, No. 4, August 1977, pp 351-353.

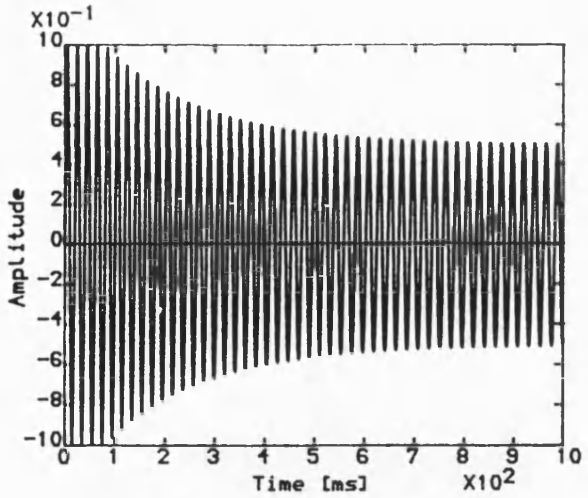

Fig. 2. Voltage with exponential decay

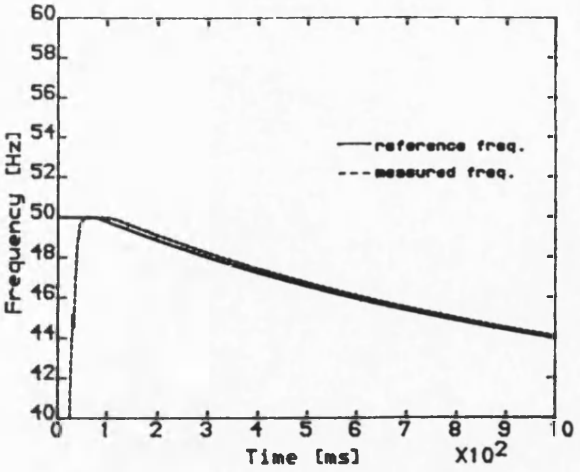

Fig. 3. Reference and measured frequencies of Fig. 2

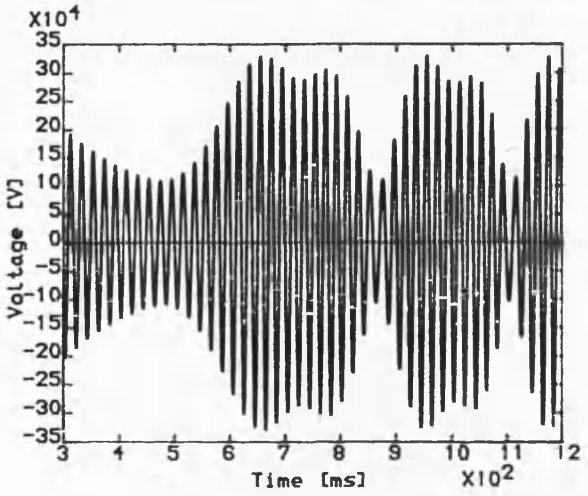

Fig. 4. Voltage during power swing and pole slip

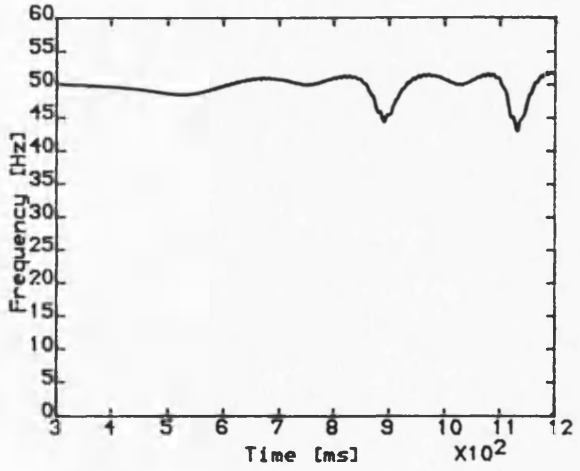

Fig. 5. Measured frequency of Fig. 4

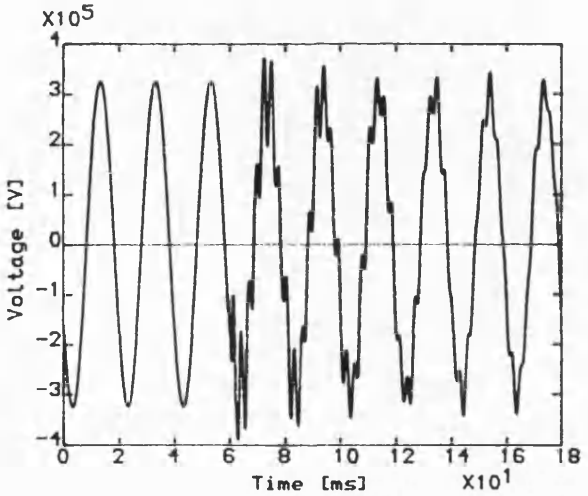

Fig. 6. Voltage with induced traveling wave noise

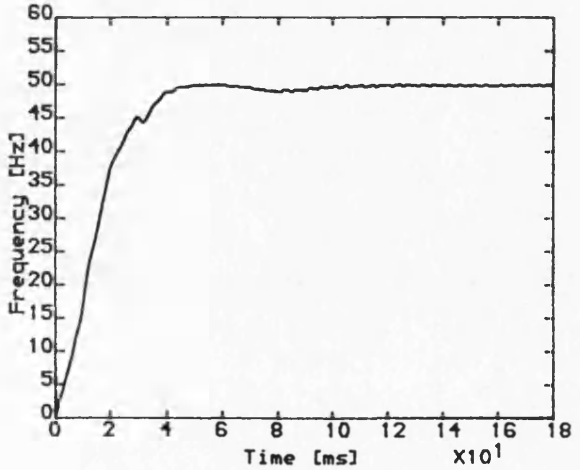

Fig. 7. Measured frequency of Fig. 6

The following paper was presented to the 28th Universities Power Engineering Conference at Staffordshire University, 21st - 23rd September 1993.

Published Work

VALIDITY OF A BANDPASS PLUS ORTHOGONAL DECOMPOSITION TECHNIQUE FOR THE DIGITAL MEASUREMENT OF POWER SYSTEM FREQUENCY

R. D. Carranza, P. J. Moore and A. T. Johns

University of Bath, UK

Abstract. A novel technique for measuring power system frequency has been recently introduced [1]: a real signal is taken from a power system bus and its instantaneous frequency (IF) is estimated by a narrow band pass and orthogonal decomposition process. Since for real conditions the power system frequency is nonstationary and the signal is seldom sinusoidal, the validity of the estimation of the IF by this technique depends on certain restrictions concerning the spectral characteristics of the measured signal which must be correctly observed by the measuring technique. In this paper is discussed the theory supporting this technique and how it satisfies the IF restrictions.

1. Introduction

The IF parameter is a well defined concept for sinusoidal signals centred at a particular carrier frequency such as FM signals. For spectral analysis of stationary signals it is appropiate to use the Fourier Transform. For wide sense stationary (WSS) or nonstationary signals any spectral analysis technique should take into account the time-varying nature of the spectral components of the signal. In this case, it is only for monocomponent signals that the IF concept has a physical interpretation.

This paper addresses the following issues: 1° The representation of a signal taken from a power system bus and the notion of its instantaneous frequency. This signal is considered as a narrow band monocomponent signal centred at the power system frequency f_o and inmersed in additive broad band noise. Both the amplitude and the phase of the monocomponent signal are regarded as random modulation processes. 2° An optimal orthogonal decomposition of a monocomponent signal for obtaining its IF. 3° A discussion about the spectral characteristics of the previously described signal will display certain theoretical conditions which must be properly observed for the correct estimation of its IF. 4° A discussion about the features of a recently introduced technique [1] and its validity for measuring the IF of a monocomponent signal according to the mentioned conditions.

2. Representation of a signal taken from a power system bus and the notion of its IF.

Let a real function $x(t)$ to represent a signal taken from a power system bus, either a voltage or a current. For real power conditions this signal is typically regarded as the sum of a narrow band pass component plus additive broad band noise. $x(t)$ may be depicted as:

$$x(t) = s(t) + v(t) \qquad ...(1)$$

where $s(t)$ represents the narrow band pass component centred at f_o: the nominal power system frequency, and $v(t)$ is the broad band noise component. The notion of the frequency of a power system has physical interpretation if it is thought as the IF of the fundamental component of $x(t)$. To do so $s(t)$ should be properly separated from the noise component by an adaptive band pass filtering procedure. A brief consideration about the spectral characteristics of $x(t)$ will render a better understanding of the concept of its IF.

2.1. The term $s(t)$ may be expressed as:

$$s(t) = a(t)\cos[\theta(t)] \qquad ...(2.a)$$
$$\theta(t) = w_o t + \alpha(t) \qquad ...(2.b)$$

Equation (2) represents a monocomponent signal with amplitude $a(t)$ and centred at a frequency $w_i(t) = d\theta(t)/dt = w_o + d\alpha(t)/dt$. Both the amplitude and the phase of $s(t)$ may be regarded as random modulation processes. For power system steady-state conditions and $v(t) = 0$ the expected values of these processes should approach: $E\{a(t)\} = V$ or I: the nominal voltage or current peak values, and $E\{d\theta(t)/dt \mid \alpha(t)=0\} = w_o$: the nominal power system frequency. In this representation $a(t)$ will account for amplitude variations of $s(t)$, eg: sudden overloads and recovering transients of voltage controllers such as AVR's or tap-changing transformers. The spectrum $A(w)$ of these disturbances has a bandwidth of a few hertz centred at dc. The term $\cos[w_o t + \alpha(t)]$ is regarded as a carrier signal centred at w_o. In the time domain the IF of this carrier accounts for excursions of the power system frequency about f_o: synchronising oscillations, frequency decay during power imbalance.

2.2. The term $v(t)$ is intended to represent any other frequency component present in $x(t)$ appart from $s(t)$. For instance: harmonics of f_o, travelling waves, arcing voltages, electro-magnetic induced voltages, etc.

At this stage, the concept of the IF of a power system would be better understood by performing a simultaneous analysis of $x(t)$ in the time and the frequency domains. Under such an approach it would be shown that the product $a(t)cos[\theta(t)]$ behavies as a single impulse function with a time-varying magnitude driven by $A(w,t)$ and wandering about w_o within a bandwidth $w_o \pm d\alpha(t)/dt$, and the components of $v(t)$ would be seen as an infinite set of impulses with magnitude and central frequencies varying randomly in time.

3. Estimation of the IF of a monocomponent signal.

To illustrate the estimation of the IF of a monocomponent signal like $s(t)$, let us firstly consider that $s(t)$ is separated from $v(t)$ by a linear-phase band pass filter centred at f_o. This consideration implies that neither the amplitude nor the phase of $s(t)$ would be distorted by this filter. Therefore, an adaptive finite impulse response (FIR) band pass filter with unit gain in its band pass interval is required. For a real narrow band mononocomponent signal like $s(t)$, it is possible to estimate its IF by performing an analytic signal $z(t)$ associated to $s(t)$. This procedure provides an optimal orthogonal decomposition of $s(t)$. Gabor [2] and Ville [3] proposed a method for generating such an analytic signal. This method uses the Hilbert Transform (HT) of $s(t)$ to produce a unique representation of $z(t)$:

$$z(t) = s(t) + j\hat{s}(t) \qquad ...(3)$$

where:

$$\hat{s}(t) = HT\{s(t)\} = PV\int_{-\infty}^{\infty} \frac{s(\tau)}{\pi(t-\tau)} d\tau \qquad ...(4.a)$$

$$\hat{S}(w) = FT\{\hat{s}(t)\} = -jS(w)sgn(w) \qquad ...(4.b)$$

PV is the Cauchy's principal value at $t = \tau$. The complex signal $z(t)$ is such that its Fourier Transform Z(w) vanishes for negative frequencies:

$$Z(w) = \begin{cases} 2S(w) & for\ w \geq 0 \qquad ...(5.a) \\ 0 & for\ w < 0 \qquad ...(5.b) \end{cases}$$

From the analytic signal procedure the IF of the monocomponent signal the IF of the monocomponent signal $s(t)$ is defined as first the derivative in time of its phase:

$$w_i(t) = \frac{d}{dt}[arg\ z(t)] \qquad ...(6.a)$$

$$= \frac{s(t)\frac{d}{dt}\hat{s}(t) - \hat{s}(t)\frac{d}{dt}s(t)}{s^2(t) + \hat{s}^2(t)} \qquad ...(6.b)$$

4. Restrictions on the estimation of the IF.

It is noticed from equation (6.b) that a correct estimation of $w_i(t)$ is provided if $\hat{s}(t)$, the Hilbert Transform of $s(t)$, is in quadrature phase with $s(t)$ in the frequency domain. This assumption is correct under the following conditions:

4.1. Spectral overlapping.

Spectral overlapping occurs whenever the spectrum of a signal interferes with the spectrum of another signal at a given instant of time. Now we will be study the spectral characteristics of $a(t)$ and $cos\ [\theta(t)]$ in signal $s(t)$. Following the procedure of section 3 and the expression of $w_i(t)$ given in equation (6.b) we want to estimate the IF of $s(t)$. To do so we need two real functions $i(t)$ and $q(t)$ in order to form an orthogonalization process $z(t)$ as in Figure 1 where $s(t)$ is time-convolved with $h_i(t)$ and $h_q(t)$: two FIR filters yielding $i(t)$: "in-phase" and $q(t)$: "quadrature" components of $s(t)$.

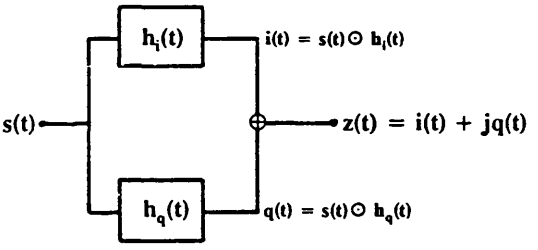

Figure 1. Schematic diagram of the orthogonal decomposition.

The orthogonal decomposition must be such that:

$$i(t) = |s(t)|\angle[w_o t + \alpha(t) + \phi] \qquad ..(7.a)$$

$$q(t) = |s(t)|\angle[w_o t + \alpha(t) + \phi - \frac{\pi}{2}] \qquad ..(7.b)$$

Note that: 1) there is a -90° phase difference between the outputs, 2) both of the convolution processes contribute with a phase delay ϕ without modifying the magnitude of $s(t)$, 3) ϕ is not a function of time. The complex function $z(t)$ may be expressed as:

$$z(t) = |z(t)|\exp[j\gamma(t)] \qquad (8.a)$$

$$|z(t)| = [i^2(t) + q^2(t)]^{1/2} \qquad (8.b)$$

$$\gamma(t) = w_o t + \alpha(t) + \Phi \qquad (8.c)$$

Let us represent the carrier component of $s(t)$ by $c(t) = cos[w_o t + \alpha(t) + \Phi]$, and let the Fourier Transforms of $a(t)$, $c(t)$, $i(t)$ *and* $q(t)$ to be $A(w)$, $C(w)$, $I(w)$ and $Q(w)$, respectively. Now, if $i(t)$ and $q(t)$ truely represent the "in-phase" and "quadrature" components of $s(t)$, that is: $h_i(t)$ and $h_q(t)$ exhibit unit gain and equal group delays such that $q(t)$ equals the Hilbert Transform of $i(t)$ as in equation (4.b), i.e.:

$$Q(w) = -jI(w)sgn(w) \qquad (9)$$

then $z(t)$ can be expressed as:

$$z(t) = s_i(t) + js_q(t) \qquad ...(10)$$

Hence, $z(t)$ may also be expressed in terms of $a(t)$ and $c(t)$ as:

$$\begin{aligned} z(t) &= a(t)\cos[\gamma(t)] + j\, HT\{\, a(t)\cos[\gamma(t)]\,\} \\ z(t) &= a(t)\cos[\gamma(t)] + j\, a(t) HT\{\, \cos[\gamma(t)]\,\} \\ z(t) &= a(t)\exp[j\gamma(t)] \qquad ...(11) \end{aligned}$$

Following the Bedrosian's theorem [4], equation (11) holds true if, and only if (iff), $|A(w)| \leq C(w)$. Note that in this case equation (11) follows equation (8.a). Therefore an optimal orthogonalization of $s(t)$ will be achieved iff the spectrum of the amplitude does not overlap with the spectrum of the carrier. Considering the random nature of both $a(t)$ and $c(t)$ of a power system signal, this condition means that $A(w)$ and $C(w)$ must be narrow band pass processes centred at dc and at f_o, respectively. This condition will prevail if both $a(t)$ and $c(t)$ are constrained to their nominal values by the use of protective and corrective schemes attached to the power system.

4.2. Approximation to the ideal discrete Hilbert Transform.

The discrete Hilbert Transform (dHT) has a finite impulse response $dht[k]$ and a discrete Fourier Transform as follows:

$$\begin{aligned} dht[k] &= \frac{2}{\pi}\frac{\sin^2[\frac{\pi k}{2}]}{k} \qquad for\ k \neq 0 \\ &= 0 \qquad for\ k = 0 \quad ..(12.a) \\ dHT(\Omega) &= -jsgn(\Omega) \quad for\ -\pi<\Omega<\pi \quad ..(12.b) \end{aligned}$$

Implementation of equation (12) requires an ideal differentiator and an ideal low pass filter, i.e.: two noncausal filters. However, a practical implementation can be achieved if the dHT is approximated only over the limited frequency bandwidth of $s(t)$ provided that a unit gain and linear phase are achieved within such an interval. Note that for a discrete-time signal the concept of analyticity is impractical. However, for a causal sequence $s[n]$ representing a unique signal $s(t)$, we can define a complex signal $z[n] = s[n] + j\hat{s}[n]$ whose spectrum is zero on the bottom half of the unit circle for $-\pi < \Omega \leq 0$, where $\Omega = 2\pi freq/f_s$. In this sense:

$$Z(\Omega) = \begin{cases} 2S(\Omega) & for\ 0 \leq \Omega < \pi \quad ...(13.a) \\ 0 & for\ -\pi < \Omega < 0 \quad ...(13.b) \end{cases}$$

4.3 Bandwidth of the monocomponent signal.

Biased estimates of the IF of $s(t)$ will result if an implementation of the discrete Hilbert Transform allows a single noise component from $v(t)$ to pass into $z[n]$. The reasons: A) as in equation (11), the Hilbert Transform will inherently select the highest frequency cosine component for replacement by an exponential, thus, spectral overlapping may occur; B) the differentiator in equation (6.b) is a high pass filter amplifying any noise. Therefore, a narrow band pass filter should be used to extract $s(t)$ from $x(t)$.

5. Characteristics of the IF measuring technique.

Following the schematic diagram of Figure 1, the proposed IF measuring technique [1] uses a couple of band pass orthogonal (BO) FIR filters $h_i[k]$ and $h_q[k]$ to implement equation (6.b). The discrete Fourier Transforms $H_i(\Omega)$ and $H_q(\Omega)$ of these filters are expressed as follows in terms of their magnitude and phase:

$$\begin{aligned} H_i(\Omega) &= -\, mag_i(\Omega)\angle\Phi_i(\Omega) \qquad ...(14.a) \\ H_q(\Omega) &= j\, mag_q(\Omega)\angle\Phi_q(\Omega) \qquad ...(14.b) \end{aligned}$$

where:

$$\begin{aligned} mag_i(\Omega) &= \frac{2\cos(\Omega_o/2)\sin(\Omega N/2)\sin(\Omega/2)}{\cos(\Omega) - \cos(\Omega_o)} \\ mag_q(\Omega) &= \frac{2\sin(\Omega_o/2)\sin(\Omega N/2)\cos(\Omega/2)}{\cos(\Omega) - \cos(\Omega_o)} \\ \Phi_i(\Omega) &= \Phi_q(\Omega) = -\Omega(N-1)/2 \qquad ...(15) \end{aligned}$$

It should be noticed that:
i) there is a -90° phase shift between $H_i(\Omega)$ and $H_q(\Omega)$ valid for $-\pi < \Omega < \pi$ as in equation (7).
ii) the BO filters have the same group delay: $(N-1)/2$, for N a number of samples in the observation window, complying with the condition in equation (10).
iii) Both of the filters have zeros at dc and the harmonics of f_o. The effective band pass interval of the filters was designed to $B = f_o \pm 20\ Hz$. A low pass filter with a cut-off frequency $f_c > B$ precedes the BO filters to ensure that no noisy components will be allowed to pass by the BO frequency sidelobes.
iv)an adaptive algorithm was developed in this technique to recursively adjust the magnitudes of $H_i(\Omega)$ and $H_q(\Omega)$ for achieving a flat unit gain within the bandwidth B. In that case the BO filters comply with

equation (9), i.e.:

$$H_q(\Omega) = -jH_i(\Omega)sgn(\Omega) \quad for \ |\Omega| \leq B \quad ...(16)$$

Note that neither $H_i(\Omega)$ nor $H_q(\Omega)$ are the dHT of $s(t)$, but they are the dHT of each other. The adaptive algorithm performs an estimation of the weighted average of $w_i(t)$ [5] which accounts for the time-varying nature of the amplitude-carrier product in $s(t)$ [6].

6. Performance of the IF technique.

Figure 2 shows a simulated "chirp" signal with both its amplitude and frequency modulated in time and corrupted by 0.1 p.u. zero mean Gaussian noise with $\sigma = 0.6$. Figure 3 shows the true IF of the signal and the measured IF, solid and broken line, respectively. The frequency range of the signal is 30Hz - 70Hz. The sampling frequency is 8 kHz. Note: 1) the first 60 ms are an initialization period of the algorithm, 2) there is a constant group delay of 25 ms between the measured and the true IF.

7. Conclusions.

In section 4 have been presented the theoretical conditions for the correct estimation of the IF of a monocomponent signal $s(t)$ when using the process of orthogonal decomposition of $s(t)$ as discussed in section 3. It was also shown in section 4 that these conditions follow the time-frequency characteristics of the power system signal under study as presented in section 2. Consequently, a given IF estimation technique should obey with these conditions. Finally, section 5 has shown the main features of the proposed IF measuring technique which have been developed following the mentioned theoretical conditions. Satisfactory results where also displayed which confirm the validity of this approach.

8. Acknowledgments.

The authors would like to thank to the University of Bath for the facilities provided for this work. The first author would like to thank to CONACYT, Mexico, for financial support.

9. References.

1. P.J. Moore, R.D. Carranza and A.T. Johns, "Performance of a New High Speed Digital Technique for Measuring Power System Frequency", IEE Int. Conf. on DPSP, York, U.K., pp. 73-77, Apr. 1993.

2. D. Gabor, "Theory of Communications", J. of the IEE, Vol. 93, Part 3, pp. 429-441, Nov. 1946.

3. J. Ville, "Theorie et Applications de la Notion de Signal Analytique", Cables et Transmissions, Vol. 2A, pp. 61-74, Jan. 1948.

4. E. Bedrosian, "A Product Theorem for Hilbert Transforms", Proc. IEEE, pp. 868-869, May 1963.

5. A. Papoulis, "Random Modulation: A Review", IEEE Trans. on ASSP, Vol. 31, No. 1, pp.96-105, Feb. 1983.

6. T. Strõm, "On Amplitude-Weighted Instantaneous Frequency", IEEE Trans. on ASSP, Vol. 25, No. 4, pp. 351-352, Aug. 1977.

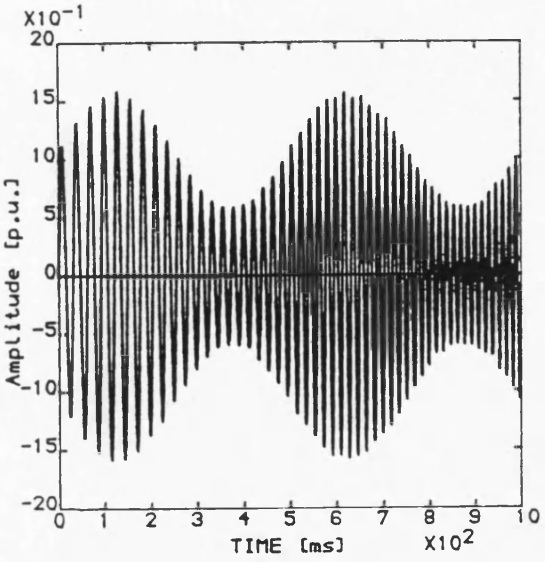

Figure 2. Simulation input signal.

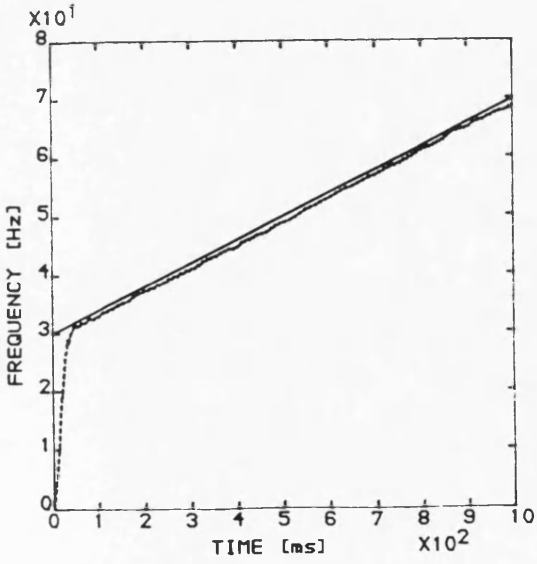

Figure 3. Reference and measured IF.

The following paper was presented to IEE Proceedings on Generation, Transmission and Distribution, Vol. 141, No. 5, September 1994.

A new numeric technique for high-speed evaluation of power system frequency

P.J. Moore, PhD, CEng, MIEE
R.D. Carranza, MSc
A.T. Johns, DSc, CEng, FIEE

Indexing terms: Power system, Frequency measurement

Abstract: A new numeric technique for evaluating power system frequency from either a voltage or current signal is presented. The technique uses discrete time values of the input signal, taken at a fixed sampling rate, to provide an estimate of power system frequency accurate to within typically 0.001 Hz. The technique is shown to be capable of tracking frequency under dynamic power systems conditions and is immune to the effect of harmonics. It is further shown that the algorithm can be easily adapted to process three-phase signals such that the positive phase sequence component can be utilised thus increasing the reliability of the measurement under fault conditions.

List of symbols

$x(t)$ = continuous form of measured power system quantity (e.g. voltage or current)
$x'(t)$ = time derivative of $x(t)$
$x(n\Delta T)$ = discrete time form of measured power system quantity (e.g. voltage or current), usually abbreviated to $x(n)$
ΔT = sampling interval
f_s = sampling frequency, $f_s = 1/\Delta T$
f = apparent power system frequency
f_0 = nominal power system frequency
$H(k)$ = coefficients of finite impulse response filter (for $k = 0, \ldots, N-1$, $N = f_s/f_0$)
z = Z transform operator
Ω = normalised frequency, $\Omega = 2\pi f/f_s$

1 Introduction

Accurate monitoring of the frequency of a power system is essential to optimum operation. Variations in frequency from a nominal value can be, for example, indicative of unexpected system disturbances for which some corrective action must be taken. On a large, stiff power system, variations in frequency will usually be slow due to the large mechanical inertia of the system. However, on smaller systems, changes in frequency will be correspondingly faster. In either case, it is imperative to determine frequency deviations at the earliest stage.

The use of microprocessor technology has produced many benefits in the field of power system protection, monitoring and control. The ability of microprocessor-based devices to provide fast response to changing system conditions is well known and their use for measuring power system frequency is well established. Early work reported in this area [1, 2] suffered from excessively long frequency evaluation times although more recent work has seen a steady improvement. The simplest method of frequency evaluation involves timing signal zero crossings [3, 4] although this approach is still relatively slow since it requires a large amount of input data to detect small deviations. Adaptation of the sampling interval to ensure correct measurement using an algorithm based on the discrete Fourier transform is feasible [5] although it is prone to round off oscillations since the sampling interval cannot be infinitely varied. Most of these methods assume that the statistics of the power system are stationary, that is, do not vary with time. Alternatively, assumptions based on known power system statistics can be used [6]. Several authors have incorporated least mean squares estimation theory using both stationary models [7, 8] and adaptive estimation, where the frequency is tracked without any prior statistical knowledge [9, 10]. However, all such methods involve a compromise between the accuracy of the frequency measurement and the length of the observation period; accuracy decreases as the period becomes smaller.

The algorithm described herein is designed to provide the fastest estimate of power system frequency based upon analysis of approximately one cycle of a sampled power system waveform. To ensure high accuracy, the algorithm uses a relatively high sampling frequency (4 kHz) to give good numeric representation of the input signal. Unlike other methods, the algorithm does not rely on zero crossings or statistical knowledge of the power system. It does not require any special hardware other than that usually found within microprocessor based protection relay equipment, and it uses a fixed sampling frequency, thus avoiding the need for, and practical problems associated with, the use of sampling frequency variation means.

The authors are grateful for the provision of facilities in the Power and Energy Systems Research Group at the University of Bath. The second author would like to thank CONACYT-Mexico for financial support.

Paper 1360C (P11), received 8th February 1994

The authors are with the School of Electronic and Electrical Engineering, University of Bath, Bath, BA2 7AY, United Kingdom

2 Algorithm development

2.1 Basic principle

Let a continuous power system voltage or current be denoted by $x(t)$. Decomposing $x(t)$ into two components which are orthogonal in phase gives

$$x_{1(t)} = X \sin(2\pi ft + \phi) \tag{1}$$

and

$$x_2(t) = X \cos(2\pi ft + \phi) \tag{2}$$

where subscripts 1 and 2 denote the individual components, X is the magnitude and f is the frequency of the signal $x(t)$, and ϕ is an arbitrary phase shift.

Differentiating eqns. 1 and 2 with respect to time gives:

$$\frac{d[x_1(t)]}{dt} = 2\pi fX \cos(2\pi ft + \phi) = x'_1(t) \tag{3}$$

and

$$\frac{d[x_2(t)]}{dt} = -2\pi fX \sin(2\pi ft + \phi) = x'_2(t) \tag{4}$$

Eqns. 1 to 4 may be rearranged as

$$\begin{aligned} &x_2(t)x'_1(t) - x_1(t)x'_2(t) \\ &\quad = 2\pi fX^2 \cos^2(2\pi ft + \phi) + 2\pi fX^2 \sin^2(2\pi ft + \phi) \\ &\quad = 2\pi fX^2 \end{aligned} \tag{5}$$

which is seen to be directly proportional to the product of the frequency and the square of the amplitude. To remove the amplitude dependency, the following expression is used:

$$\begin{aligned} &x_1^2(t) + x_2^2(t) \\ &\quad = X^2 \cos^2(2\pi ft + \phi) + X^2 \sin^2(2\pi ft + \phi) \\ &\quad = X^2 \end{aligned} \tag{6}$$

Thus, combining eqns. 5 and 6 yields

$$f = \frac{x_2(t)x'_1(t) - x_1(t)x'_2(t)}{2\pi[x_1^2(t) + x_2^2(t)]} \tag{7}$$

Eqn. 7 is an analytic expression for the frequency of $x(t)$ derived from its two orthogonal components and their time derivatives.

2.2 Frequency calculation from discrete time signals

Eqn. 7 may be applied to discrete time signals by replacing $x(t)$ with $x(n\Delta T)$ where ΔT is the sampling period and $\Delta T = 1/f_s$ where f_s is the sampling frequency. For clarity, $x(n\Delta T)$ will be written simply as $x(n)$ from here on.

The discrete time signal $x(n)$ may be decomposed into two components, each orthogonal in phase, by the use of two finite impulse response (FIR) filters based upon sine and cosine impulse responses. This technique is actually identical to the discrete Fourier transform evaluated for the fundamental component. However, it is more convenient to consider the orthogonalisation being effected by two FIR filters. The coefficients of the FIR filters are evaluated as

$$H_s(k) = \sin\left(\frac{2\pi k}{N} + \frac{\pi}{N}\right) \tag{8}$$

and

$$H_c(k) = \cos\left(\frac{2\pi k}{N} + \frac{\pi}{N}\right) \tag{9}$$

where $k = 0, 1, 2, \ldots, N-1$, $N = f_s/f_0$, f_0 = nominal power system frequency.

Hence, the two orthogonal components of $x(n)$ may be evaluated by digital convolution as

$$x_1(n) = \sum_{k=0}^{N-1} x(n-k)H_s(k) \tag{10}$$

and

$$x_2(n) = \sum_{k=0}^{N-1} x(n-k)H_c(k) \tag{11}$$

To calculate the time derivative of the orthogonalised signals, piecewise linearity between the samples is assumed which allows the following backward difference equation to be used:

$$x'(n) = \frac{[x(n) - x(n-1)]}{\Delta T} \tag{12}$$

Eqn. 12 can be applied to both orthogonal components of $x(n)$. To retain accuracy of the derivative, it is advantageous to keep the time difference between the two elements of the right hand side of eqn. 12 as small as possible; the equation thus represents the minimum situation. However, a drawback to this approach lies in the fact that the derivative approximated is most representative of a point mid-way between the two samples of $x(n)$. Potential errors arising from this may be compensated for by substituting $x(n)$ with the arithmetic mean of $x(n)$ and $x(n-1)$. Hence the discrete time equivalent of eqn. 7 is given by

$$f \approx \frac{1}{2\pi} \frac{\left(\frac{x_2(n) + x_2(n-1)}{2}\right)x'_1(n) - \left(\frac{x_1(n) + x_1(n-1)}{2}\right)x'_2(n)}{\left(\frac{x_1(n) + x_1(n-1)}{2}\right)^2 + \left(\frac{x_2(n) + x_2(n-1)}{2}\right)^2} \tag{13}$$

which reduces to

$$f \approx \frac{1}{\pi T} \frac{(x_2(n) + x_2(n-1))x'_1(n) - (x_1(n) + x_1(n-1))x'_2(n)}{(x_1(n) + x_1(n-1))^2 + (x_2(n) + x_2(n-1))^2} \tag{14}$$

2.3 Errors due to discrete time representation

The discrete time representation of the input signal, and its subsequent processing, cause two significant sources of error when eqn. 14 is used to evaluate the apparent frequency of the input signal. The first, and most significant, arises due to the FIR filters having different magnitude gains at frequencies other than the nominal power system frequency. The second cause of error is introduced by the numerical computation of the derivative.

The FIR filters described by eqns. 8 to 11 are used to produce components of the input signal $x(n)$ which are orthogonal in phase. The phase characteristic of any FIR filter having an impulse response which is either symmetric or antisymmetric, is linear with frequency. The use of one FIR filter based on a cosine function (antisymmetric impulse response), and the other based on a sine function (symmetric impulse response), ensures that the filter outputs differ by 90° for all input signal frequencies. However, although the phase characteristics

of these filters perform ideally for the required function, the magnitude characteristics are far from perfect. Fig. 1*a* shows that the magnitude responses of the sine and cosine based FIR filters are not identical. Fig. 1*b* shows

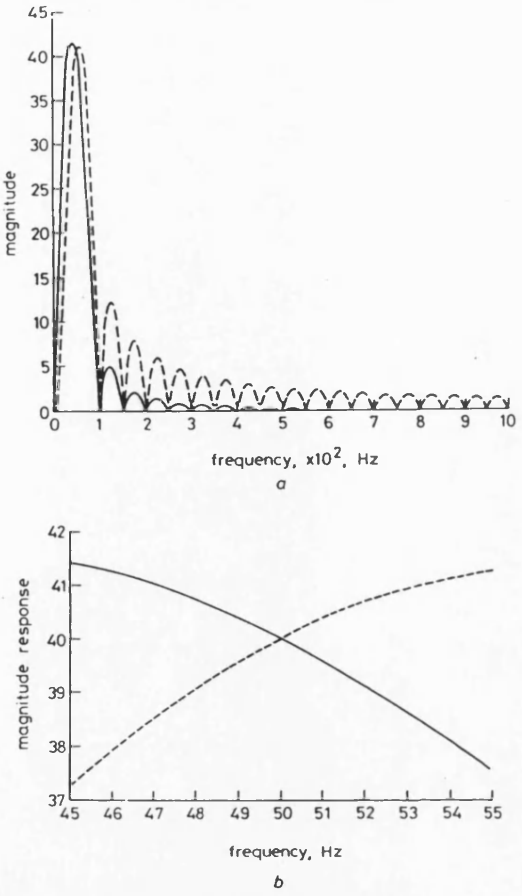

Fig. 1 *Frequency magnitude response for othogonal filters*
a Assuming f_s = 4 kHz, for clarity only 0–1 kHz range displayed
b Expanded view of *a* in the range 45–55 Hz
——— Sine filter
····· cosine filter

an expanded section of Fig. 1*a* in the region of 45–55 Hz from which it will be apparent that the magnitude gains of the filters are only equal at exactly the nominal power system frequency of, in this case, 50 Hz. This implies that the orthogonalised signals $x_1(n)$ and $x_2(n)$ have frequency dependent magnitude gains. Since eqn. 14 assumes the orthogonalised signal gains to be frequency independent, an error will be introduced if account is not taken of this effect.

It is shown in Appendix 7.1 that the magnitude gains of the sine and cosine filters are given by:

$$|H_s(f)| = \frac{2 \sin(\pi f_0/f_s) \sin(\pi N f/f_s) \cos(\pi f/f_s)}{\cos(2\pi f/f_s) - \cos(2\pi f_0/f_s)} \quad (15)$$

and

$$|H_c(f)| = \frac{2 \cos(\pi f_0/f_s) \sin(\pi N f/f_s) \sin(\pi f/f_s)}{\cos(2\pi f/f_s) - \cos(2\pi f_0/f_s)} \quad (16)$$

Compensation for the filter gains may be achieved through the use of eqns. 15 and 16. However, since the correct frequency cannot be determined without correct compensation, it is necessary to incorporate the compensation process in a feedback loop.

The second cause of error is due to the assumption to piecewise linearity between sample intervals when making the derivative calculation. It is shown in Appendix 7.2, that the right hand side of eqn. 14 equates, not simply to f, but to the term $f - 2\pi^2 f^3 \Delta T^2/3$. For a practical implementation of the frequency measurement algorithm using a microprocessor, the computation required to solve this term for f is not justified. Instead, accuracy can be improved by, firstly, evaluating the following expression:

$$f_{err} = \frac{2\pi^2 f^3 \Delta T^2}{3} \quad (17)$$

and, secondly, adding f_{err} to the current frequency estimate, that is, the measured frequency becomes $f + f_{err}$. Numerical examples of this approach, assuming a sampling frequency of 4 kHz, are shown in Table 1. This Table shows that the approach correctly evaluates the power system frequency to within three places of decimals.

Table 1: Effect of derivative error and associated compensation technique on calculation of power system frequency (for f_s = 4 kHz)

Power system frequency, Hz	f (from eqn. 14)	f_{err} (from eqn. 17)	$f + f_{err}$
48.0	47.954 52	0.045 35	47.999 87
50.0	49.948 60	0.051 25	49.999 85
52.0	51.942 18	0.057 63	51.999 81

2.4 Frequency calculation algorithm

Taking into account the factors described in the preceding sub-Sections, a new algorithm for the calculation of power system frequency is proposed. The overall structure of the algorithm is shown in Fig. 2.

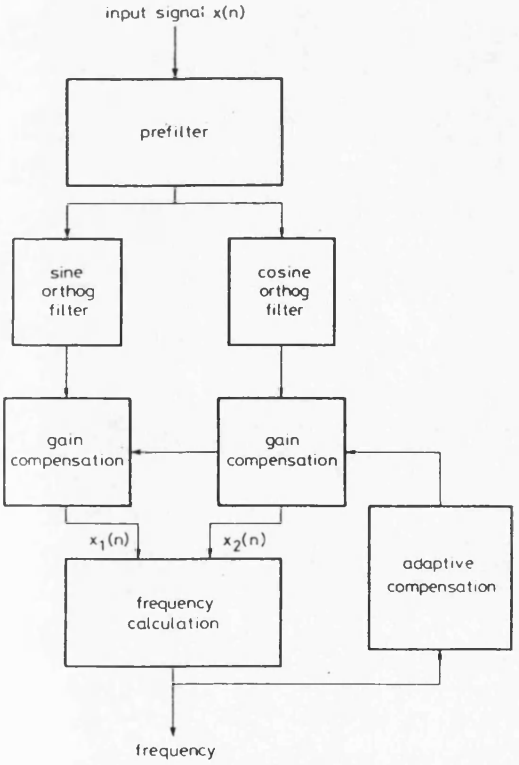

Fig. 2 *Structure of the frequency measurement algorithm*

The input to the algorithm is a sequence of discrete time values of the power system signal; it is assumed that the values have been sampled correctly and no aliasing has occurred. The prefilter is required to filter out any components contained within the sampled input signal which will not be removed by the FIR sine and cosine orthogonal filters. This is of particular relevance to power system frequency harmonics. Although the FIR filters show complete rejection of harmonics when the power system frequency is 50 Hz (Fig. 1*a*), this is not the case for other values of power system frequency. For example, if the frequency is 47 Hz, then the third harmonic frequency will consequently be 141 Hz which, from Fig. 1*a*, will not be rejected by the orthogonal filters. Thus, to ensure high accuracy under all conditions, it is necessary to include a prefilter to ensure that only signals at power system frequency are processed by the algorithm. Investigations showed that a FIR Hamming type filter with a filter length at least equal to the period of the lowest encountered power system frequency provided good rejection of likely harmonics yet retained high speed measurement of frequency.

The sine and cosine orthogonal filter blocks in Fig. 2 correspond to the implementation of the FIR filters described by eqns. 10 and 11; the coefficients of these filters are precalculated. The frequency calculation is the implementation of eqn. 14 together with the compensation for the derivative error given by eqn. 17. In order to compensate for the gains of the orthogonal filters at the most recent measurement of frequency, a feedback process is incorporated in the algorithm. However, care must be taken at this stage to ensure that the algorithm remains stable to changes in frequency and, more importantly, changes in signal amplitude. The block marked adaptive compensation performs the gain compensation by calculating the best estimate of the frequency from the previous 5 ms ($\frac{1}{4}$ cycle) history of the frequency and amplitude of the input signal. Justification for this step is given in Appendix 7.3. Having calculated the filter gains, the outputs of the orthogonal filters are multiplied by the reciprocal of the relevant gain to ensure that the magnitudes are equal.

3 Performance evaluation

Computer simulation results are presented for the frequency measuring algorithm to show its performance under steady-state conditions, dynamic conditions, and to signals containing harmonic content. The algorithm was simulated with a sampling frequency of 4 kHz and included a 100 coefficient Hamming type prefilter.

Figs. 3*a* and *b* show the response of the algorithm to steady state sinusoids at 52, 50 and 48 Hz, respectively. The accuracy of the algorithm is seen from these results to be within 0.001 Hz as predicted in Section 2.3. For all results in this section, the operation of a 16 bit analogue to digital converter was included to simulate the effects of quantisation. The accuracy of the frequency measurement was consistent for all amplitudes of the unquantised input signal in the range 1.0 to 0.05 p.u. An important feature of the algorithm is that a new measurement of frequency is made during every sampling interval, i.e., 4000 measurements are made every second. Frequency measurement is made irrespective of the phase of the input signal.

Dynamic conditions were investigated by using the 'electromagnetics transient program' (EMTP) to simulate the simple system of Fig. 4*a* which shows a 75 MVA generator connected to, initially, a load of 36.2 MW. Parameters used in this simulation are shown in Appendix 7.4. At time $t = 15.205$ s the switch is closed, thus loading the generator with an additional 17.8 MW. In this simulation, the operation of the speeder motor in the governor is disabled and hence the new loading condition results in a new steady state system frequency below the

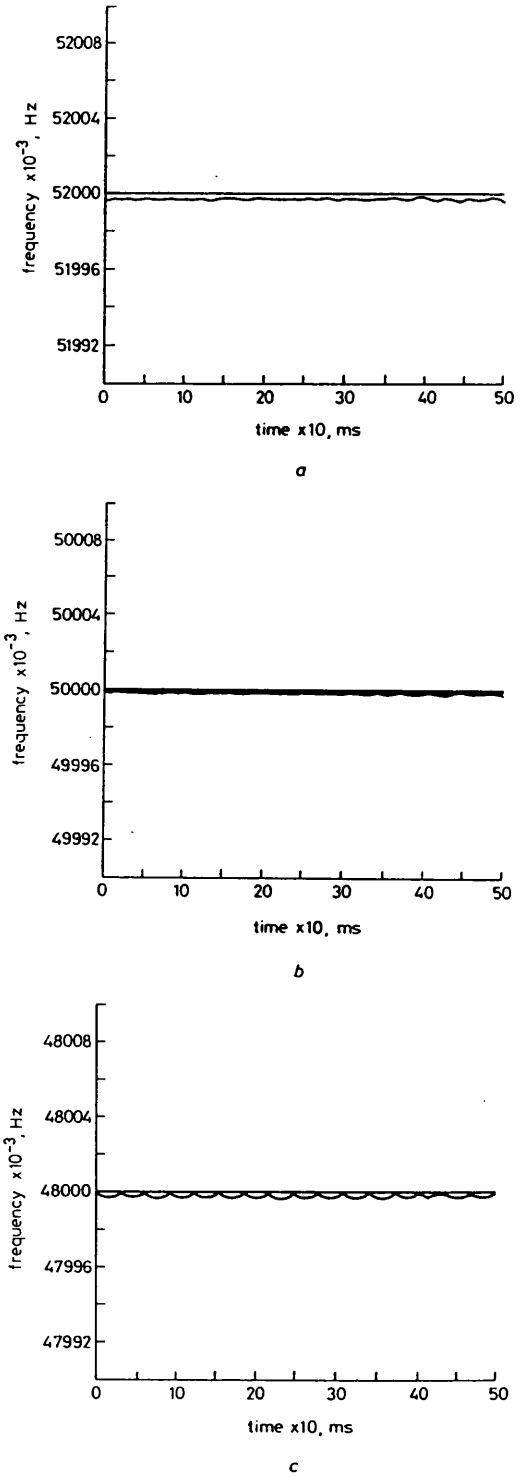

Fig. 3 *Response of algorithm to steady-state sinusoid*
a At 52 Hz
b At 50 Hz
c At 48 Hz

nominal. Fig. 4*b* shows the generator terminal voltage which is both frequency and amplitude modulated. This voltage was processed by the algorithm and the resulting frequency is depicted in Fig. 4*c* together with the generator rotor speed obtained from the EMTP simulation.

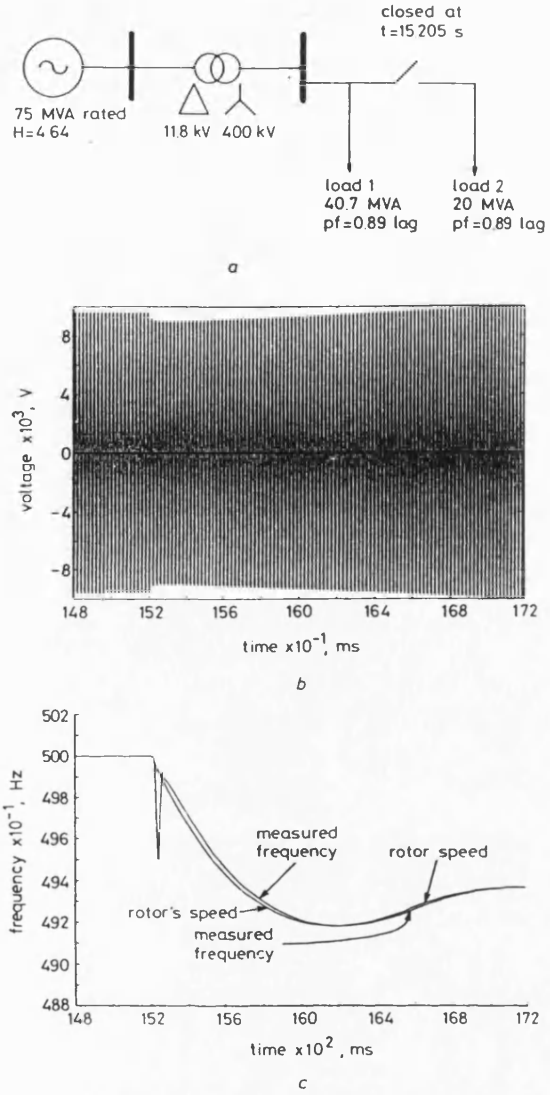

Fig. 4 *Algorithm performance for single machine power system*
a Simple single machine power system
b Generator terminal voltage
c Measured frequency and rotor speed

When the switch is closed, an instantaneous change in the terminal voltage occurs due to the redistribution of power. This is responsible for the initial 0.5 Hz 'spike' in the algorithm output at 15.2 s and is a consequence of measuring frequency from the terminal voltage. There is, of course, no corresponding instantaneous change in the rotor position and so the rotor speed is not seen to vary in the same way. Ignoring this effect, it can be clearly seen from Fig. 4*c* that the algorithm closely follows the rotor speed and exhibits a constant delay in frequency measurement of approximately 25 ms. Both rotor speed and algorithm output settle to a constant frequency of 49.37 Hz at approximately 2 s after the initial overload.

Fig. 5 shows a more complicated power system section with two generators connected to a common busbar via transmission line sections. Parameters used in this simulation may be found in Appendix 7.5. Initially, the generators at P and Q are loaded to 831.2 MW whereas the infinite bus infeed is 249.4 MW. At time $t = 15.015$ s the connection to the infinite bus is removed, the system becomes isolated, and thus the two generators take up the total load. Fig. 6 shows the frequency measured from

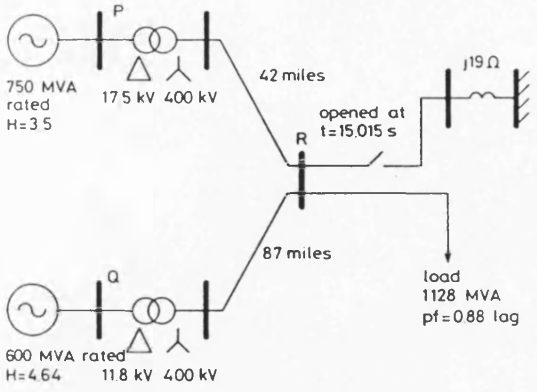

Fig. 5 *Two machine system with infinite bus connection*

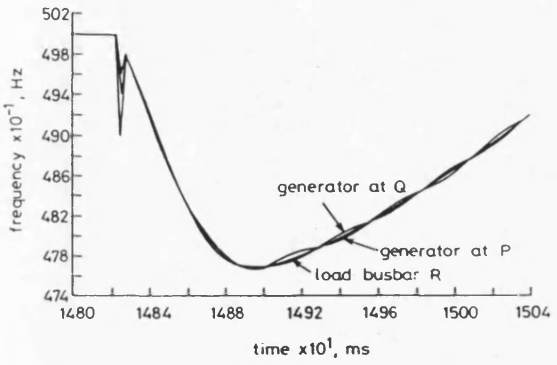

Fig. 6 *Frequencies evaluated from voltages measured at generator terminals and busbar R*

voltages taken from the terminals of the two generators, i.e., busbars P, Q and the load busbar R. For clarity, the EMTP output frequencies apparent at these positions are not shown in Fig. 6. However, as with the previous results, the algorithm exhibited perfect tracking of the frequencies with a 25 ms delay. The algorithm clearly shows the frequency oscillations resulting from power swings between the two generators in the isolated power island; the load bus frequency is observed to be approximately the mean of the two generator frequencies. These results show that the algorithm can track relatively fast frequency variations.

Finally, Fig. 7 shows the response of the algorithm to a dynamically changing power system signal having 10% of third harmonic and 5% of fifth harmonic. The signal has constant fundamental and harmonic amplitudes but exponentially decaying frequency. This is a particularly severe test because, due to the change in the power system frequency from 50 to 41 Hz, the third and fifth harmonic will vary from 150–123 Hz and 250–205 Hz, respectively. It is the action of the Hamming prefilter which ensures correct frequency measurement for this case; examination of Fig. 7 will reveal no discernable effect from the harmonics.

4 Algorithm structure for multiple input signals

The input signal to the algorithm can be either a voltage or current signal, although, in most practical cases, the input is likely to be a voltage signal. In the event that the single input signal to the algorithm is lost, either due to a fault on the chosen phase, or due to voltage transformer failure, then the frequency output of the algorithm will be similarly lost. To safeguard against this occurrence in situations where the measurement of frequency by the algorithm is critical to the correct operation of the power system, a structure for the algorithm has been developed where all three phases voltages are used. This is shown in Fig. 8 where the orthogonalisation of the three inputs signals is used to form a positive phase sequence component of the input voltage. The frequency is consequently calculated from this pps signal. The results of using this structure do not significantly vary from those shown in the previous section except that the algorithm still gives correct operation even if one of the input signals is removed. In general, under fault conditions, pps quantities are always present and so the correct measurement of frequency is ensured under even the most onerous conditions.

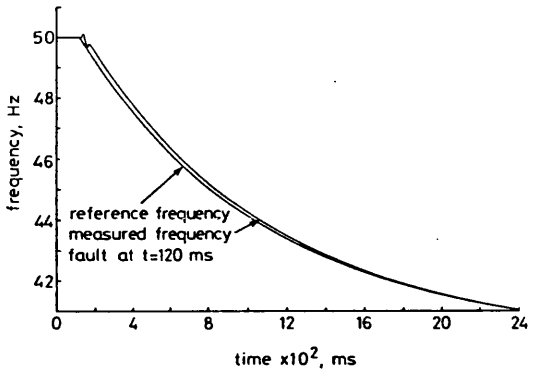

Fig. 7 *Response of algorithm to signal with exponentially decaying fundamental frequency plus 10% 3rd and 5% 5th harmonically related components*

5 Conclusions

A frequency measurement algorithm capable of evaluating power system frequency from discrete time signals has been shown to be accurate to within 0.001 Hz. The algorithm calculates a new estimate of frequency at every sampling interval irrespective of the phase of the input signal. The algorithm is capable of accurately tracking frequency under dynamic power systems conditions and provides high-speed measurement, exhibiting a delay of only 25 ms. The algorithm has shown immunity to the presence of harmonics and can be based on a three signal input with positive phase sequence component evaluation to provide a highly reliable frequency measuring function.

An important benefit of the algorithm is that it calculates frequency through a wholly numeric process and is based upon discrete time signals captured at a fixed sampling rate. It is thus suitable for implementation in current numeric protection relay hardware. The algorithm will find applications where high-speed frequency measurement is critical such as in under frequency relays and load shedding schemes.

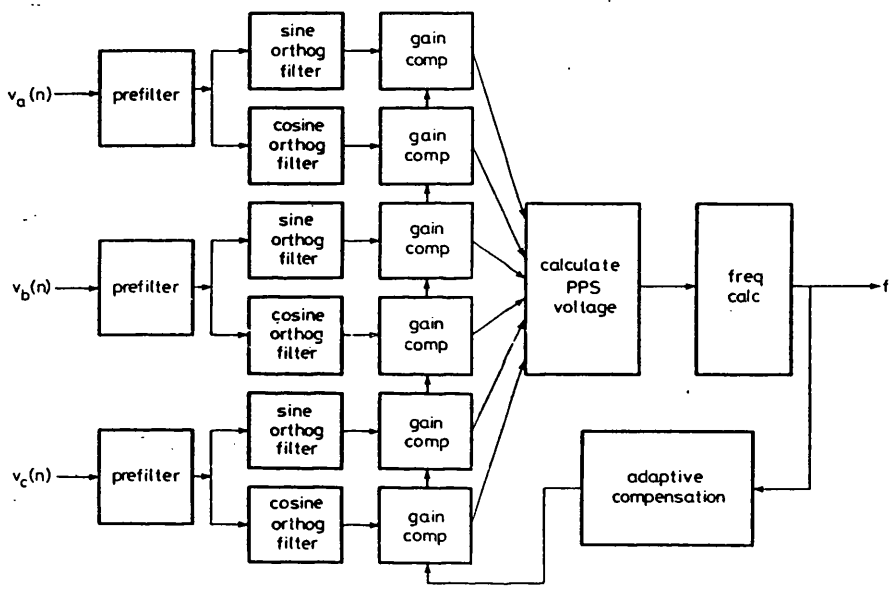

Fig. 8 *Structure of frequency measurement algorithm capable of deriving positive phase sequence component of three phase input signals*

Currently, work is progressing on the implementation of the algorithm on hardware incorporating a digital signal processor. It is hoped to report on this development in due course.

6 References

1 GIRGIS, A.A., and HAM, F.M.: 'A new FFT-based digital frequency relay for load shedding', *IEEE Trans. Power Appar. & Syst'*. Feb. 1982, **PAS-101**, (2), pp. 433–439

2 PHADKE, A.D., THORP, J.S., and ADAMIAK, M.G.: 'A new measurement technique for tracking voltage phasors, local system frequency and rate of change of frequency', *IEEE Trans. Power Appar. & Syst.*, May 1983, **PAS-102**, (5), pp. 1025–1038

3 MALIK, O.P., HOPE, G.S., HANCOCK, G.C., ZHAOHUI, L., LUQING, Y., and SHOUPING, W.: Frequency measurement for use with a microprocessor-based turbine governor'. Paper No. 91 WM 140-4EC, IEEE PES Winter meeting, New York, Feb. 1991

4 McILWAINE, S.A., TINDALL, C.E., and McCLAY, W.: 'Frequency tracking for power system control', *Proc. IEE, C.*, March 1986, **133**, (2), pp. 95–98

5 BENMOUYAL, G.: 'Design of a combined global differential and volt/hertz relay for step-up transformers', *IEEE Trans. Power Delivery*, July 1991, 6, (3), pp. 1000–1007

6 GIRAY, M.M., and SACHDEV, M.S.: 'Off nominal frequency measurements in electric power systems', *IEEE Trans. Power Delivery*, July 1989, 4, (3), pp. 1573–1578

7 GIRGIS, A.A., and HWANG, D.: 'Optimal estimation of voltage phasors and frequency deviations using linear and nonlinear Kalman filtering: theory and limitations', *IEEE Trans. Power Appar. & Syst.*, Oct. 1984, PAS-103, (10), pp. 2943–2949

8 SACHDEV, M.S., WOOD, H.C., and JOHNSON, N.: 'Kalman filtering applied to power systems measurements for relaying', *IEEE Trans. Power Appar. & Syst.*, Dec. 1985, PAS-104, (2), pp. 3565–3573

9 GIRGIS, A.A., and PETERSON, L.W.: 'Adaptive estimation of power system frequency deviation and its rate of deviation for calculating sudden power system overloads', *IEEE Trans. Power Delivery*, Apr. 1990, 3, (2), pp. 585–594

10 KAMWA, I., and GRONDIN, R.: 'Fast adaptive schemes for tracking voltage phasor and local frequency in power transmission and distribution systems', *IEEE Trans. Power Delivery*, Apr. 1992, 7, (2), pp. 789–795

11 PAPOULIS, A.: 'Random modulation: a review', *IEEE Trans. Acoust., Speech & Signal Process.*, Feb. 1983, ASSP-31, (1), pp. 96–105

12 MASON, T.H., AYLETT, P.D., and BIRCH, F.H.: 'Turbogenerator performance under exceptional operating conditions', *IEE Proc. A*, Jan. 1959, paper 2846-S, pp. 357–373

7 Appendices

7.1 Magnitude gains of the sine and cosine filters

The FIR expression for the sine filter is given by

$$H_s(k) = \sin\left(\frac{2\pi K}{N} + \frac{\pi}{N}\right) \quad \text{for } k = 0, 1, \ldots, N-1 \tag{18}$$

which is the product of a sinusoidal function and a rectangular window $p(k)$, where $p(k) = 1$ for $k = 0, 1, 2, \ldots, N-1$ and $p(k) = 0$ otherwise. An expansion of eqn. 18 will yield:

$$H_s(k) = p(k)\sin\left(\frac{2\pi k}{N}\right)\cos\left(\frac{\pi}{N}\right) + p(k)\cos\left(\frac{2\pi k}{N}\right)\sin\left(\frac{\pi}{N}\right) \tag{19}$$

In the frequency domain, the Z transform of eqn. 19 is

$$H_s(z) = \tfrac{1}{2}\sin\left(\frac{\pi}{N}\right)[P(ze^{j\Omega_0}) - P(ze^{-j\Omega_0})] + j\tfrac{1}{2}\cos\left(\frac{\pi}{N}\right)[P(ze^{j\Omega_0}) + P(ze^{-j\Omega_0})] \tag{20}$$

where

$$P(z) = \frac{z - z^{-(N-1)}}{z+1}, \quad \Omega_0 = \frac{2\pi f_0}{f_s} \tag{21}$$

which includes f_0, the frequency of sinusoid of eqn. 18, and f_s is the sampling frequency.

Solving for $P(z)$, the Z transform of eqn. 18 becomes

$$H_s(z) = \frac{\sin\left(\frac{\Omega_0}{2}\right)(1 - z^{-N})(z+1)}{z - 2\cos\Omega_0 + z^{-1}} \tag{22}$$

Since the filters are causal, the one-sided Z transform may be used where $z = re^{j\Omega}$ for $r = 1$, i.e., lying on the unit circle in the Z plane. From eqn. 22,

$$H_s(e^{j\Omega}) = \frac{j2e^{-j\Omega(N-1)/2}\sin(\Omega_0/2)\sin(N\Omega/2)\cos(\Omega/2)}{\cos\Omega - \cos\Omega_0} \tag{23}$$

By a similar procedure, the frequency domain expression of the cosine filter may be derived,

$$H_c(e^{j\Omega}) = \frac{-2e^{-j\Omega(N-1)/2}\cos(\Omega_0/2)\sin(N\Omega/2)\sin(\Omega/2)}{\cos\Omega - \cos\Omega_0} \tag{24}$$

Eqns. 23 and 24 can be expressed in terms of their magnitude and phase response for $\Omega = 2\pi f/f_s$,

$$|H_s(f)| = \frac{2\sin(\pi f_0/f_s)\sin(\pi N f/f_s)\cos(\pi f/f_s)}{\cos(2\pi f/f_s) - \cos(2\pi f_0/f_s)} \tag{25}$$

and

$$\angle H_s(f) = je^{-j\pi f(N-1)/f_s} \tag{26}$$

Similarly for the cosine filter,

$$|H_c(f)| = \frac{2\cos(\pi f_0/f_s)\sin(\pi N f/f_s)\sin(\pi f/f_s)}{\cos(2\pi f/f_s) - \cos(2\pi f_0/f_s)} \tag{27}$$

and

$$\angle H_c(f) = -e^{-j\pi f(N-1)/f_s} \tag{28}$$

7.2 Frequency error due to numerical derivative calculation

The assumption of piecewise linearity between samples, and the subsequent derivative calculation using eqn. 12, causes a time invariant frequency error to occur. This error may be conveniently derived with reference to two, unity amplitude, orthogonalised signals:

$$x_1(t) = \sin(\omega t + \phi) \quad x_2(t) = \cos(\omega t + \phi) \tag{29}$$

Thus, applying eqn. 12 to $x_1(t)$ gives

$$x_1'(t) = \frac{\sin(\omega t + \phi) - \sin(\omega(t - \Delta T) + \phi)}{\Delta T} \tag{30}$$

which may be re-expressed as

$$x_1'(t) = \frac{\sin(\omega t + \phi) - (\sin(\omega t + \phi)\cos(\omega\Delta T) - \cos(\omega t + \phi)\sin(\omega\Delta T))}{\Delta T} \tag{31}$$

Replacing $\cos(\omega\Delta T)$ and $\sin(\omega\Delta T)$ with the first two terms of the relevant Maclaurin series, eqn. 31 may be written as

$$x_1'(t) = \frac{\sin(\omega t + \phi) - \left[\sin(\omega t + \phi)\left(1 - \frac{(\omega\Delta T)^2}{2!}\right) - \cos(\omega t + \phi)\left(\omega\Delta T - \frac{(\omega\Delta T)^3}{3!}\right)\right]}{\Delta T} \tag{32}$$

which simplifies to

$$x_1'(t) = \omega\cos(\omega t + \phi) + \sin(\omega t + \phi)\frac{\omega^2\Delta T}{2} - \cos(\omega t + \phi)\frac{\omega^3\Delta T^2}{6} \tag{33}$$

An expression for $x_2'(t)$ may be similarly derived:

$$x_2'(t) = -\omega\sin(\omega t + \phi) + \cos(\omega t + \phi)\frac{\omega^2\Delta T}{2} + \sin(\omega t + \phi)\frac{\omega^3\Delta T^2}{6} \tag{34}$$

The analytic expressions for $x'_1(t)$ and $x'_2(t)$ may now be substituted into the frequency evaluation expression, eqn. 5, to yield the following result:

$$x_2(t)x'_1(t) - x_1(t)x'_2(t) = \omega - \frac{\omega^3 \Delta T^2}{6} = 2\pi\left(f - \frac{2\pi^2 f^3 \Delta T^2}{3}\right) \quad (35)$$

Thus it will be apparent from eqn. 35 that the numerical derivative calculation introduces a nonlinear error in the frequency evaluation process.

7.3 Adaptive compensation

The input signal to the frequency measurement algorithm may be considered to be both frequency modulated and amplitude modulated, in either case the modulation is taken to be random. It has been shown [11] that the optimum estimation of the frequency, $f^*(t)$, of a signal having a randomly varying amplitude $X(t)$ is given by

$$f^*(t) = \frac{E[X^2(t)f(t)]}{E[X^2(t)]} \quad (36)$$

where $E[\cdot]$ denotes the expected, or mean, value of the variable in parenthesis. In the frequency measurement algorithm, the expected value can be approximated by a moving average filter, for example, the expected value of some discrete time variable $x(n)$ can be calculated from its previous time history:

$$E[x(n)] \approx \frac{\sum_{i=0}^{N-1} x(n-i)}{N} \quad (37)$$

Thus eqn. 37 is applied individually to the square of the amplitude, $X(t)$, of the input signal (given by eqn. 6) and to the product of the amplitude squared and the frequency estimate from the algorithm output. The quotient of these terms, i.e., eqn. 36, is then used to calculate the filter gains from eqns. 15 and 16. A series of tests showed that moving average filter lengths of 5 ms (i.e., $N = 20$ for $f_0 = 50$ Hz and $f_s = 4$ kHz) promoted the best algorithmic response to typical dynamic power system input signals.

7.4 Parameters used to model single machine system (Fig. 4a)

Units in ohms unless otherwise stated.

Transformer:	leakage reactance (LV side) = 0.0435 leakage reactance (HV side) = 37.51
Generator:	75 MVA rated, 50 Hz, 2 pole, 11.8 kV, $H = 4.64$ s $x_d = 2.0$, $x_q = 1.9$, $x'_d = 0.2$, $x'_q = 0.19$. For further details, see Reference 12.

7.5 Parameters used to model two machine system (Fig. 5a)

Units in ohms unless otherwise stated.

Transmission lines:	modelled as pi equivalents, = circuit parameters per mile: $R = 0.039$, $L = 62.4$ mH, $C = 20.3$ nF.
Transformer at P:	leakage reactance (LV side) = 0.0833 leakage reactance (HV side) = 26.03
Transformer at Q:	leakage reactance (LV side) = 0.0435 leakage reactance (HV side) = 37.51
Generator at P:	750 MVA rated, 50 Hz, 2 pole, 17.5 kV, $H = 3.5$ s $x_d = 1.75$, $x_q = 1.75$, $x'_d = 0.265$, $x'_q = 0.265$
Generator at Q:	modelled as eight parallel 75 MVA units as described in Fig. 4a. For further details, see Reference 12.